On Large Scale Convection in the Atmosphere over the Tropical Western Pacific and Eastern Indian Ocean

By

Zhenjie Lin (M. Sc.)

submitted in fulfilment of the

requirements for the degree of

Doctor of Philosophy

in the Department of Geography and Environmental Studies

University of Tasmania

Hobart, Australia

December, 1991

To

My father Jinliang, mother Chunmei, wife Qingping, and daughter Susan.

Statement

This thesis contains no material which has been accepted for the award of any other higher degree or graduate diploma in any tertiary institution and, to the best of my knowledge and belief, this thesis contains no material previously published or written by another person, except where due reference is made in the text of the thesis.

Zhenjie Lin

Acknowledgement

Upon completion of this study, I would like to pay special tribute to my two supervisors: Dr Manuel Nunez, of the Department of Geography and Environmental Studies, University of Tasmania, and Dr Gary Meyers, of the CSIRO Division of Oceanography, Hobart. I am deeply grateful to Manuel Nunez for his constant guidance and help, and his efforts in correcting the draft of this thesis. My heartful thanks to Gary Meyers, for his invaluable advice and assistance, from acquiring the data to correcting my draft.

There are many people in the Department of Geography and Environmental Studies of the University of Tasmania who have encouraged and helped me. I would like to specially thank Professor Jamie Kirkpatrick, Dr Les Wood and Dr Peter Wilde for their consistent help and concern. Thanks also to the departmental secretaries Miss Sally Banks, Miss Ifay Tsang, and Mrs. Kerrie Green.

It has been a very nice experience to study in the department. I would like to express my thanks to my fellow students. They include Dr Kelvin Michael, Dr Maxim Shoshany, Dr David Hood, Dr Jocelyn Hughes, Dr Jane Williams, Mr. Ge Wang, Ms. Louis Gilfedder, and Mrs Shirley Grosvenor. My special thanks to Dr Kelvin Michael for his continuous help in many areas.

The staff in the Computing Centre of the University of Tasmania have given me invaluable support. Special thanks to Bob Allan, Paul Stevenson and Sue Mulcahy. Many thanks to the staff at the CSIRO Marine Laboratory in Hobart, for allowing me to use their computers, library and other facilities. My sincere thanks to Peter Campbell, Paul Tildesley, Ken Ridgeway and Helen Phillips, for their help in computing.

It would be impossible to use such extensive data sets in this study without the kindness and help from many people. Special thanks to Dr Robert Bernstein of SeaSpace in San Diego for his kindness in providing the MCSST data, the Australian Bureau of Meteorology in Melbourne for providing the wind data, Dr Roger Lukas of the University of Hawaii for providing sea surface temperature from *RV Moana Wave*, Dr Eric Lindstrom and Dr John Church of the CSIRO Division of Oceanography, for providing data from *RV Franklin*, Dr Richard Reynolds, Climate Analysis Center, NOAA for providing monthly SST and OLR data, and NOAA NESDIS for providing the TOVS sounding product.

I would not have been able to finish my study without the understanding and support of my wife, Qingping Huang. She has sacrificed all of her leisure time to support our family. Her encouragement and understanding have been an inspiration to me. I am grateful to my mother Chunmei Qiu who came to Australia twice to help us during my studies, my father who has supported my studies from his meagre financial resources since I was young, and my parents-in-law and brother and sisters for their love, care, encouragement and support.

I would also like to express my sincere thanks to Professor Sizhong Zheng of the Institute of Geography, the Chinese Academy of Science. He gave me special help and encouragement to come to Australia to pursue the PhD degree.

The study was supported jointly by a University of Tasmania Postgraduate Scholarship and a University of Tasmania/CSIRO Research Grant.

Abstract

The motivation for this study came from the variation of deep convection during the anomalous climatological events known as El Nino/Southern Oscillation (ENSO). Various environmental variables, mainly sea surface temperature (SST), wind and precipitation affect various stages of the convection process. Despite the considerable work that has been done in this area, there are gaps in our knowledge of deep convection and its relationship to SST.

The study encompassed an area from 70°E to 180°E and from 45°S to 45°N, but concentrated on the tropical region which is considered to be of primary importance to the development of ENSO events. The data sets used consistd of satellite-derived SST fields, wind fields from Australian Bureau of Meteorology, precipitable water vapour from NOAA/TOVS and outgoing longwave radiation (OLR), all for the period 1984 to 1986. This period lies between the 1982/83 and 1986/87 ENSO events, and therefore provides information on the character of convection prior to and at the early stages of the 1986/87 event.

The annual variation of SST, wind, OLR and precipitable water were mapped during the study period. A wind divergence analysis at 200 mb revealed a zone of convergence over northern Australia from June to November. Over the ocean, the maximum convection is generally located west of the SST warm centre, and convection follows changes in the location of the warm centre. A conceptual model relating OLR to SST and upper level wind divergence has been developed. It successfully explains the relationship between these three variables, especially above the threshold temperature of 27.5°C, and points to the importance of upper level divergence in the development of deep convection.

Some interesting features were found to be related to the 1986/87 ENSO event. A positive SST anomaly developed over the tropical mid-Pacific during the study period. By contrast a negative anomaly developed simultaneously over the south Indian Ocean west of Australia. Evidence of a weak convection signal, much before the ENSO anomaly was fully developed, was observed in the Philippines Sea region from May 1986 onward.

Table of Contents

1986

List of Figures

List of Tables

List of Acronyms

ATRA	Australian Tropical Region Analysis
AVHRR	Advanced Very High Resolution Radiometer
COARE	Coupled Ocean-Atmosphere Responses Experiment
COADS	Comprehensive Ocean-Atmosphere Data Set
CTD	Conductivity-Temperature-Depth
DJF	December-January-February
ECMWF	European Centre for Medium Range Weather Forecasting
ENSO	El Nino/Southern Oscillation
EOF	Empirical Orthogonal Function
GCM	General Circulation Model
HIRS	High-Resolution Infrared Radiation Sounder
HRC	Highly Reflective Cloud
ITCZ	Intertropical Convergence Zone
JJA	June-July-August
LLPW	Low-Level Precipitable Water
LUCIE	Leeuwin Current Interdisciplinary Experiment
MAM	March-April-May
MCA	Meso-scale Convective Area
MCSST	Multichannel Sea Surface Temperature
MSU	Microwave Sounding Unit
NESDIS	National Environmental Satellite Data and Information Service
NOAA	National Oceanic and Atmospheric Administration
NODC	National Oceanographic Data Center
PW	Precipitable Water
OLR	Outgoing Longwave Radiation
RMSD	Root Mean Square Difference

SON	September-October-November
SOI	Southern Oscillation Index
SPCZ	South Pacific Convergence Zone
SST	Sea Surface Temperature
SSU	Stratospheric Sounding Unit
TOGA	Tropical Ocean Global Atmosphere
TOVS	TIROS Operational Vertical Sounder
WCRP	World Climate Research Programme
WEPOCS	Western Equatorial Pacific Ocean Circulation Study
WMO	World Meteorological Organisation
WOCE	World Ocean Circulation Experiment
XBT	Expendable Bathythermograph

Chapter 1. Introduction

1.1 Motivation

Disastrous climatic events associated with droughts in the Australian region have been related to the El Nino/Southern Oscillation (ENSO) phenomenon (Horel and Wallace, 1981; Philander, 1983). Various researchers (Rasmusson and Carpenter, 1982; Gill and Rasmusson, 1983; Lau and Chan, 1985, 1986a, 1986b; Knutson *et al.*, 1986; Ardanuy and Kyle, 1986; Ardanuy *et al.*, 1987) have reported an eastward movement of the centre of deep convection in the atmosphere from the Indonesian region to the mid-Pacific during an El Nino year. The western Pacific Ocean plays an important role in this process because the western branch of the Walker Circulation rises here and thus forms a large-scale convection centre while the warm pool with greater than 28°C water enhances the latent heat flux.

With the increasing understanding of the important role played by the tropical ocean in the development of ENSO, an international program, the Tropical Ocean Global Atmosphere Program (TOGA), has been organized to integrate research in this area (World Meteorological Organization, 1985). The TOGA Programme is a specific project within the World Climate Research Programme (WCRP), and its implementation is an essential part of achieving the overall objectives of the WCRP. The TOGA programme recognized the importance of the western Pacific by establishing the Coupled Ocean Atmosphere Response Experiment (COARE) (Lukas and Webster, 1988). COARE recognises the western Pacific as a very active source region of equatorial waves in the ocean. The meteorology is also important on both a global and regional scale. The warm water regions are the largest and strongest heat sources for the atmosphere on the globe. Since the sensitivity of the atmosphere in regions of warm sea surface temperature is principally a Clausius-Clapeyron effect,

small changes in the warm moist structure of the western and central Pacific Ocean, such as occurring during ENSO phenomena, have a profound effect on the atmospheric structure simply because of this nonlinear relationship between the saturation vapour pressure and temperature of the underlying ocean. That is, small changes in the boundary forcing may invoke very large changes in the atmospheric heating.

In terms of air/sea heat exchange, the sensible and latent heat convective fluxes form an important source of heat release to the atmosphere. Once in the atmosphere, moisture may condense as convective rainfall, a crucial rainfall mechanism in the tropics. Lack of convection during ENSO years has created droughts in the Indonesian and Australian region, with negative effects on the agriculture and economy of the recipient nations (McBride and Nicholls, 1983; Ropelewski and Halpert, 1987; Nicholls, 1989).

Studies on convection have shown that it may act on a variety of temporal scales ranging from weeks to years (Gill and Rasmusson, 1983; Knutson *et al.*, 1986; Knutson and Weickmann, 1987). Links between convection and sea surface temperature (SST) have also been explored, especially at the interannual scale. Gill and Rasmusson (1983) showed that during the 1982-83 ENSO event, the eastward migration of maximum SST was followed by an outgoing longwave radiation (OLR) anomaly, which in turn, was followed by the easterly wind anomaly at 200 mb and westerly wind anomaly at 850 mb (see also Figure 5.1 of World Meteorological Organization, 1985). The study supports the earlier hypotheses of Bjerknes (1969) who argued that the strength of the Walker circulation decreased during ENSO years with a weakening of convection in the western tropical Pacific.

Subsequent studies revealed that the relationship between SST and convection is more complex, especially over the western Pacific (Gadgil *et al.*, 1984; Graham and Barnett, 1987). It was found that there is a critical temperature, approximately 27.5°C, under which no strong convection can develop. Above this temperature, there is no clear relationship between these two variables. These observations illustrate the complexity

of the processes governing the starting, development, maintenance and collapse of convection. Clearly, there is a need for further studies to investigate these processes in more detail.

1.2 Objectives

The purpose of this dissertation is to study the character of the large-scale tropical convection process over the eastern Indian Ocean and the western Pacific. Using extensive simultaneous data sets, it is expected that this study will illuminate the relationships between convection and various oceanographic and meteorological parameters. These parameters include OLR as an index of convection, and SST, wind and precipitable water fields. They were collected over an area bounded by latitudes 45°S to 45°N, longitude 70°E to 180°E, and for the period 1984-86. The region is unique in that it encompasses the upwelling end of the Walker Circulation as well as all the processes associated with the beginning of an ENSO event. Unlike other studies, the data sets used here are very comprehensive, therefore allowing a detailed description of the spatial and temporal structure of the processes involved in convection. In particular, the wind fields at both 850 mb and 200 mb are examined in detail to determine the divergence field in a column of air. The study provides a climatology of convection in the region in preparation for TOGA-COARE.

The study period covers a time span between the 1982/83 ENSO event, the most intense such event this century, and the 1986/87 event. It should therefore illuminate the period of recovery after the 1982/83 event, and a gradual build-up of the anomalies prior to the 1986/87 event. This period has not been examined in great detail previously.

A detailed examination of each individual field is necessary in order to gain a better understanding of the convection process. The spatial and temporal patterns of each data set have been described in terms of annual, interannual and intraseasonal variations. This procedure highlights the regional characteristics important to the

development of convection. The integration of the various data sets will then provide a comprehensive description.

1.3 Thesis structure

A general review of studies related to large-scale convection is presented in Chapter 2. The convection process and estimates of large-scale convection using precipitation, outgoing longwave radiation and wind divergence data are discussed. Various spatial and temporal features of convection from interannual, intraseasonal to even shorter time scales are then discussed. Relationships between large-scale convection and sea surface temperature, wind field and water vapour convergence are then reviewed. A review of various numerical models of air-sea interaction, especially related to interannual variations, is presented. The last section discusses the remaining important issues related to large-scale convection.

A detailed description of the data sets used in this study is given in Chapter 3. These data include satellite-derived multichannel sea surface temperature (MCSST), wind data from the Australian Tropical Region Analysis (ATRA), prepared by the Bureau of Meteorology of Australia, outgoing longwave radiation (OLR) and TIROS Operational Vertical Sounding (TOVS) data product. Validations on MCSST and wind data are presented using independent *in situ* data sets. Various analysing techniques will be discussed in detail. They include harmonic analysis, filtering techniques and empirical orthogonal function (EOF) analysis.

The character of the SST field is described in Chapter 4. The seasonal means during the period 1984-86 are analysed and compared to earlier studies on the climatological SST distribution. The annual and semi-annual cycles of SST are then examined using harmonic analysis, and the results are compared with earlier results from the literature. The spatial patterns of SST at different time scales are examined using empirical orthogonal function (EOF) analysis. Some interesting spatial features in SST of the tropical mid-Pacific and the southeast Indian Ocean are discussed.

The wind field is analysed in Chapter 5. The seasonal means of wind at 850 mb and 200 mb during the study period of 1984-86 are described to provide a background knowledge of the wind fields in the lower and middle troposphere. The annual and semi-annual cycles depicted by harmonic analysis are then discussed. This is followed by an analysis of the intraseasonal variations using bandpass-filtered (from 30-65 days) data along longitudinal and latitudinal lines. Longitude-time diagrams of these filtered wind data at different zonal bands are then presented.

A comprehensive study of convection is presented in Chapter 6. The main features of OLR during these three years are compared with those from earlier studies at different time scales. Whilst OLR provides dynamic evidence that convection is taking place, precipitable water in the low and middle troposphere provides information on potential areas of convection. The spatial feature and annual variation of precipitable water are therefore addressed. Estimates of convection are linked to the main variables which comprise SST and the wind field. A conceptual model is developed to examine the relationship between convection and these variables.

A summary of the main findings and suggestions for future research are presented in the final chapter.

Chapter 2. A General Review

2.1 Introduction

For time scales longer than a week air-sea interactions, especially over tropical areas, play a crucial role in the coupled ocean-atmosphere dynamic system (Rasmusson and Carpenter, 1982; Gill and Rasmusson, 1983). Because of the ocean's huge thermal capacity, it acts as an energy reservoir for the earth-atmosphere system. In the tropics, where oceans cover more than 75% of the surface (Riehl, 1979), SST is the primary forcing of the atmosphere. Currents control the SST pattern, and evaporation at the sea surface returns latent heat energy to the atmosphere. The solar radiation, on the other hand, warms the upper layers of the ocean. Through wind-stress, the atmosphere modifies the ocean currents, therefore changing the distribution of SST. The year-to-year variation of global climate has been greatly affected by this interaction.

The convection process involved in air-sea interaction provides a huge amount of energy to the atmosphere-ocean heat engine system (Gill, 1985). Detailed studies of the convection process will help to better understand, simulate and eventually forecast the behaviour of various aspects of the climate system. As illustrated by Heddinghaus and Krueger (1981) who used mean OLR for 45 months from June 1974 to February 1978, it can be seen that large-scale intense convective centres are mainly located over Central and South America, Central and North Africa, the western Pacific-Indonesian "Maritime Continent" region, and northern Australia. These processes of convection operating at large temporal and spatial scales are of fundamental importance to the climate system and as a result have received much attention.

This chapter reviews previous studies of large-scale convection, especially in the region encompassed by the eastern Indian Ocean to the western Pacific. Section 2.2 discusses the convection process and measurement of large-scale convection through

precipitation, OLR and wind divergence. Section 2.3 discusses the spatial and temporal features of convection, from interannual, intraseasonal and even shorter time scales. Sections 2.4, 2.5 and 2.6 review relationships between large-scale convection and sea surface temperature, wind field and water vapour convergence, respectively. Section 2.7 discusses various numerical models of air-sea interaction. The last section discusses the main findings and outlines the problems yet to be solved.

2.2 The convection process and measurements

Convection in the atmosphere over tropical regions is often regarded as a heat-induced event. An air mass will ascend upon being warmed. The water vapour in the air condenses as a result of dry or wet adiabatic cooling and releases latent heat to the air. In order to form organized convection, a continuous energy supply and a generally unstable environment are needed. Sensible and latent heat fluxes from the earth's surface are often considered as the two major important energy sources. Over the tropical oceans, however, latent heat associated with evaporation comprises the major part of its energy supply. For a circumpolar belt 10° latitude wide bordering on the equatorial trough, latent heat accounts 84% of total energy flowing into the atmosphere from the earth surface (Riehl, 1979).

As summarized by Barry and Chorley (1987), five categories of tropical weather systems can be distinguished according to their space and time scales (Figure 2.1). The smallest, with a life span of a few hours, is the individual cumulus, 1-10 km in diameter, which is generated by dynamically-induced convergence in the Trade Wind boundary layer. In fair weather, cumulus clouds are generally aligned in "cloud streets", more or less parallel to the wind direction. Individual cumulus towers, associated with thunderstorms in the Intertropical Convergence Zone (ITCZ), may sometimes reach more than 20 km in height with updraughts of 10-14 ms^{-1}. In this way, the smallest system may aid in the development of larger disturbances.

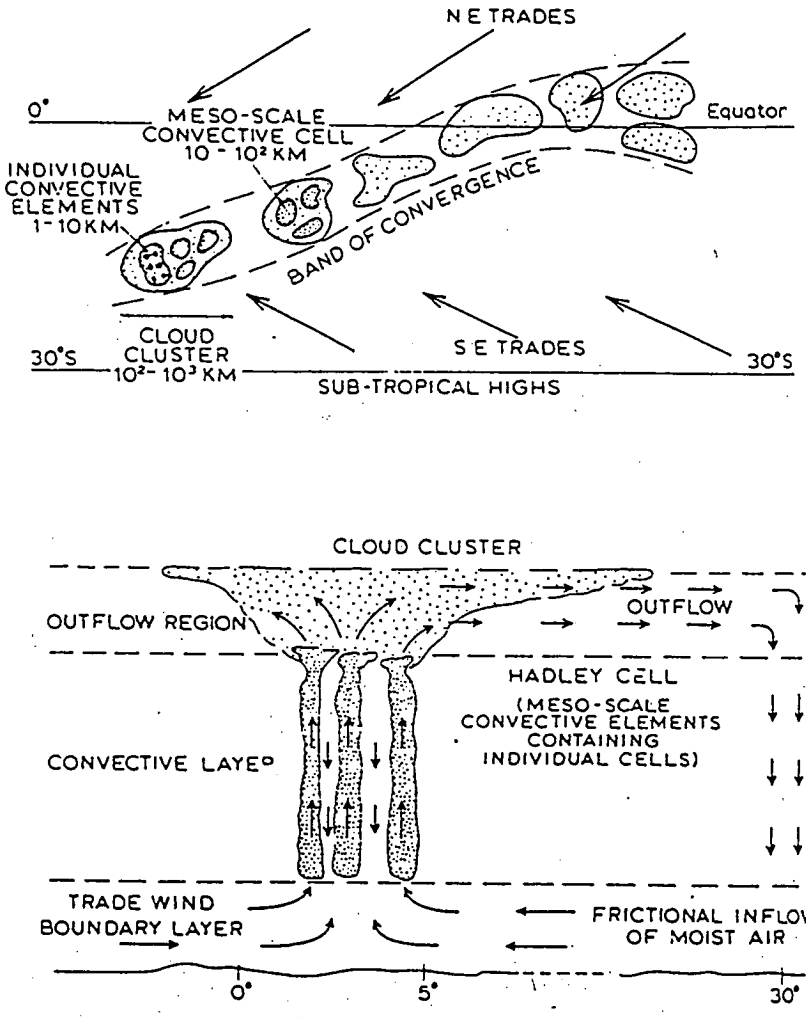

Figure 2.1 The meso-scale and synoptic structure of the equatorial trough zone (ITCZ), showing a model of the spatial distribution and vertical structure of convective elements which form the cloud clusters (from Mason, 1970)

The second category of the system is those cumulus clouds which group into meso-scale convective areas (MCAs) up to 100 km across. In turn, several MCAs may comprise a cloud cluster, i.e. the third category, with 100-1000 km in diameter. It should be noted that peak convective activity has passed when cloud cover becomes extensive through the spreading of cirrus canopies. A cluster meso-scale of convective cells often has a deep layer of convergent airflow (Figure 2.1). Some persist for only 1-2 days but others develop within synoptic-scale waves.

The fourth category of tropical weather system includes the synoptic-scale waves and cyclonic vortices, and the fifth group is represented by planetary-scale waves. The planetary waves have a scale of 10,000 to 40,000 km. Categories 3 and 4, mesoscale to synoptic-scale systems, are taken in this study to be representative of large-scale convection. Therefore their spatial and temporal variation are of special interest.

Direct measurements of convection are difficult since the vertical velocities are small (in the order of a few centimetres per second). Instead, indirect techniques are used. Precipitation, which is one of most significant results when water vapour condenses, often is used as an index to measure large-scale convection. It has been found that precipitation over Indonesia is reduced when an ENSO event begins, and reaches its maximum negative anomaly at the mature stage of an ENSO event (Rasmusson and Carpenter, 1982) , while rainfall in the central Pacific is exceptionally high. Severe rainfall in northern Peru has also been associated with ENSO (Horel and Cornejo-Garrido, 1983).

Because of the scarcity of precipitation measurements over tropical oceans, OLR estimates obtained from the NOAA operational satellites have attracted much attention in recent years. The OLR data were described in detail by Gruber and Krueger (1984). OLR data sets were first used in earth radiation budget studies (Gruber and Winston, 1978; Winston *et al.*, 1979). They became useful proxy data for convection studies due to the following theoretical consideration (Morrissey, 1986a). If it is assumed that

convective clouds exist at essentially the same temperatures as the surrounding atmosphere, and if a representative temperature sounding is used, infrared temperature isopleths can be converted to minimum cloud-top height fields (Martin and Scherer, 1973). The relationship between infrared radiation, effective blackbody temperature and height is shown graphically in Figure 2.2 (Morrissey, 1986a), where the standard atmosphere was obtained from Anderson and Oliver (1970). It is assumed that the stronger convection is, the higher the convective clouds extend, and therefore, the lower the cloud-top temperatures.

It has been widely accepted that convection is the primary rain-producing mechanism in the tropics and that contamination of cloud-top height fields by cirrus and cirrostratus is minor (Morrissey, 1986a, b). Therefore, for the tropics, cloud height and cloud area derived from satellite infrared data should be well correlated with the degree of convective activity. It has been noted that the OLR associated with strong convection is frequently of the order of 225 Wm^{-2} or less (Heddinghaus and Krueger, 1981). In contrast, the trade wind cumulus regime, extending a kilometre or so above the ocean surface, appears relatively warm and emits higher radiation, usually of the order of 275 Wm^{-2} or more. Thus it is possible to separate the major areas of strong convection from the relatively inactive trade wind or subsidence regimes (Heddinghaus and Krueger, 1981). Due to their continuity and availability, the OLR data sets have been widely used to study variations of convective activity at annual, interannual, intraseasonal, and even shorter time scales. These studies will be extensively reviewed in the next section.

Highly Reflective Clouds (HRCs) have also been examined and used as another important index for large-scale convection (Garcia and Anderson, 1984; Garcia, 1985; Steiner, 1987). In the visible and infrared satellite image mosaics, HRCs appear as large and bright cloud masses, thus implying intense convection. Their identification and use in precipitation estimates is discussed by Kilonsky and Ramage (1976) and Garcia (1981). The data are produced in NOAA on daily $1° \times 1°$ grids. The treatment

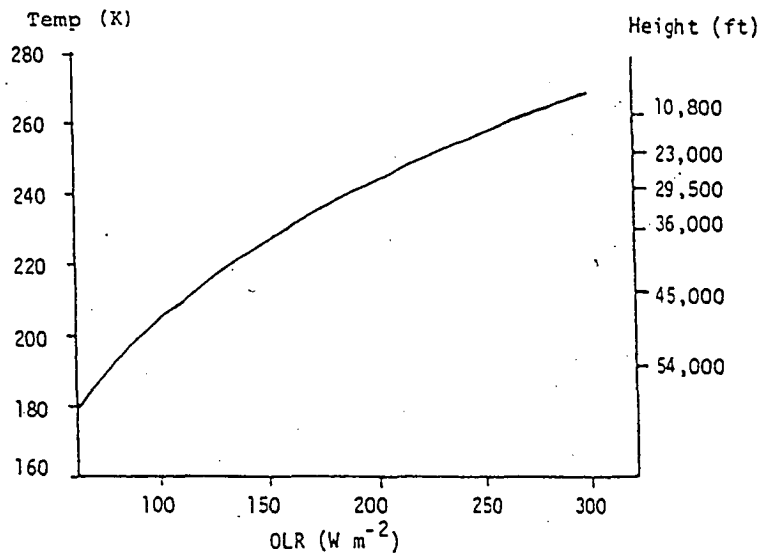

Figure 2.2 The relationship between infrared radiation, effective blackbody temperature and height as computed from the standard atmosphere (15°N, annual) (after Morrissey, 1986a)

to date of these data is subjective since the criteria used to denote convection is left to visual interpretation.

2.3 Variation of large-scale convection

Large-scale convection has a wide spectrum of variation from the interannual to the intraseasonal scales. Heddinghaus and Krueger (1981) used an EOF approach to study the monthly OLR data at the spatial scale of 10° latitude by 20° longitude from 1974 to 1978. They examined annual and interannual variations of OLR over the tropics. Most variation of OLR can be depicted by the first three EOF modes. The first one represents the winter-summer migration of convective centres between the northern and southern hemispheres. The second represents variation in the intensity of the ITCZ from spring to fall. The third mode shows a semiannual component which depicts the Indian Monsoon. Liebmann and Hartmann (1982) used the same period of data but with a higher spatial resolution (5° latitude by 5° longitude) to describe the annual and interannual variations of OLR. They noticed that the ITCZ is clearly most intense during June-July-August whist an OLR minimum (denoted by the 240 Wm^{-2} contour) exists in all seasons near Indonesia. Furthermore they showed that during December-January-February and March-April-May the eastward extension of the low OLR zone is associated with the enhanced Southern Pacific Convergence Zone (SPCZ). Horel (1982) used the same data set and found that on the equatorward side of the annual mean position of the ITCZ (along 5°N), OLR is least in April and May, while on the poleward side (along 10°N) it is least in August and September. In the region of the SPCZ, OLR is least during the summer season of the southern hemisphere when rainfall is usually greatest. Meehl (1987) used extended data covering a period from 1974 to 1982 and presented similar results. He found that the convective centre migrates from the northern hemisphere to the southern hemisphere and shifts eastward at the same time.

The interannual variations are largely related to the ENSO events. After removing annual variations, Heddinghaus and Krueger (1981) noted that the first eigenvector of OLR data exhibited a major anomaly centre southeastward from the central equatorial Pacific. It is located just northeast of the SPCZ and to a large extent it represents fluctuations in the position of this major cloud band. The time series associated with this pattern has been found to closely parallel Southern Oscillation Index (SOI) which is derived from the Easter Island / Darwin pressure difference anomaly (Quinn and Burt, 1972). It has also been found that convection centres, usually in the Indonesian maritime continent in non-ENSO years, move to the mid-Pacific region during the ENSO year (Liebmann and Hartmann, 1982; Rasmusson and Carpenter, 1982; Gill and Rasmusson, 1983; Meehl, 1987). This eastward shift can be seen clearly in a schematic diagram of the zonal circulations along the equator during ENSO and non-ENSO periods (Figure 2.3).

Large-scale convection possesses a striking intraseasonal oscillation. Yasunari (1980, 1981) was among the first to reveal such features in the Indian Monsoon region convective activity. There are some comprehensive reviews on this subject by Knutson *et al.* (1986) and Knutson and Weickmann (1987). A few important characteristics of the oscillation extracted from their summaries, together with some more recent studies, are listed below:

- The oscillation is characterized by global-scale tropical wind and convection anomalies, including a modulation of the northern hemisphere and southern hemisphere summer monsoon activity;

- The oscillation is not strictly periodic, but has a preferred time scale of about 30 to 60 days;

- The eastward propagation of 30-60 day OLR anomalies has been noted by Weickmann (1983), Weickmann *et al.* (1985), Knutson *et al.* (1986), Lau and Chan (1985; 1986a,b), Murakami *et al.* (1986) and others. The characteristic propagation speed

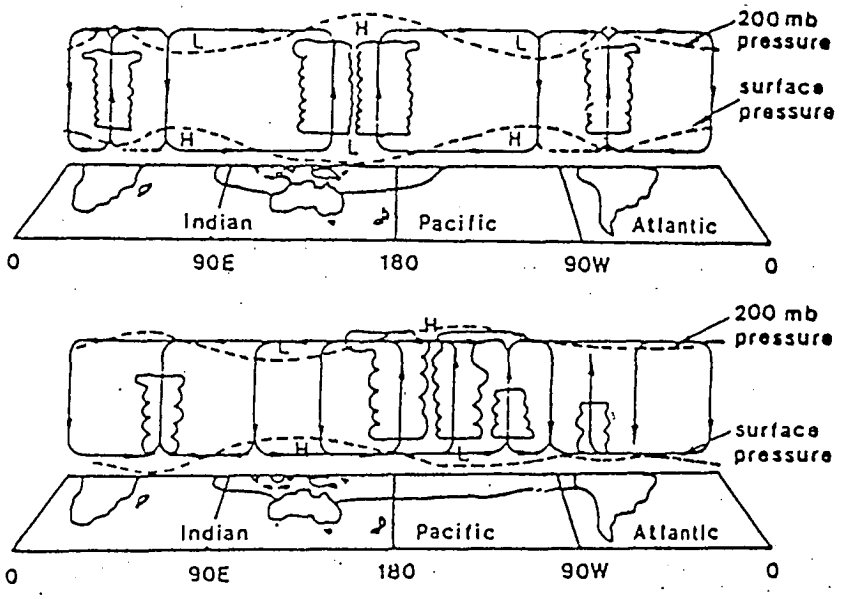

Figure 2.3 Schematic diagram of the zonal circulations ("Walker Circulation") along the equator during ENSO and non-ENSO periods (after Webster, 1983, Webster and Chang, 1987)

for this phenomenon is 3-6 ms^{-1} and mainly occurs over the tropical Indian and western Pacific areas. The circulation, however, noted by Lorenc (1984) and Krishnamurti *et al.* (1985), propagates around the entire globe with propagation speeds of 10 ms^{-1};

• The 30-60 day oscillation occurs throughout the seasonal cycle with no systematic seasonal variation in amplitude or periodicity (Anderson *et al.*, 1984), but does show seasonality in the locations of maximum OLR variability and in the extra-tropical response. The largest OLR anomalies, located around 150°E in the western Pacific, exhibit a slightly slower eastward progression, particularly during May-October (Knutson and Weickmann 1987);

• Some evidence exists for an association between tropical convection fluctuations and mid-latitude circulation anomalies on a 30-60 day time scale (Weickmann *et al.*, 1985; Lau and Phillips, 1986);

• Oscillations of a similar time scale have been observed in the tropical oceans. For example, Mysak and Mertz (1984) reported 40-60 day oscillations of longshore currents and ocean temperatures in the western Indian Ocean;

• Intraseasonal (25-40 days) atmospheric oscillations, characterized by eastward propagation of large-scale tropical wind anomalies, have been found in general circulation models (GCMs) by Lau and Lau (1986) and Hayashi and Sumi (1986). Goswami and Shukla (1984) have found 20-40 day oscillations in a zonally symmetric GCM.

The variability of OLR at shorter time scales has also been studied. Murakami (1980a) applied the EOF analysis to the OLR data during the winter months in 1974-77 over the monsoon region from 50°E to the dateline and from 30°N to 20°S. He presented the composite pattern of the first 10 eigenvectors after the data was passed through a 15-30 day filter. He noted that distinct southward propagation of OLR perturbations along 100-115°E from about 25°N to 20°S. In a similar study (1980b), he also examined the

behaviour of OLR at the time scale of 4-6 days. Further work (Murakami, 1983) also details the diurnal variation of OLR over the western Pacific and Southeast Asia during the northern winter (December 1978 - January 1979) and summer (July-August 1979).

2.4 Large-scale convection and SST

There is considerable observational evidence (Cornejo-Garrdio and Stone, 1977; Ramage and Hori, 1981; Rasmusson and Carpenter, 1982; Horel, 1982; Liebmann and Hartmann, 1982) which suggests that convection anomalies in the tropics are closely associated with anomalies in sea surface temperature.

Philander and Rasmusson (1985) showed a climatology of SST from the Indian Ocean to the mid Pacific in March and September. They compared this climatology with similar data for OLR. Their results showed that seasonal migration of the atmospheric convective zones are associated with seasonal changes in the SST. The isoline of 240 Wm^{-2} OLR, which delineates the region of most intense convection, is usually enclosed by the 27.5°C isotherm through the year. These warm surface waters are predominantly found in the western equatorial Pacific and off the coast of Central America (Philander and Rasmusson, 1985).

Although the warmest ocean area in the western central Pacific exhibits very little seasonal variation, it is very sensitive to ENSO, displaying large variability during such episodes. The eastward migration of this warmest area (28.5°C) is a common feature in the developing stage of ENSO events since 1940 (Fu *et al.*, 1986). The extent of its eastward migration varies from event to event and represents a large contribution to the interannual variability of zonal SST distribution in the equatorial Pacific. In terms of spatial extent, it is comparable to the behaviour of the equatorial cold tongue in the east. The spread of the warmest water constitutes an active factor in the development of ENSO events.

The relationship between SST and convection has been studied widely over a number of years. Researchers assumed a direct link between warm water and convection since elevated SSTs can increase surface evaporation, and in turn convection (Bjerknes, 1969; Rowntree, 1972; Julian and Chervin, 1978). The comparison of SST and large-scale convection shows that these two variables are closely related. Gill and Rasmusson (1983) show longitude-time plots along the Equator of anomalies in monthly mean OLR and SST (4°S-4°N) during 1982-83. They suggest that the warm pool over 29°C (which is normally located over the western Pacific) migrated eastwards, followed by the zone of anomalous convection.

Recent studies show that SST and convection are not so well correlated. Gadgil *et al.* (1984) found that over the Indian Ocean on a monthly basis the degree of cloudiness correlates well with SST for the relatively colder ocean, but when SST is maintained above 28°C it ceases to be an important factor in determining the variability of cloudiness. Over the major regions of convection east of 70°E, the observed cloudiness can not be correlated with variations in SST.

Graham and Barnett (1987) confirmed and extended the above results over broad regions of the Indian and Pacific oceans. SST's in excess of 27.5°C are required for large-scale deep convection to occur (Figure 2.4). However, SSTs above that temperature are not sufficient condition for convection to develop and further increases in SST appear to have little effect on the intensity of convection. This problem will be studied in more detail in Chapter 6, which addresses other conditions related to convection over warm ocean waters.

2.5 Large-scale convection and the wind field

The wind field over the tropical Pacific has been found to be closely associated with large-scale convection on a wide spectrum of time scales. The large-scale convection in the tropical area develops mainly in the ITCZ and SPCZ, which in turn are closely linked with the trades and monsoons.

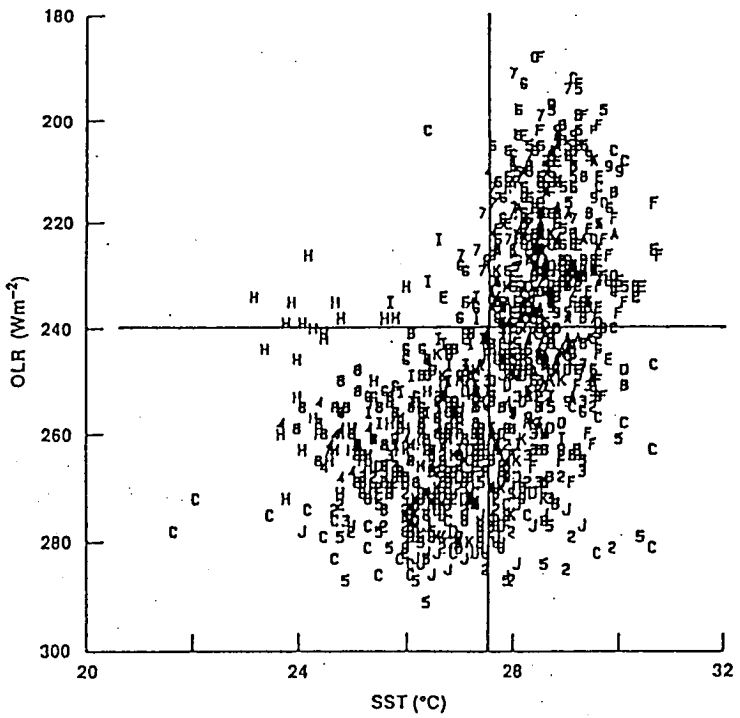

Figure 2.4 Scatter plot of SST and OLR. OLR values decrease (convection increases) toward the top; SSTs are warmer to the right. Note the break at SSTs of ~27.5°C (vertical line) that is associated with OLR values of ~240 Wm^{-2} (horizontal line), a threshold often associated with deep convection. Also note that there is little relation between SSTs and OLR when SSTs exceed 27.5°C. These are monthly data for 1974 to 1979. Separate symbols are used to represent different locations (after Graham and Barnett, 1987).

The annual cycle of the wind field has been extensively studied. Brooks and Brady (1921) were among the the first to study the annual variation of pressure and wind in the central equatorial Pacific. Crowe (1951) showed that the strength of the southeast and northeast trades over the Pacific were inversely related, i.e. during January the northeast trades are stronger than the annual mean and the southeast trades are weaker, while the opposite conditions prevail during July.

This relationship has been shown to exist at the interannual time scale. Tropical wind observations from merchant ships compiled by Wyrtki and Meyers (1975a, 1975b, 1976) have been used in earlier studies to demonstrate the existence of interannual variability of the tropical wind field. Wyrtki (1975) found that strong easterlies in the central Pacific lasting a year or more precede the occurrence of El Nino, and decrease afterwards. The existence of large-scale spatial coherence in wind field variations throughout the tropical Pacific was demonstrated by Barnett (1977) using EOF analysis. Reiter (1978) showed that the meridional wind component of the trades in both hemispheres is strengthened during El Nino and is associated with increased rainfall near the ITCZ. Pazan and Meyers (1982) used the same data to study the relationship between the wind field and the Southern Oscillation Index. They found that when the SOI is low the largest anomalies are in the westerlies on the equator and in the subtropics west of the dateline. Goldenberg and O'Brien (1981) subjectively re-analysed the data set and used them to detail the distributions of frequency and zonal wavenumber spectra from 29°S - 29°N. They found three areas of high interannual variability: a band stretching from Chile to Australia (where the Southern Oscillation Index is measured), a region over the central equatorial Pacific and a region poleward of 21°N in the central Pacific.

Wind data from tropical Pacific islands have also been used to study the interannual variation of the wind field and its relationship to ENSO events. Harrison and Gutzler (1986) found that westerly wind anomalies associated with warm central Pacific sea surface temperature are stronger at 850 mb than at the surface. By constructing an

ENSO event composite, Harrison (1987) pointed out that the westerly anomalies near the equator during ENSO years first appeared west of the dateline in the northern summer and autumn. An eastward spread across the dateline follows later on in the year. The anomalies then suddenly jumped southward to 5°S in January to February where they were greatly reduced two months later.

Studies of the Pacific wind field and ENSO have tended to stop at 120°E, the western limit of the Wyrtki and Meyers (1976) data set. The wind system has also been studied over tropical areas of the Indian Ocean. Hastenrath and Lamb (1979) have developed climatological wind statistics over the Indian Ocean. Hellerman and Rosenstein (1983) used all the available surface observations collected by the National Climatic Center to calculate normals and standard errors of the global monthly wind stress. These data were then used as boundary conditions for models of the ocean circulation. At almost the same time, Barnett (1983, 1984a, b, c) used complex EOF analysis to show that anomalies related to ENSO in zonal wind, sea level pressure and equatorial precipitation originate in the Indian Ocean and propagate eastward into the Pacific. He suggested that the mechanism that drives this propagation appears to be latent heat release associated with precipitation anomalies that are phase-locked to and propagate with surface wind anomalies.

Since large-scale convection occurs in the whole troposphere, it is important to study the upper level as well as the near-surface fields. While near-surface wind fields are important for air-sea interaction studies, other data for upper tropospheric processes has also been collected. Krueger and Gray (1969) and Krueger and Winston (1974) contrasted the tropical circulation for northern hemisphere winters during ENSO and non-ENSO periods, and found that zonal wind anomalies in the upper and lower troposphere over the central Pacific had opposing signs. By merging wind observations from aircraft, radiowinds and radarwinds, Sadler (1975) created an excellent atlas of mean monthly wind at the 200 mb and 300 mb levels. Sadler (1980) showed substantial changes in the 200 mb zonal and meridional winds when comparing

two Januaries that had opposite phase in the Southern Oscillation. Horel and Wallace (1981) found above normal 200 mb geopotential heights in the tropics during northern hemisphere winters following El Nino events. Hastenrath and Wu (1982) confirmed the negative correlation between low-frequency fluctuations of upper and lower tropospheric winds. Yasunari (1985) documented the existence of eastward-propagating signals in the filtered near-equatorial 200 mb wind field.

Later studies documented the eastward propagating character in the upper-level wind field. Gill and Rasmusson (1983) concluded that, during the 1982-83 ENSO event, the easterly wind anomaly at 200 mb and the westerly wind anomaly at 850 mb agreed well with the development of the OLR anomaly along equatorial areas. They ran a simple model which showed that anomalous heating, located where the large OLR anomalies were found, produced strong westerly anomalies. In turn the westerly anomalies brought in more moisture to fuel the heating. Gutzler and Harrison (1987) examined the longitude-height-time evolution of seasonally averaged wind anomalies by using tropical island data. They found that wind anomalies are negatively correlated in the upper and lower troposphere, and are out of phase between the southern tip of India and the central Pacific.

The intraseasonal oscillation of wind along tropical areas was first described by Madden and Julian (1971, 1972). They presented evidence for a statistically significant zonal wind oscillation in the tropics and described some of the features of the oscillation, which they noted had a quasi-periodic nature with a time scale of 40-50 days. They described the phenomenon as a gobal-scale zonally oriented circulation cell that propagated eastward around the globe. They noted that the oscillation primarily involved the zonal wind with upper and lower tropospheric wind anomalies being out of phase with each other. Yasunari (1980, 1981) found evidence for a 40-day fluctuation in the Indian Monsoon convective activity during the northern hemisphere summer. The anomalies generally propagate northward from the equator to the northern extent of the monsoon region. He concluded that the oscillations were related

to the active-break cycles in the Indian monsoon. Julian and Madden (1981) presented further evidence for the role of convection in the oscillation and agreed with Yasunari's conclusion that the northward-propagating monsoon oscillations were part of the same phenomenon as the eastward-propagating tropical oscillations.

Many studies regarding intraseasonal oscillations done in the 1980s, used OLR data. Knutson *et al.* (1986) found that intraseasonal OLR fluctuations had their greatest amplitude in the Indian Monsoon region and north of the equator in the western tropical Pacific. These two regions have out-of-phase fluctuations and appear to be linked by OLR anomalies propagating eastward (at 3-6 ms^{-1}) along the equator between 50° and 160°E.

The even shorter time scale of westerly bursts has attracted attention in recent years. Westerly bursts are most common during the Northwest Monsoon. They generally last 3-5 days, though week-long events are not uncommon (Keen, 1984; 1987). Westerlies are convergent along the equator owing to the Coriolis effect and thus represent a dynamical forcing for convection. Westerlies also contribute to moisture convergence by advection of moist air from the west (Steiner and Khalsa, 1987). Strong convergence in the lower troposphere occurs at the eastern boundary of a westerly burst, and deep convection is often greatly enhanced (Steiner, 1987). Since considerable interannual variability of the westerly burst is observed, with its greatest frequency during the early stages of ENSO events, it has been suggested that the westerly burst phenomenon may play an important role in the onset phase of at least some ENSO events (Steiner and Khalsa, 1987).

2.6 Large-scale convection and water vapour convergence

The importance of water vapour convergence did not attract much attention until Cornejo-Garrido and Stone (1977) pointed out that the region of enhanced condensation is associated with a region of moisture convergence rather than with a region of enhanced evaporation. Ramage (1977) further demonstrated the important

contribution of moisture convergence to the overall tropical heat balance. This idea has been tested further in models by Zebiak (1986) and Zebiak and Cane (1987) which resulted in a possible prediction of ENSO. Garcia *et al.* (1986) found that a moist unstable lower troposphere in the eastern Pacific had developed in advance of deep convection during the 1982-1983 ENSO.

Knowledge about the distribution of water vapour over the tropical areas is still very poor because of the limited observations or short period of observations. The development of recent data acquisition has gone far to remedy the situation. The TIROS-N Operational Vertical Sounder (TOVS) unit, aboard the NOAA series of polar orbiting satellites, provides moisture and temperature profiles of the atmosphere. Processed data are available from the National Environmental Satellite Data and Information Service (NESDIS) using methods described by Smith and Woolf (1976), Smith *et al.* (1979) and Hayden *et al.* (1981). Until recently, TOVS data had been mainly used in operational analyses. However, Cadet (1983) and Garcia *et al.* (1986) have begun to demonstrate the value of this data source in climate research. Using HRC as a proxy for convection (see Section 2.2), Steiner (1985, 1987) and Steiner and Khalsa (1987) analyse the relationship between this variable and low-level moisture (from TOVS) and SST in the tropical Pacific. They found that although the large-scale features of SST, low level precipitable water (LLPW), and HRC agreed well in each month, the maxima and minima of the three variables were found to be offset in both time and space. In the eastern equatorial Pacific, seasonally occurring minima of SST and LLPW were often offset by as much as 20° to 30° longitude, with LLPW minima to the west of those of SST, while increases of SST and LLPW were found to precede rises of HRC by 1 or more months. These discrepancies implied that other factors have to be considered to explain the relationship between convection process and surface heating.

2.7 Numerical models

Along with statistical studies, numerical models for ENSO have also been developed, both from atmospheric and oceanic prospectives. It was natural for meteorologists to consider the Southern Oscillation as a response to ocean conditions, and for oceanographers to consider El Nino as a response to atmospheric conditions. From the atmospheric side, a few researchers using both complex and simple models pointed to the importance of tropical Pacific SST anomalies in producing observed atmospheric anomalies during ENSO (e.g. Rowntree, 1972; Wells, 1979; Webster, 1981; Keshavamurty, 1983; Shukla and Wallace, 1983; Zebiak, 1982, 1986).

Oceanographic studies show that the observed tropical Pacific SST and sea level anomalies during ENSO result primarily from the influence of surface wind stress anomalies (e.g. Busalacchi and O'Brien, 1981; Cane, 1984; Philander and Siegel, 1985).

With coupled atmosphere-ocean models, McWilliams and Gent (1978) and Lau (1981) used highly idealized models and demonstrated the possibility of frequency variability. McCreary (1983) and McCreary and Anderson (1984) derived the interannual variability by using models with explicit ocean dynamics, but a highly idealized atmosphere. Philander *et al.* (1984) developed a model with explicit linear dynamics for both the atmosphere and ocean. They found a coupled instability which led to the growth of large-scale atmospheric and oceanic anomalies. The linearization of the model does not permit equilibration and the subsequent decay of anomalies. That is, no ENSO cycle is reproduced. Zebiak and Cane (1987) designed an atmospheric and oceanic model in which the atmosphere model is a steady-state, linear shallow-water equations on an equatorial beta plane; while the ocean model is linear, and describes the low-frequency motion of a two-layer ocean in which the lower (sub-thermocline) layer is motionless. The model reproduces the major features of ENSO.

After some understanding of the statistical and dynamical features of ENSO, it is natural to try to develop techniques to predict ENSO. From the purely dynamical approach, Cane *et al.* (1986) claimed from their numerical modeling results "that El Nino is generally predictable one or two years ahead". On the other hand, from traditional statistical forecasting techniques, Barnett (1984a) claimed that the sea surface temperature anomalies during 1982-83 in the equatorial Pacific could have been predicted 4-5 months in advance. Fraedrich (1988) went further to discuss the predictability time scales of ENSO events by analysing annual time series of ENSO. He concludes that e-folding predictability time scales up to 1.5 years would indicate that at least a skillful nowcasting of ENSO may be possible.

2.8 Discussions

From the above review, there are various topics which need further attention and which are appropriate to the present study. They are as follows:

a) Seasonal variations

The annual cycle of various atmospheric and oceanic features has long been studied since they are usually the most evident and most important to human life. Detailed studies of these annual cycles revealed various mechanisms behind the variations. For example, during earlier periods of this century, annual cycles in temperature, rainfall and pressure at various stations around the globe were studied in order to classify regional climates (e.g., Koppen, 1923; Kendrew, 1937; Trewartha, 1937). Such classification schemes have been very successful in identifying regions where the physical mechanisms responsible for the annual cycle may be similar (Horel, 1982). For example, monsoonal climate denotes a seasonal response to an air-sea interaction which is quite unique to a particular region of the world.

Studies of annual cycles have also served as a background to explain interannual variations. This approach was first used by Walker (1923, 1924). Bjerknes (1969)

introduced the term "Walker Circulation" to describe large-scale zonal circulation between the western and eastern tropical Pacific. Some recent studies have provided more detailed information (Heddinghaus and Krueger, 1981; Horel, 1982; Meehl, 1987). The higher resolution data used in this study (see Chapter 3), will allow the seasonal variations of SST, winds, OLR and precipitable water vapour to be studied, and provide a more complete description of these fields. Relevant climatologies will be compared with the three years long (1984-86) data set developed in this study.

b) Interannual variations

Studies of interannual variations of the atmosphere and the ocean have become increasingly popular in the last two decades. This is mainly due to two reasons. Firstly, large quantities of atmospheric and oceanic data have become available from satellites and specialized observation networks (such as expendable bathythermographs (XBTs)). Increasingly more accurate observations at higher spatial and temporal resolution can be provided by satellite retrieval techniques (such as NOAA Advanced Very High Resolution Radiometer (AVHRR) and TOVS Sounding Products). Secondly, since the 1982/83 ENSO event, several international research programs, such as TOGA, TOGA-COARE and World Ocean Circulation Experiment (WOCE), have been organized to coordinate research from different countries. By a process of coordination and information exchange, broad knowledge has been gained about the coupled atmospheric-oceanic system. Their results have been continuously incorporated into various numerical models to reproduce some important features for forecasting.

Studies of interannual variations conducted in the past decade are largely related to ENSO events. Bjerknes (1966, 1969, 1972) first linked El Nino to the Southern Oscillation processes. Wyrtki (1974) pointed out the possible mechanism of El Nino and Southern Oscillation through wind stress and mass transport (reflected in the variation of sea level). By surveying the literature from the 1920s to 1970s, Julian and

Chervin (1978) examined various phenomena related to ENSO events. Using SST, wind, precipitation and OLR data from past ENSO events, Rasmusson and Carpenter (1982) presented a composite description of the above phenomenon. Since the time of this publication two ENSO events have occurred (1982/83 and 1986/87) which have been closely monitored. It is therefore worthwhile to examine if those precursors that signalled past ENSO events also appear in the data sets used in this study, from 1984 to 1986.

c) Intraseasonal variations

There have been many studies in the last decades of the intraseasonal variations of wind and convection. Madden and Julian (1971, 1972) were the first to document the existence of eastward propagating zonal circulation cells in the tropics with periods between 40-70 days. Knutson *et al.* (1986) and Knutson and Weickmann (1987) have provided very good reviews of the intraseasonal variation of convection (OLR). It is of interest in this study to observe if the main intraseasonal features can be replicated here using the data sets of wind and SST.

d) SST and convection

The relationship of SST and convection has long been regarded as important in understanding the coupled atmosphere and ocean system. The warm sea surface provides a huge energy reservoir through vaporization, while convection provides a very effective mechanism to release the latent energy trapped in the air mass. Viewed from wide range of SST variability, it has been assumed that the SST and OLR correlate closely. Earlier studies assumed a direct link between warm surface water and convection by which an elevated SST can increase surface evaporation, and in turn, convection (Bjerknes, 1969; Rowntree, 1972; Julian and Chervin, 1978). Comparison of SST and large-scale convection shows a tight connection between these two variables. Gill and Rasmusson (1983) shows longitude-time plots along the Equator of monthly mean values of OLR anomaly and SST (4°S-4°N) during 1982-83. They

suggest that the warm pool over 29°C (which is normally located over the western Pacific) migrated eastwards and the zone of anomalous convection followed it.

More recent studies suggest that SST and convection are not so directly correlated (Gadgil *et al.*, 1984; Graham and Barnett, 1987). Over the Indian Ocean on a monthly basis the degree of cloudiness correlates well with SST for the relatively colder ocean, but when SST is maintained above 27.5-28°C it ceases to be an important factor in determining the variability of cloudiness. Since the SSTs over the major regions of convection east of 70°E in the tropics are higher than this critical temperature, the observed cloudiness does not correlate well with variations in SST.

From the above studies it seems that there are still some problems which remain unsolved. Why does the critical temperature lie at about 27.5-28°C? Why are SST and convection not well correlated above this threshold temperature? What is the relationship between SST and convection above this threshold temperature? This study will attempt to answer some of these questions.

e) Upper level divergence and convection

It has long been assumed that the upper level divergence and convection have a very close relationship. However, partly due to the accuacy of divergence data, detailed relationship between these two fields is still not well documented. Regarding the spatial structure of convection, it is worthwhile to examine the spatial scales associated with regions of convergence and divergence. From general circulation theory, at the global scale the Hadley circulation describes a convection process originating at the tropics and subsiding in the subtropical areas. However the existence of dry/wet seasons in the northern/southern hemisphere at certain times of the year in the study region suggests that the global model of convection may be too simple. The data sets used in this study (OLR, wind and SST) provide an opportunity to investigate their spatial relationship in more detail.

f) Precipitable water and convection

The importance of water vapour convergence was relised only after Cornejo-Garrido and Stone (1977) pointed out that the region of enhanced condensation was associated with a region of moisture convergence rather than with a region of enhanced evaporation. Ramage (1977) further demonstrated the important contribution of moisture convergence to the overall tropical heat balance. This idea has been tested further in models by Zebiak (1986) and Zebiak and Cane (1987) which resulted in a possible prediction of ENSO. Garcia *et al.* (1986) found that a moist unstable lower troposphere in the eastern Pacific had developed in advance of deep convection during the 1982-1983 ENSO. By using the precipitable water data from the NOAA TOVS Sounding product, Steiner (1985, 1987), Steiner and Khalsa (1987) used TOVS data incorporated with SST, HRC data, to analyse the relationship between convection in the tropical Pacific with SST and low-level moisture. They found that the maxima and minima of the three variables were offset in both time and space, demonstrating that high SST does not always result in enhanced local convection. In the eastern equatorial Pacific, increases of SST and low level precipitable water (LLPW) were found to precede rises of HRC by 1 or more months. However, knowledge about the distribution of water vapour over the tropical areas is still very poor because of the quality of the satellite retrieval process and the need to provide high frequency data. It is therefore interesting to further examine the spatial and temporal features of the precipitable water and its relationship to the distribution of convective centres.

Chapter 3. Data and Methodology

3.1 Introduction

This chapter describes the main data sets used in this study, SST, wind and OLR, as well as precipitable water data from TOVS. Their sources and methods of acquisition are described. Some validation is done on SST and wind fields in order to assess their suitability for analysis as described in later chapters. The SST, wind, OLR and TOVS precipitable water data sets are discussed in sections 3.2, 3.3, 3.4 and 3.5 respectively.

The analysis techniques used in this study follow a conventional approach. Harmonic analysis, used to describe the annual variation of the above parameters, is discussed in Section 3.6. A high-pass filtering technique, outlined in Section 3.7, is applied to the wind data to study their intraseasonal variations. Finally, empirical orthogonal function (EOF) analysis, used in the description of SST variation is presented in Section 3.7.

3.2 Sea Surface Temperature (SST)

3.2.1 Data Description

3.2.1.1 Multichannel Sea Surface Temperature (MCSST)

The common *in situ* SST observations in the open ocean presently available from World Weather Watch are mainly confined to shipping routes. Sadler *et al.* (1987a,b) and Reynolds (1988) used all the available data to calculate the average monthly SST field over the global ocean from 1900-1979. Data coverage in portions of the seas north of Australia, the central Pacific and the Southern Ocean is not entirely satisfactory for monitoring global air/sea interactions. On the other hand, satellite-observed SST data have much better spatial and temporal resolution than World Weather Watch data. The technique has been greatly developed and improved since the launching of NOAA

7 in 1981, which carried the AVHRR. A five-channel, three-window AVHRR is now being used to calculate the multichannel sea-surface temperature (MCSST) (McClain *et al.*, 1985), which is an operational daily product of the global SST field on a 1° latitude/longitude grid. The MCSST data permit studies on time scales smaller than one month, as required for this study.

At present, MCSST is being used to produce global monthly-averaged SST (Reynolds,1988) and to support other climate studies (Legeckis, 1986; Strong, 1986). Validation of MCSST against *in situ* temperature measurements has been mainly restricted to monthly averages (McClain *et al.*, 1985; Reynolds, 1988) and therefore it is worthwhile to examine the validation of MCSST using additional *in situ* data on a short time-scale, especially over the western Pacific.

The MCSST data used in this study are daily, global analyses from 70°S to 70°N on a 1° latitude/longitude grid. The calculation of these fields has been reported in detail in several papers (Strong and McClain, 1984; McClain *et al.*, 1985). The processing of the data before it was acquired for this study is briefly summarized below:

a) Data retrieval: The AVHRRs deliver 1.1 km (at nadir) resolution measurements in four or five channels (depending on the satellite): 0.58-0.68, 0.725-1.10, 3.55-3.93, and 10.3-11.3 μm and an additional 11.5-12.5 μm channel for the five channel AVHRRs. The recorded onboard data with global area coverage (GAC) is transmitted to ground stations twice daily at a nominal resolution of 4 km (four of every five samples along the scan line are used to to compute one average value, and data from only every third scan line are processed). The data set consists of the raw sensor data and quality control information, calibration coefficients and earth positions.

b) Quality Control: A quality control procedure is used to eliminate pixels that are contaminated by cloud cover. Every 6 hours, all MCSST observations are organized into basic units of 50 km × 50 km. A series of cloud filtering techniques are applied and cloud contaminated pixels are removed. Each unit is then assigned a particular SST value using regression formulae relating channel grey level values to SST (Strong and

McClain, 1984; McClain *et al.*, 1985). Daily MCSST values at grid points of 1° longitude × 1° latitude are calculated from the MCSST values on basic units through objective analysis. Other operational products, such as isotherm contour charts, archive tapes, and teletype transmissions on the Global Telecommunications System, are produced regularly from the MCSST fields.

For this study, the daily MCSSTs were filtered by a 5 day running average and subsampled every second day.

3.2.1.2. Ground-truth data description

Three sources of ground-truth data, mostly from the western equatorial Pacific, were available for the present study:

a) Mooring data: A moored surface buoy was maintained on the Equator at 150°E during the Western Equatorial Pacific Ocean Circulation Study (WEPOCS) conducted from June 1985 to February 1986 (Lindstrom *et al.*, 1987). Near-surface temperature was measured at 2 m depth by the weather station for a period of 10 weeks, and at 15-m depth by an Aanderaa current meter for six months. The SST measurements at 2-m were made every 2 hours, and at 15 m every 50 minutes. These data were then averaged to get daily values for this study.

b) Research Vessels. The SST at approximately 3 m depth was recorded with thermosalinographs on the research vessels *Franklin* and *Moana Wave* during three cruises in 1986. SST was measured every minute. Observations in a day within a 1° × 1° bin were averaged to get a daily gridded value.

c) Expendable bathythermograph (XBT) temperatures: Two XBT data sets were used in this comparison. The first was composed of individual transects along shipping routes in the seas north of Australia (see Figure 3.1). At 4 to 6 hour intervals an XBT cast is taken and each route is repeated every 2-4 weeks. The temperature recorded at 5 m was used since there are errors associated with the measurement at the surface (Roemmich and Cornuelle, 1987). The final step involves grouping all the SST data

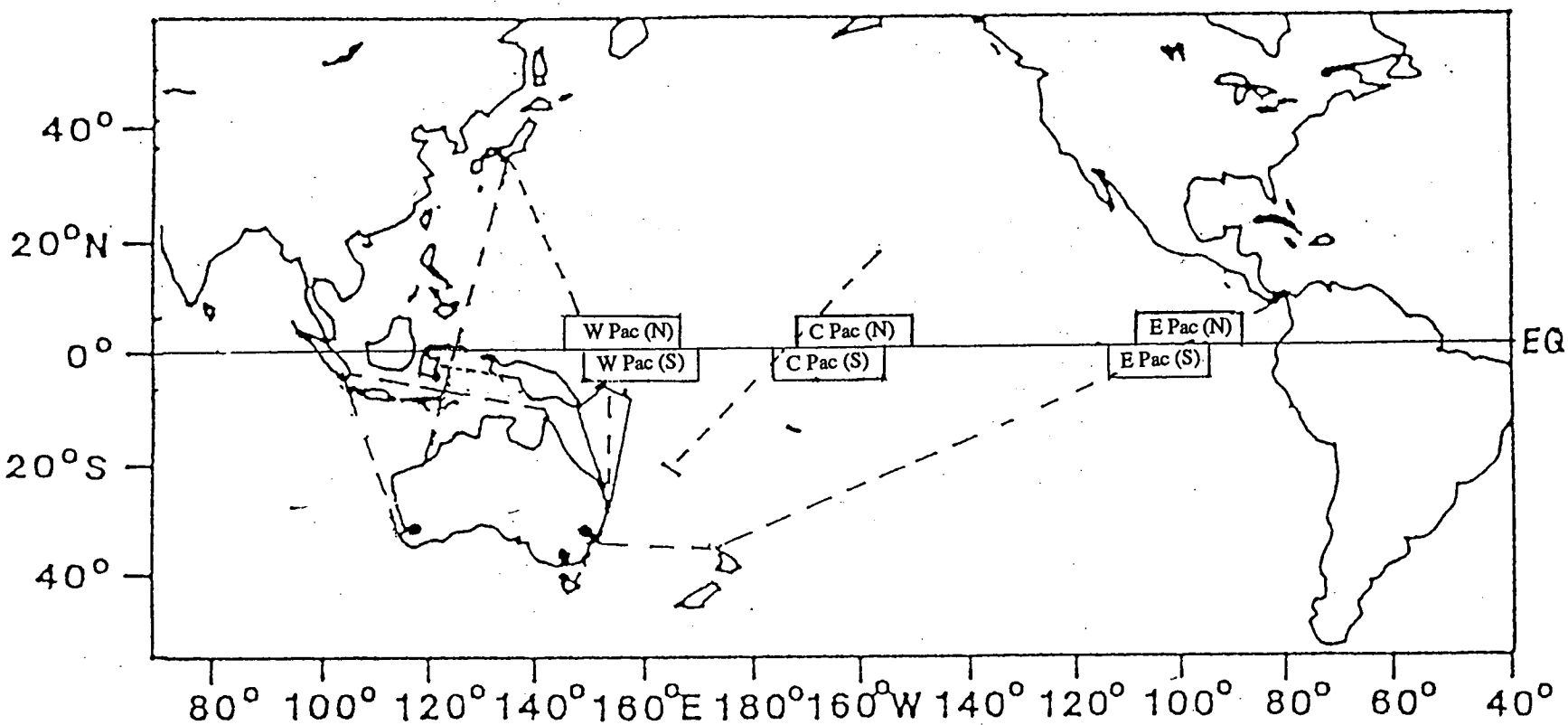

Figure 3.1 XBT ship of opportunity lines selected for validation of MCSST

into 1° latitude × 1° longitude squares to obtain a daily value. Typically, it took the ship between 3 to 4 hours to sail through one of the 1° squares so that in this comparisonindividual XBT drops are being compared to the gridded MCSST values.

The second data set comprised transects located in the western, central and eastern Pacific. The XBT data was averaged in large areas (Figure 3.1). Typically each area was criss-crossed by transects, and each transect was repeated 18 times a year. The monthly-averaged temperature at 5 m depth was calculated in the areas 0-6°N and 0-6°S near 160°E, 165°W and 100°W, during 1979-1984 (Figure 3.1).

3.2.2. Comparison

3.2.2.1. Comparison of daily averages

The daily-averaged SST from the mooring and research vessels are compared to MCSST in Table 3.1, which also gives the location of each *in situ* measurement. The root mean square differences (RMSD) of SST to MCSST values at the nearest grid point vary from 0.54 to 0.92°C, and the biases vary from -0.54 to 0.29°C depending on location. The area-averaged MCSST in 2° latitude × 3° longitude boxes surrounding the daily SST location are also compared, giving a RMSD from 0.43 to 0.72°C, and biases from -0.48 to 0.20°C. The area-averaged RMSD are smaller than grid-point RMSD, which implies that the MCSST are more representative of an area. It should be pointed out that high correlation coefficients (0.97 and 0.98) in the Tasman Sea (Row (d) in Table 3.1) are due to a broader range of SST from 12 to 24°C (12° difference), while SSTs from other areas vary only from 25 to 31°C (6° difference). A better indication of the overall accuracy is given by the RMSD figures: there are no significant differences in RMSDs between the Tasman Sea area and other areas.

3.2.2.2. Comparison of monthly averages

Comparisons of monthly-averaged XBT SST to MCSST for five near-equatorial areas over the Pacific are presented in Table 3.2. The correlation coefficients between these two data sets in all areas are quite high, varying from 0.75 to 0.97. The biases are

Data Source	Period (yymmdd)	Grid Point Values				Area Averages			
		n	Bias	RMSD	R	n	Bias	RMSD	R
Mooring 0°, 150°E									
(a) 2 m depth	850801-851012	73	-0.54	0.72	0.49	73	-0.48	0.62	0.55
(b) 15 m depth	850802-860201	185	-0.34	0.54	0.57	185	-0.23	0.43	0.61
RV Franklin									
(c) 17°S-7°N 143°E-153°E	860107-860212	113	0.29	0.78	0.55	18	0.20	0.55	0.71
(d) 28°S-42°S 148°E-155°E	861104-861120	50	-0.19	0.87	0.97	11	-0.19	0.72	0.98
RV Moana Wave									
(e) 8°S-7°N 143°E-159°E	860112-860213	107	0.13	0.92	0.69	13	0.17	0.69	0.84

Table 3.1 Comparisons between daily-averaged MCSST and SST from mooring and research vessels. n = number of observations, Bias = mean of (MCSST - SST), RMSD = root mean square difference, R = correlation coefficient. See the text about the exact meanings of the grid point values and area averages.

Data Source	Period (yymm)	n	Bias	RMSD	R	Time Derivative	
						NSS	PSS (%)
W Pac(S)	8202-8503	38	-0.04	0.44	0.75	30	81
W Pac(N)	8202-8506	41	-0.12	0.40	0.85	30	75
C Pac(S)	8202-8412	35	-0.24	0.50	0.83	24	71
C Pac(N)	8202-8412	35	-0.35	0.55	0.89	25	74
E Pac(S)	8202-8411	34	-0.26	0.54	0.97	31	94

Table 3.2 Comparisons between monthly-averaged MCSST and XBT SST over the equatorial Pacific. W Pac(S) = 0°-6°S, 150°-170°E; W Pac(N) = 0°-6°N, 145°-165°E; C Pac(S) = 0°-6°S, 175°-155°W; C Pac(N) = 0°-6°N, 170°-150°W; E Pac(S) = 0°-6°S, 115°-95°W. NSS is the number of the same sign between time derivatives of MCSST and XBT SST. PSS is the percentage of the same sign, i.e. NSS/(n-1). Other table headings are same as Table 3.1.

between -0.04 and -0.35, and RMSD are between 0.40 and 0.55. These results are almost the same as those of Bernstein and Chelton (1985), McClain *et al.* (1985) and Reynolds (1988). As the variation of SST over the western Pacific is only about 1°C, the usefulness of MCSST over this area might seem doubtful. The time derivatives of both XBT SST and MCSST were therefore calculated (Table 3.2) to see whether MCSST can reflect relative temperature change. The results are encouraging: although the changes from month to month are small, the derivative has the same sign 71% to 94% of the time for the five areas.

To show how MCSST depicted the real variations of SST, the time series of monthly-averaged SST and MCSST in the area of 0°-6°N, 150°-170°E are presented in Figure 3.2. The two time series are consistent in both the long-term, and short-term trend (for example, the peak in October 1982). Similar results were found in the time series of other areas.

3.2.2.3. The systematic shift of bias (MCSST-SST) over the western Pacific

A temperature-dependent bias is one of most important features obtained in this MCSST-SST comparison. It can be seen clearly in a plot of individual values of *in situ* SST (x-axis) against MCSST (y-axis). Figure 3.3 shows the daily area-averaged values used in Tables 3.1, and Figure 3.4 shows the monthly values used in Table 3.2. Both figures show that under warm conditions (SST > 28.5°C), large and positive (MCSST-SST) differences tend to occur more frequently than at lower SST. In order to see this feature clearly, daily area-averaged values from data sources described in Rows (c) and (e) of Table 3.1 and daily XBT data have been combined and analysed for different temperature bands (Table 3.3). The biases (MCSST-SST) vary steadily from about 0.34 to -0.59.

There may be two explanations for this effect. Firstly, it may be caused by temperature-dependent biases in the AVHRR brightness temperature sensors (Brown *et al.*, 1985). The 11 and 12 μm detectors in the AVHRR have a non-linear response to infrared radiation. This response is measured when the instrument is on the ground,

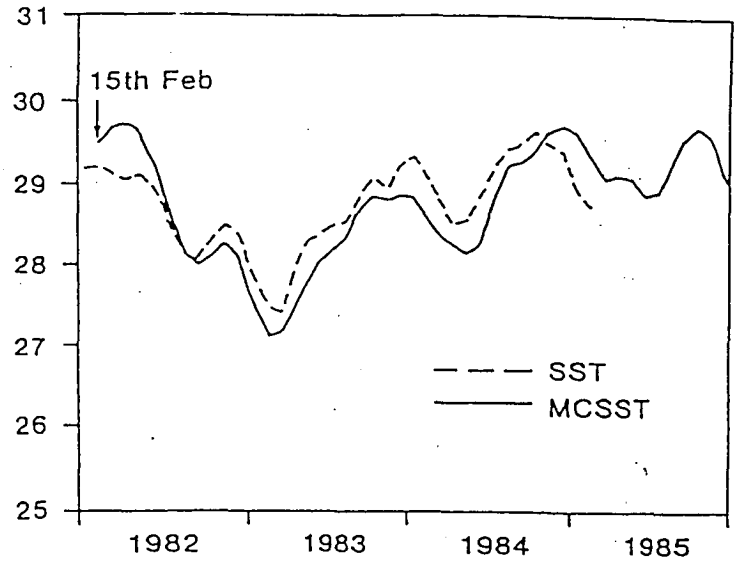

Figure 3.2 Time series of monthly MCSST (solid line) and XBT SST (dashed line) over the area of 0-6°N, 150°-170°E.

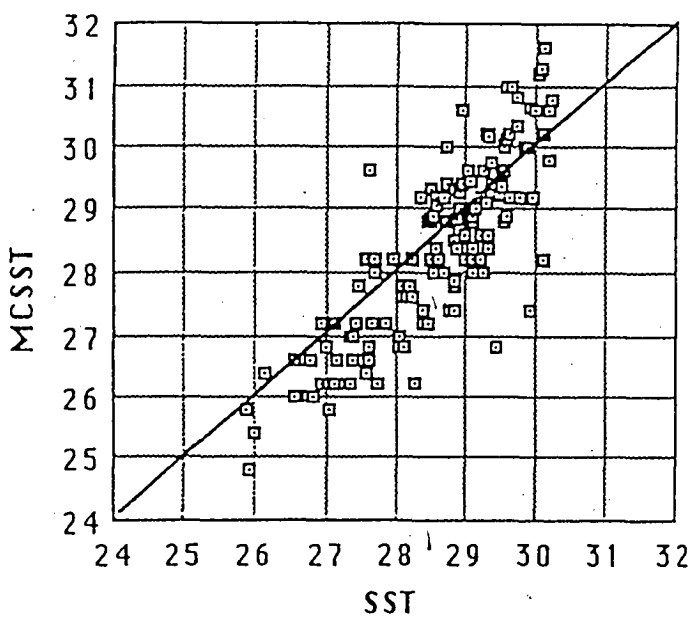

Figure 3.3 Comparison of daily MCSST to in situ SSTs measured at the moorings, research vessels and XBT transects described in Table 3.1.

Temperature Range	n	Bias	RMSD
>30	9	0.34	1.03
29 - < 30	47	-0.15	0.85
28 - < 29	47	-0.22	0.80
27 - < 28	27	-0.39	0.84
26 - < 27	9	-0.29	0.50
25 - < 26	3	-0.59	0.72

Table 3.3 Daily area-averaged values compared according to SST range. Data are from*in situ* SSTs measured at the mooring, reasearch vessels and XBT transects.

and is published by NOAA along with all the other calibration information. For a variety of reasons, mostly errors in human communication between operational groups at NOAA, this non-linearity was not taken into account until January 1985.

To test whether calibration could account for the temperature-dependent bias, the data in Table 3.3 were divided into two groups: before and after 1 January 85 (Group B-Before and Group A-After) (Table 3.4). The number of observations in Group B is too small to provide any meaningful result except for the general negative biases: MCSST underestimates the SST. For Group A, it still can be seen clearly that MCSST-SST tends to be positive at higher temperatures. Therefore, the bias at higer temperature ranges may be only partly due to the calibration problem.

A detailed check of the high SST values in Figure 3.4 suggests that the trend is more marked over the western Pacific. This raises another possibility. Over the western Pacific, around 28°C, a threshold for the development of large-scale convection is established (Gadgil *et al.*, 1984; Graham and Barnett, 1987). Under this condition, the water vapour within the atmospheric layer is very high, causing attenuation of radiation emitted by the sea surface. The regression formulae used to calculate the MCSST were not developed in this type of atmosphere and may not be accurate enough to cover this situation. Other authors have also pointed out this problem (e.g. Barton, 1985).

3.2.3. Concluding Remarks

Operational MCSST data provides regular and informative SST measurements for meteorological and oceanographic studies. The comparisons have indicated an RMS difference of about 0.7 °C for daily values and 0.5°C for monthly values. These satellite-derived SST measurements can generally pick up the real variation of SST, and thus can be used to monitor the field of sea-surface temperature. They are quite appropriate for calculating the monthly average values in combination with ship-of-opportunity data, and provide reasonably good estimates for short time-scales of weeks to months.

Period	Temperature Range	n	Bias	RMSD
Before Jan. 1, 1985	>30	2	-1.17	1.95
	29 - < 30	10	-1.09	1.85
	28 - < 29	9	-0.92	1.20
	27 - < 28	7	-0.67	0.62
	26 - < 27	3	-0.44	0.43
	25 - < 26	2	-0.85	0.78
After Jan. 1, 1985	>30	7	0.77	0.80
	29 - < 30	37	0.10	0.41
	28 - < 29	38	-0.05	0.51
	27 - < 28	20	-0.29	0.74
	26 - < 27	6	-0.22	0.16
	25 - < 26	1	-0.08	0.01
	>29	44	0.20	0.47
	27 - < 29	58	-0.13	0.59
	25 - < 27	7	-0.20	0.14

Table 3.4. Daily area-averaged values compared according to SST range before and after 1 January, 1985. Data sources and table headings are same as Table 3.3.

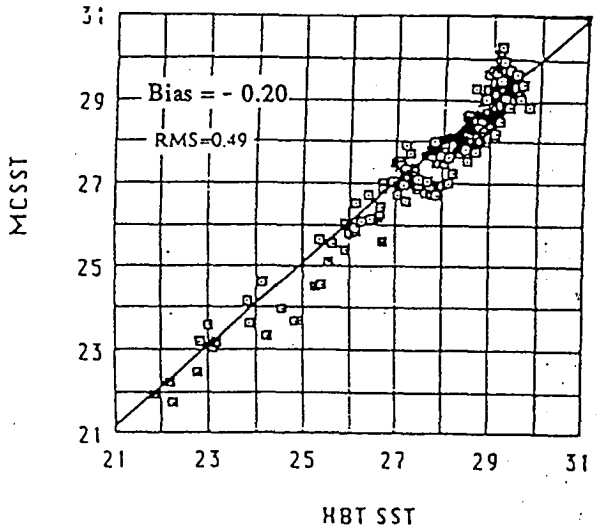

Figure 3.4 Comparison of monthly MCSST to in situ XBT SSTs over the equatorial Pacific described in Table 3.2.

In this study, 5-day running averages are calculated to remove the short term variation, and then sampled every second day. There are a total of 548 samples for the period from 1984 to 1986. The 1° Lat × 1° Long data are then averaged into 2.5° Lat × 5° Long bins. There are a total of 507 grids in the research area.

3.3 Wind Data and Validation

3.3.1 Calculation

The Australian Tropical Region Analysis (ATRA) produced by Bureau of Meteorology, Australia is a three-dimensional, univariate optimum interpolation of all available wind data (ships, aircraft, radiosondes, surface land stations, satellite-determined winds, etc.) (Davidson and McAvaney, 1981; Davidson *et al.*, 1983). Variables are analyzed at eight levels in the vertical on a twice daily basis at 11 and 23 GMT. Data for this validation were taken from the lowest level, which corresponds closely to a pressure level at 950 mb, and projected to the surface using the same boundary layer model as the optimum interpolation procedures for surface winds from ship and land stations. In the optimum interpolation technique, the first guess field for an analysis is the analysis from 12 hours earlier. The Bureau of Meteorology began to apply this analysis routinely in September 1983, and the data from January 1984 to December 1986 have been used in this report.

3.3.2 Data Validation

The advantages and disadvantages of the ATRA analysis can be partly assessed in the light of earlier studies. In many oceanographic studies the curl of wind stress is the most important parameter. A careful comparison between the ATRA analysis and that of ECMWF by Hendon (1988) showed major differences in low level wind, particularly off the west coast of Australia, where gradients in the wind field are large. Differences in the structure of derived wind divergence (both horizontally and vertically) were documented and in some cases the sign of wind vorticity (which is very

similar in pattern to wind stress curl) did not agree. It is likely the differences arise because no forecast model or initialization is used in the ATRA analysis, so that the analyzed wind fields are essentially the optionally interpolated observations. Thus, while the ECMWF analysis has the advantage of having global coverage, the ATRA analysis preserved the observed spatial structure in the wind field, and may be more useful when wind stress curl is needed. Hendon (1988) went on to show that divergence derived from the ATRA analysis is consistent with patterns of outgoing long-wave radiation, which give a qualitative assessment of the validity of gradients in the wind field analysis.

In this section, the ATRA analysis is compared with four independent wind data sets collected by the CSIRO Division of Oceanography and the University of Tasmania at marine weather stations and buoys, representing conditions on the Equator, and in tropical and extra-tropical areas.

3.3.2.1 John Brewer Reef

Wind measurements from a tower at John Brewer Reef (18°38'S, 147°4'E) provided data in a tropical area. Michael (1988) calculated the surface heat fluxes using *in situ* and satellite-derived parameters. Wind, sea surface temperature, humidity, air temperature, and various radiation parameters were measured from the 16th of June 1985 to the 7th of July 1986 (Michael and Nunez, 1991). A comparison of these data with weekly-averaged wind speed from the ATRA analysis over a 26 week period showed good agreement. A mean difference of 0.34 ms^{-1} (measured > analysis) was obtained, which was 5% of the mean speed recorded at the tower. The RMSD was 1.22 ms^{-1}, and the correlation coefficient was 0.84 (Figure 3.5). Michael (1988) reduced the 950 mb wind speed by 20% as required in a boundary layer model (Davidson and McAvaney, 1981).

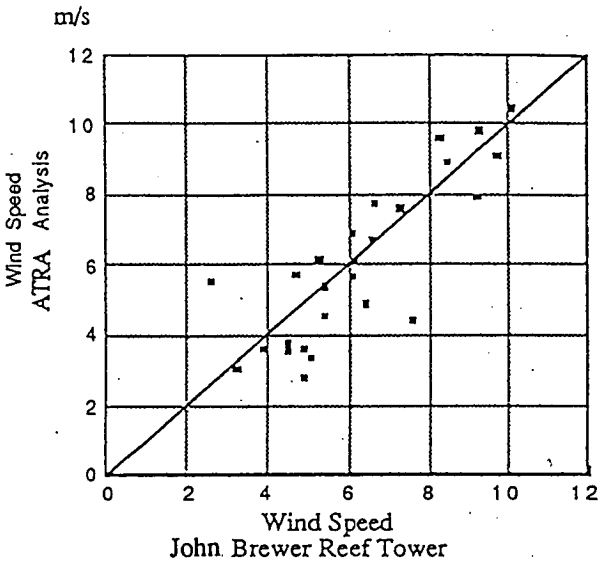

Figure 3.5 Scatter plot of wind speed of John Brewer Reef tower vs ATRA wind analysis

3.3.2.2 150°E mooring during the WEPOCS

Wind measurements on a mooring at 0°, 150°E during WEPOCS provided another independent data set (Lindstrom *et al.*, 1987). WEPOCS was organized by investigators from Australia and the United States with the objective to test a hypothetical ocean model, and to describe the effect of the monsoon on the upper ocean circulation in this region. Two research vessel expeditions were conducted in June-August 1985 (WEPOCS I) and January-February 1986 (WEPOCS II) to coincide with the peaks of the southeast and northwest monsoon (Lindstrom *et al.*, 1987). One of the main elements of the experiment involved in the deployment of current and wind moorings from July, 1985 to January, 1986 at 0°,150°E. The wind measurements were available only from 31/7/85 to 12/10/85 due to a failure of the anemometer.

The mooring wind vector averaged over five days is compared to the ATRA analysis in Figure 3.6, which shows the zonal and meridional components of the wind vectors in panels a and b, the wind speeds in c, and the difference in wind direction in panel d. A similar comparison of daily-averaged wind is also conducted. Table 3.5 gives a comparison of wind statistics: average components, speed and direction for the observing period, average difference in these parameters, root mean squared (RMS) differences and correlation coefficients for daily and five-day mean values. For daily values, the averaged wind speed difference is only 0.25 ms^{-1} (Table 3.5), or 10% of the mean speed for the observing period. The difference indicates again that the boundary layer model has not reduced the 950 mb wind enough for an estimate at the surface. The RMS difference in wind speed is 1.45 ms^{-1}. The difference in direction is near zero or small when wind speed measured at the mooring approaches 4 ms^{-1}, but can be very large when wind speed is small (Figure 3.6c and 3.6d). The time series of zonal five-day averaged wind shows excellent agreement (Figure 3.6a) as indicated by the correlation coefficient (0.95) in Table 3.5; however, meridional wind (Figure 3.6b) is not represented very well by the ATRA analysis, which registers the wrong sign on 5 of 15 occasions.

		u	v	w	Dir.
a) (0°, 150°E) 850731 ~ 851012	ATRA wind	-1.12	0.72	2.78	156.14
	Mooring	-0.99	0.54	2.52	148.42
	Bias (ATRA-mooring)	-0.14	0.19	0.25	2.79
	RMSD (daily)	1.33	1.78	1.45	60.66
	R (daily)	0.80	0.47	0.43	
	RMSD (5d mean)	0.46	1.17	0.76	24.15
	R (5d mean)	0.95	0.17	0.66	
b) (34°01'S, 114°28'E) 870211 ~ 870526	ATRA Analysis	0.68	1.36	7.19	176.30
	Mooring	0.26	2.03	5.16	185.56
	Bias (ATRA-mooring)	0.41	-0.67	2.02	-3.73
	RMSD (twice daily)	3.35	2.95	3.42	37.94
	R (twice daily)	0.87	0.83	0.55	
	RMSD (5d mean)	2.02	1.18	2.25	25.13
	R (5d mean)	0.94	0.92	0.83	
c) (29°32'S, 114°16'E) 870210 ~ 870331	ATRA Analysis	-2.18	1.69	7.33	160.01
	Mooring	-0.55	4.00	5.34	179.97
	Bias (ATRA-mooring)	-1.63	-2.32	1.98	-23.56
	RMSD (twice daily)	4.31	5.18	3.36	58.15
	R (twice daily)	0.69	0.48	0.51	
	RMSD (5d mean)	2.05	2.48	2.08	27.47
	R (5d mean)	0.96	0.87	0.95	

Table 3.5 Comparison of wind at moorings to ATRA wind analysis: zonal wind (u), meridional wind (v), wind speed (w) and direction (Dir.).

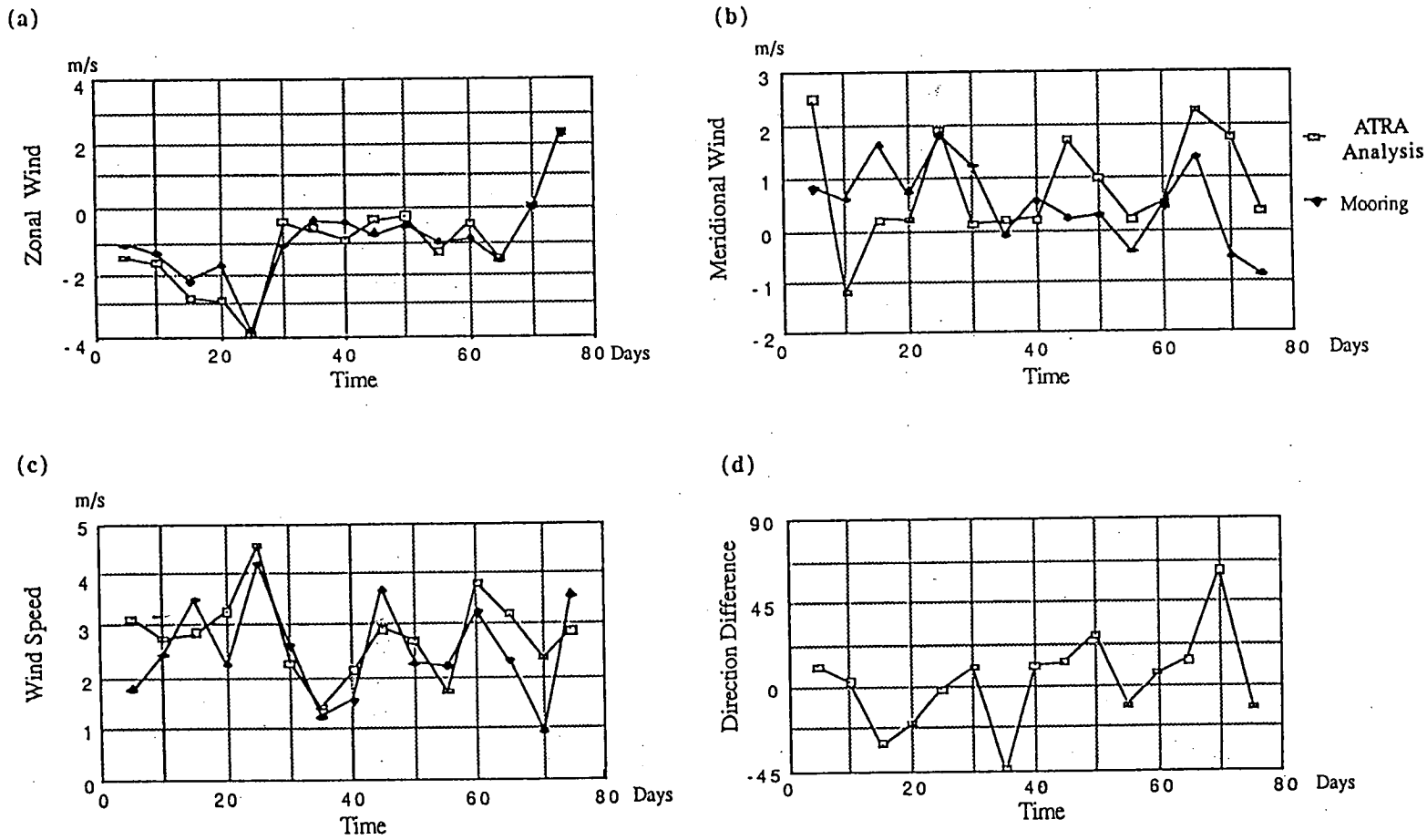

Figure 3.6 Time series of 5-day averaged wind components of mooring on Equator at 150°E and ATRA wind analysis: (a) zonal wind; (b) meridional wind; (c) wind speed; and (d) direction difference (ATRA analysis minus mooring).

3.3.2.3 Mooring off Cape Naturaliste

Wind measurement from a mooring (34°01'S, 114°28'E) off Cape Naturaliste, West Australia provided data in an extratropical region. The mooring was maintained as part of the Leeuwin Current Interdisciplinary Experiment (LUCIE), a multi-ship, year long survey designed to investigate the dynamics of the Leeuwin Current (Church *et al.*, 1989). The second mooring deployment provided useful wind data during the period 11/2/87 to 26/5/87. (The first deployment provided too short a record (35 days) for useful validation). The five-day averaged winds are compared in Figure 3.7, using the same format as the comparison for the equatorial mooring. Statistics are presented in Table 3.5. The mooring data are averaged over 12-hour intervals. Time series of the twice-daily values are compared. For twice daily values the mean wind speed bias (ATRA - Mooring) is 2.02 ms^{-1}. Again the ATRA analysis shows higher wind speeds indicating that the boundary layer model has not sufficiently reduced wind speeds at 950 mb to approximate speeds at the surface. The mean bias in direction (ATRA - mooring) is only -3.73°, indicating that rotation of the wind vector due to friction in the boundary layer is on average a good correction to the 950 mb wind. The time series of 5-day averaged zonal and meridional wind (Figure 3.7) are in excellent agreement and give correlation coefficients of 0.94 and 0.92 respectively. This high correlation may partly reflect the high span in wind speeds exhibited in this region.

3.3.2.4 Mooring off Dongara

Wind measurement from a mooring (29°32'S, 114°16'E) off Dongara, west Australia were obtained as part of the LUCIE research project during 10/2/87 to 31/3/87. A comparison of five day averages from the ATRA analysis, in the same format as earlier comparisons is presented in Figure 3.8. A comparison of twice-daily values is also conducted, and the statistics are summarized in Table 3.5. A striking discrepancy appears in the mean bias in direction (Table 3.5, Figure 3.8d). The discrepancy is due to a sharp change in wind direction at the continental boundary. It is likely that the

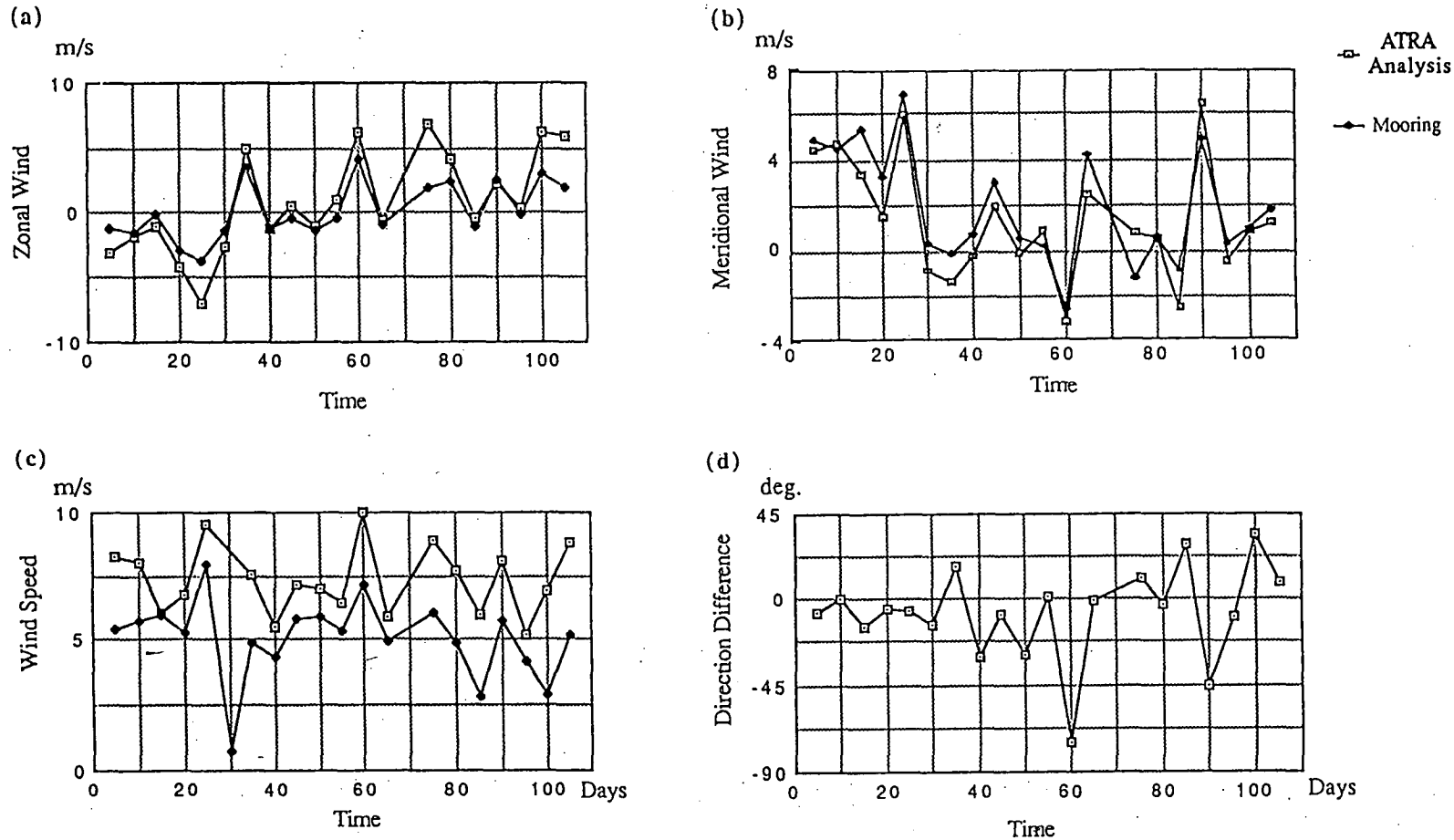

Figure 3.7 Time series of 5-day averaged wind components of mooring (34°01'S, 114°28'E) off Cape Naturaliste and ATRA wind analysis: (a) zonal wind; (b) meridional wind; (c) wind speed; and (d) direction difference (ATRA analysis minus mooring).

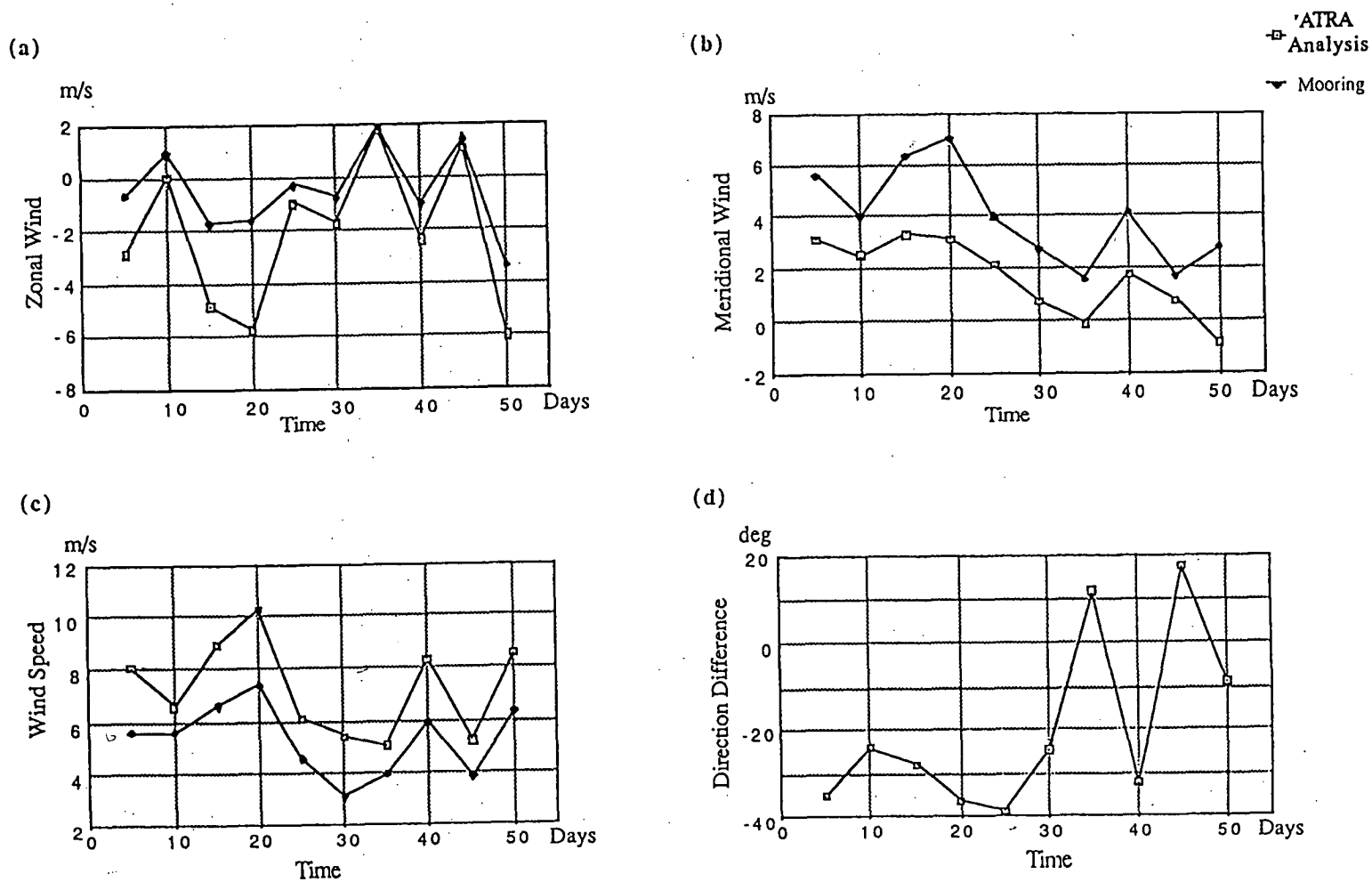

Figure 3.8 Time series of 5-day averaged wind components of mooring (29°32'S, 114°16'E) off Port Dongara and ATRA wind analysis: (a) zonal wind; (b) meridional wind; (c) wind speed; and (d) direction difference (ATRA analysis minus mooring).

mooring has come under the influence of continental winds, whilst the ATRA analysis has smeared the open-ocean winds into the coastal region. Despite this discrepancy, time-series of five-day wind speeds are highly correlated (0.96 and 0.87 for zonal and meridional wind speed components respectively). The twice-daily values are not as highly correlated (Table 3.7), probably due to a daily sea-breeze in the ATRA analysis which is filtered out by the 12-hour averaging in the mooring data.

3.3.2.5 Summary of validation

The 950 mb wind from the ATRA analysis corrected for friction in the surface boundary layer (Davidson and McAvaney 1981) is highly representative of variations in the surface wind (see correlation coefficients in Tables 3.5-3.7). A 20% reduction in wind speed as calculated in a boundary layer model overestimates the magnitude of surface wind by 5% to 40%, the larger values occurring in extra-tropical regions. Predicted directions in the ATRA analysis may be seriously in error in coastal regions, and under weak wind speeds (<4 ms^{-1}), but are usually within 10° from the measured value when wind speeds are high.

3.4 Outgoing Longwave Radiation (OLR)

OLR data used in this study was obtained from the NOAA polar orbiting satellites. They are sun-synchronous satellites, having an inclination of about 99° (the angle the satellite track makes with the equator), a nominal height above the earth of 833 km, and a period of about 102 minutes. The equator crossing times of the NOAA satellites are at about 0900 LST southbound and 2100 LST northbound. The local area coverage or "pixel" resolution is about 1.1 km. Further details concerning the determination of this radiation budget component are given in Winston and Krueger (1977).

The instrument scan was perpendicular to the orbital plane at a rate of six scans per second. From 833 km, the observed swath on either side of the suborbital track extends approximately 13° of geocentric arc (approximately 2,866 km at the equator).

Due to the volume of data involved, larger data elements are produced by spatially averaging the pixels along the scan. Mercator arrays on a 2.5° × 2.5° latitude-longitude grid are produced by bi-linear interpolation of stereographic arrays where data has been digitized. The data are organized into two sets, one with night-time values and one with daytime values. Daily OLR is then obtained by averaging the twice daily values. From these daily values, monthly averages are then calculated.

3.5 TIROS-N Operational Vertical Soundings

The TIROS Operational Vertical Sounder (TOVS) on board the TIROS-N (now called NOAA) series of polar-orbiting satellites provides global coverage of temperature and moisture for selected layers of the atmosphere. Since mid-1979, the goal has been to have two of these satellites in sun-synchronous orbit at all times, permitting most of the earth to be sampled at roughly 6-hour intervals. The TOVS itself consists of three instruments: (1) the second version of the High-Resolution Infrared Radiation Sounder (HIRS/2), (2) the Microwave Sounding Unit (MSU), and (3) the Stratospheric Sounding Unit (SSU). These instruments together measure radiances in 27 spectral intervals. Detailed descriptions of the TOVS retrieval techniques can be found in the literature by Smith and Woolf (1976), Smith *et al.* (1979) and Hayden *et al.* (1981).

The operational product obtainable from the National Environmental Satellite Data and Information Service (NESDIS) contains temperature for 15 layers from 1000 to 1 mb and precipitable water (PW) for three layers from 1000 to 300 mb. TOVS PW data from 1000 to 700 mb are used in this study to provide information on the large-scale distribution of low level moisture.

Several studies have examined the accuracy of the TOVS PW data. Since moisture retrievals are not possible under completely cloudy conditions, the PW data may have a bias under heavy convection condition. Gruber and Watkins (1979) found a RMSD of about 5mm between daily low-level PW (1000-700 mb) derived from TOVS and co-located radiosonde observations over continental United States. Again, Gruber and

Watkins (1982) compared TOVS and radiosonde temperature data from July 1979 through May 1980 and found that the RMSD are larger for cloudy retrieval paths (2-3 mm) than for clear retrieval paths (1-2 mm). Garcia *et al.* (1986) did a similar validation using aircraft observation over the eastern Pacific from November 1980 to January 1983. He found that the biases are larger than those of Gruber and Watkins, but the RMSD are smaller for the lowest two layers.

3.6 Harmonic Analysis and Filtering techniques

3.6.1 Harmonic analysis

Harmonic analysis is one of the conventional techniques used to detect oscillations with known frequencies. Using Fourier analysis, a time series can be represented by a linear combination of a given number of periodic functions (sine and cosine functions). All of these periodic functions are orthogonal and the coefficients can be determined independently of one another. Since it is well known that annual and semiannual cycles of atmospheric and oceanic variables in tropical areas are dominated by solar movement, harmonic analysis has been widely used to describe their seasonal oscillations. A brief description of the technique is presented below. A comprehensive treatment can be found in Jenkins and Watts (1968) and Chatfield (1975).

For a time series x(t) sampled at a unit interval for N times: $\{x_t\}$ for k=1, 2, ... , N, x(t) can be represented by a Fourier series:

$$x(t) = A_0 + \sum_{k=0}^{\frac{N}{2}-1} [A_k \cos(\omega_k t) + B_k \sin(\omega_k t)] + A_{\frac{N}{2}} \cos \pi t \qquad (3.1)$$

the component at frequency $\omega_k = \frac{2\pi k}{N}$ is often called the kth harmonic. For $k \neq \frac{N}{2}$, the kth harmonic is often written in the equivalent form

$$A_k \cos(\omega_k t) + B_k \sin(\omega_k t) = C_k \cos(\omega_k t - \phi_k) \qquad (3.2)$$

$$C_k = \sqrt{A_k^2 + B_k^2} \qquad (3.3)$$

$$\varphi_k = \tan^{-1}\left(\frac{B_k}{A_k}\right) \tag{3.4}$$

where C_k and ϕ_k represent the amplitude and phase of the cycle respectively.

Using the least squares approach, A_k and B_k can be estimated by the following formulae:

$$\begin{aligned} A_0 &= \bar{x} \\ A_k &= \frac{2}{N}\sum_{m=1}^{N} x_m \cos\ \omega_m m \\ B_k &= \frac{2}{N}\sum_{m=1}^{N} x_m \sin\ \omega_m m \\ A_{\frac{N}{2}} &= \frac{1}{N}\sum_{m=1}^{N}(-1)^m x_m \end{aligned} \tag{3.5}$$

It can be shown that

$$\frac{1}{N}\sum_{t=1}^{N}(x_t - \bar{x})^2 = \sum_{k=1}^{\frac{N}{2}-1}\frac{C_k^2}{2} + A_{\frac{N}{2}}^2 \tag{3.6}$$

That is, the variance of a time series can be represented by a sum of their individual harmonic contributions. By plotting $\frac{C_k^2}{2}$ against ω_k, a line spectrum is obtained to describe discrete spectra. Since most time series have continuous spectra, it is more appropriate to use a continous curve so that its area can be used to represent the variance. By plotting the heights of histogram $I(\omega_k)$ against ω_k, a periodogram is obtained, where

$$\begin{aligned} I(\omega_k) &= \frac{N}{4\pi}C_k^2 \quad (\text{for } k \neq \frac{N}{2}) \\ I(\pi) &= \frac{N}{\pi}A_{N/2}^2 \end{aligned} \tag{3.7}$$

Harmonic analysis is used in Chapter 4 and 5 to study the annual and semiannual cycles of SST and wind field. Smothing of the periodogram is necessary to estimate the continuous spectrum.

3.6.2 Spectral analysis

Harmonic analysis is appropriate for studies of oscillations with known frequencies. However, there are still many variations of atmospheric and oceanic phenomena with unknown and continuous frequencies. It is often more suitable to use a spectral density function $f(\omega)$ (i.e. spectrum) to describe the contribution at a band of frequencies. The spectrum $f(\omega)$ can be shown as the limit of the periodogram when the number of samples $N \to \infty$. While the $I(\omega)$ is asymptotically unbiased, it can be shown that the variance of $I(\omega)$ does not decrease as the number of sampling N increase. Therefore, $I(\omega)$ is not a consistent estimator for $f(\omega)$ (Chatfield, 1975).

It can be shown that by smoothing the periodogram, that is

$$\hat{f}(\omega) = \sum_{k=-N/2}^{N/2} I(\omega_k) W(\omega - \omega_k) \tag{3.8}$$

where $W(\theta)$ is a spectral window with some conditions, the $\hat{f}(\omega)$ is an asymptotically unbiased estimate of $f(\omega)$, and is a consistent estimate due to its variance tending to zero when $N \to \infty$. (Chatfield, 1975; Priestley, 1981). In Chapter 4, an IMSL subroutine SSWD is used to estimate the spectral density of SST.

It can be shown that $\nu \hat{f}(\omega)/f(\omega)$ is approximately distributed as χ^2_ν (Chatfield, 1975: Section 7.5) where ν is called the number of degrees of freedom. Therefore, the 100(1-α)% confidence interval is given by

$$\frac{\nu \hat{f}(\omega)}{\chi^2_{\nu,\alpha/2}} \text{ to } \frac{\nu \hat{f}(\omega)}{\chi^2_{\nu,1-\alpha/2}}.$$

It can be seen that by plotting spectral estimates on a logarithmic scale, the confidence interval for the spectrum is simply represented by a constant interval about the spectral estimates (Jenkins and Watts, 1968: Section 6.4.2):

$$\log \hat{f}(\omega) + \log \frac{\nu}{\chi^2_{\nu,\alpha/2}} \quad \text{to} \quad \log \hat{f}(\omega) + \log \frac{\nu}{\chi^2_{\nu,1-\alpha/2}}$$

When smoothing the periodogram in groups of size m, it can be seen that ν equals to 2m.

3.6.3 Filtering techniques

Filtering techniques are often used to pre-process the data before any analysis is done. This technique allows a particular band of frequencies to be highlighted for further study. Filters may be sub-divided into low-pass, high-pass, band-pass and band-rejection depending on their frequency response (Bellanger, 1984). It may be shown that all the above filters can be easily constructed from the low-pass filter (Bellanger, 1984; Hamming, 1983). Therefore the design of a low-pass filter will be discussed below:

The design of digital filters is based on Fourier transform theory. For a function x(t), its Fourier transform X(f) in frequency domain can be written as

$$X(f) = \int_{-\infty}^{\infty} x(t) e^{-j2\pi ft} dt \tag{3.9}$$

where $$x(t) = \int_{-\infty}^{\infty} X(f) e^{j2\pi ft} df \tag{3.10}$$

x(t) can be seen as the inverse Fourier transform of X(f) through (3.10).

Physically, the Fourier transform X(f) describes how the power distribution of a function x(t) varies with frequency (Jenkins and Watts, 1968). Suppose a new function y(t) can be defined as

$$y(t) = \int_{-\infty}^{\infty} h(u)x(t-u)du \tag{3.11}$$

It can be shown that

$$Y(f) = H(f)\, X(f) \tag{3.12}$$

where Y(f), H(f) and X(f) are the Fourier transforms of y(t), h(t) and x(t) respectively (Jenkins and Watts, 1968).

According to the Parseval theorem, the energy of Y can be expressed as

$$|Y(f)| = |H(f)| \bullet |X(f)|$$

therefore, if the amplitude response of a low-pass filter is one between 0 and a cut-off frequency f_c, its properties may be described as (Hamming, 1983):

$$\begin{aligned} H(f) &= 1 \qquad \text{for } 0 \leq |f| < f_c \\ &= 0 \qquad \text{elsewhere} \end{aligned} \tag{3.13}$$

and, of course

$$H(-f) = H(f)$$

The amplitude response of filtered data should have the following properties:

$$\begin{aligned} |Y(f)| &= |X(f)| \qquad \text{for } 0 \leq |f| < f_c \\ &= 0 \qquad \text{elsewhere} \end{aligned}$$

Therefore, the Fourier explanation of H(f) could be written as

$$h_k = 4\int_0^{0.5} H(f)\cos(2\pi kf)df \tag{3.14}$$

$$= 4\int_0^{f_c} \cos(2\pi kf)df$$

$$= 2f_c \frac{\sin 2\pi\, kf_c}{2\pi\, kf_c} \tag{3.15}$$

Therefore, the corresponding Fourier series is

$$H(f) = 2f_c + 2\sum_{k=1}^{\infty}\left[\frac{\sin 2\pi kf_c}{\pi k}\right]\cos 2\pi kf \tag{3.16}$$

In practice, it is necessary to limit the number of coefficients in h_i to N_0, where $N_0 \leq N$. This truncation in fact can be seen as multiplying the impulse response h_i by a time window g_i which has the following properties:

$$\begin{aligned} g_i &= 1 && \text{for} -\frac{N_0}{2} \leq t \leq \frac{N_0}{2} \\ &0 && \text{elsewhere} \end{aligned} \tag{3.17}$$

The Fourier transform of this function is written:

$$G(f) = N_0\frac{\sin \pi fN_0}{\pi fN_0} \tag{3.18}$$

Therefore, the real filter, with a limited number of coefficients N, has the following convolution product $H_g(f)$ as its transfer function (Jenkins and Watts, 1968):

$$H_g(f) = \int_{-\infty}^{\infty} H(f)G(f - f')df' \tag{3.19}$$

By limiting the number of coefficients, ripples are introduced and the steepness of the cut-off filter is limited. These problems can be further ameliorated by designing special windows. For the present study, equation (3.16) will be used.

It has been pointed out that the number of coefficients and filter characteristic have the following relationship (Maurice, 1984):

$$N_e = \frac{2}{3}\log\left(\frac{1}{10\delta_1\delta_2}\right)f_s/\Delta f \tag{3.20}$$

where δ_1 is the passband ripple, δ_2 is the stop band ripple, f_s is sampling frequency and Δf is the transition band.

In the present study, f_c=1/7, let $\delta_1 = 0.05$, $\delta_2 = 0.05$ and $\Delta f = 0.04$, we have N_e=27. For f_c=1/60, let $\delta_1 = 0.1$, $\delta_2 = 0.1$ and $\Delta f = 0.005$, we have N_e=133.

3.7 Empirical Orthogonal Functions (EOF) Analysis

In the last two decades EOF analysis has become very popular in meteorological and oceanographic studies (Barnett, 1977; Weare, 1977). There are three important reasons for its popularity (Weare and Nasstrom, 1982). The first is that this method often enables a description of the spatial and temporal variability of a complex geophysical field with a relatively small number of functions and associated time coefficients. The second reason is that the most important of the derived empirical functions often are amenable to physical interpretation which may give substantial insight into complex processes such as oceanographic variations (Weare *et al.*, 1976) or short-term climatic changes (Weare, 1979). The third major reason is that the method is applicable to any variable observed on any grid, regardless of whether the grid is regular or not. Whetton (1986) provided a comprehensive review of this method.

In this section, the method will be briefly described. For the simplicity of the discussion, it is assumed that the mean of the data have been removed, so that $\overline{X} = 0$.

Now, in meteorological and oceanographic studies, it is often necessary to examine a spatial feature and temporal features of a variable field. One way to do it is to partition the field into two; a temporal and a spatial field. This can be done by EOF analysis.

A field X, consisting of m stations with n observations (in time), may be expressed in a matrix format as follows:

$$X = \begin{array}{l} \longrightarrow \text{stations} \\ \Big\downarrow \text{time} \end{array} \begin{bmatrix} x_{11} & x_{12} & \cdots & x_{1m} \\ x_{21} & x_{22} & \cdots & x_{2m} \\ \vdots & \vdots & \ddots & \vdots \\ x_{n1} & x_{n2} & \cdots & x_{nm} \end{bmatrix} \tag{3.21}$$

Suppose X (m stations and n observations) can be expressed as a linear combination of two matrices C and V, i.e.

$$X = CV' \tag{3.22}$$

In the following analysis, it will be shown that C and V can be derived from X. Furthermore C is a time dependent matrix whist V describes the spatial domain.

A matrix A may be derived such that

$$A = \frac{1}{m} X'X \tag{3.23}$$

then keeping in mind that $\overline{X}=0$, it can be seen that the diagonal elements of A are the variances of the data for each of the m stations, and the off-diagonal terms are the covariances between stations. It is clear that A is real and symmetric. From the theory of linear algebra (Hohn, 1964, Chapter 8), there will exist an orthogonal matrix V and a unique diagonal matrix D which meet the relation:

$$D=V'AV \tag{3.24}$$

and

$$V'V=VV'=I \tag{3.25}$$

It can be shown that the columns of V are eigenvectors of A and the diagonal elements of D are the corresponding eigenvalues. Formula (3.25) shows that the eigenvectors (columns of V) are of unit length.

In other words,

$$D = V'AV = V'\frac{1}{m}X'XV = \frac{1}{m}(XV)'(XV) \tag{3.26}$$

let C=XV, (3.27)

i.e.

$$\begin{bmatrix} c_{11} & c_{12} & \cdots & c_{1m} \\ c_{21} & c_{22} & \cdots & c_{2m} \\ \vdots & \vdots & \ddots & \vdots \\ c_{n1} & c_{n2} & \cdots & c_{nm} \end{bmatrix} = \begin{bmatrix} x_{11} & x_{12} & \cdots & x_{1m} \\ x_{21} & x_{22} & \cdots & x_{2m} \\ \vdots & \vdots & \ddots & \vdots \\ x_{n1} & x_{n2} & \cdots & x_{nm} \end{bmatrix} \times \begin{bmatrix} v_{11} & v_{12} & \cdots & v_{1m} \\ v_{21} & v_{22} & \cdots & v_{2m} \\ \vdots & \vdots & \ddots & \vdots \\ v_{m1} & v_{m2} & \cdots & v_{mm} \end{bmatrix}$$

then X=CV' (3.28)

that is

$$\begin{bmatrix} x_{11} & x_{12} & \cdots & x_{1m} \\ x_{21} & x_{22} & \cdots & x_{2m} \\ \vdots & \vdots & \ddots & \vdots \\ x_{n1} & x_{n2} & \cdots & x_{nm} \end{bmatrix} = \begin{bmatrix} c_{11} & c_{12} & \cdots & c_{1m} \\ c_{21} & c_{22} & \cdots & c_{2m} \\ \vdots & \vdots & \ddots & \vdots \\ c_{n1} & c_{n2} & \cdots & c_{nm} \end{bmatrix} \cdot \begin{bmatrix} v_{11} & v_{21} & \cdots & v_{m1} \\ v_{12} & v_{22} & \cdots & v_{m2} \\ \vdots & \vdots & \ddots & \vdots \\ v_{1m} & v_{2m} & \cdots & v_{mm} \end{bmatrix}$$

This row corresponds to the first eigenvector

This column corresponds to the time series for pattern 1

then $$D = \frac{1}{m}C'C \tag{3.29}$$

Formula (3.28) shows that a data field X can be represented by a product of C and V, where V is a matrix consisting of the eigenvectors of matrix A (3.23 and 3.24), representing spatial patterns, and C is a matrix calculated from (3.27), consising time series corresponding each spatial patterns.

Chapter 4. The Variability of Sea Surface Temperature

4.1 Introduction

SST has been found to be one of the most important factors in the global climatic system, especially over tropical oceans. SST, wind, water vapour and deep convection in the tropical atmosphere are closely correlated through the action of sensible and latent heat fluxes. The apparent correlation between the location of the maximum centre of convection and the SST maximum in tropical areas has highlighted the importance of SST (Figure 4.1, after Lukas, 1987; World Meteorological Organization: Figure 5.1, 1985). Along the equator, a warm pool with an annual mean SST greater than 30°C is located near Papua New Guinea, while a cold tongue of 20°C, related to the Peru current and upwelling (Wyrtki, 1982), stretches from the coast of South America along the equator to the central Pacific. This distribution of SST in the Pacific maintains the zonal Walker circulation, with large-scale convection in the Indonesia-North Australian area, and descending air prevailing in the eastern Pacific Ocean.

The seasonal variation of SST suggests another aspect of its correlation with convection. There are systematic longitudinal changes in phase and amplitude of the seasonal cycle in SST. Near the coast of Peru, the highest SST occur during March, while further west along the equator, the highest SST occur progressively later and with diminished amplitude (Wyrtki, 1965; Horel, 1982; Rasmusson and Carpenter, 1982). While the first harmonic component of the annual cycle is dominant in the area beyond the tropics and northwest Indian ocean, the second harmonic component contributes more than 60% of the variance of the seasonal cycles in the region extending southeastward from the Arabian coast , and 30-60% in the western equatorial Pacific (Levitus, 1987). The seasonal SST variation is consistent with the analysis of convection presented by Meehl (1987) who showed that the

a)

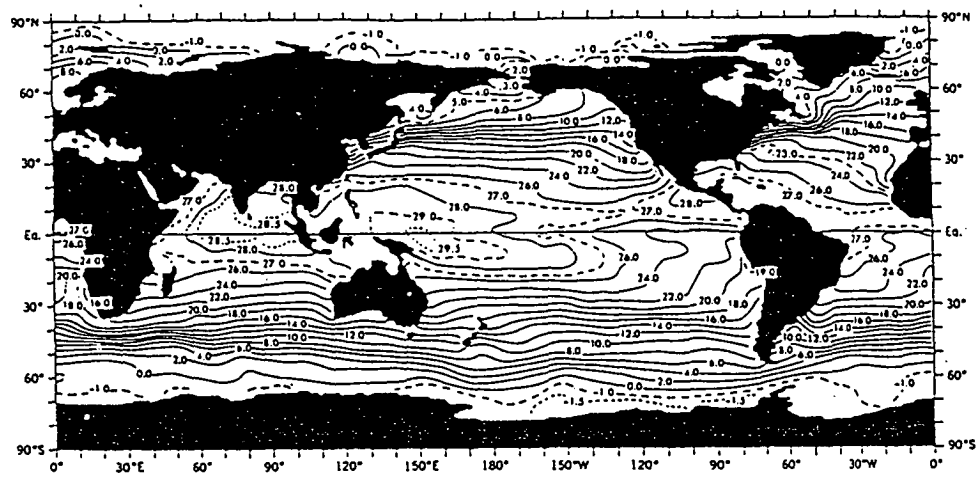

b)

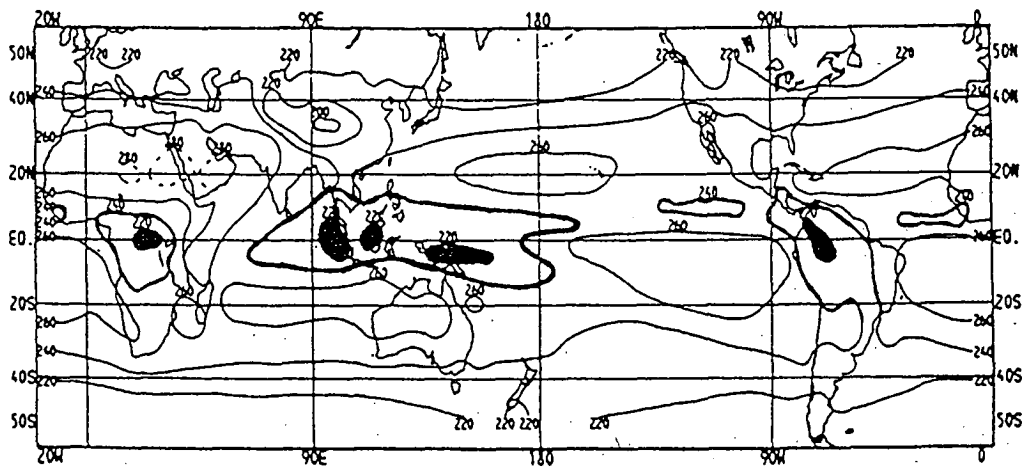

Figure 4.1 Annual mean sea surface temperature (a) from Levitus (1982) and annual mean outgoing longwave radiation (b) from NOAA Atlas #6. OLR values of less than 240 Wm^{-2} are considered to be indicative of intense convection in the tropics. This contour line is darkened. The regions of most intense convection with OLR < 220 Wm^{-2} are shaded. Note that with exception of the western Pacific warm pool core, these regions are found over land masses (From Lukas, 1987).

longitude-time contour map of outgoing longwave radiation (OLR) has a clear semiannual cycle in the western Pacific (100°-170°E) and an annual cycle in the eastern Pacific (Meehl, 1987: Figure 3a). This coherence between SST and convection suggests that there are strong connections between them which justify further study.

Interannual variations of SST provide further evidence regarding its relationship with convection. While the annual variation of SST in the warm pool from the mid-Indian Ocean to the western Pacific is very small, the interannual variation of SST in this area could be larger (World Meteorological Organization, 1985). Gill and Rasmusson (1983) documented that this warm pool migrated eastwards and a zone of anomalous convection followed it in 1982-1983. By studying the SST data of 1984-86 we can examine whether this relationship is unique to the 1982/83 ENSO event or whether it is a feature of other ENSO events.

Recent studies of SST and convection reveal the complexity of their relationship, especially in the western Pacific. Graham and Barnett (1987) have documented two important links between SST, surface wind divergence, and convection. First, over broad regions of the Indian and Pacific oceans, SSTs in excess of 27.5°C are required for large-scale deep convection to occur. However, SSTs above that temperature are not a sufficient condition for convection and further increases in SST appear to have little effect on the intensity of convection. Second, when SSTs are above 27.5°C, surface wind divergence is closely associated with the presence or absence of deep convection. Steiner and Khalsa (1987) obtained similar results by studying the relationship between SST, HRCs. They show that convection was poorly correlated with SST and lower tropospheric moisture in the western Pacific, but was highly correlated in the eastern Pacific. Gutzler and Wood (1989) find that OLR anomalies are significantly correlated with SST and surface convergence anomalies in the eastern Pacific but are uncorrelated in the western Pacific. On the other hand, OLR and 850 mb convergence anomalies are significantly correlated from about 120°W westward but are uncorrelated in the eastern Pacific.

In spite of the studies on the annual and interannual variations of SST mentioned above, questions on the SST/convection relationship still remain unanswered. Firstly, what are the main features of SST over the western Pacific before and during the 1986/87 ENSO? What are the similarities and differences of this event compared with other ENSO events? What are their implications to convection in the area? Secondly, strong semiannual cycles of SST and OLR have been shown over the area from the Bay of Bengal to the ocean north of Australia (Levitus, 1987; Meehl, 1987). What are the reasons for these cycles? Although solar radiation has a semiannual peak in tropical regions, the process would not explain the lack of semiannual cycles in the eastern tropical Pacific. Are there any thermal or dynamical connection between SST and convection in this aspect? Are there any corresponding semiannual cycles of OLR over the same area? Thirdly, Steiner and Khalsa (1987) and Gutzler and Wood (1989) reported no close relationship between SST and convection over the western Pacific, while the study of Gill and Rasmusson (1983) suggests a connection. Graham and Barnett's (1987) result suggests that SST is not the only factor controlling convection in the western Pacific. What are the missing factors? How do they interact each other? We will try to answer some of these questions in this chapter and leave some for discussion in later chapters.

The contents of this chapter are organized as follows: in Section 4.2, the seasonal and annual average during the period 1984-86 are analysed and compared to the climatological SST distribution. In Section 4.3, the annual and semiannual cycles of SST will be examined using harmonic analysis, and the results will be compared with earlier studies. In Section 4.4, the spatial patterns of SST at different time scales will be examined using EOF analysis. The dominated patterns and their corresponding time series are discussed. A summary and discussion will be presented in the last section.

4.2 Seasonal Means of SST

Understanding the SST climatologies in the area from the mid-Indian ocean to the western Pacific would help us to identify the special features of SST during 1984-86, thus providing a background to understand convection in this area. The compilation of SST climatologies has been long an important task for oceanographers and meteorologists. SST climatologies derived from different observation systems and with different spatial scales are presently available (Robinson, 1976; Levitus and Oort, 1977; Robinson *et al.*, 1979; Strong and Pritchard, 1980; Levitus, 1982; Reynolds, 1982; Sadler, 1987a, b; Japan Meteorological Agency, 1989). Reynolds (1983) has compared several SST climatologies based on either surface marine observations (bucket, engine intakes, buoy readings) or oceanographic cast observations (Nansen and conductivity-temperature-depth (CTD) hydrographic stations and XBTs) by examining difference fields of these climatologies for individual months as well as computing root-mean-square differences between them. He concluded that the surface marine climatologies were generally superior to the cast climatologies due to the higher data density of surface marine data. Levitus (1987) further examined two climatologies based on data sets from the National Oceanographic Data Centre (NODC), Washington DC (consisting in one-degree objectively analyzed monthly means, based on approximately 1.5 million temperature soundings) and the Comprehensive Ocean-Atmosphere Data Set (COADS, based on monthly objective analyses of a subset of the 70 million historical merchant ship reports), respectively. By examining the amplitude and phase of the first two harmonics of each climatology, as well as the percent variance contributed by each harmonic to the annual cycle, he found excellent agreement between the two sea surface temperature climatologies in the first two harmonics.

From the above studies it is possible to list the main features of the SST climatology of the study area: 1) The western Pacific contains the warm pool of high SST which is responsible for the maintenance of large-scale convection in the northern Australian and Indonesian areas. A small variation of SST in this area will greatly influence the development of ENSO events; 2) The amplitude of the annual variation in the tropical band decreases from its largest magnitude in the eastern Pacific to a very small value in the western Pacific. In turn, the time of the warmest SST is earliest near the coast of Peru (occurring in March), and is delayed in the westward direction; 3) In the western equatorial Pacific, the amplitude of the annual cycle of SST is generally smaller than the amplitude of its interannual variation. On the other hand, the amplitude of the interannual variations are linked to the build up and collapse of ENSO events; 4) semiannual cycles develop in the area of the Asian and Australian Monsoons.

The annual mean of SST in the period 1984-86 estimated from the MCSST data is presented in Figure 4.2a. It shows that the 28°C pool is mainly confined between 10°S and 10°N while the 29°C pool is located to the east of Papua New Guinea between 7°S and 2°N. The eastward shift of this warm centre during ENSO events is thought to be the mechanism that controls anomalous deep convection in the atmosphere (Rasmusson and Carpenter, 1982; Gill and Rasmusson, 1983). The results presented in Figure 4.2 are very similar to those presented by the climatologies cited above, especially Levitus (1982) and the Japan Meteorological Agency (1989), which used long-term observations of temperature profiles and surface weather reports to arrive at mean climatologies for the study area. Both of them show that the 28°C isotherm stretches eastward from the southeast end of Papua New Guinea, crosses the Philippine Islands north of Manila, dips down to about 5°N in the South China Sea and back up to the south end of Vietnam, touches Jakarta and meets Darwin in northern Australia. The agreement with the data presented in this study is encouraging in that it suggests that the three year mean field is similar to the long term climatology. Furthermore, the

a)

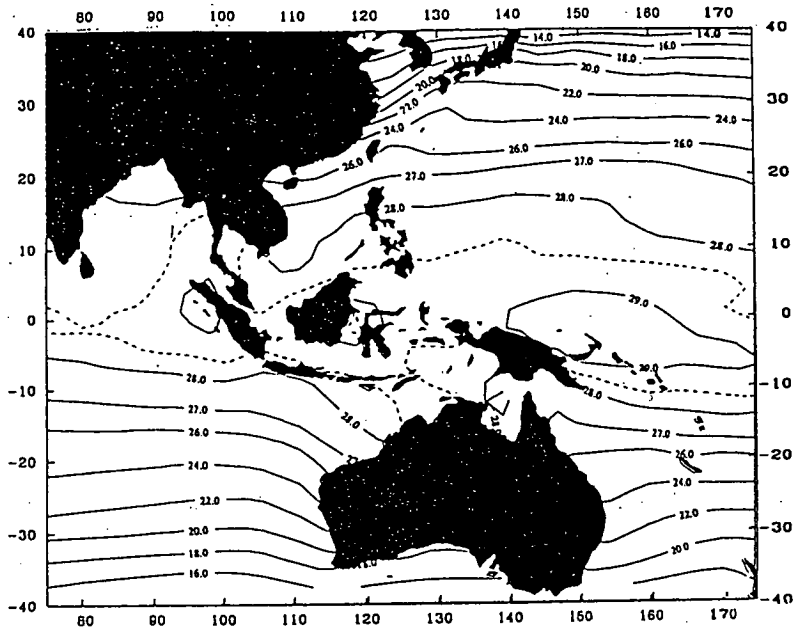

b)

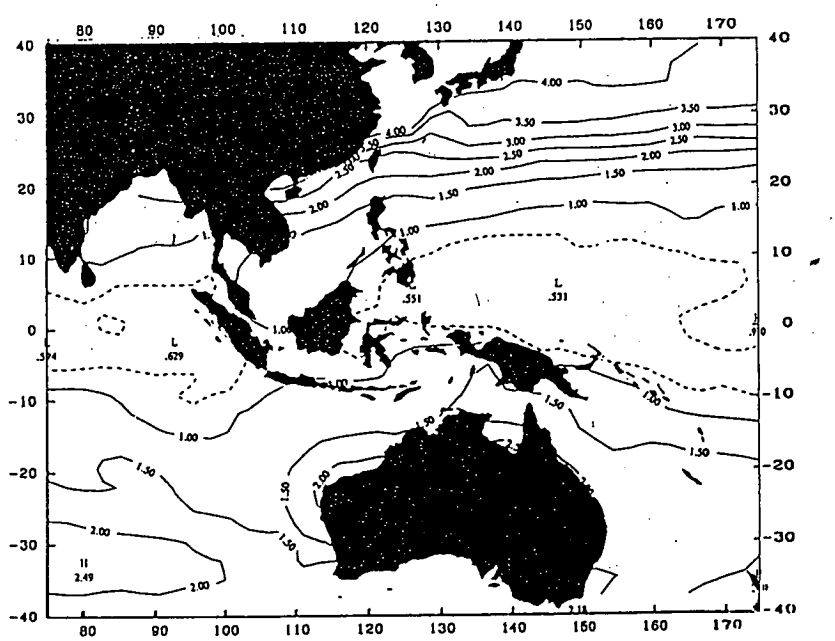

Figure 4.2 Annual mean (a) and standard deviation (b) of sea surface temperature (°C) during the period of 1984 to 1986.

a)

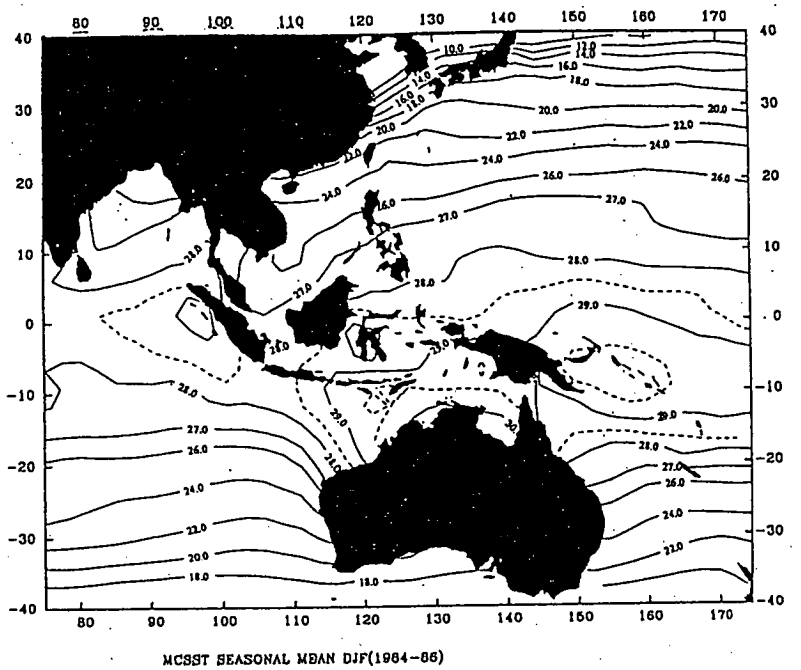

b)

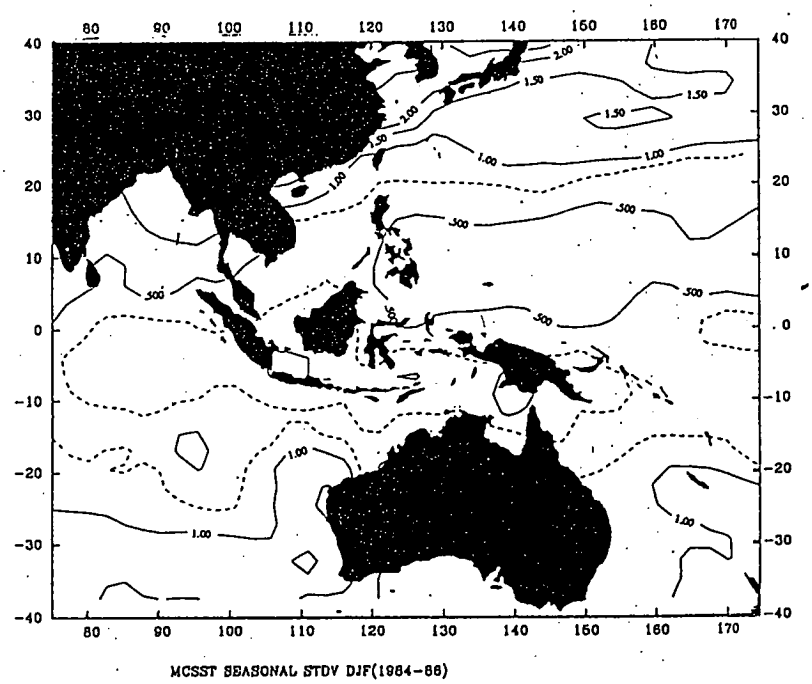

Figure 4.3 Seasonal mean (a) and standard deviation (b) of sea surface temperature during the period of 1984 to 1986: December-January-February.

a)

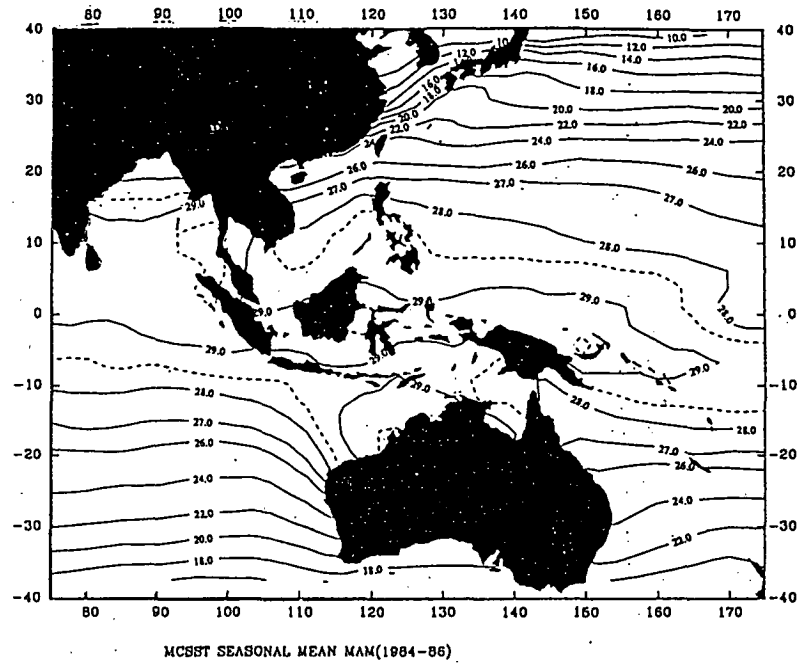

b)

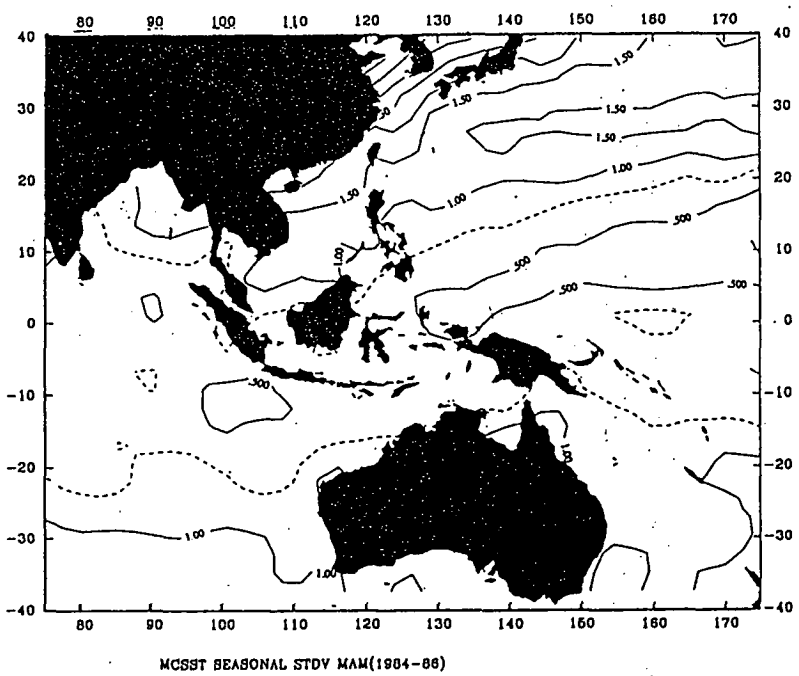

Figure 4.4 Seasonal mean (a) and standard deviation (b) of sea surface temperature during the period of 1984 to 1986: March-April-May.

a)

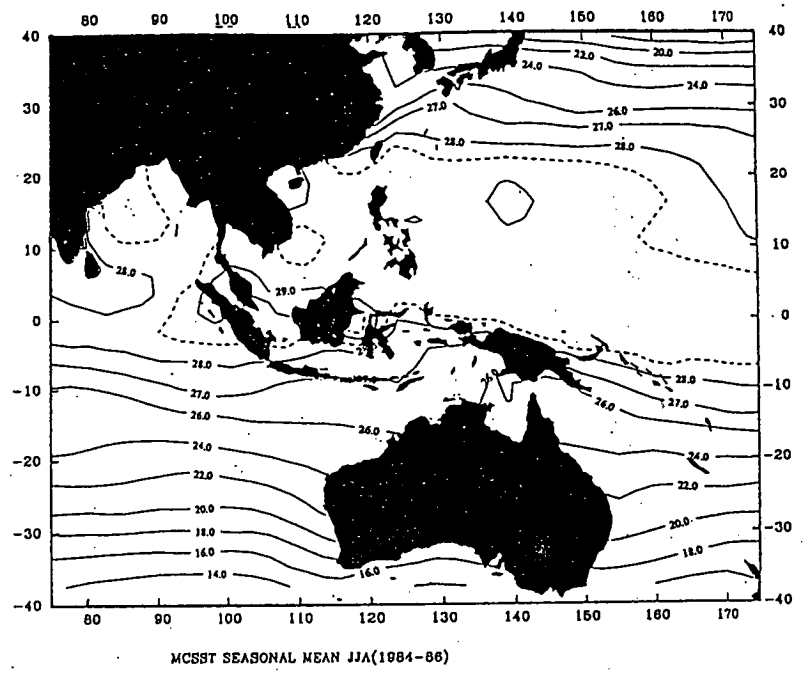

b)

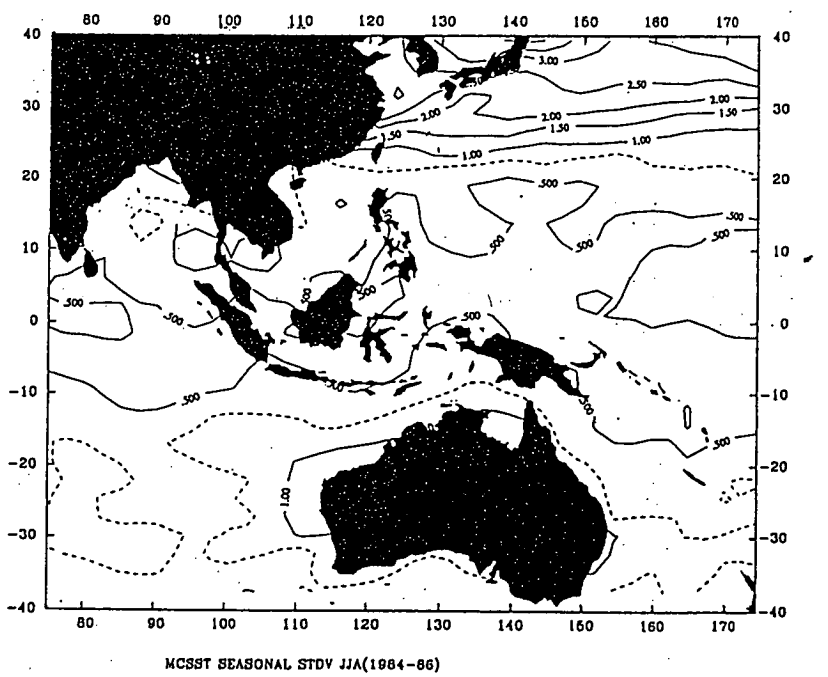

Figure 4.5 Seasonal mean (a) and standard deviation (b) of sea surface temperature during the period of 1984 to 1986: June-July-August.

a)

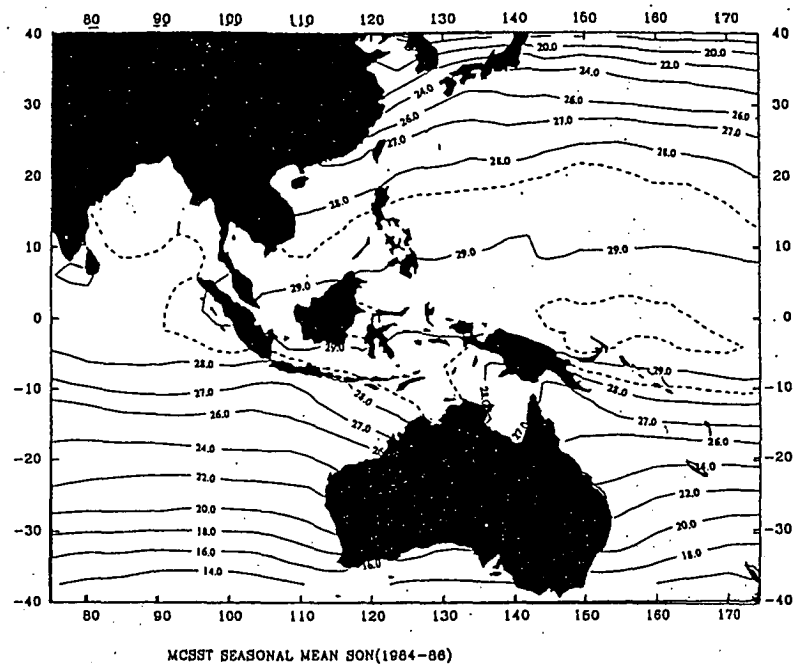

b)

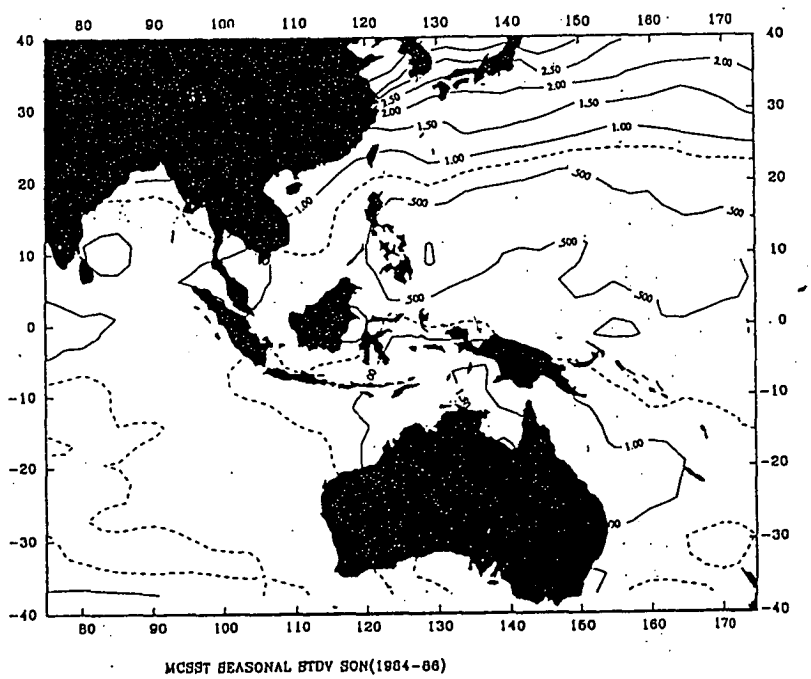

Figure 4.6 Seasonal mean (a) and standard deviation (b) of sea surface temperature during the period of 1984 to 1986: September-October-November.

agreement also points to the general reliability of the satellite technique used in this study to derive the SSTs.

The standard deviation was calculated from five-day running mean temperatures and as such represents variances with time scales ranging from days to years (Figure 4.2b). It is very obvious that the standard deviation of SST north of 20°N is much higher than the equivalent value for the same latitude in the southern hemisphere. This is due to the strong influence of the Asian Monsoon. The standard deviation near the equator is smaller, and the 1°C isotherm is mainly confined to latitudes between 10°S to 10°N. The importance of small changes in temperature in this region has been discussed in terms of dynamic models constructed by Keshavamurty (1982) and Palmer and Mansfield (1985). They argue that on physical grounds, the relation between saturated vapour pressure and temperature is exponential in nature. Therefore a small change in temperature of a warm ocean will create a very large change of vapour pressure which is critical to the development of convection. Their models support this argument. The observations of the shift in the 29°C isotherm, followed by the shift in deep convection in the 1982/83 ENSO event (Figure 5 of Gill and Rasmusson, 1983; Figure 5.1 of World Meteorological Organization, 1985), further supports the importance of small temperature changes. Also, the observational studies by Nicholls (1989) show that the warm water region of the eastern Indian Ocean is also an important control on the climate system.

Four seasons are defined to observe the seasonal patterns. They are DJF (December-January-February), MAM (March-April-May), JJA (June-July-August) and SON (September-October-November). The main features of the mean field and its standard deviation are described below to give a general description of the annual march of isotherms.

Figure 4.3 shows the seasonal mean and standard deviation of SSTs in DJF. One of its major features is that the 29°C isotherm extends to the west of Papua New Guinea and

covers the seas north of Australia in the eastern Indian Ocean. The western edge of the 29°C pool almost exactly matches other climatologies (Sadler, 1987a, b; Japan Meteorological Agency, 1989). The standard deviation of SST in DJF in Figure 4.3b shows that the minimum centre is along the zonal band from 5°N to 15°N, which implies that SST varies very little in the three months in this area. This feature is consistent with the region of maximum solar radiation in the southern hemisphere, and the southward shift of the ITCZ is in agreement with the region of maximum SST. The minimum standard deviation zone is not coincident with the 29°C isotherm, but usually encompassed the 27° to 29° isotherm region. This is a consistent feature of all the seasonal diagrams to be shown. This observation will be discussed further in Chapter 6.

Figure 4.4a shows the mean SST in MAM. The 29°C isotherm moves westward, covers most areas around Malaysia and Papua New Guinea, i.e. from 110°E to 170°E, and extends as far as the Arabian Sea. The 0.5°C isotherm in the standard deviation distribution (Figure 4.4b) shows a southwest-northeast orientation structure.

The virtual disappearance of the 29°C isotherm in JJA is the most striking feature of Figure 4.5a. This feature accompanies a northward movement of the 28°C pool. The standard deviation isotherms in Figure 4.5b loses its band structure which was evident in the previous seasons. The 0.5° C standard deviation is spread evenly in the area between 15°S and 20°N, while the whole area south of 27°N is covered by the 1.0°C isotherm.

The 29°C isotherm, covering the area between 8°S and 8°N, again appears in the mean SST pattern for SON (Figure 4.6a). The 0.5°C isotherm of standard deviation in Figure 4.6b covers the area from 5°N to 20°N.

The annual and seasonal mean SST fields for the period of 1984-86 show a good agreement with other SST climatologies. This fact further confirms the validity of MCSST for use in studies of air-sea interaction. In addition, it suggests that the SST fields in the three years of this study have not shown any significant departures from

the long-term climatology. Therefore they provide a background to judge the other features of the SST field and their relationship with large-scale convection.

4.3 Annual and semiannual cycles of SST

Harmonic analysis (see Chapter 3) has been applied to each grid point of the MCSST field to study their annual and semiannual cycles. The number of observations (N) is 548 representing SST at two-day time intervals during 1984-86. The results of the analysis will be described and mainly compared to a similar study by Levitus (1987) who composited all available historical data into monthly climatologies for the two climatological data sets (>100 years), respectively.

The results for the annual oscillation have been presented in Figure 4.7a. The amplitude of the oscillation is represented by the length while the phase of the oscillation is represented by the direction of arrow. An arrow pointing east means that SST reaches its annual maximum on the 1st of January, while north represent the 1st of April. It is noted that maximum amplitudes occur in the northern hemisphere offshore of Japan where a cold winter mass breaks out from the adjacent continent. The large transfer of heat from the ocean to the atmosphere determines, at least in part, the magnitude and position of the maxima. It should be seen clearly that the amplitudes of the annual cycle in the area north of 25°N are much larger than those at the same latitude in the southern hemisphere. This is mainly due to the response of the stronger Asian monsoon compared to the Australian monsoon. It should be noted that while most of the area in the northern Pacific has similar phase angle, the oscillation phase in the north Indian Ocean is similar to that in the southern hemisphere as far north as 10°N. The boundary between these two areas runs from Sri Lanka to the Malaysian peninsula, to the Moluccas and Irian Jaya. This boundary might also partition the effective area dominated by the Asian Monsoon and the Australian Monsoon. It should be also noted that the amplitudes of annual oscillation in the areas from South China/Southeast Asia to the northwest Australia are largest among those at same

a)

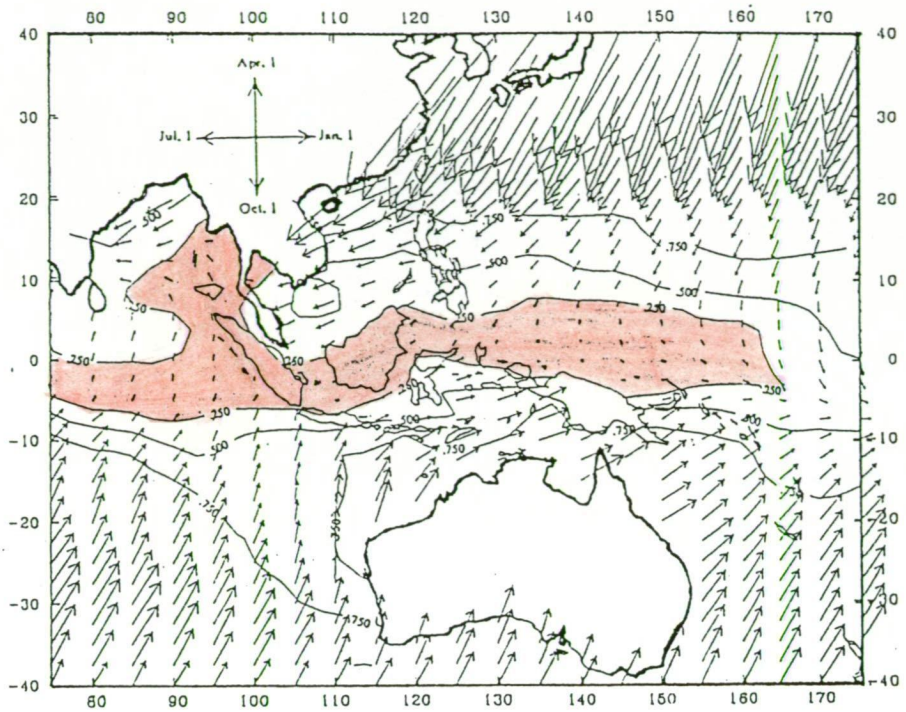

b)

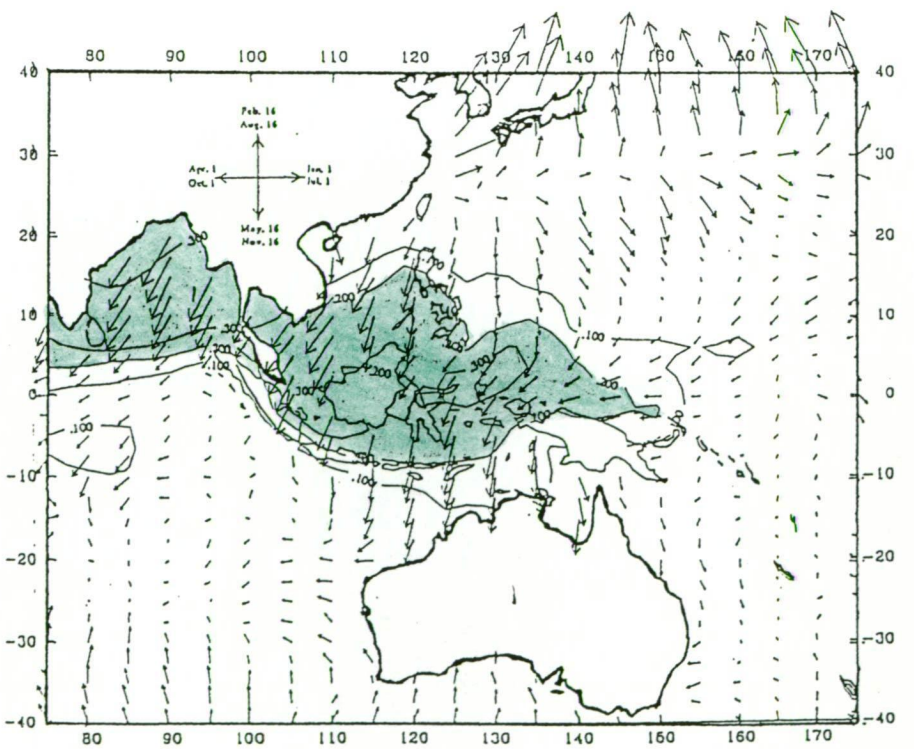

Figure 4.7 The amplitude, phase and percentage of contribution to the total variance of annual (a) and semiannual (b) cycles of MCSST: Areas with contribution less than 25% by annual cycles (a) are shaded in red whilst larger than 20% by semiannual cycles (b) are shaded in green.

latitudes. The relationship between SST and monsoons will be further discussed in the next chapter.

Levitus (1987) was interested in comparing the COADS merchant ship data set with the NODC temperature soundings. In his analysis he included global maps of the amplitude of the first and second harmonics as well as their phase. In a similar fashion to this study, maximum amplitudes were also reported along 47°N out of the coast of Japan. The amplitudes of annual cycles are also much higher in the northern hemisphere than in the southern hemisphere for the same latitude. He found his results are highly consistent with other earlier studies (Wyrtki, 1965; Tchernia, 1980; Horel, 1982; Merle, 1983). Agreement is also good in phase angles of annual cycles between the Levitus analysis and this study.

The contour map of the percentage variance of the annual cycle over the total variance give further insight into the annual cycle (Figure 4.7a). It is noted that the 75% contour line lies at 15°N in the northern hemisphere, and around 10°S in the southern hemisphere. The equatorial areas from mid-Indian Ocean to 165°E in the western Pacific are confined to the 25% contour line. These patterns are similar to those presented by Levitus (1987) except that for any specific locations, the value of the percentage in this study is generally lower than those in Levitus' studies by 10-20%. This is mainly due to two reasons. Firstly, the Levitus analysis was performed on long term monthly averaged SST fields, therefore, the interannual variance has been incorporated into the annual variance or filtered out. Secondly, Levitus used monthly mean SST data which eliminates most of the short time scale variance. In contrast, in this study the five-day running average MCSST data (sampled every second day) has been used. Therefore, the total variance includes considerable high frequency variance as well as interannual variance.

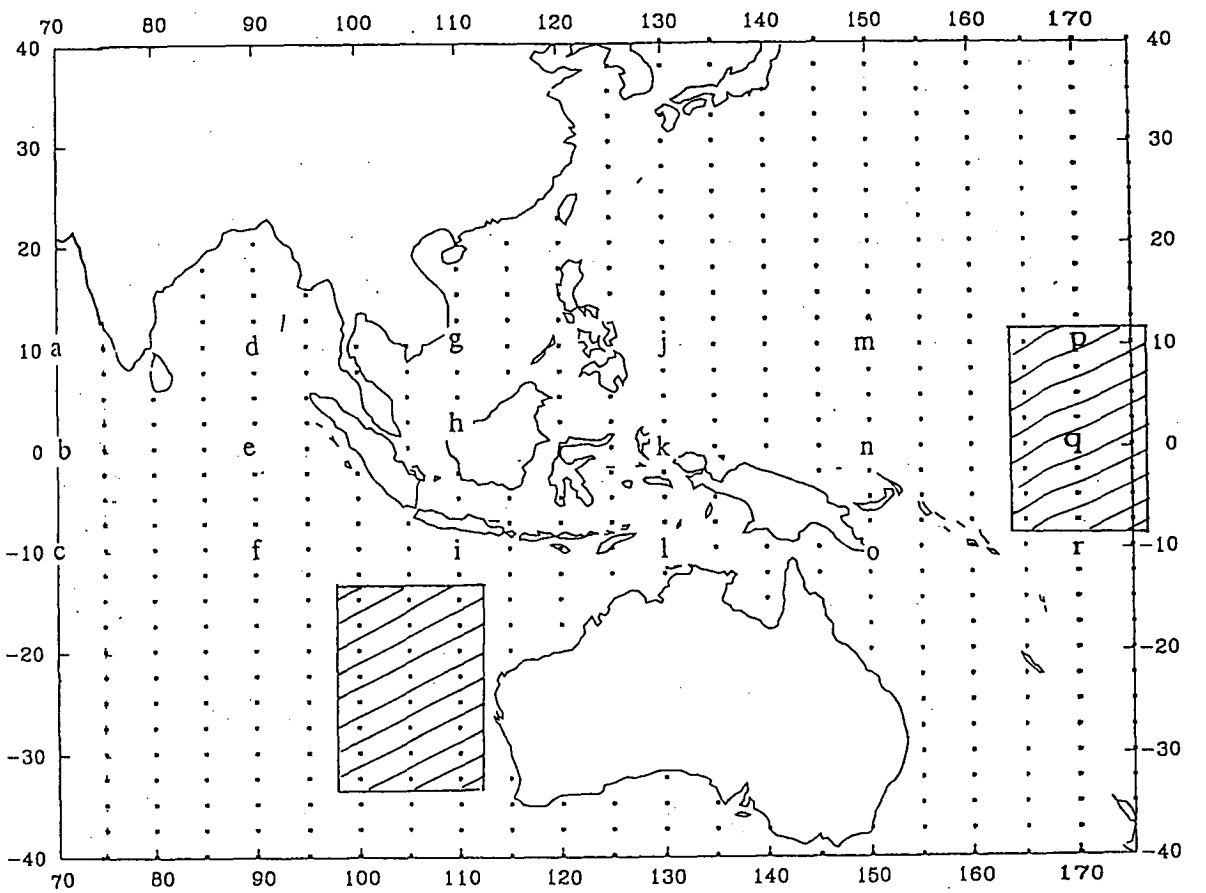

Figure 4.8 Gridpoints of MCSST field and 18 sampling locations (marked by a ~ r) selected for monthly time series in Figure 4.9. Two shading areas represent the centres revealed by the first EOF pattern of anomalous MCSST discussed in Section 4.4.

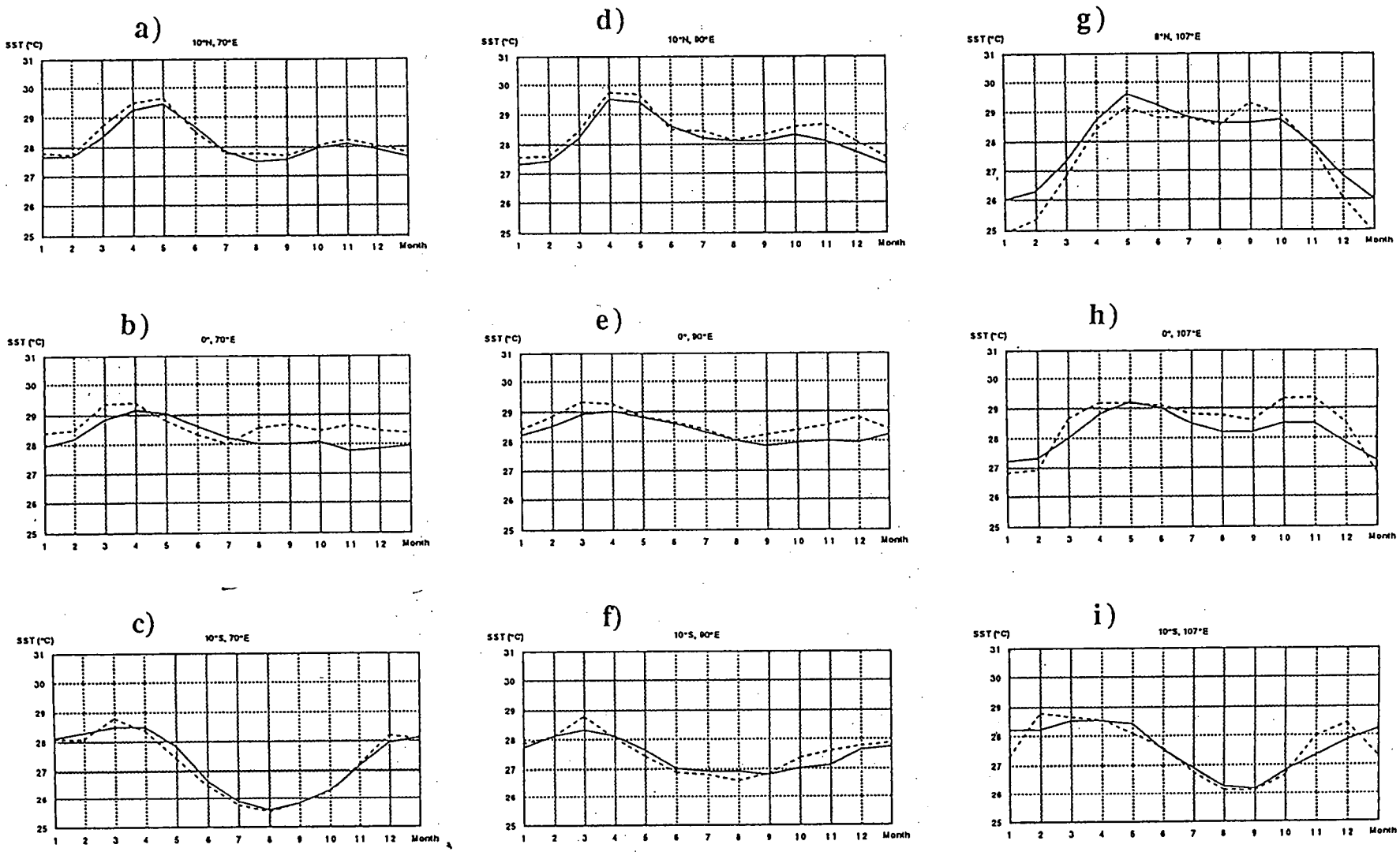

Figure 4.9 Time series of three-year averaged monthly MCSST and Sadler's (1987a,b) SST climatologies at 18 selected locations along the equatorial zone.

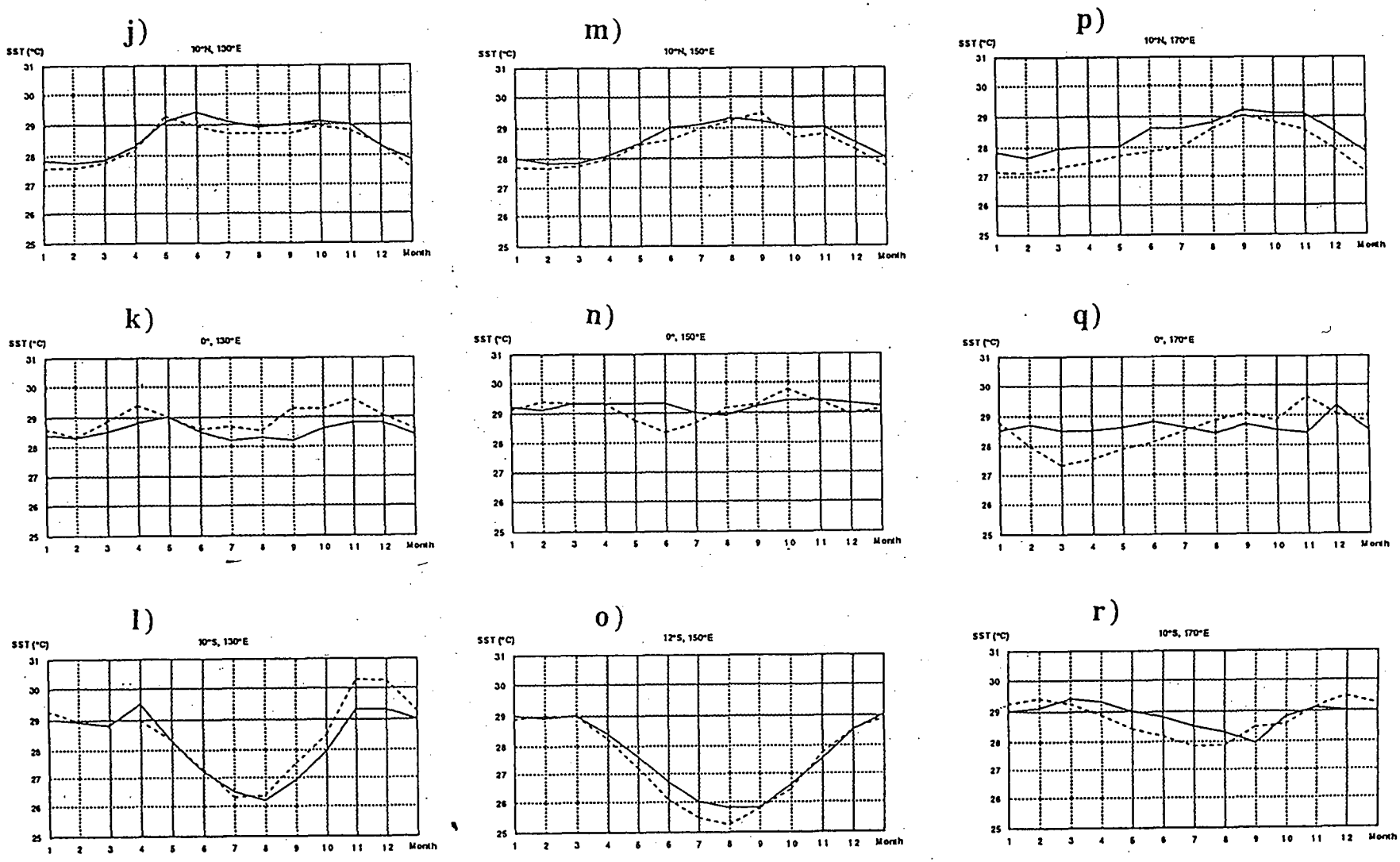

Figure 4.9 (Continued)

These main features of the annual cycle can be further confirmed and visualized in the annual variation of SST at 18 locations (Figure 4.8) presented in Figure 4.9. The solid lines represent monthly SST climatologies from Sadler (1987a, b) and the dashed lines represent the 3-year averaged monthly MCSST. It can be seen firstly that the monthly MCSST agrees well with Sadler's SST. Secondly, it is of interest to see that the phases of the annual cycles along the 10°S are almost the same for various longitudinal zones, i.e. the minimum SST occurs in July-August-September and the maximum in February-March-April. By contrast, along 10°N there is a marked longitudinal shift in the time of the maximum SST. The maximum SST occurs in May along 70°E, June along 130°E, August along 150°E and in September along 170°E.

The semiannual oscillation is presented in Figure 4.7b where the arrow pointing to the east represents both the 1st of January and the 1st of July, while the arrow pointing to the north represents both the 16th of February and the 16th of August. Large amplitudes occur in the area north of 30°N due to the asymmetry of the SST annual oscillation. Of more interest, is the Indonesian and northern Australian area which shows the largest amplitude in the region. In addition, the oscillation phase in this area shows similar phase to those in the both hemispheres from 20°N to 20°S. The phase poleward of 30° latitude in both hemispheres is different from that in the tropical area, suggesting that the semiannual oscillation is dominant in tropical areas and is generated by different mechanisms than those in higher latitude. The entire region from South China/Southeast Asia to Northwest Australia experiences a semiannual oscillation with the same phase on both sides of the equator.

The contour map of the percentage of the variance related to the semiannual cycles over the total variance further supports the above features (Figure 4.7b). There are two high centres, one is in the Bay of Bengal and the other is along the Malaysian Peninsula-Papua New Guinea. Again, this pattern agrees with Levitus' results. He noted that the second harmonic component contributes more than 60% of the variance of the annual cycles in the region extending south-eastward from the Arabian coast , and 30-

60% in the western equatorial Pacific. It should be pointed out here, as in the case of the annual cycle, that the values of the percentage in this study are also smaller than those presented by Levitus. The reasons for this discrepancy have been discussed earlier when the case of the annual cycle was considered.

Further insight into the semiannual oscillation may be illustrated using the results of Meehl (1987). In his study he produced contour maps of OLR for various months. These results are presented in this thesis as Figure 4.10. The maximum OLR anomaly, which is shown shaded, undergoes a seasonal shift from west to east. Maximum intensity occurs during JJA at 90°E, which can be attributed to the Asian monsoon. As time progresses the zone of maximum OLR shifts eastward so that by February, there is a zone of convection extending from approximately 100° to 180°E. In fact, comparison with Figure 4.7 shows that the July pattern of maximum OLR (Figure 4.10a) corresponds to a large amplitude of the semiannual oscillation in the Bay of Bengal. The minimum phase angles of semiannual cycles of SST in this area are in April and October which corresponds to a time interval prior to and after the maximum OLR.

The zone of maximum semiannual amplitude between 100°E to 140°E in tropical areas, seems to be related to zones of maximum OLR. In the northern hemisphere it occurs in July and in southern hemisphere, it occurs in January (see Fig 4.7b). As in the case of the Bay of Bengal, the phase of the semiannual oscillations indicated a build up prior to the time of maximum OLR and a decay during and after the maximum OLR event.

The relationships shown here indicate that the spatial and temporal patterns of SST are intimately related to convection as evidenced by the OLR patterns. It also suggests that the pattern shown in Figure 4.7 is dominated by monsoonal events. These points will be discussed further in Chapters 5 and 6.

It is also worth investigating the contribution of higher frequencies to the total variance. This is an important task since other studies have shown convection events to have an

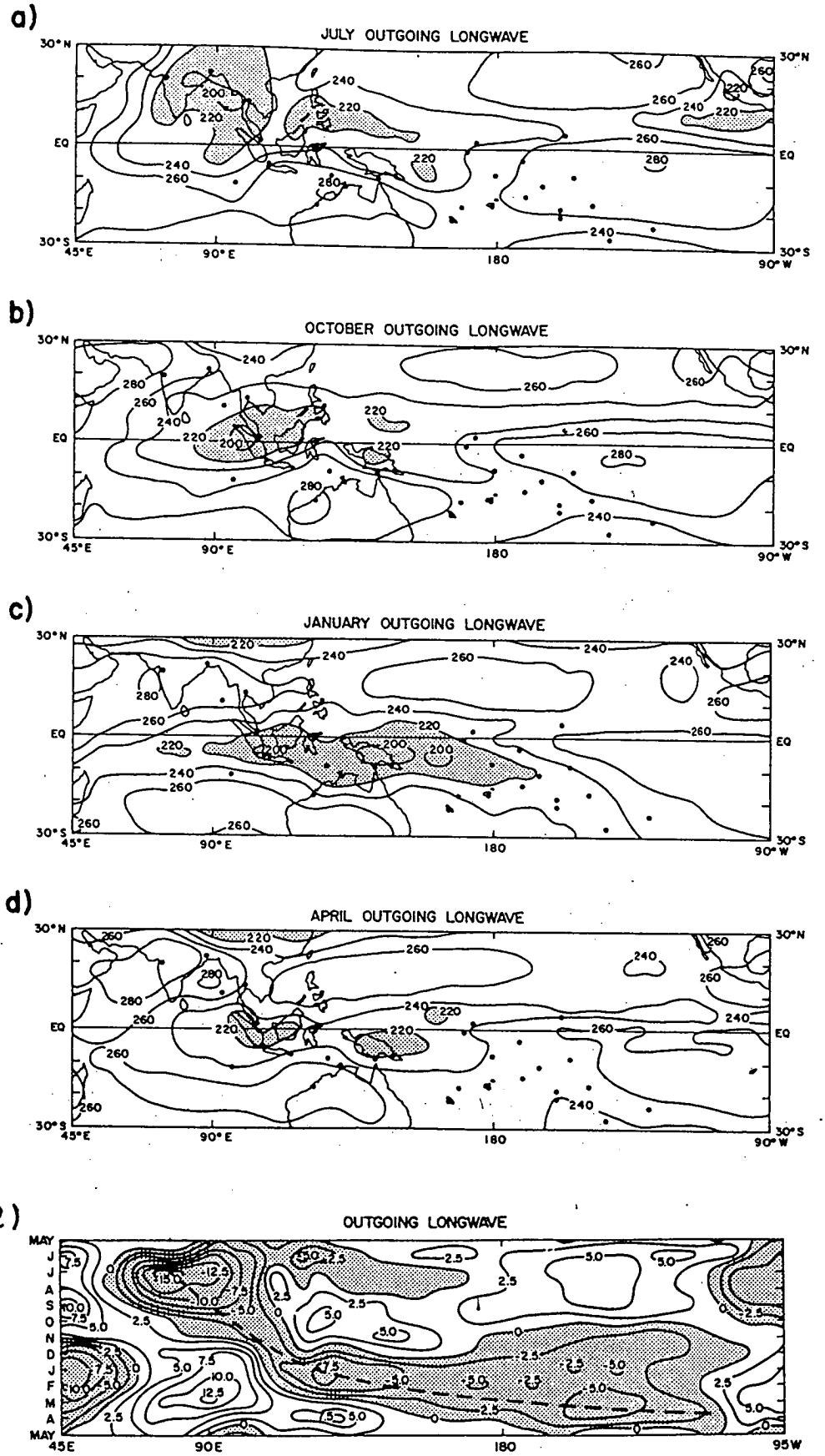

Figure 4.10 Long-term means (eight years) of OLR for the peiod covering June 1974-November (1983), for the Indian and Pacific sectors for (a) July, (b) October, (c) January, (d) April. The longitude-time contour plot is shown in (e).(after Meehl, 1987)

oscillation of 40-60 days (Lau and Chan, 1985; Knutson and Weickmann, 1987). Eighteen SST time series were selected in the study region encompassing 10°N to 10°S and longitudes 70°E to 170°E. These are shown as crosses in Figure 4.8. Spectral power analyses were carried out for these sites.

The analysis used a linear interpolation to replace missing values. These consisted of 61 missing observations out of 548. The longest continuous number of missing observations was 16. Annual and semiannual cycles have been removed before the periodograms are calculated. A subroutine in the spectral analysis (FFT technique) of the IMSL has been used to obtain the power spectra. 548 spectrum power values have been obtained for each of the 18 grid points along the equatorial area from mid-Indian Ocean to mid-Pacific. A frequency window of six equally weighted sampling points has been used to smooth each curve, and an average curve has been obtained for all 18 grid points. Since the data in its original form consisted of 5-day running averages, it is meaningless to consider frequencies of less than one cycle per ten days. The spectrum distribution has been shown in Figure 4.11. As described in Chapter 3 regarding the spectrum analysis, the number of degrees of freedom is 2m for each estimates of the spectrum where m=6. Therefore, the number of degrees of freedom of the averaged spectrum equals 2m times 18 (grid points) which equals 216. An error bar with a confidence level of 95% is also displayed. As may be noticed, there are no any noticeable peaks in the power spectrum. Therefore, when considering the studied equatorial regions as one area, the intraseasonal oscillations of SST are not significant.

4.4 EOF analysis

In the previous sections various aspects of the mean SST field were studied. The seasonal variability was observed by averaging the data on a three month period for three years. Annual and semiannual oscillations were also studied using harmonic analysis. In this section the space and time scales of variability will be studied in greater depth by the use of EOF analysis. This technique allows the identification of

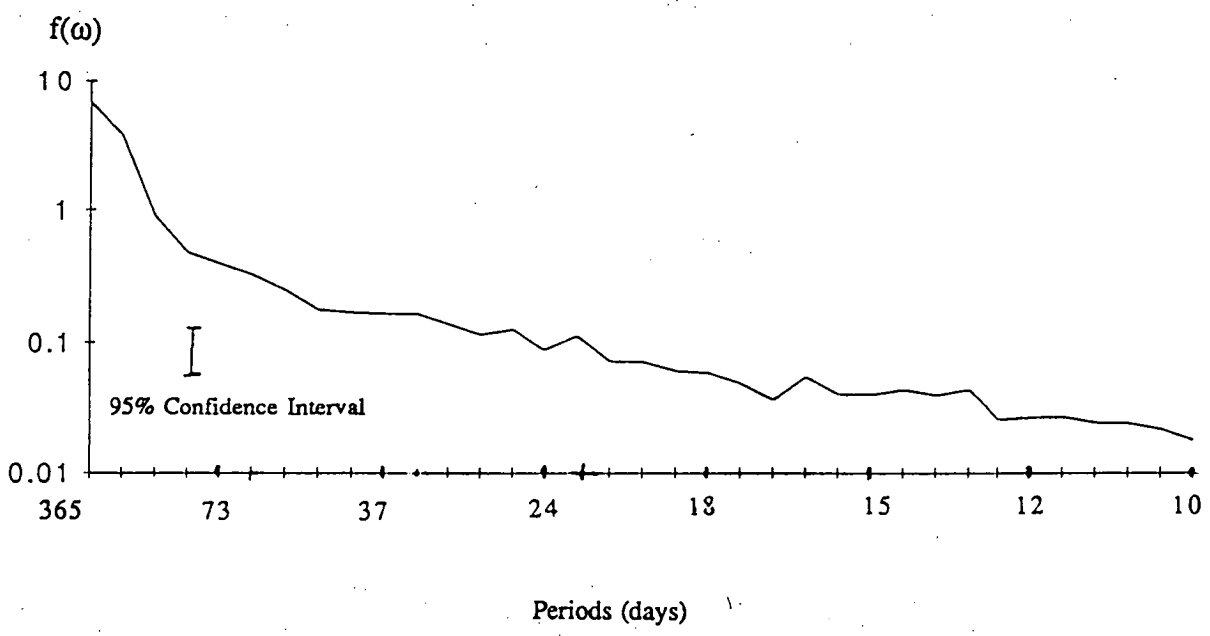

Figure 4.11 Spectral distribution of averaged 18 time series.

the dominant pattern of SST, contributing most to the variance in the SST field in the time span covering the study period. In some cases the variance may be attributed to real physical processes, and therefore these patterns may help understand the underlying causal mechanisms.

As mentioned in Chapter 3, given an anomalous SST field, denoted as X with n stations and m measurements in time, it is possible to derive an $n \times n$ correlation matrix A. Given this real and symmetric matrix A, it is possible to obtain a unique diagonal matrix D and orthogonal matrix V such that

$$D = V'AV$$

the values of the i-th element of the diagonal matrix may be ranked in order of magnitude, which corresponds to ranking the columns of V. These columns define the time-independent, spatial patterns of temperature. Alternatively, it is possible to construct the temporal matrix C such that

$$C = XV$$

Thus each column of C represents the time series corresponding to a particular eigenvector pattern. In the literature both the spatial patterns in the eigenvectors and time series are presented for analyses. In this chapter, the normal EOF technique has been applied to the deviations from the seasonal cycles of the MCSST data. The whole process can be outlined as follows: the mean value and the annual and semiannual cycles are removed from the original data, which is then normalized by its residual variance. The correlation matrix is then calculated for the EOF analysis.

Few studies have covered EOF analyses of SST for this study region and no previous studies have concentrated on the eastern Indian Ocean/western Pacific region. White *et al.* (1985) used ship observations over a four year period (1979-1982) in the Pacific basin to arrive at a series of patterns. They showed a positive anomaly off the Peruvian coast which extended westward to the dateline. A negative anomalous SST in the

western Pacific extended eastward to the dateline. The time series corresponding to this pattern is dominated by a sharp rise in the anomalies prior to the onset of the 1982/83 ENSO event. Weare (1987) used composite EOF analysis of SST to arrive at a first pattern which was quite similar to that of White *et al.* (1985).

In contrast to the above studies, high spatial and high temporal satellite-derived SSTs are used in the study region. It is expected that this analysis will highlight the spatial coherence between the eastern Indian Ocean and the western Pacific Ocean.

There are 507 grid points in the entire study area. That is to say, there are 507 EOF patterns in theory. The results of the analysis show that the first 3 patterns explain 44.3%, 15.1%, 10.3%, respectively, with the accumulating sum of 69.7%. The main features of these three patterns and their corresponding time series are discussed below. The patterns allow a compact description of SST variation during 1984-1986, however due to the short time-series they may not be stable for longer periods of time.

The first spatial pattern of EOF representing 44.3% of the total variance is shown in Figure 4.12a. It can be seen clearly that one positive centre is located at 170°E near the Equator at the western end of the Pacific equatorial cold tongue while a negative centre is located in an area from 35°S to 15°S to the west of Australia. This implies that the SST anomalies in these two areas are out of phase. The linearly increasing trend of the time series corresponding to this spatial pattern (Figure 4.12b) suggests that during these three years, positive SST anomalies have been building up in tropical areas near the dateline while negative anomalies have prevailed in the eastern Indian Ocean. This coincides with the positive anomaly build-up before the ENSO onset, also noted by White *et al.* (1985) in the Pacific basin. A trough associated with the negative centre extends from the southeast to the northwest in the south Indian Ocean while another trough in the north Pacific extends from northeast to southwest. A few major oscillations can be related to annual and semiannual cycles. Prior to 1986-87, there is a tendency for warm water to build up in the western Pacific. However the patterns are

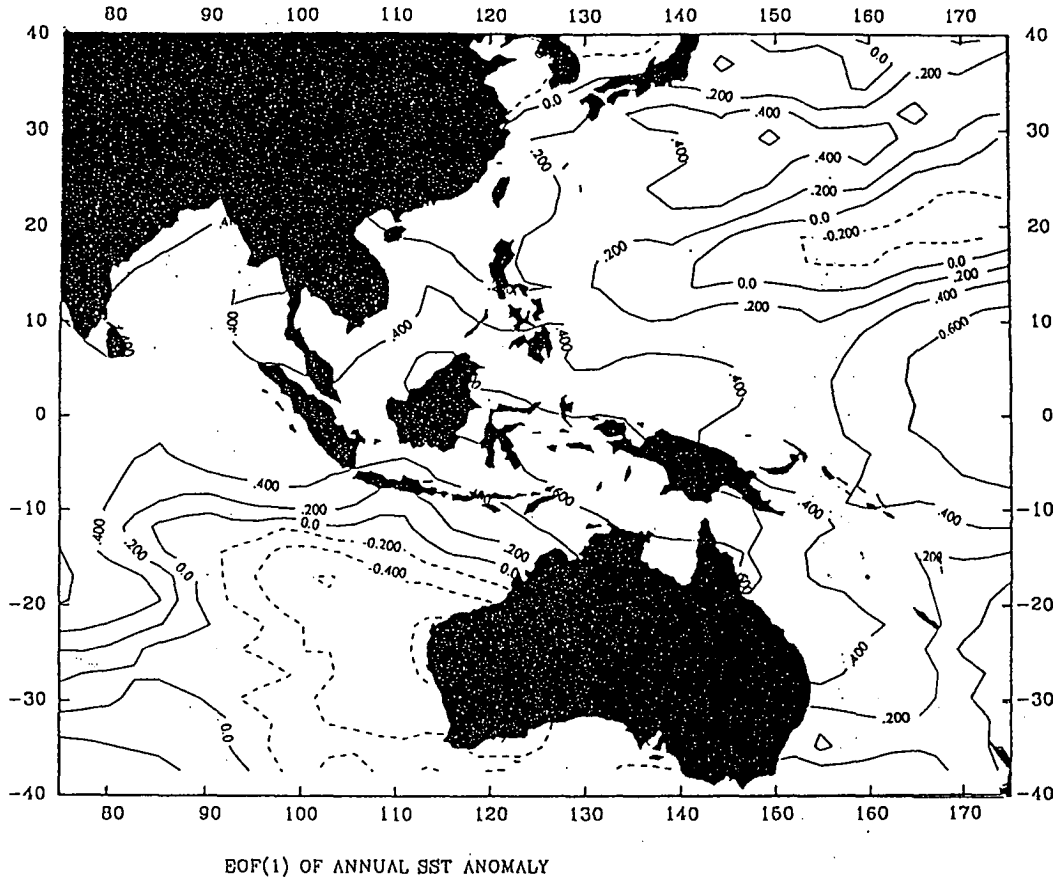

a)

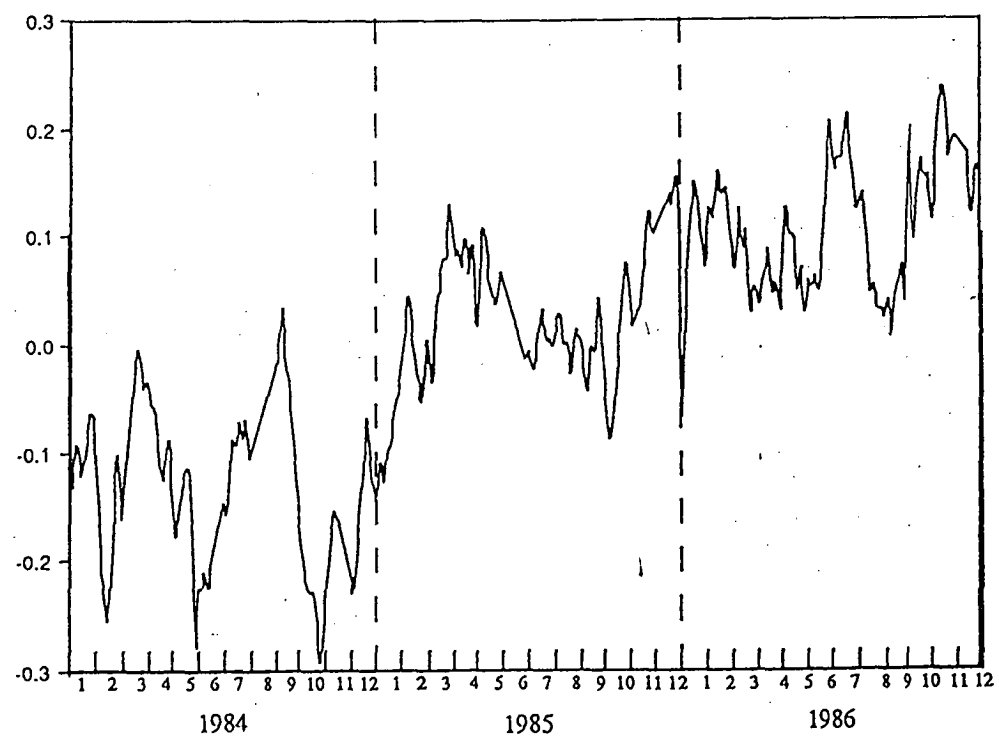

b)

Figure 4.12 The spatial pattern (a) and its time component (b) for the first eigenvector pattern EOF1 of SST anomalies. Dashed lines in (a) represent negative values..

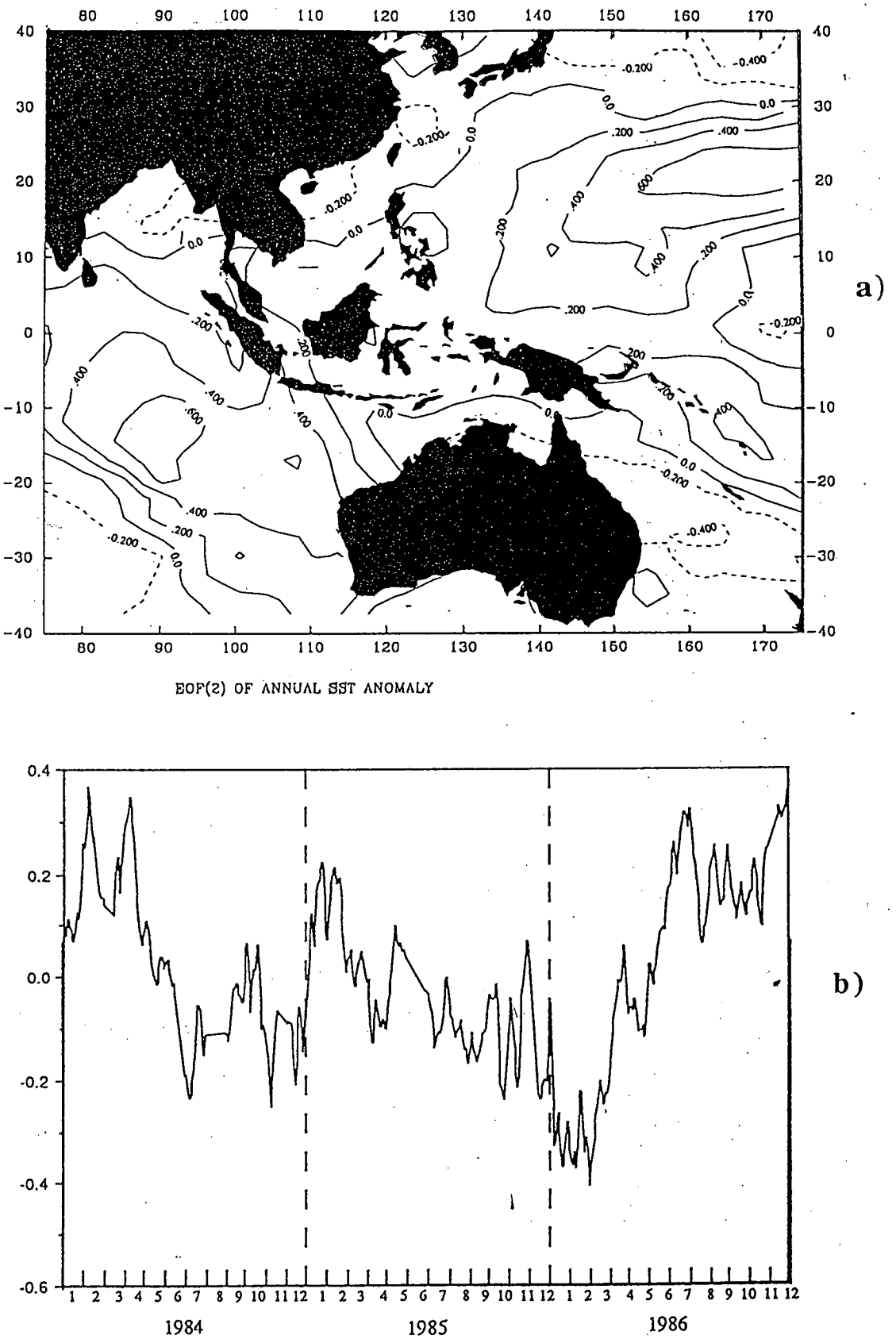

Figure 4.13 Same as Figure 4.12 except for the second eigenvector pattern EOF2

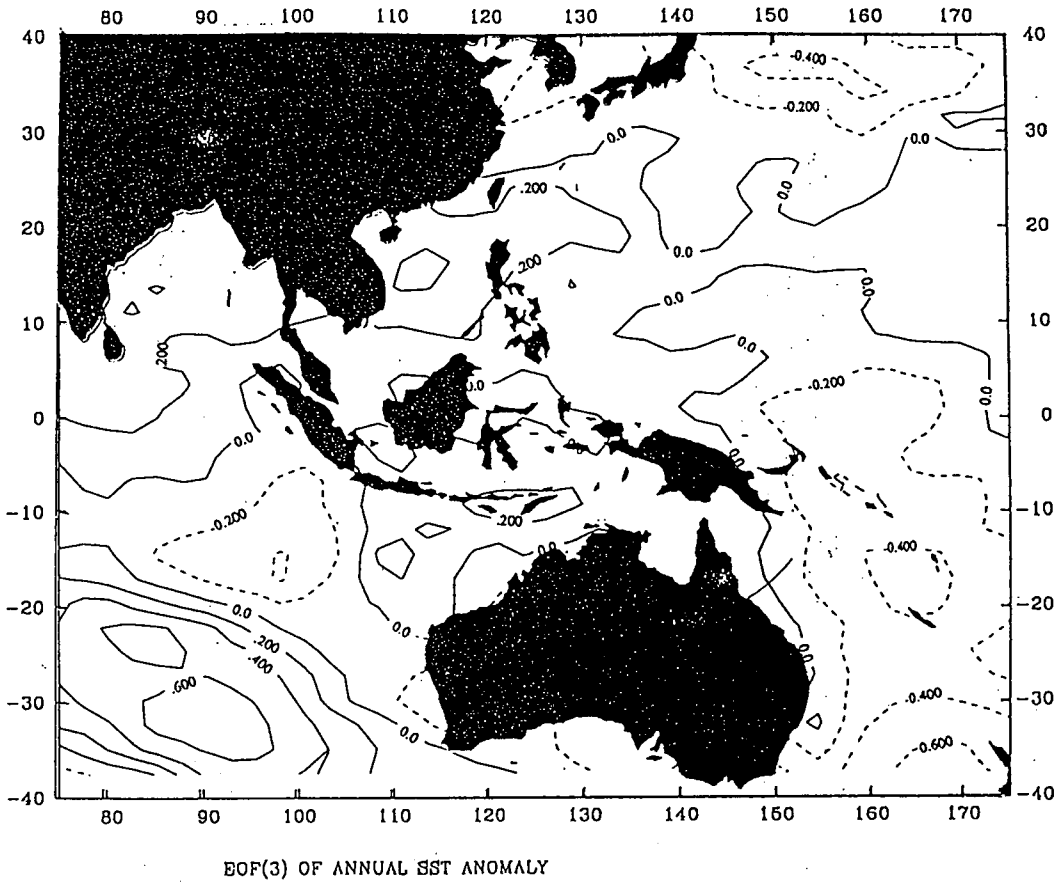

a)

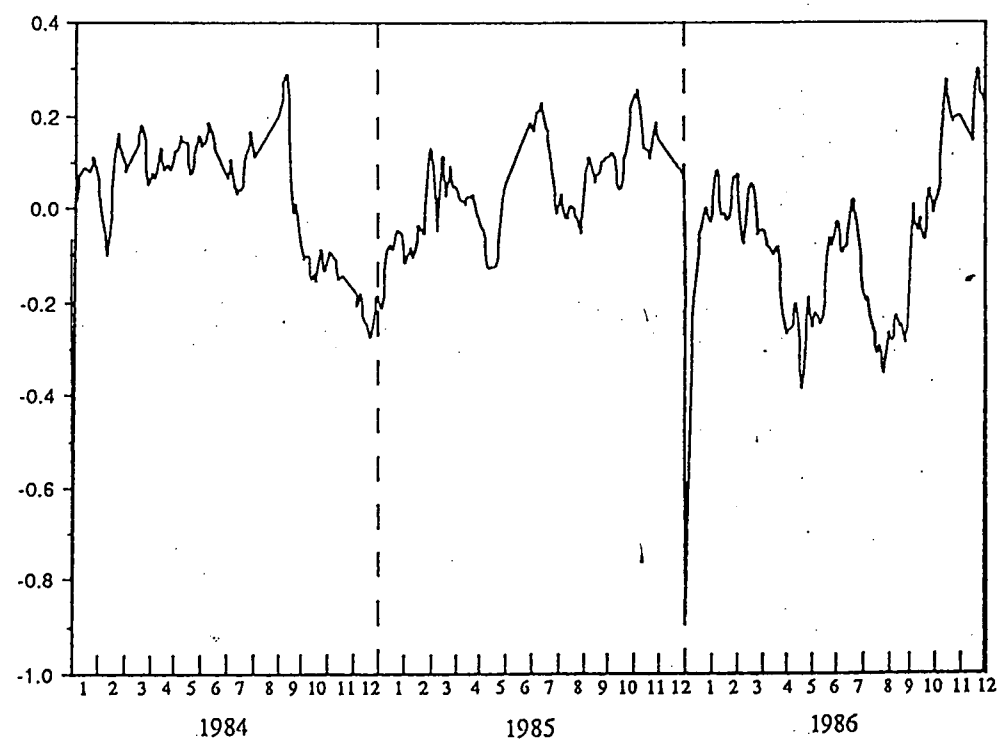

b)

Figure 4.14 Same as Figure 4.12 except for the third eigenvector pattern EOF3

still subject to modulation of the annual and semiannual cycles which dominate the SST fluctuations in this area.

In order to test whether the pattern of the first oscillation could be seen in the original MCSST data, time series of SST were chosen at two locations in the study area (Figure 4.8); one in the positive anomaly centre in the equatorial areas near the dateline, and the other in the negative centre of the west Australian coast (Figure 4.12 and Figure 4.8). The two time series are highly negatively correlated (Figure 4.15a). The cross correlation reaches a peak (-0.61) with a lead of 10 days (Figure 4.16b). That is to say, when the south eastern Indian Ocean has a positive anomaly, there will be a negative anomaly in the mid-Pacific or vice versa. The SST in the Indian Ocean will lead the Pacific by about 10 days.

To further confirm our results, a contour map of the correlation coefficients of SST at the middle equatorial Pacific (0°, 175°E) to all grid points has been presented (Figure 4.1b). It can be seen that SST in the mid Pacific is indeed negatively correlated with the SST in the south eastern Indian Ocean adjacent to Western Australia.

No obvious modulation of the annual and semiannual oscillations is evident in the time function of White *et al.* (1985) for their first eigenvector. There are a few explanations for this difference. The most important one is that the area covered in the two studies are different. White *et al.* (1985) concentrated in the entire Pacific Basin, from 50°N to 20°S. By contrast this study focused on a region bounded by 75°E to 180°E and 40°N to 40°S which is dominated by monsoons. Secondly the time span of the two studies are different, with White *et al.* (1985) concentrating in the period preceding the outbreak of the 1982/83 ENSO event. Thirdly, the temporal and spatial resolution of the data are different.

The second EOF pattern (15.1% of the total variance, see Figure 4.13a) shows another interesting feature. There are two positive centres located in the North Pacific near 20°N and the southeastern tropical Indian Ocean. The time series corresponding to this

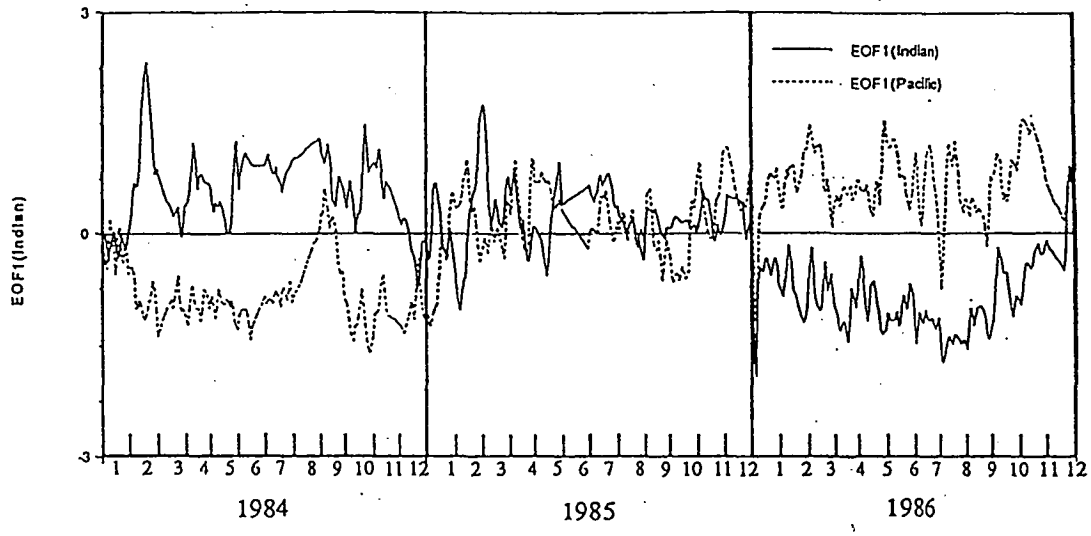

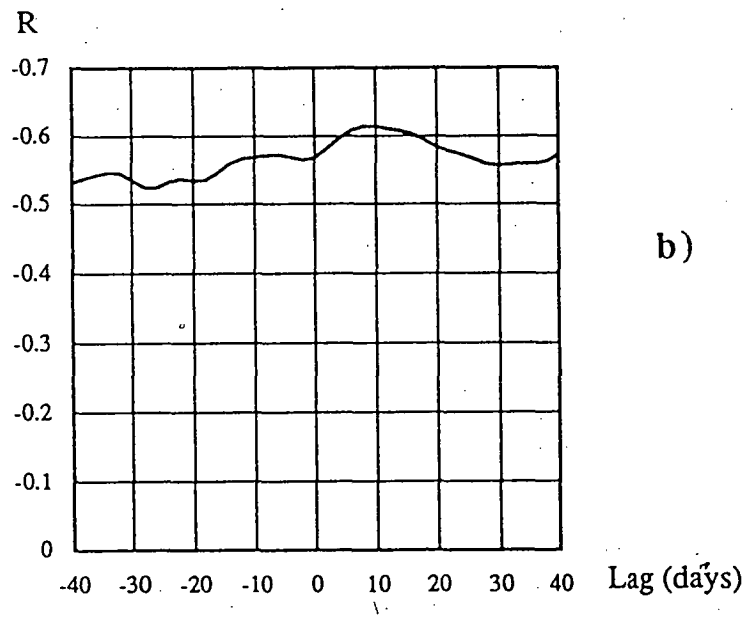

Figure 4.15 Time series (a) and their cross correlation coefficients (b) of MCSST near two centres in EOF1 during 1984-86

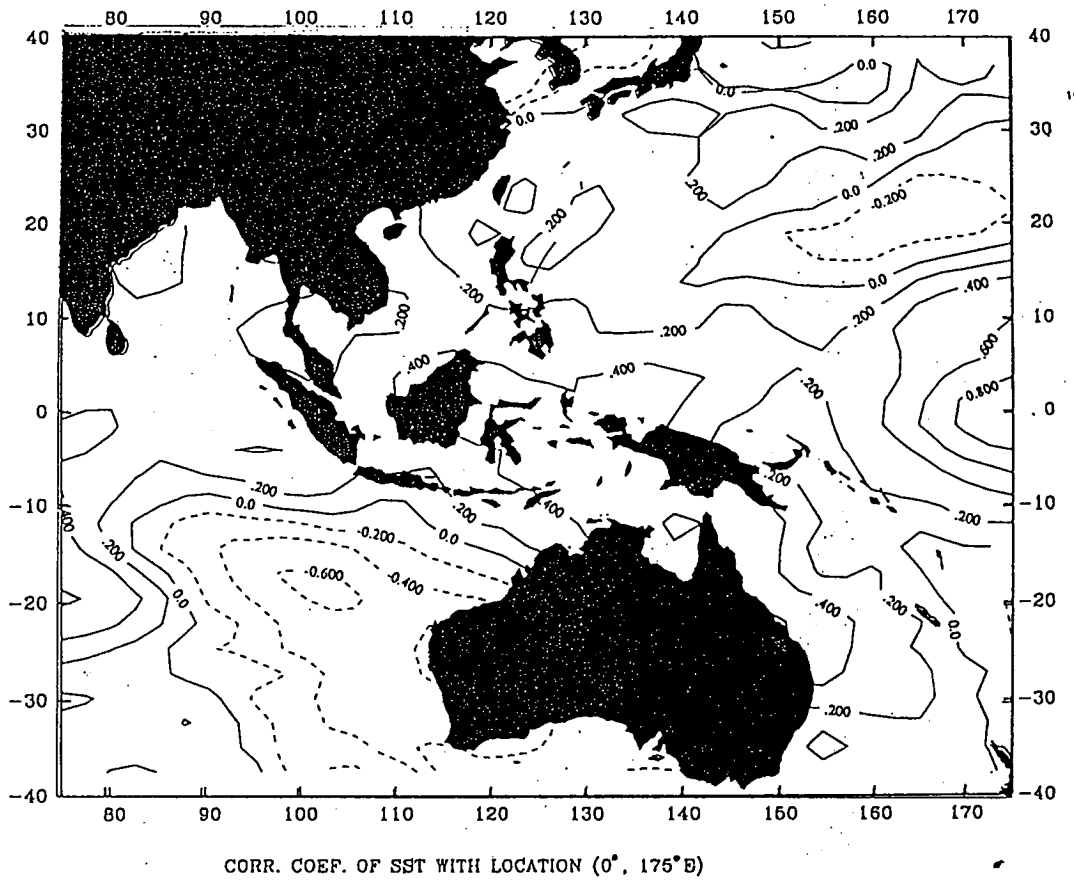

Figure 4.16 Spatial distribution of correlation coefficients related to the grid point (0°, 175°E). Dashed lines represent negative values.

pattern (Figure 4.13b) suggests these anomalies are in phase and are more likely related to interannual oscillations during 1984-1986 with a time scale of two to three years.

The two positive centres do not coincide with their corresponding centres in the first EOF pattern. Rather in the case of the Pacific centre, it is displaced northward to latitudes between 20°N to 25°N. The Indian ocean centre is also displaced from the centre in the first EOF pattern, but in a northwest direction to occupy position between 10°S to 15°S. An examination of the climatology of sea surface pressures for this region shows that these two centres coincide with the subtropical high pressure region in the case of the northern Pacific, and a local trough in the Indian ocean which is related to the ITCZ. We postulate here that the second pattern of the EOF is related to a quasi-biennial oscillation, perhaps of a global scale, but with the two centres acting in unison. By contrast the first EOF pattern shows a build-up (cooling) in the tropical Pacific (Indian ocean) in anticipation of the ENSO event.

A positive centre located in the southeastern Indian Ocean and a negative centre in the southwestern Pacific are the main features of the third EOF pattern (10.3% of the total variance, see Figure 4.14a). The time series corresponding to this pattern (Figure 4.14b) suggest an interannual oscillation mechanism as well as longer time scales.

It is worth noting that all three EOFs have produced centres of large-scale spatial coherence of SST in the Southeastern Indian Ocean near the region identified by Nicholls (1989) as an area where SST variations influence Australian rainfall. The time series suggests that positive anomalies develop in these two areas before April of 1985 while negative anomalies develop after this date. The SST pattern after April 1985 could be related to the lack of drought in Australia during the 1986-87 ENSO. According to Nicholls (1989) lower SST in the Southeastern and Central Indian Ocean is related to higher rainfall in parts of Australia.

4.5 Summary

This chapter has investigated the spatial and temporal field of SST in the study region covering 40°S to 40°N and 70°E to the dateline, in preparation for a study of the influence of SST on convection processes. Previous studies (Graham and Barnett, 1987; Steiner and Khalsa, 1987; Gutzler and Wood, 1989) have shown that an SST of about 28°C is a necessary but not sufficient condition for convection to occur. At higher temperatures, other processes dominate in the development of convection.

If an isotherm of 28°C is accepted as the boundary for potential convection to develop, then it is possible to examine the mean SST climatology of the study region to provide a background for convection. An examination of Fig 4.2 reveals that on a annual mean basis there is a wide latitudinal band (15°N to 5°S in Indian ocean; 10°N to 15°S in the Pacific Ocean) where convection can potentially develop. On a seasonal basis there is a warm zone of SST greater than 28°C in the northern winter (Figure 4.3). A general feature is that this warm zone is larger in the Pacific than in the Indian Ocean.

A number of studies (Weickmann, 1983; Lau and Chan, 1985; Meehl, 1987) have used OLR as a surrogate for convection and have examined the temporal scales of this process. They find that convection displays variability at scales ranging from weeks to years. It is clearly worth investigating whether SST varies at similar time scales. In this study a harmonic analysis has been used to analyze the annual and semiannual cycles. Spectral analyses, covering a wide range of frequencies has also been done. Finally EOF analysis have been done to observe the dominant spatial patterns and their temporal variability.

The pattern for the annual amplitude and phase (Figure 4.7a) shows very small amplitudes in the equatorial region, but opposing phases in the Equatorial Pacific and Indian Oceans. The discontinuity in phase angle in the Malaysian-Papua New Guinea region serves to partition the effective areas of the Asian and Indian Monsoon systems.

No clearcut pattern can be derived between these oscillations and the mean OLR climatology from Meehl (1987).

In contrast the semiannual pattern shows a good agreement, both in magnitude and phase with Meehl's OLR pattern. High amplitudes in the tropics are correlated with zones of high convection (Meehl, 1987), and high SSTs occur prior to the onset of maximum convection. Once convection starts the SST decreases in response to the loss of heat in the upper layers of the ocean. Beyond a certain temperature convection stops and the ocean proceeds to warm again. Typical peaks of SST for the northern hemisphere occur in May and November. Beyond November the seasonal processes cool the ocean until warming occurs again the following spring.

The results of the EOF analyses show a see-saw pattern of SST anomalies between the middle equatorial Pacific and the south eastern Indian Ocean. The time series corresponding to this pattern shows a linear interannual trend which is observed as a build up of positive SST anomaly in the western Pacific and negative anomaly in the eastern Indian Ocean. This pattern provides a background for the eastward shift of convection which is typical of ENSO events.

No evidence was found to suggest that the 30-60 day oscillations in SST are significant. While there are obvious 30-60 days oscillations of the large-scale convection, one would suspect that a similar situation may exist in the fields of SST. The spectral analyses in this chapter do not support the hypothesis. Other factors such as wind and moisture may be responsible for the 30-60 day oscillations. This will be investigated in the next chapters.

Chapter 5. The Variability of Wind Field

5.1 Introduction

Wind forcing on the ocean is one of the most important processes in climate variability because it drives ocean currents, which modify the sea surface temperature, and it affects sensible and latent heat fluxes between the ocean and the atmosphere. While it is generally understood that the pattern of SST anomalies plays an important role in the development of large scale tropical convection, the non-linear relationship between SST and convection above a threshold temperature of about 27.5°C (Graham and Barnett, 1987) suggests that other factors need to be considered. This consideration needs to be specially in focus in the western Pacific, where the global warm pool of oceans with mean sea surface temperature at about 29°C is located.

Deep convection in the tropical atmosphere arises from a combination of dynamical and thermal processes. Dynamical convection occurs when surface wind converges (or upper level wind diverges) from its surrounding area; while thermal convection occurs when the air is locally heated and becomes warmer than its surroundings. Moisture contained in the ascending air releases latent heat at some stage, thus further enhancing convection. Sources of moisture may originate locally from evaporation at the ocean surface, or be transferred from other areas by wind. Over tropical areas, these processes are actively involved with the wind field, thus making it necessary to study the wind variability in order to fully understand the convection process. In this Chapter a general description of the wind field during 1984-86 is presented to provide a background for the analysis of wind divergence and convection in Chapter 6.

This chapter will address some questions concerning the wind field of the tropical eastern Indian and western Pacific Oceans. Firstly, are there any biases in the seasonally averaged wind field during 1984-86 compared to the long term climatology?

If so, do they have any special relationship to the onset of the 1986-87 ENSO event, or to the development of large scale convection in the equatorial western Pacific? Secondly, what are the main features of the wind field at different time scales, from interannual, annual, intraseasonal, or even shorter (to cover the westerly burst)? Thirdly, what are the most important processes in the wind field associated with the development of large scale convection? Is there a specific time interval, region or layer in the wind field associated with convection?

A detailed description of the wind data and the methodology used in this chapter has been presented in Chapter 3. The data sets used in this chapter are the five-day running averages of wind velocities at 850 mb and 200 mb. Averages and standard deviations have been calculated for the four seasons as defined in Chapter 4 for the three years from 1984 to 1986. Wind divergences for the four seasons were calculated using the central finite difference approach. Harmonic analysis was then applied to derive parameters of annual and semiannual cycles. The band-pass (30-65 days) filtered wind data are then used to study the intraseasonal behaviour of the wind field.

The organization of this chapter is as follows: In Section 5.2, the seasonal means of wind at 850 mb and 200 mb during the study period of 1984-86 are described to provide a background knowledge of the wind fields in the lower and middle troposphere. The annual and semiannual cycles depicted by harmonic analysis are discussed in Section 5.3. In Section 5.4, the intraseasonal variations by using bandpass-filtered (from 30-65 days) data is presented along longitudinal and latitudinal lines, respectively to examine spatial structure in the area between the mid-Indian Ocean to mid-Pacific. Longitude-time diagrams of these filtered wind data at different zonal bands are presented in Section 5.5. A summary and discussion will be given in the last section.

5.2 Seasonal means: 1984-86

A complete set of plots of the 1984-86 seasonally averaged wind vector and the corresponding divergences at two layers, 850 mb (Figure 5.1) and 200 mb (Figure 5.2), is presented in the discussion of the wind field. The averaged wind field is represented in vector format and the averaged divergence is denoted by contour lines. Divergences are calculated using three-point central finite differences. The unit of wind velocity is in ms^{-1} and the unit of divergence is 10^{-6} sec^{-1}. For 850 mb (200 mb) divergence field, areas with value larger than 2×10^{-6} sec^{-1} (4×10^{-6} sec^{-1}) are shaded in red while areas with value less than -2×10^{-6} (-4×10^{-6} sec^{-1}) are shaded in green. The validation of the wind field has already been described in Chapter 3.

5.2.1 850 mb wind field

The Asian Winter Monsoon is the most striking feature during DJF (Figure 5.1a) at 850 mb. In the northern hemisphere, north of 23°N, the northwest wind blows down from Siberia and becomes the westerly east of Japan. South of 23°N, the northeast trade merges with the northeast monsoon in the South China Sea. This branch of the monsoon becomes a westerly wind after passing the equator due to the Coriolis effect. In the southern hemisphere, the westerly Roaring Forties are dominant in mid-latitudes, while the easterlies are dominant north of 30°S. A strong equatorward component of wind is observed in the eastern Indian Ocean. The zonal component of the northeast trade in the northern hemisphere is strong when the zonal component of the southeast trades in the southern hemisphere is weak. Such an out of phase relationship in the zonal wind field between the two hemispheres has been noted by Crowe (1951), and Wyrtki and Meyers (1976). The divergence field shows four areas of strong convergence in the tropical region: west of Java and Sumatra near 10°S and 80°E, east of the Philippines, east of Papua New Guinea and along the northwest coast of Australia respectively. The first centre is associated with the ITCZ,

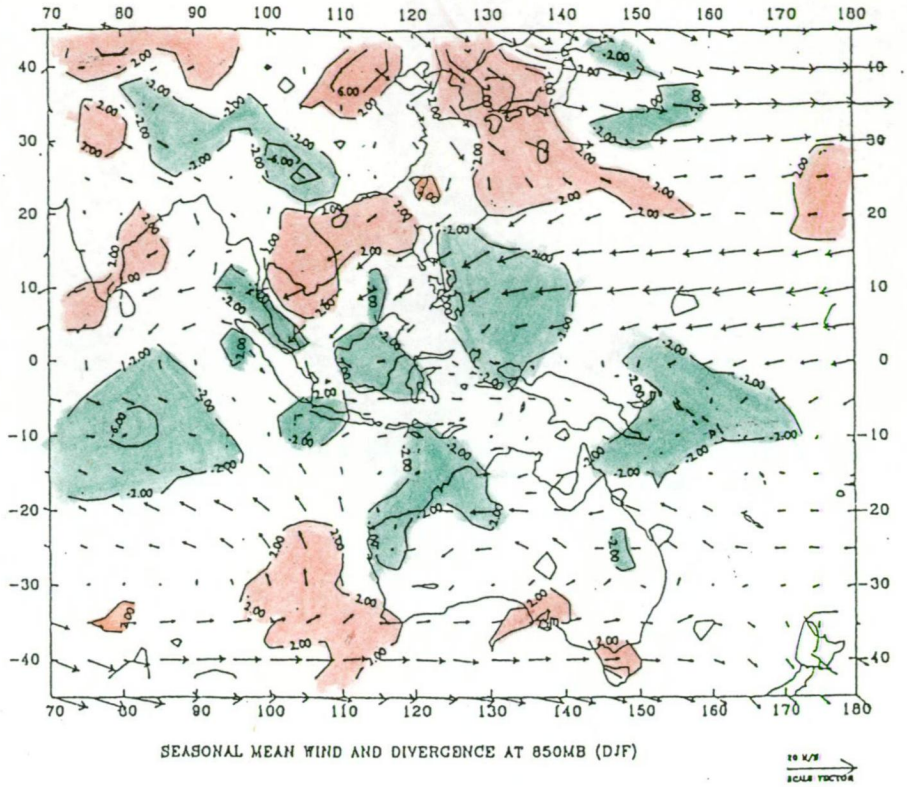

a)

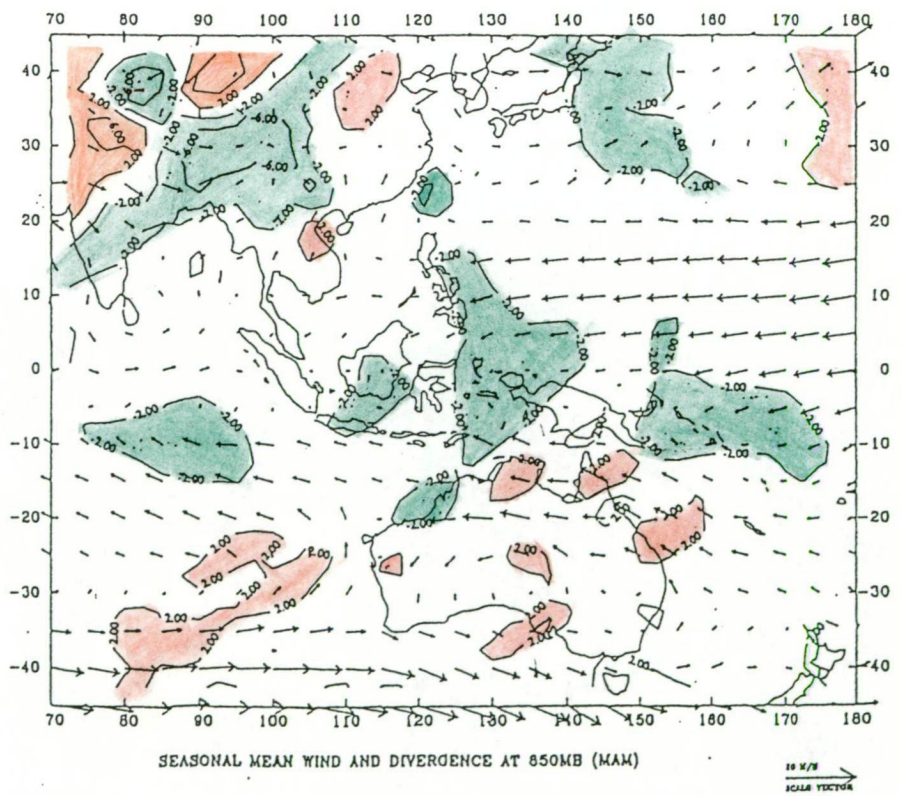

b)

Figure 5.1 Three years (1984-86) seasonal means of wind and divergence at 850 mb. (a) December-January-February (DJF); (b) March-April-May (MAM); (c) June-July-August (JJA); and (d) September-October-November (SON). The units of OLR are in Wm^{-2}. Areas with divergence larger than 2×10^{-6} sec^{-1} are shaded red, less than -2×10^{-6} sec^{-1} are shaded in green.

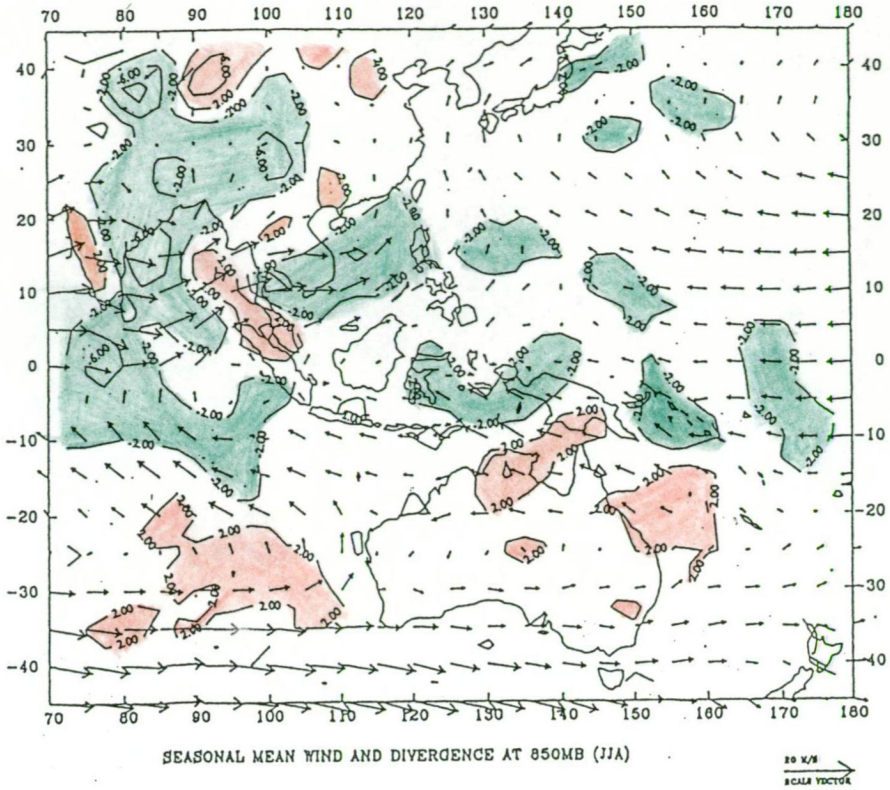

c)

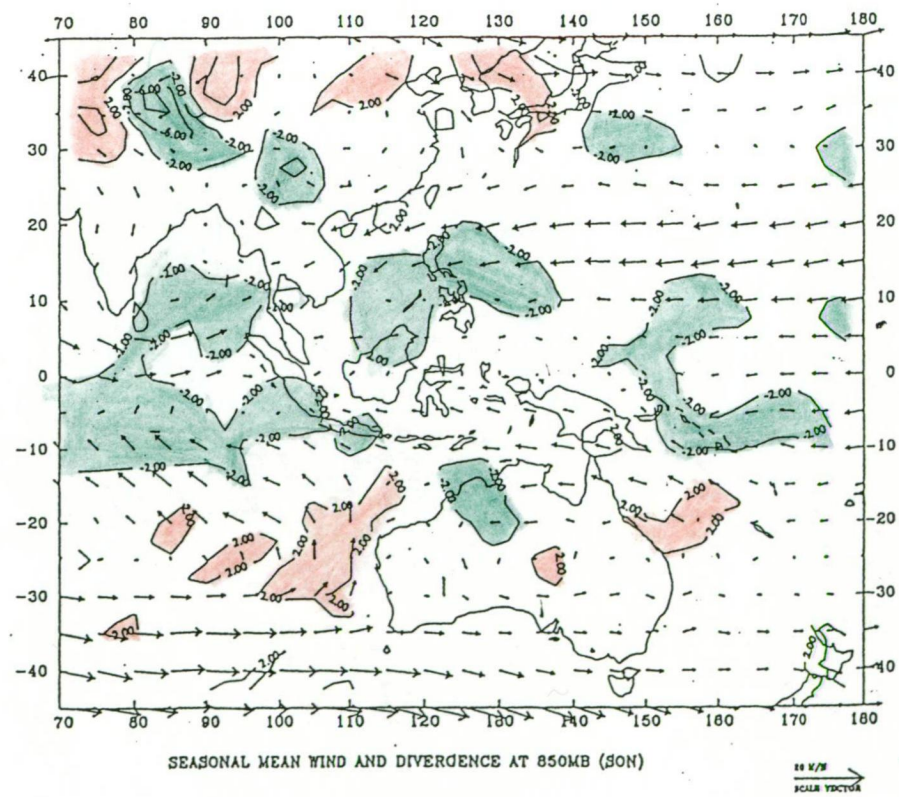

d)

Figure 5.1 (Continued)

which is in the southern hemisphere in the Indian Ocean in this season. The second is in associated with decreasing speed along the trajectory of the core of the northeast Trades and may be associated with the ITCZ of the Pacific. The third one is at the eastern end of a belt of westerlies between 0°-10°S and is mainly associated with the SPCZ. The centre of divergence located west of Australia near 30°S, 105°E is the jet of the Australian Monsoon. Rasmusson and Carpenter (1982) also documented the two areas in the western Pacific and described this region as a feature of the ITCZ and the SPCZ.

The Asian winter monsoon greatly reduces in strength and retreats northward during MAM (Figure 5.1b). The boundary between easterly and westerly winds in the north Pacific shifts northward near 30°N at the dateline and at 22.5°N near Taiwan. The convergent wind centre in the Indian Ocean shifts eastward from about 80°E to 85°E and decreases in intensity. The centre east of the Philippines weakens and moves southward to the Banda Sea while the one east of Papua New Guinea remains the same.

The Asian Summer Monsoon reaches its peak during JJA and the Bay of Bengal is associated with a large scale convergence (Figure 5.1c). The boundary between the easterly and westerly winds in the northern Pacific moves north to 35°N. A strong easterly blows in the areas north of Australia and near Papua New Guinea. The centre of convergence east of the Philippines now weakens and a new one develops in the South China Sea near 15°N at the eastern end of a belt of westerlies between 0°-20°N. Accompanied with this new convergence centre, there is a strong divergence centre in the Indo-China Peninsula.

The climatological data presented by Rasmusson and Carpenter (1982) do not show the convergence in the South China Sea, and the divergence in the Indo-China Peninsula is only weakly developed. The stronger convergence in the South China Sea may be

associated with a stronger westerly component over the same area during this study period.

The retreat of the Asian Summer Monsoon and the start of the Winter Monsoon are the main features in the SON map for northern hemisphere (Figure 5.1d). A convergent centre near the Philippines is stronger than the previous season, while the one east of Papua New Guinea weakens in strength. It should be noted that the large convergent area over the Bay of Bengal now disappears in this season and the convergent centre over the equatorial Indian Ocean expands slightly southeastward.

As mentioned in Rasmusson and Carpenter (1982), unlike the northern hemisphere ITCZ, the SPCZ shows only small seasonal changes in position. Horel (1982) also noticed the weaker annual cycle in convergence near the SPCZ. This fact has been further confirmed in this study by observing the strength and positions of the three convergent centres.

5.2.2 200 mb wind field

The wind field at the 200 mb level is described in this section to provide background knowledge on the circulation in the upper troposphere, and therefore may provide some further insights into large scale convection which will be discussed in the next chapter. The main features of the annual variation of the wind field at 200 mb are the changes in the boundaries and strength of the equatorial easterlies, and the changes in the active centres of convection such as the ITCZ and the SPCZ (Figure 5.2). The areas of divergence larger than 4×10^{-6} sec^{-1} are shaded in red and less than -4×10^{-6} sec^{-1} in green. The wind field at this level is more uniform than that at 850 mb. The wind field at lower level is more influenced by small scale and localized thermal and dynamical effects. In addition, the convergence field at 200 mb is complementary to that at 850 mb. That is to say, at 850 mb, the equatorial zone is generally a zone of convergence and the higher latitudes are zones of divergence. By contrast, at 200 mb, the equatorial

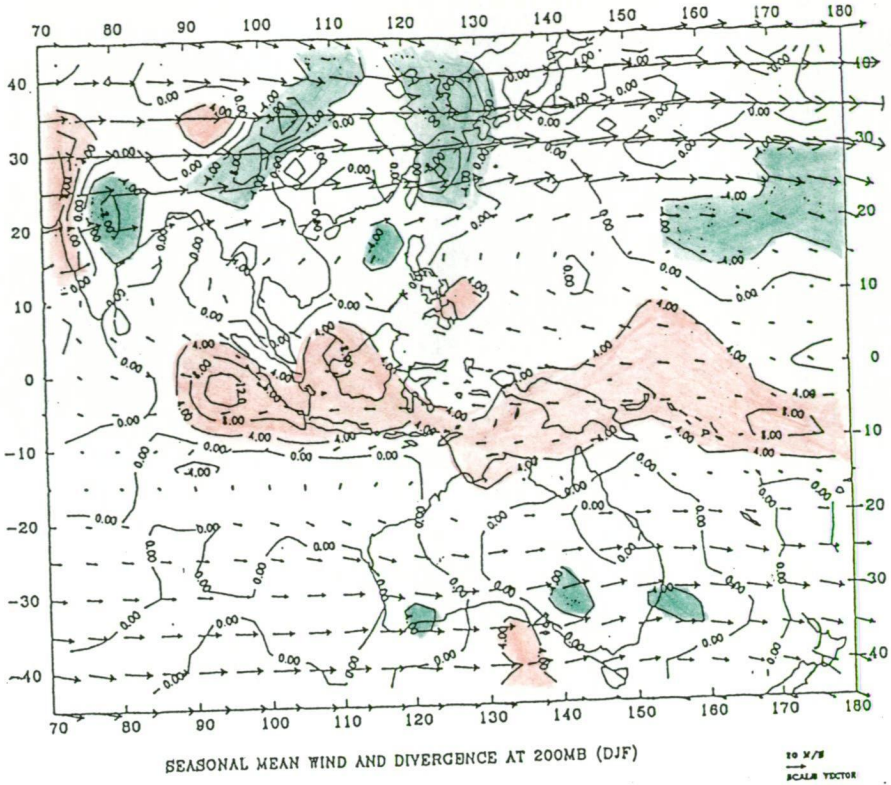

a)

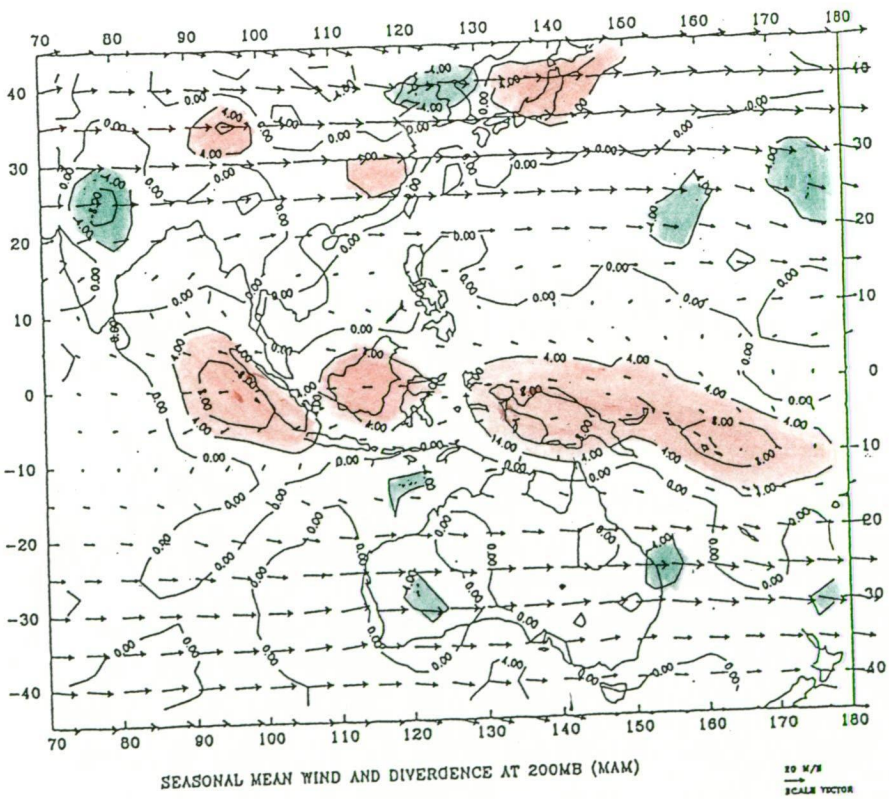

b)

Figure 5.2 Same as Figure 5.2 except for 200 mb level. Areas with divergence larger than 4×10^{-6} sec^{-1} are shaded red, less than -4×10^{-6} sec^{-1} are shaded in green.

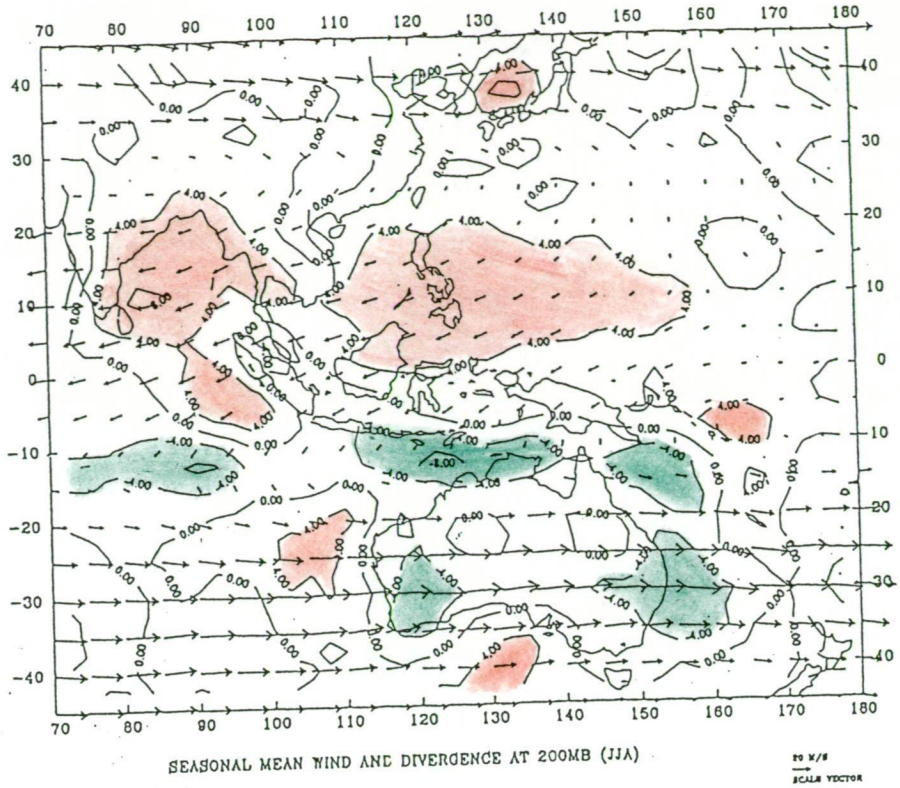

c)

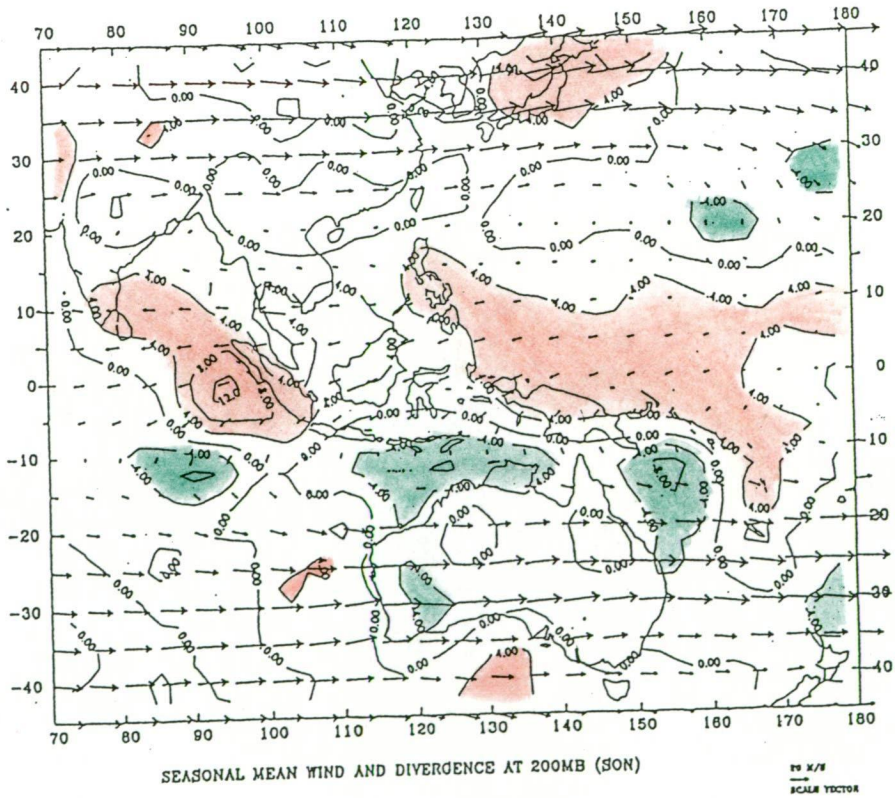

d)

Figure 5.2 (Continued)

areas are generally zones of divergence (corresponding to the large scale convection, i.e. ITCZ and SPCZ) and the higher latitudes are convergent.

In DJF, while the easterlies are prevailing in the equatorial areas from 15°S to 15°N, the westerlies are prevailing at higher latitudes in the study region (Figure 5.2a). This distribution is similar to those of Sadler (1975) with data from the 1950s to 1973 and Arkin (1982) who studied the wind field from 1968 to 1979. This agreement confirms the accuracy of the wind data and shows that the upper level circulation in DJF during the three years did not demonstrate any large bias from the long term average. The equatorial areas are divergent areas. In particular, two divergent centres are noted: one is located west of Sumatra and the other one east of Papua New Guinea near 170°E.

In MAM, the easterly wind regime contracts to a narrower band encompassing latitudes 10°N to 10°S. Furthermore the northern hemisphere westerly regime extends to the equator near the dateline (Figure 5.2b). Along with this shift, the ITCZ zone of divergence strengthens and shifts southward, especially near the dateline. The convergence centre previously located near 5°S now shifts southward to about 10°S near the dateline and extends to Sumatra. This may indicate that the merging areas of SPCZ and ITCZ shift westward.

In JJA, the wind system in the northern hemisphere changes significantly from that of the previous season. The easterly wind expands near 25°N in the equatorial mid-Indian Ocean, but changes little east of 160°E (Figure 5.2c). Again, the distribution of the wind field is similar to that reported by Arkin (1982). It is noticed that the divergent band weakens and retreats back to west of 155°E and shifts northward to near 15°N. At this time, a narrow convergent zone located near 10-15°S develops over the cooler water in the south Java upwelling zone during JJA. There was no significant convergent centre in that area during the previous two seasons. The upper level wind field shows a stream of air blowing from the divergent area off Mindanao to the convergence near 10°S, and the surface wind (Figure 5.1c) is directed back toward

Molucca Sea suggesting the presence of a largely closed convection cell within the tropical region of Australasia.

The wind field in SON is similar to that of JJA except that the easterly over the northeastern Indian Ocean is weaker (Figure 5.2d). The divergent centre just west of Indonesia strengthens and the divergent centre north of New Guinea expands. It is interesting to notice that while the divergent zone shifts southward near the Equator, the convergent zone near 10-15°S has not changed significantly in either position or strength. This convergent zone is not obvious in the two other seasons of DJF and MAM. The cause and implication of this feature will be discussed later.

The comparison of the wind fields at 200 mb and 850 mb shows several interesting features. At the 850 mb level, the tropical areas from 30°S to 30°N are generally occupied by the easterlies (both southeast and northeast trades) in the Pacific Ocean. The southwest Asian monsoon disrupts the above simple pattern. At 200 mb, the easterlies are limited to the bands of 10°S to 10°N and the westerlies prevail at higher latitudes. In other words, within the equatorial zones, both lower and upper tropospheres are occupied by easterlies, except that in northern summer, the southwest Asian monsoon crosses the equatorial Indian Ocean. Between latitudes of 10° to 30° in both hemispheres, the wind directions at the two levels are generally opposite: the easterlies blow in the lower level and westerlies in the upper level. This scenario is different again in the northern summer when the southwest Asian Monsoon goes across the zone in the northern Indian Ocean between 10°N to 30°N. Beyond the latitudes of 30° in both hemispheres, westerlies are prevalent.

The comparison between the convergence fields of 200 mb and 850 mb shows some interesting features. Firstly, the convergence fields at the two levels are generally opposite in sign. In other words, a convergent zone in the lower troposphere corresponds to a divergent zone in the upper troposphere, and vice versa. This is especially obvious in tropical areas where the ITCZ and SPCZ are located. While this

inverse relationship is expected from dynamical considerations, its appearance in the calculated divergence fields is an exacting test of the quality of the wind data, and its appearance increases the confidence in the reality of the features that were described. Secondly, the intensity of the convergence field is weaker at lower levels than at the higher levels. At 850 mb, the areas of strong convergence ($> 4\times10^{-6}$ sec^{-1})are much smaller than those at 200 mb, and are more randomly distributed. This is due to the fact that air density is not incorporated into the calculation of divergence. The rarefied air aloft has to move faster to balance the inflow of denser air at the lower level. This also suggests that the lower level convergence is more influenced by local "heat spots" while the upper level convergence is more influenced by the large scale dynamics. Thirdly, as mentioned above, there is a strong 200 mb convergent zone north of Australia in JJA and SON. This zone is also reflected in the 850 mb divergent areas in the Coral Sea and north of Australia.

The global Hadley cell circulation presented by Lockwood (1974) shows that air masses ascend over the equatorial area and then subside over the mid-latitudes. Therefore, the convergence zones near the 10°S exhibited in Figures 5.2c and 5.2d must be interpreted as "local" features. That is, both sources and sinks exist within the maritime north Australian / Indonesian area. It should be noticed that while the upper convergent zone (200 mb) is very distinct in its band shape during JJA and SON, the surface divergences at the two seasons do not have a coherent contiguous structure; rather they are scattered over a large area. The relationship between the convergent zone and the SST field in the Indonesian area will be expanded in the next chapter.

5.3 Annual and semiannual cycles

The seasonal description of the wind field has been presented in the previous section. To give a more compact description of the annual and semiannual cycles of wind field, harmonic analysis has been applied to the study area. A detailed description of harmonic analysis has been presented earlier in Chapter 3. The amplitudes and phases

of the annual cycles and semiannual cycles, and the variance contributed by the two cycles, for each of 850 mb and 200 mb are depicted in Figures 5.3 - 5.6, where the length of the arrow represents the amplitude of a cycle and the direction of the arrow represents the phase of a cycle. For the annual cycle, pointing to the east means the maximum of the cycle occurs on January 1st, pointing to the north April 1st, etc. For the semiannual cycle, pointing to the east means the maximum of the cycle occurs on January 1st and July 1st, pointing to the north February 16th and August 16th, etc. Contour lines superimposed on the maps are the percentages of variance accounted by annual (or semiannual) cycle to the total variance derived from the five-day running average (sampled every second day). For annual (semiannual) cycles, areas with values larger than 20% (5%) are shaded in red.

5.3.1. Annual cycle

5.3.1.1. 850 mb wind field

The amplitude of the annual cycle in both the zonal and meridional wind shows great spatial variation (Figure 5.3). The northern hemisphere has the largest amplitudes where the Asian monsoon is dominant. For zonal wind, an area larger than 4 ms^{-1} is located along the band covering 70°E to 150°E, and north of the Equator up to 20°N. The largest amplitudes of 8 ms^{-1} are centred near the Malaysian Peninsula (Figure 5.3a). Gutzler and Harrison (1987) obtained similar results, but with much less island station data. The observed pattern is due to the Asian Summer and the Winter Monsoons in the area. Another high is located north of 25°N and east of Japan, where the strong Asian Winter Monsoon contributes the large annual variation.

Close examination of phases of annual cycle shows some further features. It is clear that from the Equator to 15°N and eastward of the Philippines, the annual amplitude of the easterly winds decreases eastward and the timing of the maxima is gradually delayed. The annual cycle peaks in July in the Indian Ocean which corresponds to the strongest Indian Monsoon and in September near the dateline. In the Pacific Ocean

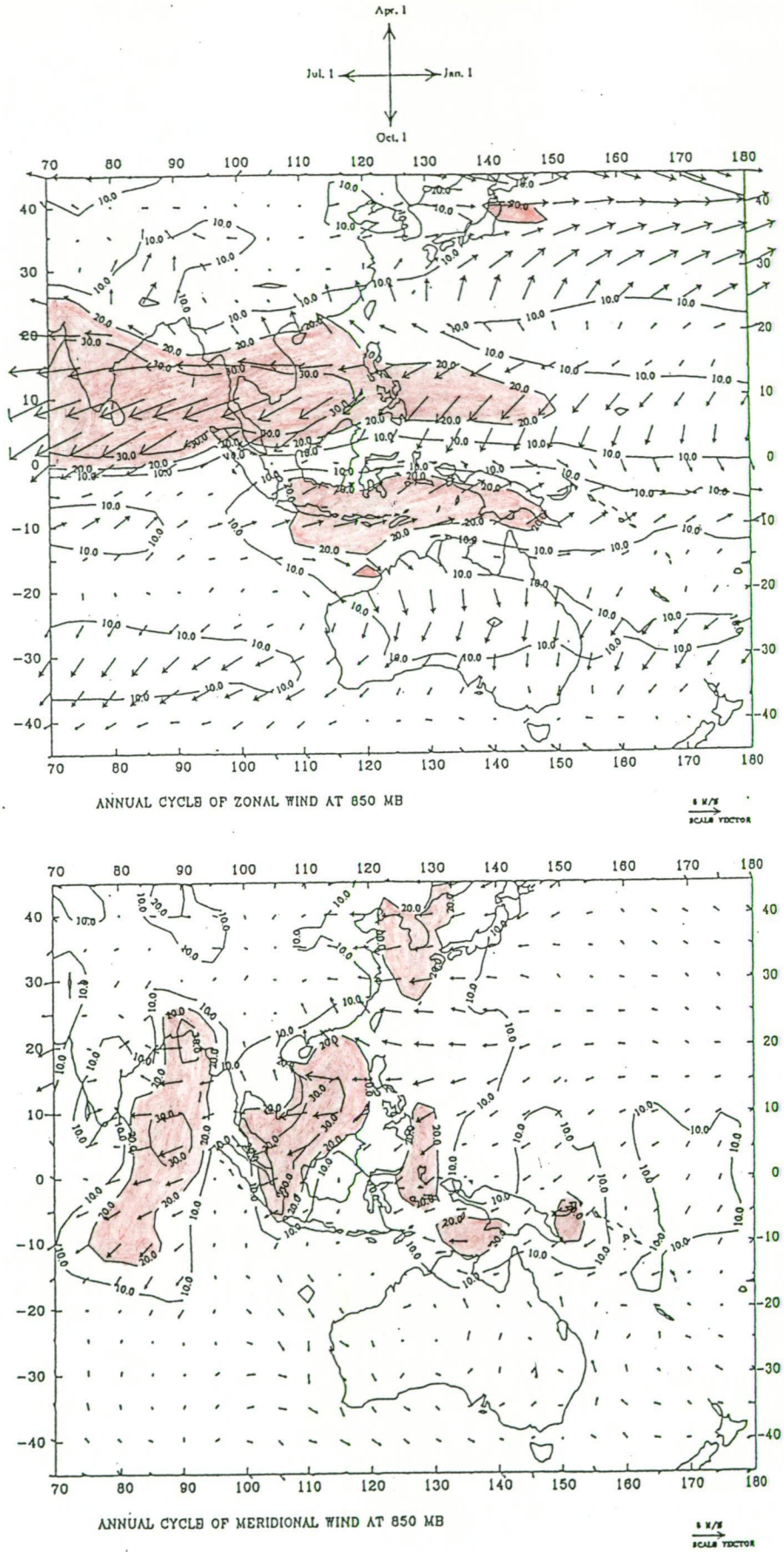

Figure 5.3 The amplitude, phase and percentage of contribution to the total variace of annual cycle of 850 mb wind field: (a) zonal component and (b) meridional component. Areas with the percentage larger than 20% are shaded in red.

north of 20°N, the westerly peaks in the northern winter from December to February, which coincides with the Asian winter monsoon. South of the equator, the area north of Australia has the largest annual amplitudes in tropical regions. The westerly in this area reaches its peak in January when the Australian Monsoon is strongest. Horel (1982) documented similar results using the zonal wind along the equator. In general, the amplitude of the annual cycles in the mid-latitudes in both hemispheres is very small, with the exception of the area east of Japan. This is especially evident south of 40°S. This implies that either the wind systems in these areas are very stable or some other cycles with different frequencies are contributing more to the total variance.

The areas with the largest annual amplitudes (the northern Indian Ocean and South China Sea and the area north of Australia) are generally consistent with the highest percentage contribution by the annual cycle. However, the contribution of the annual cycle is not very large east of Japan, since the total variance of the zonal wind component is relative high in this region.

The meridional winds also show great spatial variation in their annual cycle (Figure 5.3b). Three areas, all in the northern hemisphere, have maximum amplitudes larger than 3 ms^{-1} . One area is in the Bay of Bengal, the second is from the South China Sea and the third is in the western end of the Pacific Ocean from Korea to the east of the Philippines. These three areas are all strongly influenced by the Asian Monsoon. The southerlies in these three areas all reach their peaks in July, when the Asian Summer Monsoon is strongest. These are generally consistent with the zonal wind behaviour discussed previously that the westerlies over the Bay of Bengal and the South China Sea reach their annual maxima from July to August. However, there is one main difference over the area west of Japan. In this area, the meridional winds have larger annual variation while the zonal winds do not have a significant annual cycle. In fact, the zonal wind is not strong all year around. Figures 5.1a and 5.1c show that west of Japan, the northwesterlies are well developed in DJF, while the southerlies are well developed in JJA. As discussed before, the patterns of percentage of the variance

associated with the annual cycle are coherent with patterns of the annual amplitude. The areas with a contribution greater than 20% almost overlap the areas with amplitudes larger than 2 ms^{-1}.

Horel (1982) noticed that the amplitude of the annual cycle in the meridional wind derived from ship observations from 1946 to 1976 is much larger than that of the zonal wind at the equator, particularly from 110°E to 170°E. For the wind field at 850 mb in this study, while this feature still exists the difference between the amplitudes of the two components is not as marked. This may suggest that the meridional wind at 850 mb does not experience as large an annual cycle as that of the surface.

5.3.1.2 200 mb wind field

The 200 mb zonal pattern exhibits a typical wintertime strengthening of the westerlies. In the northern hemisphere this occurs during February at a latitude of 20-30°N (Figure 5.4a). In the southern hemisphere the annual amplitudes are smaller and the strengthening occurs in August. The annual cycle of the westerlies in the northern hemisphere contributes more (about 30-50%) to the total variance than its equivalent in the southern hemisphere (only about 20-30%). The 200 mb meridional pattern is almost exclusively dominated by the northern hemisphere monsoon (Figure 5.4b). Larger amplitudes occupy a region from the east Indian Ocean (75°E) to the western Pacific (150°E) and from the equator to 30°N. The annual cycle in these areas account for more than 20% of the total variance.

5.3.2. Semiannual cycles

5.3.2.1 850 mb wind field

One of the main features of the semiannual cycle is that the amplitudes (of both zonal and meridional fields) are much smaller than the corresponding amplitudes for the annual cycle, except in equatorial areas (Figure 5.5). The ratio of the amplitude of the annual cycle to semiannual cycle is about 2-3 for the zonal wind, and reaches more than

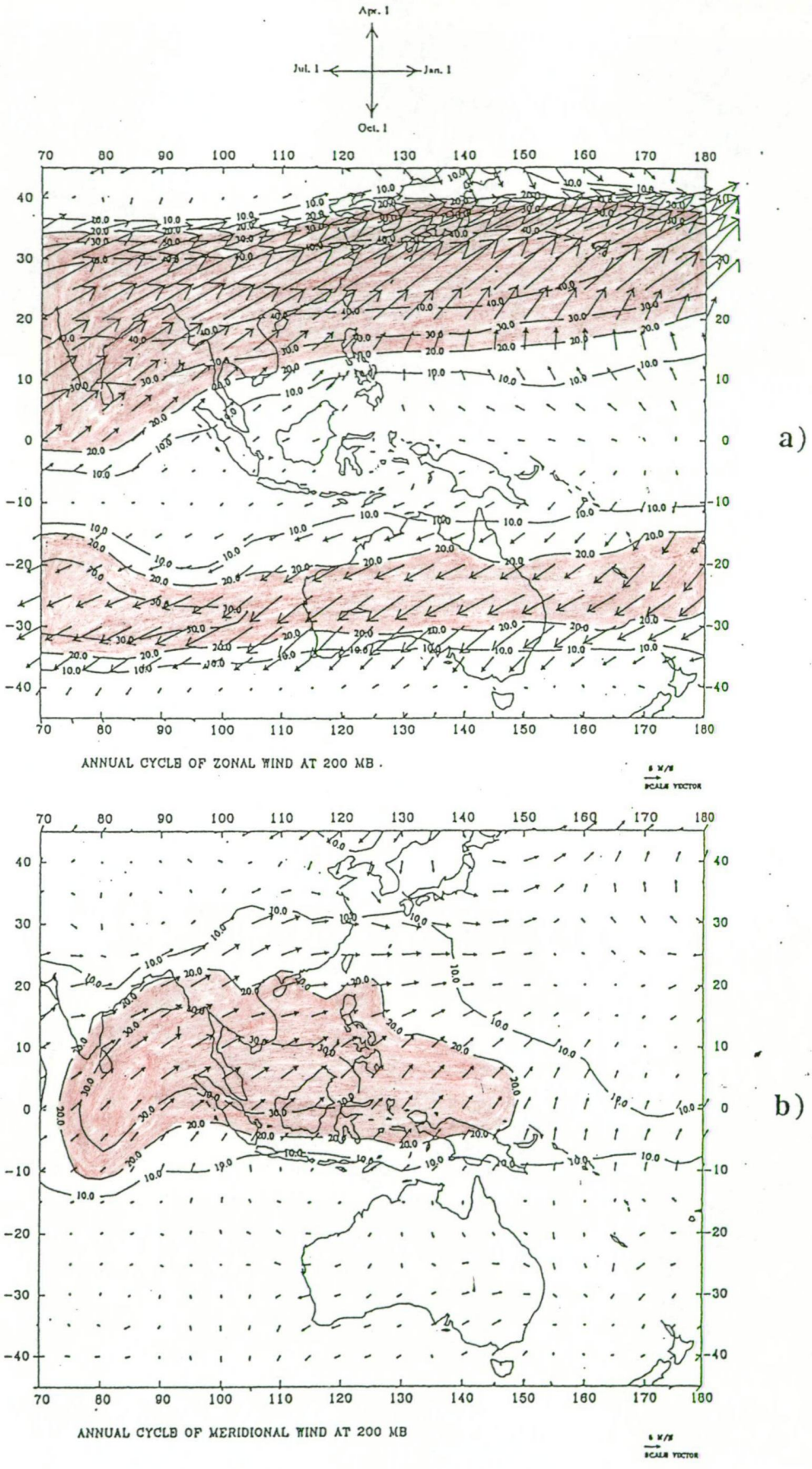

Figure 5.4 Same as Figure 5.3 but for 200 mb.

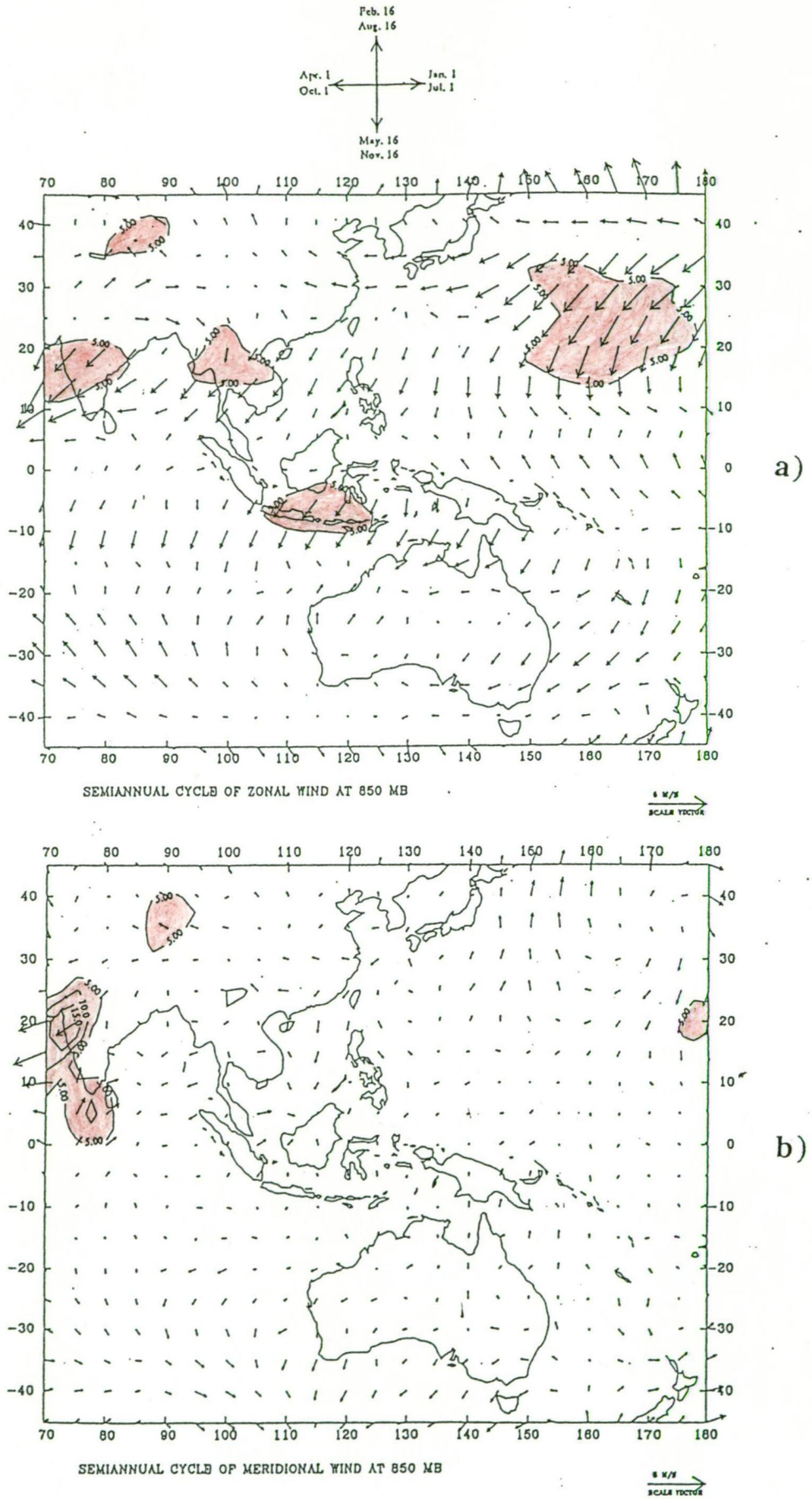

Figure 5.5 Same as Figure 5.3 but for semiannual cycle at 850 mb. Areas with the percentage larger than 5% are shaded in red.

5 for meridional wind, especially in the northern hemisphere. For the zonal component, maximum values are between 2 and 3 ms^{-1} at 850 mb (Figure 5.5a). These maximum amplitudes occur near the Indian subcontinent, Indochina area, Malaysia and northwestern Pacific, and their peaks occur in April and October, just before and after the summer monsoon. In terms of percent contribution to the total variance, these isolines correspond to regions greater than 5%. There is also a region over Indonesia with a greater than 5% contribution, although the amplitude is less than 2 ms^{-1}.

High amplitude regions in the meridional component generally coincide with the areas with high amplitude zonal components (Figures 5.5b). It is interesting to see that on a percentage basis, there are regions that account for more than 9% in the Indian subcontinent. Very little pattern is seen in the timing of the amplitudes of the meridional component.

5.3.2.2 200 mb wind field

The zonal component of the semiannual cycle at 200 mb contains two high amplitude (> 6 ms^{-1}) areas (Figure 5.6a). The first one is located east of Japan, while the second is located just west of north-west Australia. For most of the tropical regions, the timing of the maximum amplitude occurs in February and August.

It is interesting to note that the percentage contribution of the semiannual cycle (zonal component) is largest just south of the equator between 70°E and 150°E. The areas greater than 5% (shaded in Figure 5.6a) are extensive and cover a large contiguous area. The percentages are larger than 15% in the equatorial Indian Ocean from 10°S to 20°S. This is in contrast to the fact that the percentage contribution by the annual cycle is smaller than 10% over the tropical area (Figure 5.4a), which implies that the semiannual cycle in this area is more dominant. Van Loon and Jenne (1969, 1970) have documented this semiannual cycle at 200 mb in the global scale and suggested that the oscillation is associated with second harmonics of opposite phase in the temperature above the equator and in subtropics. The detailed linkage between this semiannual

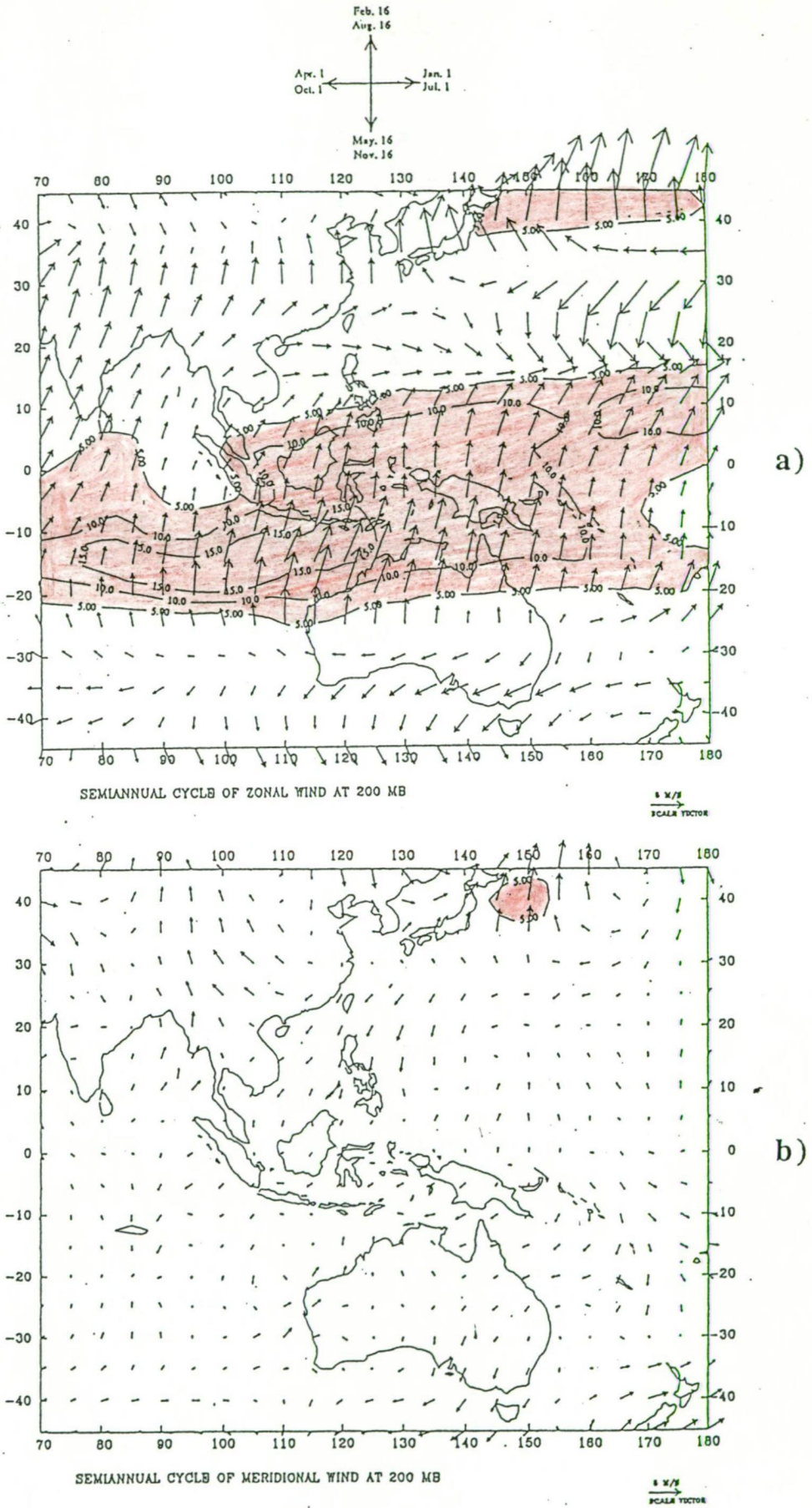

Figure 5.6 Same as Figure 5.3 but for semiannual cycle at 200 mb.

cycle of zonal wind to convection over the area has still not been well documented.

By contrast the amplitudes of the meridional component in this area are all small (Figure 5.6b), with the exception of an area near Japan where the amplitudes are greater than 3 ms^{-1} and the contribution of the total variance is greater than 5%.

5.4 Intraseasonal oscillations

The following procedure was followed to examine the intraseasonal oscillations. In a harmonic analysis, the sum of all variances contributed by each harmonic component should equal the total variance for a particular location. Harmonic analysis was performed at each grid point for both the zonal and meridional component at 850 mb and 200 mb. The total powers in the bands of period 4-10 days, 10-30 days, 30-65 days and 65-180 days were calculated. The final step involved taking a ratio between the power in a particular frequency band to the total variance. The results are presented in Figures 5.7 and 5.8. Areas with values greater than 20% are shaded in red and less than 10% in green.

Oscillations in the frequency bands 4-10 days and 65-180 days are not presented since they rarely accounted for more than 10% of the total variance. The general observation may be made that in the 10-30 days oscillation, the southern hemisphere exhibits a larger percentage contribution than in the northern hemisphere (Figure 5.7). Values are typically greater than 20% in the mid latitudes, for both the zonal and meridional components at both the 850 mb and 200 mb level. This pattern is to be expected since in the northern hemisphere the annual cycle accounts for a large percentage of the total variance. As mentioned earlier, this is due to monsoonal and other continental effects. On the other hand, the meridional components of both 850 mb and 200 mb show larger percentage of contributions by the 10-30 days oscillation (Figures 5.7b and 5.7d).

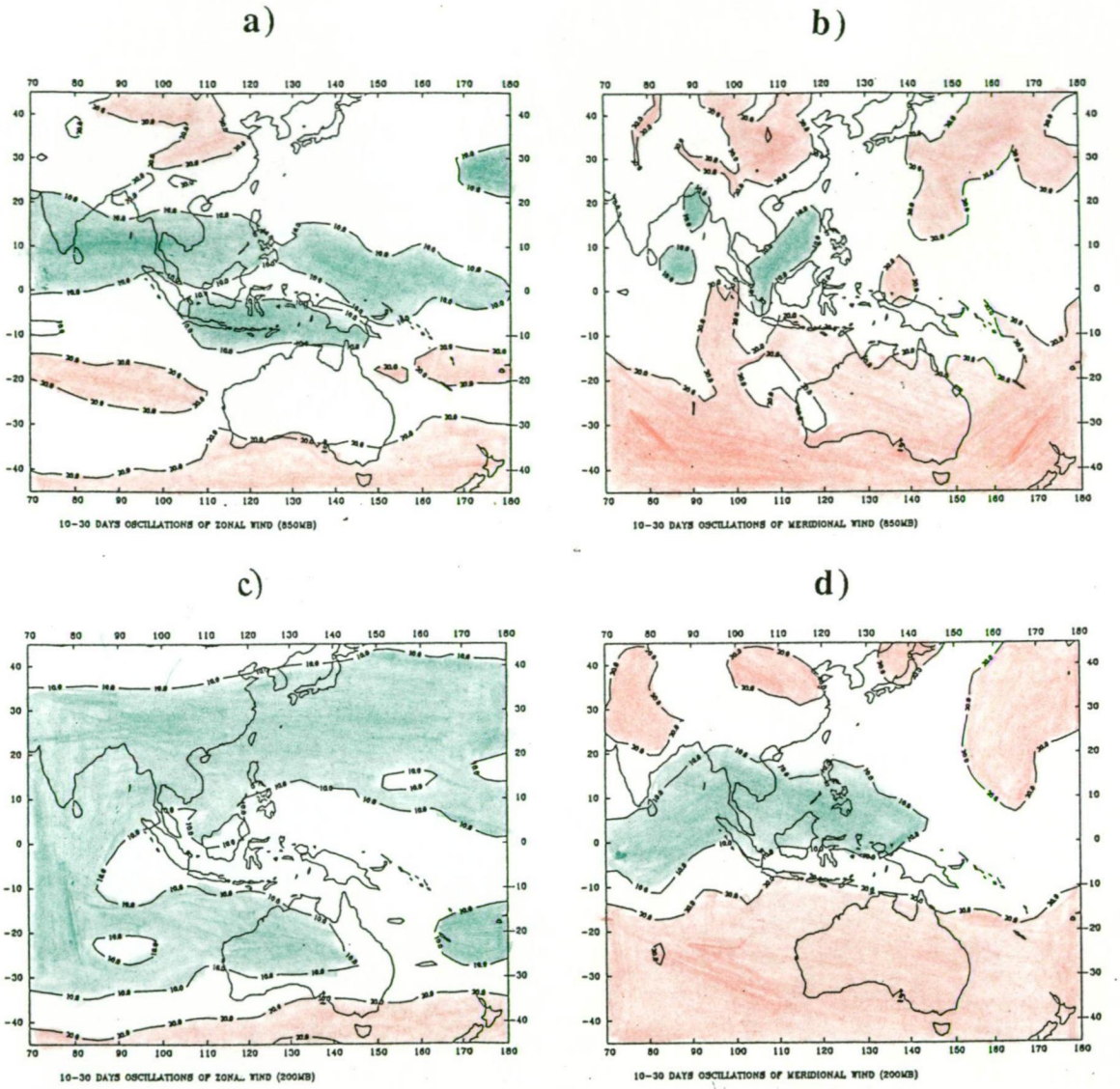

Figure 5.7 The percentage of contribution by the 10-30 day oscillation to the total variance of 5 day running averages: a) 850 mb zonal wind; b) 850 mb meridional wind; c) 200 mb zonal wind; d) 200 mb meridional wind. Areas with percentage larger than 20% are shaded in red and less than 10% in green.

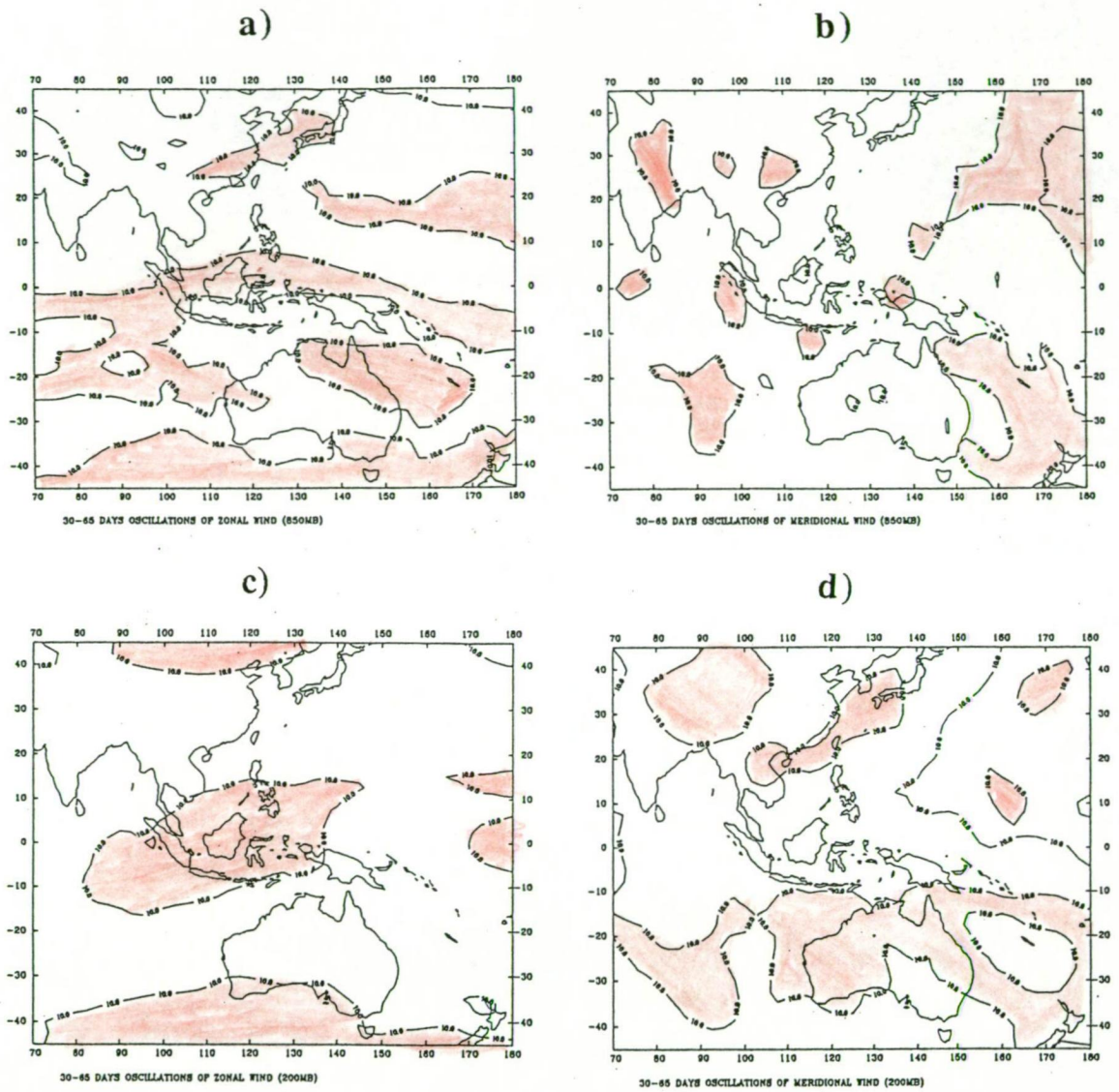

Figure 5.8 The percentage of contribution by the 30-65 day oscillation to the total variance of 5 day running averages: a) 850 mb zonal wind; b) 850 mb meridional wind; c) 200 mb zonal wind; d) 200 mb meridional wind. Areas with percentage larger than 10% are shaded in red.

At the other extreme, a region of low variance is noted from the Bay of Bengal to the Philippines and a trough of low variance extends eastward to the dateline, where it lies on the equator. Both the zonal and meridional component 850 mb map (Figures 5.7a and 5.7b) show this feature, whilst this minimum region in the 200 mb zonal component map (Figure 5.7c) has shifted by about 10 degrees northwards. This region features a strong semi-annual cycle as discussed in the previous section.

Significant areas of high variability (greater than 20%) also exist in the zonal component at 850 mb in the subtropical southern Indian Ocean and east of the Coral Sea (Figure 5.7a). The meridional component, both 850 mb and 200 mb, also exhibits a high variability in the north Pacific Ocean east of Japan.

Contributions by 30-65 day oscillations are generally smaller than those by 10-30 day oscillations (Figure 5.8). Areas with contributions greater than 10% are shaded in red. The most outstanding feature in the 30-65 day oscillation of zonal wind at 850 mb is a ridge of maximum variance extending along the equator in the Indian Ocean and Indonesian region and deflecting southward into the southern hemisphere along the SPCZ (Figure 5.8a). The maximum variance in the Malaysian region suggests generation or amplification of variability with this time scale in this area. The pattern of the contribution by zonal wind at 200 mb is more uniform (Figure 5.8c), with a maximum over the Indonesian region.

5.5 Longitude-time diagrams

The longitude-time diagrams of zonal and meridional winds at both 850 mb and 200 mb levels for different zonal bands are examined. A 30-65 day bandpass filter has been applied to the wind data. The filtered data have been averaged over six zonal bands, where each band extends over 10 degrees of latitude. The zonal bands are as follows: 20-30°S, 10-20°S, 0-10°S, 0-10°N, 10-20°N and 20-30°N. Only a small part of the longitude-time diagrams are presented in the following pages (Figures 5.9 - 5.12).

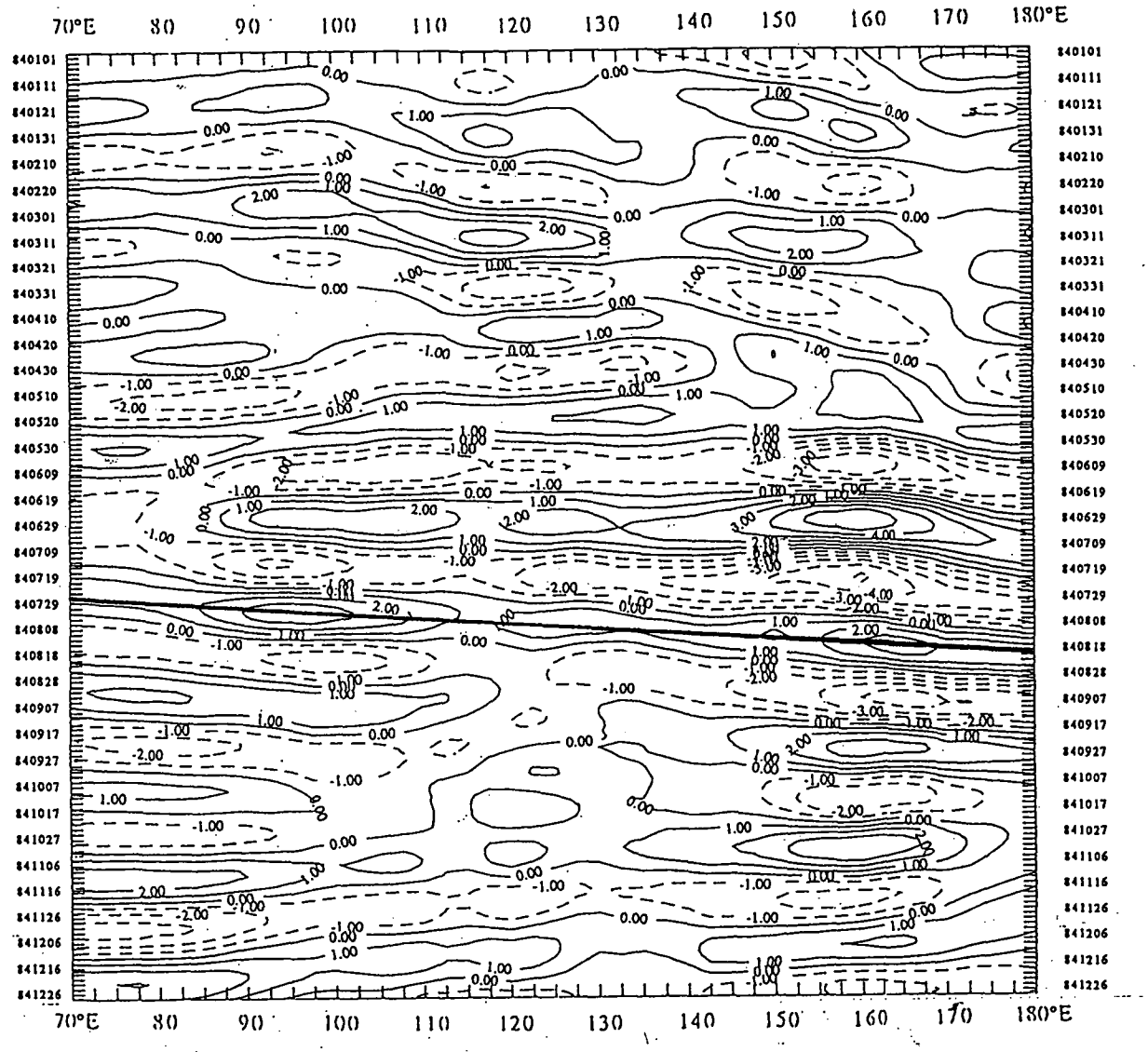

Figure 5.9 Time-longitude diagram of 30-65 day bandpass filtered zonal wind at 850 mb in the bands of 20°S-30°S in 1984.

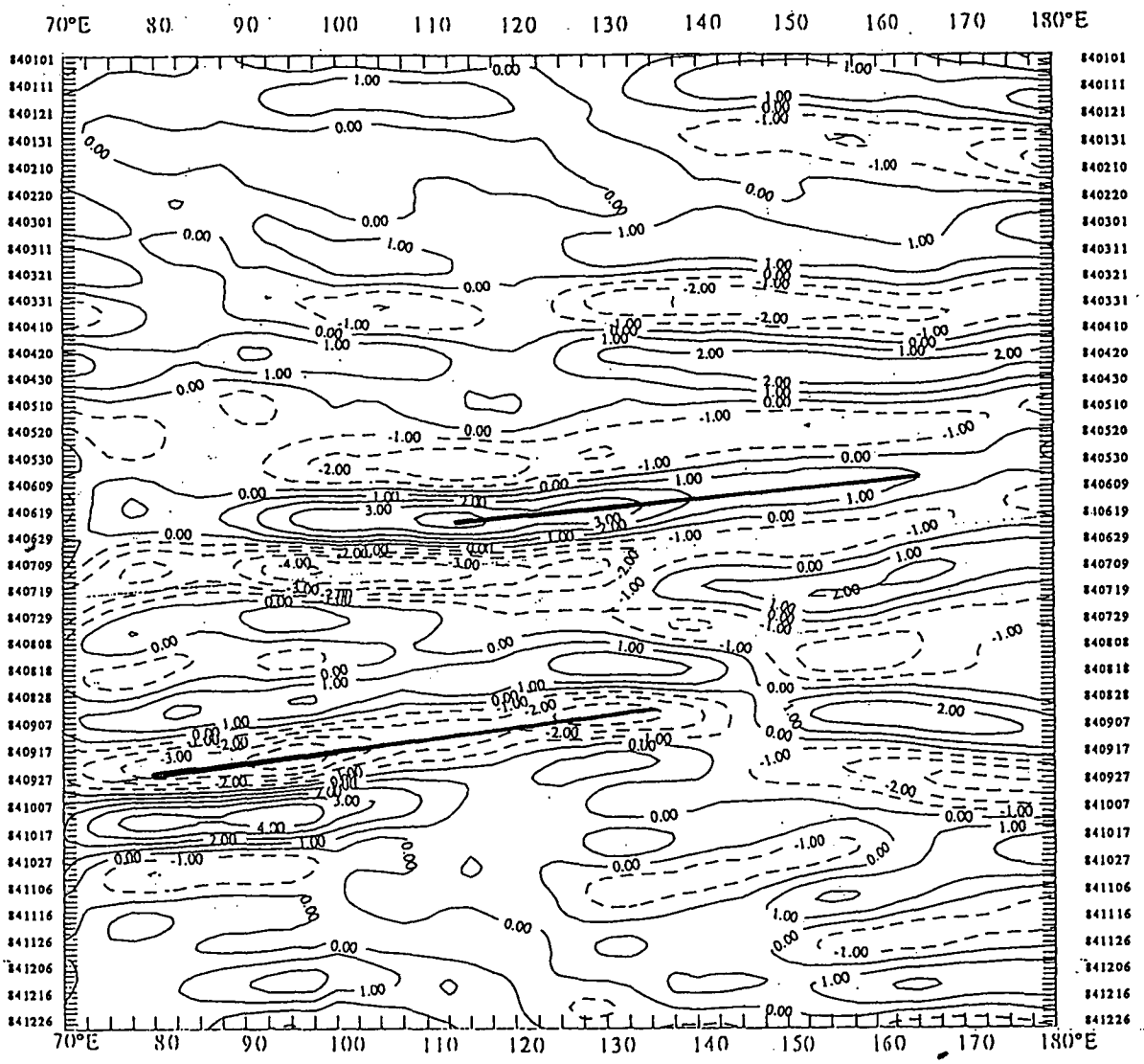

Figure 5.10 Time-longitude diagram of 30-65 day bandpass filtered zonal wind at 850 mb in the bands of 10°N-20°N in 1984.

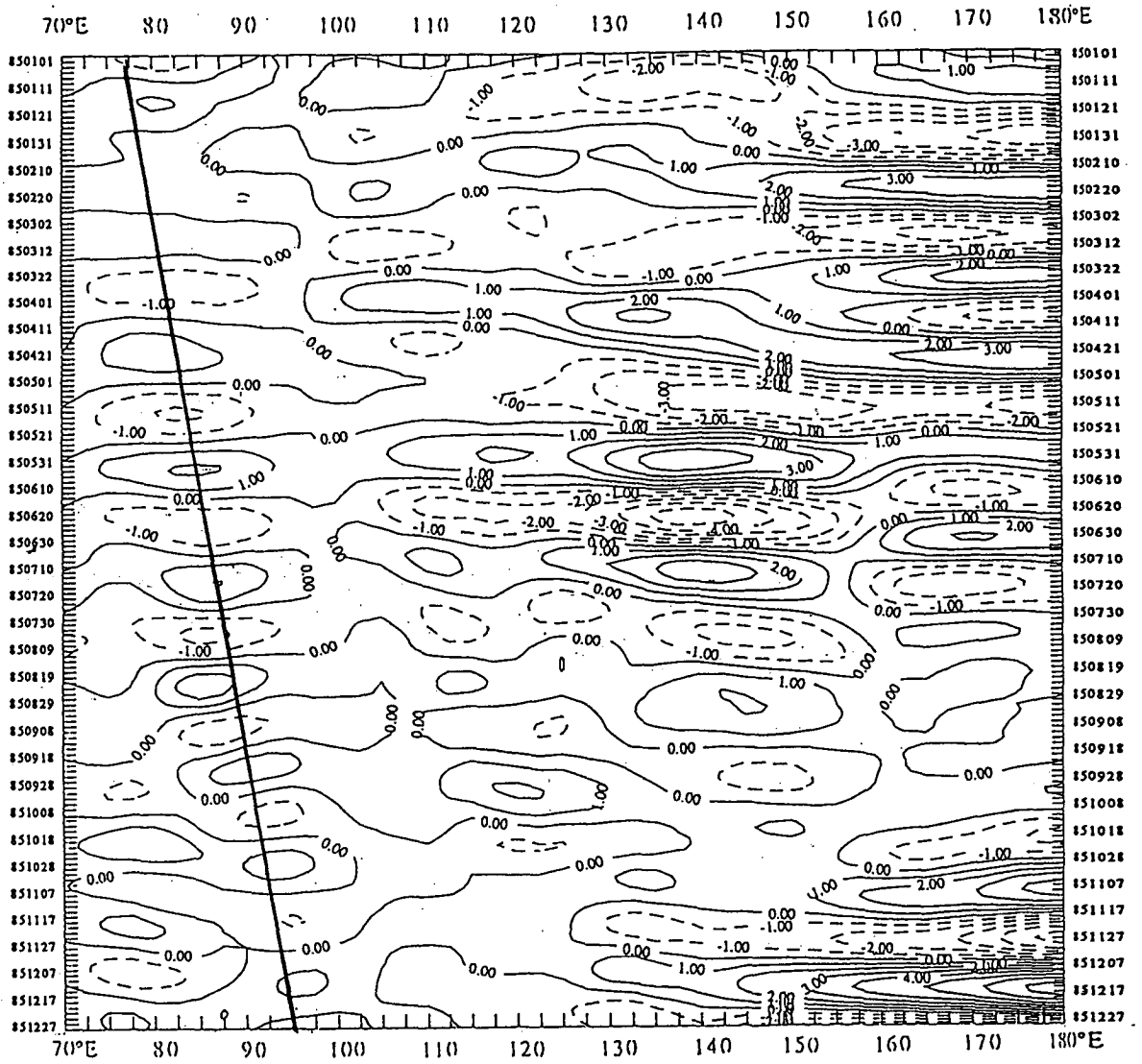

Figure 5.11 Time-longitude diagram of 30-65 day bandpass filtered zonal wind at 850 mb in the bands of 20°N-30°N in 1985.

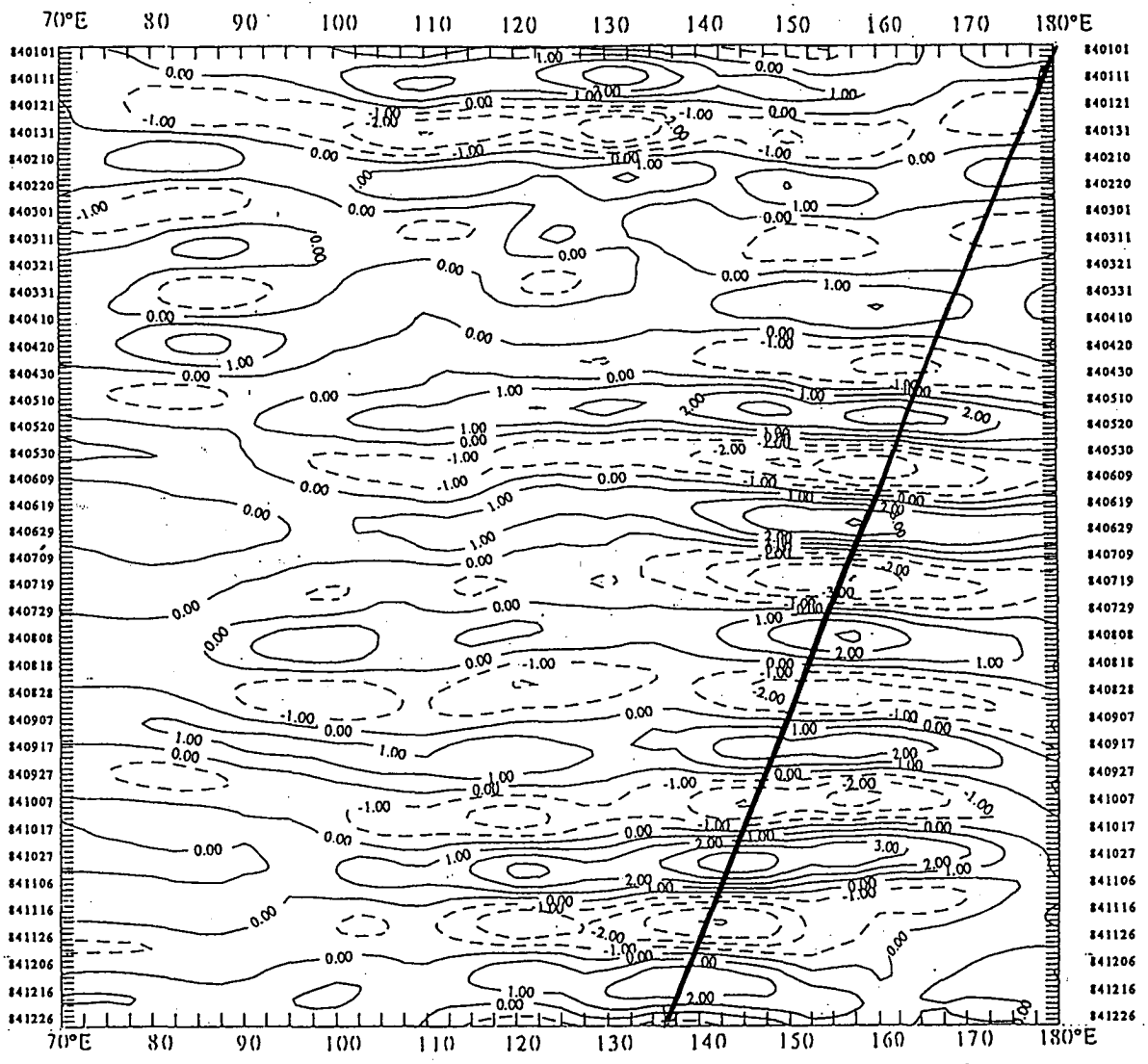

Figure 5.12 Time-longitude diagram of 30-65 day bandpass filtered zonal wind at 850 mb in the bands of 10°S-20°S in 1984.

While these diagrams confirm some results by earlier studies, a few outstanding features can be summarized as follows:

1) Zonal anomalies usually propagate eastward from the eastern Indian Ocean to the western Pacific (Figure 5.9). It takes about 50 days for an anomaly to propagate from the mid-Indian Ocean to the dateline.

2) During the northern summer and autumn, the zonal anomalies in the band of 10-20°N propagate from east to west (Figure 5.10)

3) East of Indonesia, the extreme centre will usually propagate westward (Figure 5.11) while west of Indonesia, the extreme centre propagates eastward (Figure 5.12).

5.6 Summary

As mentioned earlier, the three year wind data set used in this chapter is too short to obtain reliable climatic statistics on indications of interannual variability. Nevertheless, on a qualitative basis at least, it is possible to note similarities in the seasonal means with other studies. Whilst the general features of the seasonal means (zonal and meridional components at 850 and 200 mb) are similar to long term climate studies, the zonal winds in the tropical Indian Ocean were found to be stronger in this data set. This feature might explain the stronger low level convergence east of New Guinea and in the tropical Indian Ocean. In addition, the convergence zone east of the Philippines was not replicated elsewhere (Rasmusson and Carpenter, 1982). It is important to keep in mind that the data sets used for comparison are not exactly similar since Rasmusson and Carpenter used surface observations as opposed to the 850 mb data used in this study.

The 200 mb divergence map reveals an interesting feature during the northern hemisphere summer and autumn (Figure 5.2c, 5.2d). The zones of convergence and divergence each occur along distinct contiguous zonal bands in the tropical regions. During these two seasons there is very little evidence of extratropical convergence and

divergence occurring. This feature suggests that the two zones (convergent and divergent zones) are intrinsically linked by an intertropical convection cell, although judging by their areas, they are not exactly balanced.

By using harmonic analysis, this study has described the main features of the annual, semiannual, 30-65 day and 10-30 day oscillation in the wind field. The annual cycle exhibits a much stronger amplitude (both in the zonal and meridional components at the two levels, Figure 5.3, 5.4) in the northern hemisphere than in the southern hemisphere, and this is very likely due to the dominance of the Asian Monsoon. In terms of the percentage contribution to the total variance of 5-day running average, values higher than 30 percent are reported in the monsoon region.

By contrast, the contribution to the total variance by the semiannual cycle is much smaller, with the exception of the zonal wind at 200 mb (Figure 5.6a). In the southern tropical areas west of 150°E, the contribution by the semiannual cycle is greater than 10%. Van Loon and Jenne (1969, 1970) observed a similar effect, and they argued that the semi-annual wind oscillation is induced by the semiannual temperature cycle, which in term is originated by latent heat release from convection. An examination of the seasonal convergence distribution (Figures 5.1, 5.2) does not indicate a strong semi-annual thermal wind effect. However, it is quite possible that a strong semi-annual signal will emerge after removal of the annual signal.

A strong intraseasonal 30-65 day oscillation (850 and 200 mb) is also observed in approximately the same area where the 200 mb semiannual cycles are distinctive. A high intraseasonal oscillation in OLR has also been reported in this area (Knutson *et al.*, 1986), which suggests that wind and convection are actively correlated at these time scales.

At even shorter time scales (10-30 days) the contribution is large at higher latitudes (see Figures 5.7). This is to be expected since the annual semi-annual and intraseasonal

cycles are low in these regions. Rather, the wind field is dominated by synoptic mid-latitude events of short duration.

From the above discussion, it is evident that the annual, semiannual and intraseasonal wind fluctuations are all important to the convection process. The annual cycle describes the monsoon activity which is important in the Indian and southeast Asia region. Higher wind frequencies are also contributing to the convection process, although their contribution to the total variance is relatively smaller to the large yearly signal. By contrast both the semiannual and intraseasonal oscillations have a large contribution in the western equatorial Pacific and Indian Ocean. These two time scales in the wind field are intricately linked with convection processes as discussed above.

In the next chapter the various parameters contributing to the convection process will be linked together to provide further insights into cause and effect relationships dealing with convection.

Chapter 6. The Variability of Convection

6.1 Introduction

Large scale, deep convection over tropical areas provides an effective means by which energy is transferred to the atmosphere (Ramage, 1968). When an air mass has been warmed, it will ascend until its temperature is the same as that of the surroundings. If saturation has occurred, the water vapour trapped in the air mass condenses and releases latent heat to the air. In order to form organized convection, a supply of continuous energy in a generally unstable environment is required. Sensible and latent heat fluxes from the Earth's surface are often considered as two major important energy sources. However the release of latent heat of condensation during convection is the most important energy transfer.

Even though convection can not be observed very readily, precipitation is one of its significant results and is used as an index to measure large scale convection. It has been found that precipitation over Indonesia drops when ENSO events begin, and reaches its maximum negative anomaly at the peak time of ENSO events (Rasmusson and Carpenter, 1982). During this time rainfall in the central Pacific is exceptionally high. Over South America, severe rainfall in northern Peru has also been observed during this time (Horel and Cornejo-Garrido, 1986).

OLR has been widely used as proxy data for convection in recent years (Heddinghaus and Krueger, 1981; Gill and Rasmusson, 1983; Gadgil *et al.*, 1984; Meehl, 1987; Graham and Barnett, 1987; Liebmann, 1987; Weickmann and Khalsa, 1990). Low OLR values in the tropics are associated with convective cloudiness (Griffith *et al.*, 1978). Anomalously low OLR indicates either more than usual cloudiness within the grid box or more well-developed clouds than normal. Therefore, anomalously low

OLR is indicative of anomalous forcing of the atmosphere by radiation and latent heating.

Many studies have examined the seasonal and interannual variation of the major convective cloud bands in the tropics. It has been shown that the intensive convective centres are mainly located over Africa, Central and South America, the western Pacific - Indonesian "Maritime Continent" region, northern Australia, and along the ITCZ and SPCZ (Heddinghaus and Krueger, 1981). The convective centres connected with the ITCZ and SPCZ move meridionally with the seasons, or towards the summer hemisphere (Meehl, 1987). It has been documented that the interannual variation of convection is closely related to the development of ENSO events. By applying EOF analysis to the OLR data set during 1974 to 1978, Heddinghaus and Krueger (1981) found that the interannual variation associated with the development of the 1976-77 ENSO event was dominated by a strong see-saw feature over the Indonesian region and the mid-Pacific. Gill and Rasmusson (1983) noted an eastward shift of OLR during the 1982-83 event. When the warm pool over the western Pacific migrated eastward, the convection centre moved eastward steadily.

The details of annual variation of convection has some interesting features. By applying EOF analyses to the OLR data, Heddinghaus and Krueger (1981) showed that most of the annual variation is depicted by the first eigenvector which essentially represents a migration of the rainfall between the northern and southern hemispheres. The second EOF mode reveals that the northern ITCZ is best developed in the northern fall. The third mode shows a semiannual component and is essential for defining the Indian monsoon over the Indian Subcontinent: the convection is strong during spring and drops in summer, rises again in autumn and falls in winter. Meehl (1987) also noted that an area of intense convection moves seasonally from the northwest in the Indian summer monsoon to the southeast during the Australian monsoon.

A number of past studies of convection use both OLR and other data sets (Rasmusson and Carpenter, 1982; Liebmann, 1987; Meehl, 1987; Weickmann and Khalsa,1990). This study is one of the first to be conducted by considering the OLR, wind field, SST and precipitable water altogether. While Meehl (1987) documented the annual and interannual variations of convection over the area, he did not use wind data. Although Weickmann and Khalsa (1990) used the detailed wind, OLR and TOVS precipitable water to describe the onset of ENSO, they did not incorporate SST into their study. And, their data sets were mainly limited to only two months from November to December of 1981. By using the comprehensive data sets from 1984 to 1986, the following questions will be addressed in this chapter:

Firstly, what are the main features of OLR during these three years compared with those earlier studies at different time scales? This will be discussed in Section 6.2.

Secondly, whilst OLR provides dynamic evidence that convection is taking place, precipitable water in the low and middle troposphere provides information on potential areas of convection and hints at the sources of moisture for convection. The spatial feature and annual variation of precipitable water are therefore addressed in Section 6.3.

In Section 6.4 estimates of convection will be linked to the main variables which comprise SST and the wind field. A conceptual model will be developed to examine the relationship between convection and these variables. The localized divergence cells of 200 mb wind field will also be discussed.

The implications of the above results for other studies will be discussed in Section 6.5 , the conclusion section.

6.2 General features of OLR

Three-month averaged OLRs for the period of 1984-86 are presented to give a general description of convection in this area (Figure 6.1). A value less than 220 Wm^{-2} has been widely regarded as being indicative of deep, tropical convection (Rasmusson and Carpenter, 1982). It should be pointed out that in MAM and DJF there are also large areas of OLR less than 220 Wm^{-2} which appear north of 30°N. These areas are partly caused by cold surface temperatures rather than being only related to large scale thick convective clouds. These features will not be further addressed in this thesis.

The convective maximum has a distinctive annual variation. In JJA, it is located in its extreme west and north positions, north of 5°S and west of 150°E. The strongest convective centre (lower than 200 Wm^{-2}) is located in the Bay of Bengal. This feature is consistent with the out-break of the Asian Summer Monsoon and the northward shift of the ITCZ. In SON, with the development of the Asian Winter Monsoon, the convective area weakens and retreats southeastward to the equatorial area from 85°E to 165°E and from 10°S to 10°N. The strongest centre is now found in the Malaysian area. In DJF, the convective area strengthens again and moves further southeastward with the strongest centre now located in the area encompassed by the Malaysian Peninsula and Papua New Guinea. This convective pattern is a response to the development of the Australian Summer Monsoon. The season of MAM has the weakest convection, since the convective area contracts and weakens without an obvious shift of its centre. The above description of the seasonal features of OLR is very similar to the description by Meehl (1987), who used monthly averages of OLR for 8 years from 1974 to 1982.

All 36 monthly maps of OLR covered in this study are in the Appendix. An examination of the individual months reveals some outstanding features not covered in

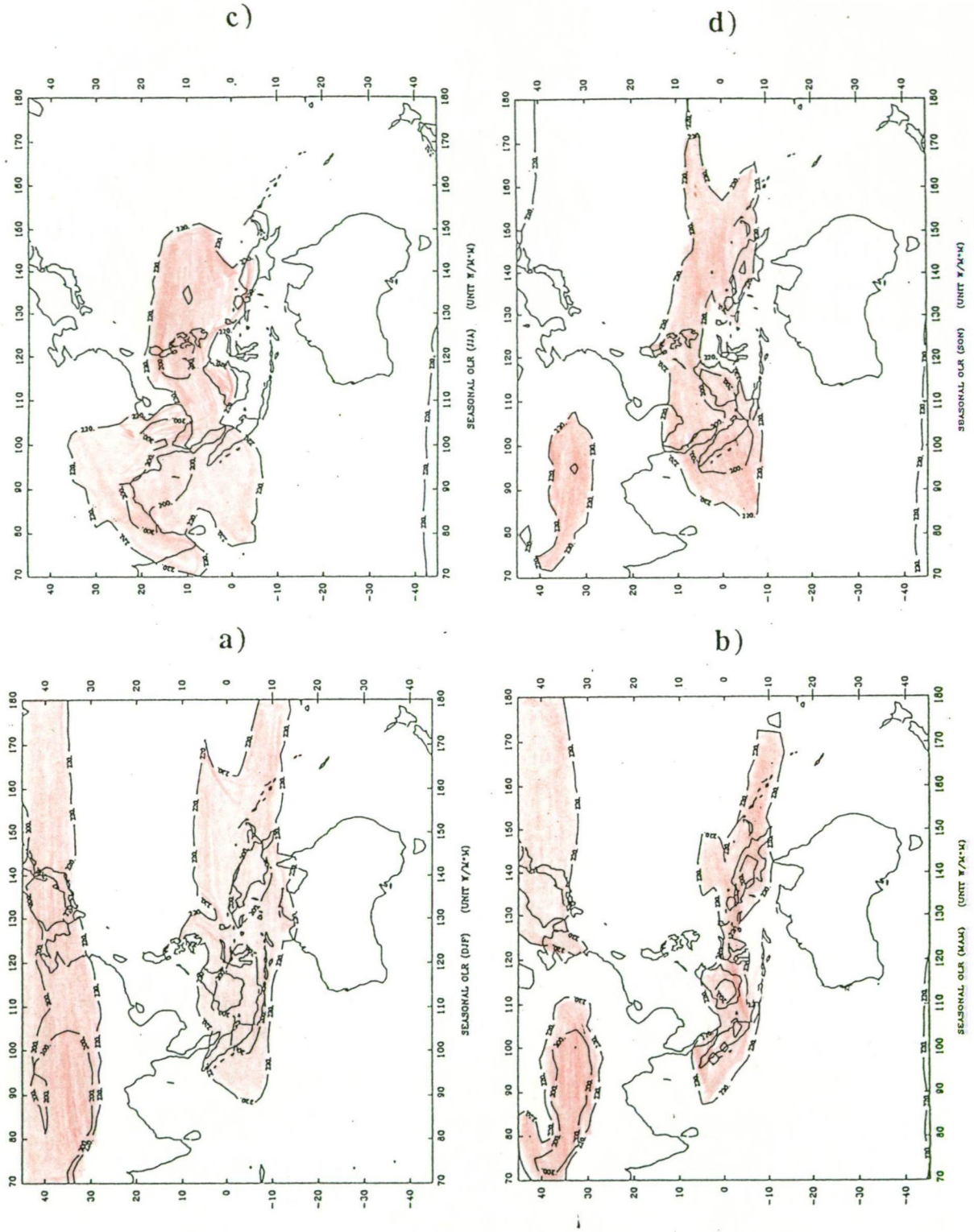

Figure 6.1 Three years (1984-86) seasonal means of OLR. (a) December-January-February (DJF); (b) March-April-May (MAM); (c) June-July-August (JJA); and (d) September-October-November (SON). The units of OLR are in Wm^{-2}. Areas with OLR less than 220 Wm-2 are shaded red.

the seasonal trends. It can be seen that the convection reaches its weakest intensity during May. In June the convection abruptly develops in the Bay of Bengal and quickly reaches its strongest intensity in July when it moves southeastward. It continues to move southeastward in September, gradually weakening until it reaches its second weakest season in November. The highly convective area is now located along the equator, from 80°E to 165°E, with a gap of "relatively clear sky" between Malaysia and Papua New Guinea over the Banda and Molucca Seas (Figure 6.2). The convection again gets stronger from December to February, reaching its most southeast position in February. From March to May, the convection again weakens and gradually moves northwestward back to the equatorial area north of Australia.

An examination of the monthly patterns also reveals an eastward shift (about 10°-20° longitudes) from the three year mean of the convection centres during August to December 1986. This pattern follows the warm SST shift which was discussed in Chapter 4. This feature can be shown clearly on the longitude-time contour map of three years monthly OLR averaged in the bands of 5°N-15°N (Figure 6.3a) and 5°S-5°N (Figure 6.3b). In addition, it is interesting to note that convection as a whole in 1986 is much weaker than previous years. After the weak period of convection in May 1986, the convection did not fully develop as in 1984 and 1985. Rather, the dry areas expanded westward as far as 100°E and eastward as far as 150°E. From November 1986, the convection quickly developed east of New Guinea and moved eastward to the dateline in December. This obvious shift forms a major feature of ENSO events during 1986/87. It is interesting to note that there is relatively weak convection in the Banda Sea area during May in all three years (see Appendix). Especially in 1986 the weak convection appears to develop from this region. This observation seems to support the hypothesis that the Banda Sea region is linked to the development of drought in Australia (Nicholls, 1989).

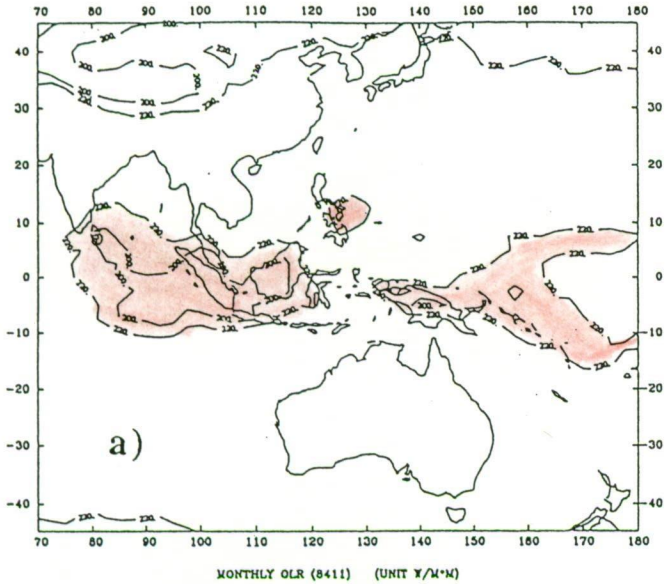

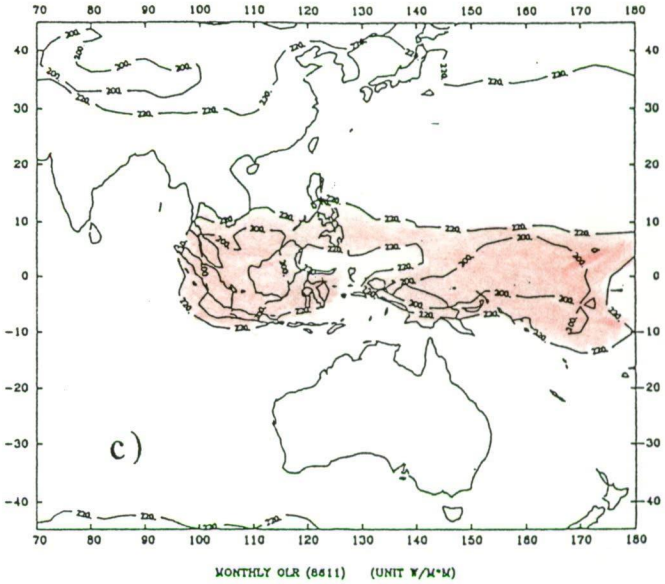

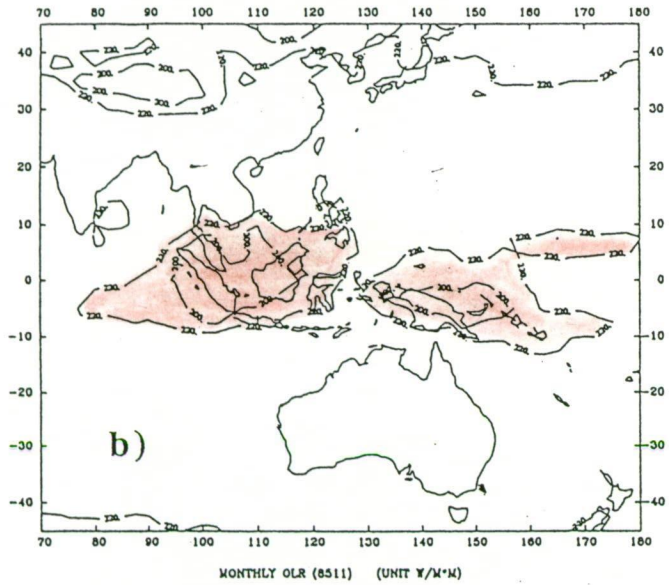

Figure 6.2 Monthly mean of OLR in November 1984 to 1986. (a) 1984; (b) 1985; and (c) 1984. Units and shading are the same as those in Figure 6.1. Notice the "convection-free" area in the Banda Sea.

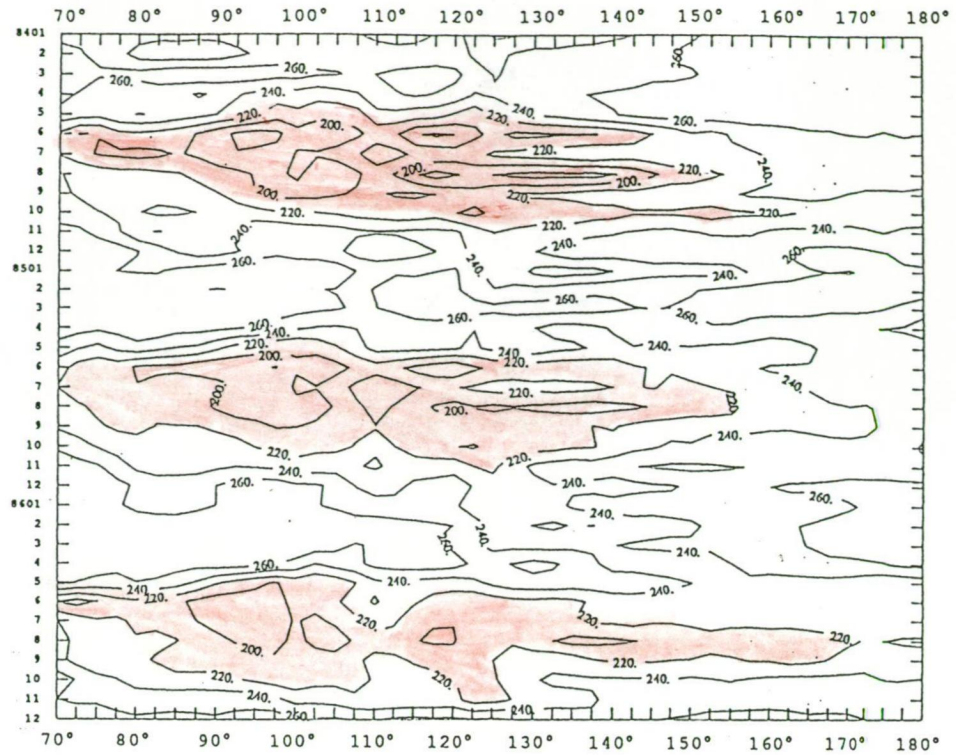

a)

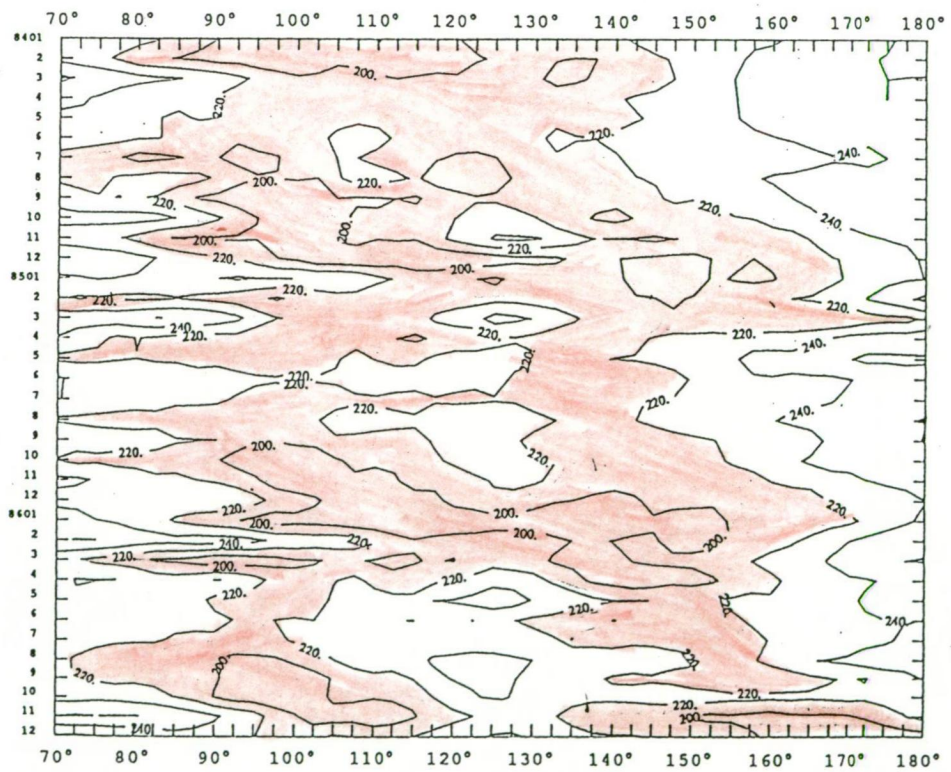

b)

Figure 6.3 Time-Longitude diagram of monthly mean OLR in the zones of 5°N to 15°N (a) and 5°S to 5°N (b) for the period 1984-86. Units and shading are the same as those in Figure 6.1. Notice the eastward shift of the convection centre (a) in 1986 and the large "convection-free" area near 130°E from May 1986 to December 1986 (b).

6.3 Precipitable water

While OLR provides important "dynamic evidence" of large scale convection, data on precipitable water is useful because it provides insight into sources and sinks of moisture flux. LLPW in the surface to 700 mb layer was obtained from the TOVS aboard the NOAA series of polar orbiting satellites. The determination of TOVS temperature and moisture profiles from radiances is described by Smith and Woolf (1976), Smith *et al.* (1979), and Hayden *et al.* (1981). Since the TOVS instruments do not measure precipitable water under completely cloudy conditions, the average LLPW has a dry bias in the presence of heavy convection. Comparisons of TOVS data with radiosonde observations were discussed by Gruber and Watkins (1982). They found RMS differences of about 5 mm precipitable water between TOVS-derived low-level moisture and co-located radiosonde observations over the continental United States. Khalsa (1986) and Steiner (1987) found similar results over the Pacific islands.

Monthly LLPWs were calculated over the study region from January to December, 1986. The four maps of January, April, July and October are shown in Figure 6.4. The shading represents moist areas, with LLPW > 35 mm. These shaded areas coincide well with the region of less than 220 Wm^{-2} in the OLR contour maps (Figure 6.1). It is interesting to note that the moist area varies markedly in the region, with an obvious annual course similar to the OLR. In January the more moist area is located north of Australia, with a central core with LLPW greater than 40 mm in Papua New Guinea. February is considered the driest season (not shown) when the wet band is limited to a region eastward of 115°E and from the Equator to 15°S. This wet band expands northwestward in March and by April, it is located from 80°E to the dateline, with a 20° zonal band extending from 5°N to 15°S. The wettest season occurs in July (Figure 6.4c), when the Indian monsoon reaches its strongest intensity. The centre is located in the Indian Continent with a maximum core of over 45 mm. From August onward, the wet area moves southeastward and the humidity at the centre decreases. In

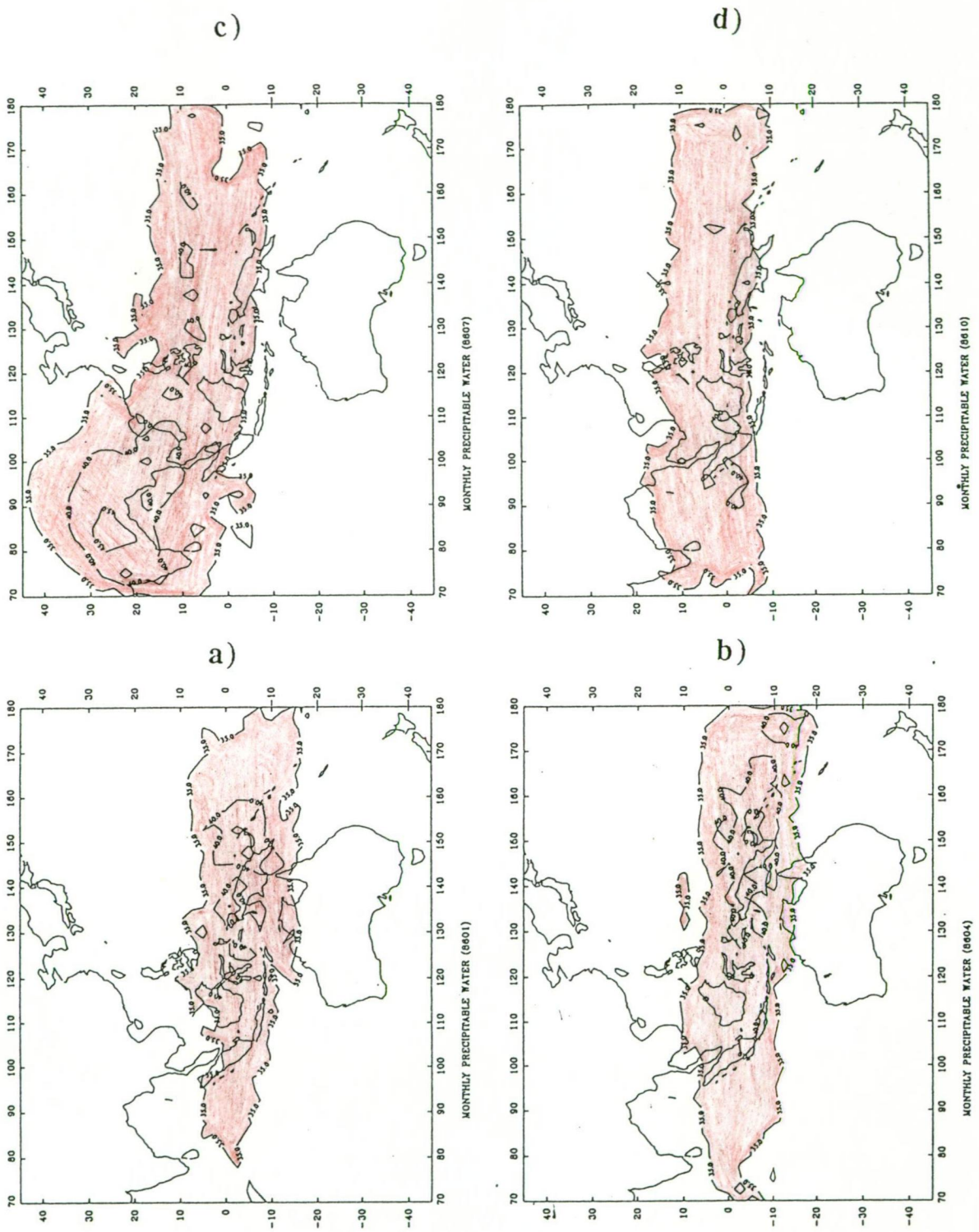

Figure 6.4 Monthly mean of TOVS precipitable water vapour in the layer from surface to 700mb (LLPW) in 1986. (a) January; (b) April; (c) July; and (d) October. The units of precipitable water vapour are in mm. Areas with LLPW greater than 35 mm are shaded red. Notice the agreement of the shaded areas with the shaded areas in Figure 6.1.

October (Figure 6.4d), the wet band is located over the equatorial area from 10°S to 10°N.

The agreement between the annual course of OLR and precipitable water suggests a strong relationship between the two. While SSTs of at least 27.5-28°C have been regarded as one necessary condition for deep convection, it is proposed here that the 35 mm in LLPW is another "necessary" condition. Steiner (1985) obtained similar results.

6.4 Comprehensive study of convection

The analysis done so far is mainly limited to investigating the effects of individual variables related on convection. It is therefore interesting to examine and summarize the relationship among those variables whilst at the same time observing their spatial and temporal features. The spatial features will be discussed in section 6.4.1, while the temporal features will be discussed in section 6.4.2. A conceptual model of convection, related to SST in the 200 mb wind field will be developed in section 6.4.3. Finally some features of localized divergence cells at 200 mb wind field will be presented in section 6.4.4.

6.4.1 Spatial features

a) OLR vs SST

It has been widely believed that OLR and SST are negatively correlated (Bjerknes, 1969; Rowntree, 1972; Julian and Chervin, 1978). This is generally true for large scale global relationships. However, there is much scatter in the relationship, so that it might be statistically less significant over a smaller region covering a subset of the OLR and SST bands. Gadgil *et al.* (1984) and Graham and Barnett (1987) argued that SST above 28°C is a critical value for convection to develop, and that above this threshold, the relationship between the two variables is not obviously established. This study confirms this observation. As an example, the monthly OLR map for January 1984 with its associated high SST centres is shown in Figure 6.5a. However, the following

comments are representative of most monthly maps. Firstly, the 28°C isotherm is located within an area encompassed by latitudes 20°N to 20°S for most of the year. It is also noticed that the deep convection denoted by 240 Wm^{-2} is generally within the 28°C contour lines and follows the annual course of SST. Secondly, while deep convection occurs in high SST areas, not all high SST areas generate convection (Figure 6.5a). This feature confirms that warm SST is only a necessary condition and not a sufficient condition to generate convection. Thirdly, convective centres do not generally overlap the areas of maximum SST, but instead are located west of the high SST centres.

To show that this description is representative of convection centres and high SST centres during other months, indices of convection and warm SST centres were devised to represent the maxima as a function of longitude. The index of convection centre was calculated along longitude. At each 2.5° × 2.5° grid point the value 400-OLR is calculated. If this value is greater than 200, it is then indicative of deep convection and used for the index. Otherwise it is ignored and not used in the subsequent sum. Once this value is calculated for all the grid points, they are then summed between latitudes 30°N and 30°S and for a constant longitude.

A similar procedure is followed in defining an index of SST centre. Values greater than 29.5°C are registered in the 2.5° × 2.5° grid point and added between latitudes 30°N and 30°S and for a constant longitude. As in the previous index, values less than the treshold value (29.5°C) are not used in the sum.

Areas with convection index larger than 600 are shaded in red and SST index larger than 90 in green in Figure 6.5b. It can be seen clearly that maximum convection centres and maximum SST warm centres seldom overlap. Furthermore, there seems to be some differences in their temporal variation at different longitudes. West of 110°E, the SST maximum mainly occurs from April to May, just before convection starts to increase to the annual maxima from June to August. The SST warm centre then

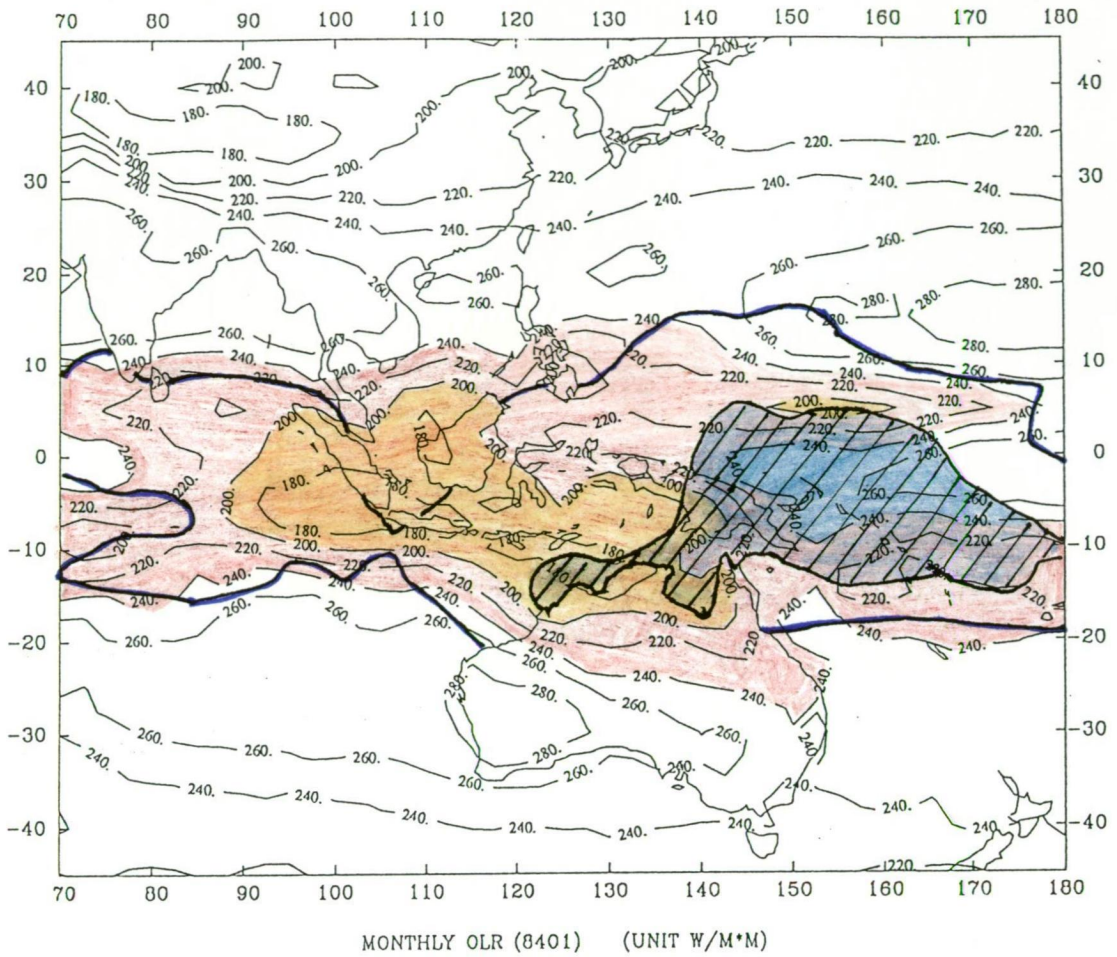

a)

Figure 6.5 Monthly mean of OLR (Wm^{-2}) in January 1984 (a). Areas with OLR value less than 240 Wm^{-2} are shaded in red. Areas with OLR value less than 200 Wm^{-2} are shaded in yellow. The blue lines superimposed compound the area of SST warmer than 28°C, and the areas with blue shading are of SST warmer than 29.5°C. Notice the "convection-free" area in the Caroline Sea. The time-longitude diagram of indices of convection and warm SST centres is in (b). Areas with value of index of convection centre larger than 800 are shaded in red and areas with value of index of SST centre larger than 120 are shaded in green. See text for detail to calculate such indices.

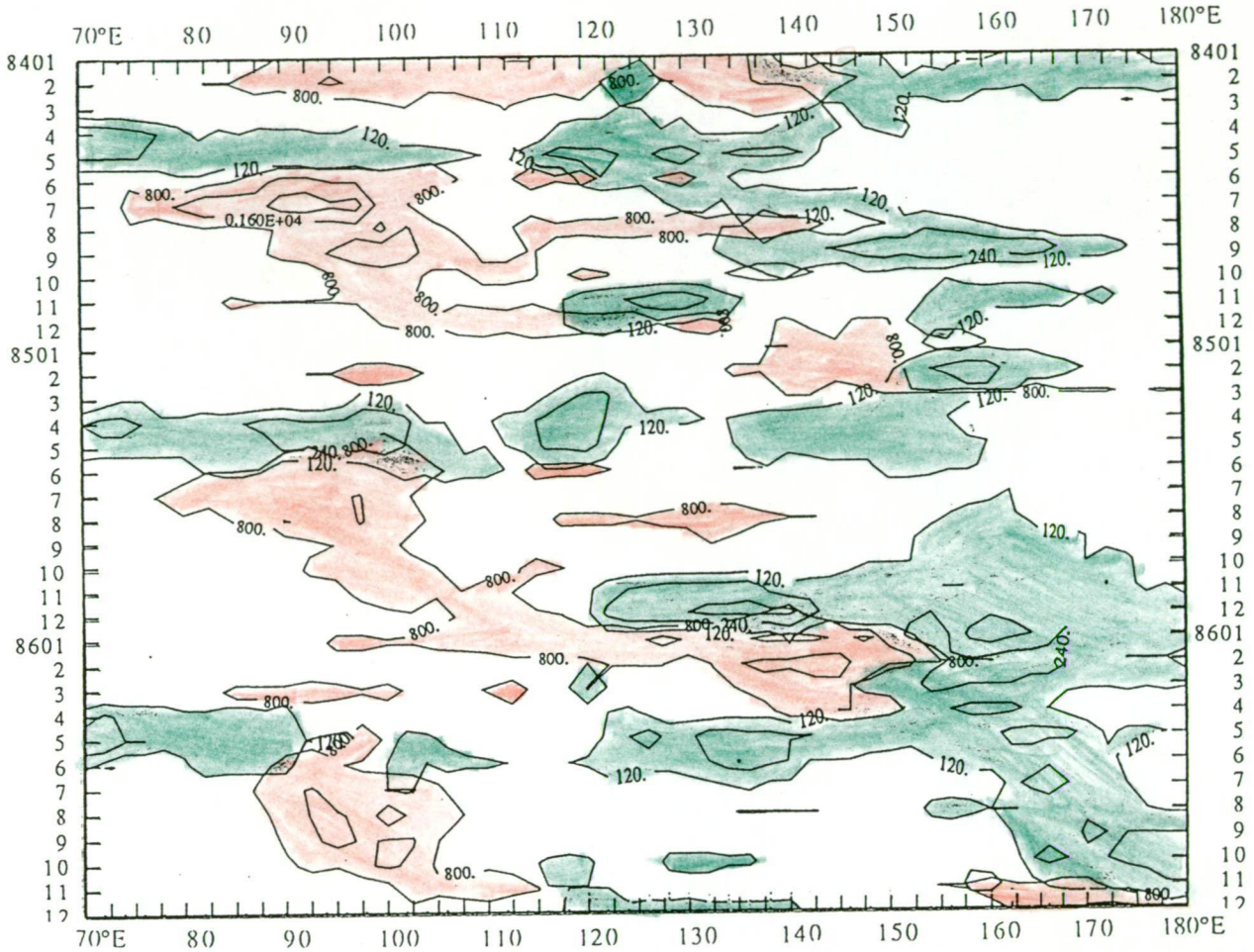

Figure 6.5 (Continued).

disappears. In the region east of 110°E, the SST maxima occur east of, and before, maximum convection. The high SST centres shift eastward from April to the end of the year, and the convection centres follow the SST pattern. The difference between these two meridional bands therefore suggests that in the Indian Ocean, while SSTs provide a precursor for convection to develop and may initiate convection, other processes must contribute to the development of the convection maxima since the two indices do not overlap and show different orientations. It is likely that the wind convergence at lower level and divergence at higher level may play more important roles to maintain and accelerate convection. In contrast, in the area of Indonesia and eastward, the SSTs may play a more important role in initiating and controlling the convection centre. More specifically, the convection centres follow the high SST centres and are located west of them. The major events in the OLR-SST relationship indicated by Figure 6.5b can be seen in the original, monthly OLR and SST maps in the Appendix.

b) OLR vs 200 mb divergence

The relationship between mean monthly OLR and mean monthly 200 mb divergence is next examined. To illustrate the discussion, Figure 6.6 presents the pattern for January 1984. As may be noticed, the areas of maximum convection (OLR < 200 Wm^{-2}) encompass the zones of maximum 200 mb divergence. Furthermore although the OLR pattern is spatially coherent, the regions of maximum convergence appear as localized cells. This cell-like feature might be partly due to errors introduced by the finite difference method of estimating wind divergence. On the other hand, local cells of both wind divergence and OLR are often exhibited suggesting that the divergence calculation is realistic.

6.4.2 Temporal features

In the above sections OLR has been related to individual variables such as SST and LLPW. The analyses concentrated mostly on their spatial interrelation at various times

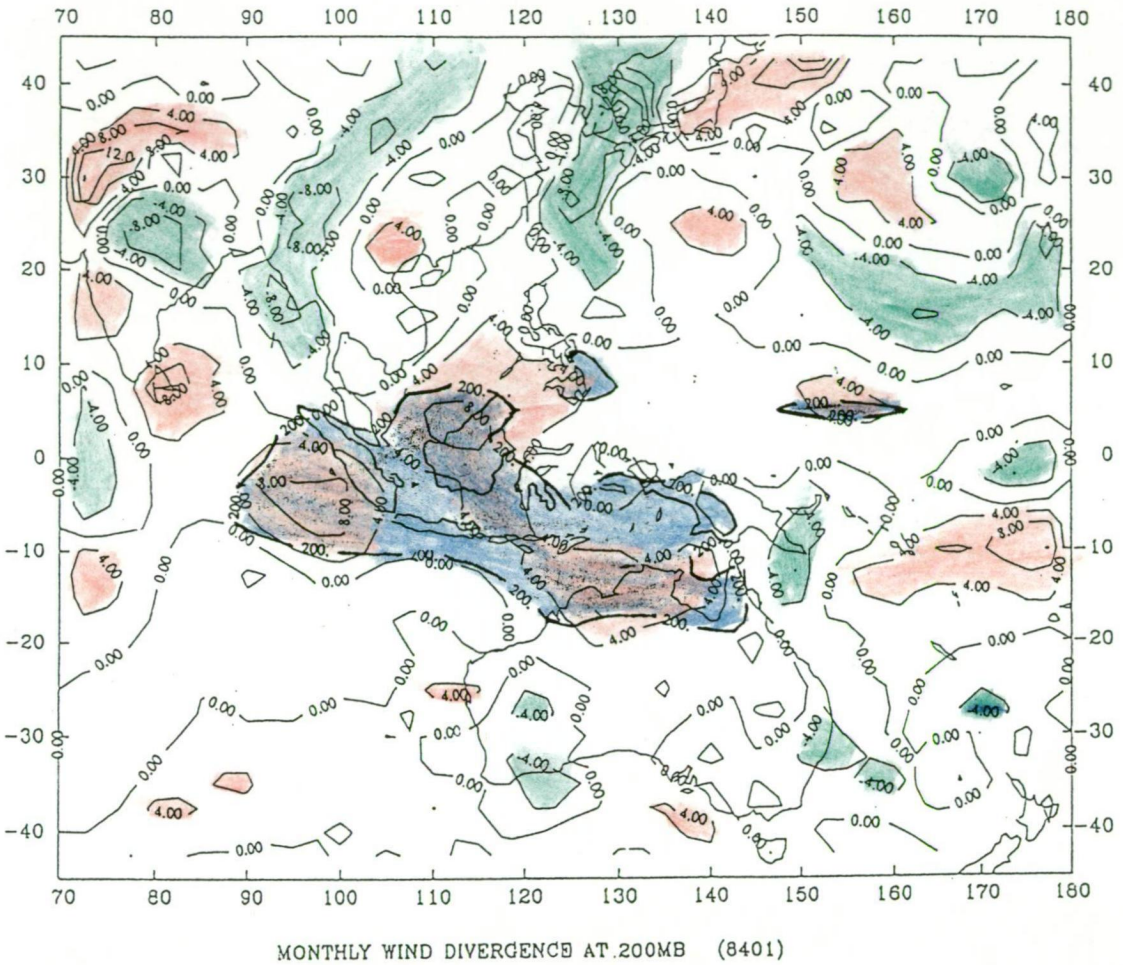

Figure 6.6 Monthly wind divergence at 200 mb in January 1984. Areas of divergence larger than 4×10^{-6} sec^{-1} are shaded in red and areas less than -4×10^{-6} sec^{-1} in green. Contour interval is 4×10^{-6} sec^{-1}. Superimposed are OLRs during the same period with values less than 200 Wm^{-2} (blue areas). Notice the agreement between these two fields.

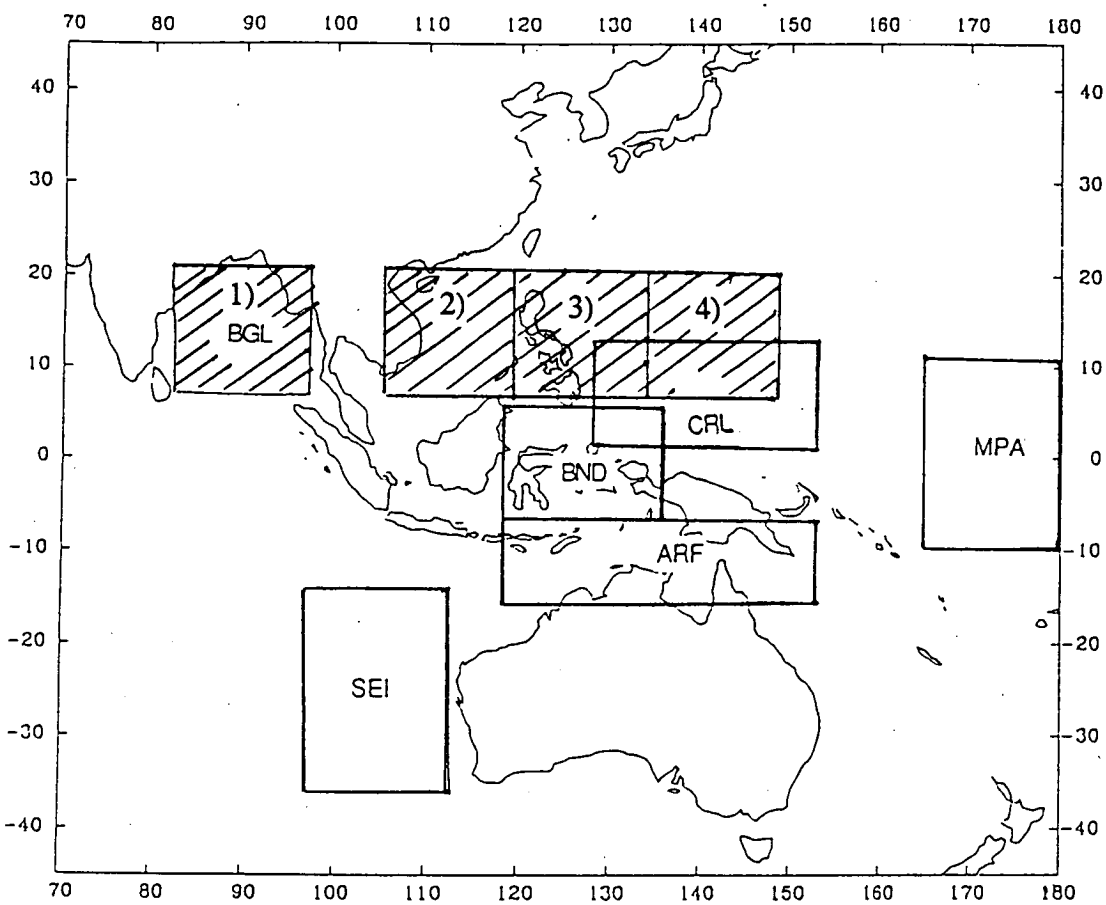

Figure 6.7 Locations of six regions with some interesting features: the Bay of Bengal (BGL) exhibited semiannual cycles of SST; the southeast Indian Ocean (SEI) and the tropical mid-Pacific near the dateline (MPA) experienced a see-saw feature of SST during 1984-86; the 200 mb divergence centres in the Caroline Sea (CRL) and the convergence centres in the Arafura Sea (ARF) suggest localized circulation cells; and a relatively convection-free area in the Banda Sea (BND), which expanded dramatically from May 1986 onwards. Four shaded bins marked by 1 ~ 4 represent areas selected to construct the conceptual model discussed in Section 6.4.3.

of the year. In this section the controlling factors of SST and the wind field will be integrated to gain further insight into thermal and dynamic processes behind convection. The analysis is done by selecting six regions which exhibit special features in previous chapters (see below for brief explanation), and by observing the temporal variation of each parameter. The data to be examined for each region includes OLR, SST, 200 mb divergence and the U and V components of the 200 mb wind fields. The regions are shown in Figure 6.7; they are: 1) the Bay of Bengal (BGL) which has obvious annual and semiannual cycles of SST and the OLR minimum (maximum convection), 2) the Southeast Indian Ocean (SEI) and 3) the Mid-Pacific area (MPA) which indicated a see-saw feature of SST in 1984-86, 4), the Arafura Sea (ARF), and 5), the Caroline Sea (CRL) which exhibited recurrent, localized cells in divergence at 200 mb level.

a) Bay of Bengal (BGL)

The time series shows some interesting features including strong seasonal variation (Figure 6.8). The SST shows obvious semiannual cycles, with the annual maximum in April to May and the second relative maximum in October. The annual minimum occurs in January, with a relative minimum in July to August. The increase of SST from the annual minimum to the maximum value takes only three to four months. The convection (OLR), on the other hand, shows only an annual cycle. The strongest convection happens in June and the weakest convection in February to March. The sharp decrease of convection almost always happens when the SST is in its second minimum, then SST reaches a second maximum as convection collapses. These observations confirm that maximum convection does not always overlap the maximum SST in time.

The above processes are interpreted as follows: in the first half of the annual cycle of convection, i.e. from its bottom to its peak, the SST is positively related to convection with a lead of one month. Once the convection reaches a certain intensity (around 220

a)

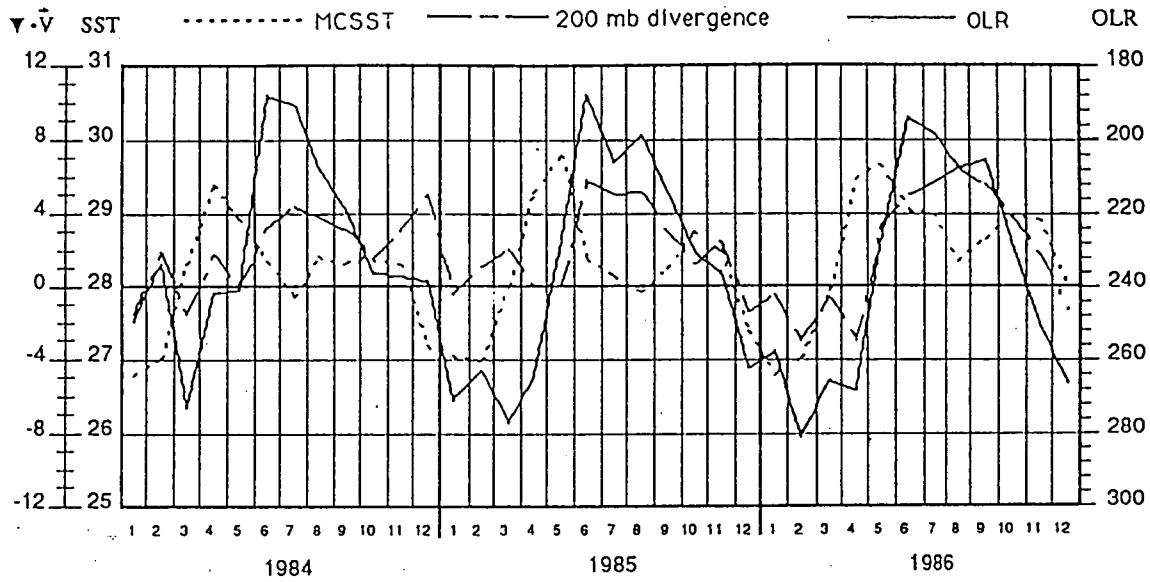

Monthly OLR, MCSST and 200 mb divergence during 1984 - 86 in the region of BGL.

b)

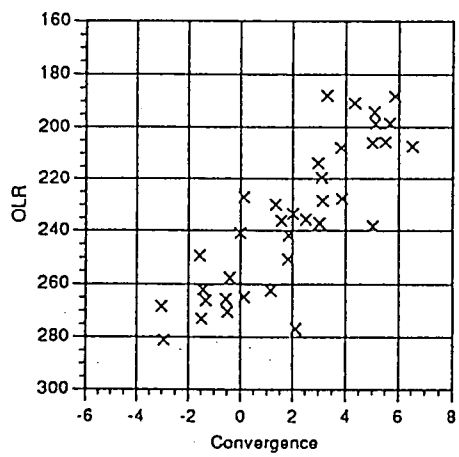

Monthly OLR vs convergence during 1984 - 86 in the region of BGL

c)

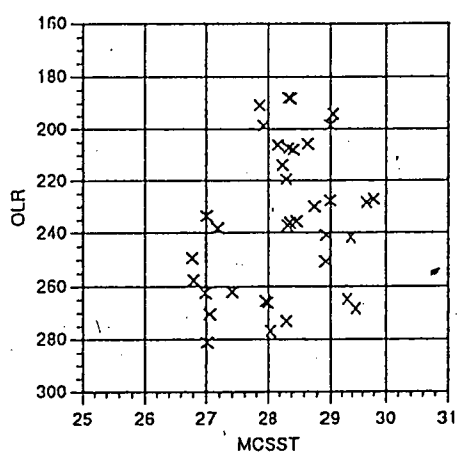

Monthly OLR vs MCSST during 1984 - 86 in the region of BGL

Figure 6.8 The time series of monthly MCSST, 200mb wind divergence and OLR during 1984-86 in the region of BGL (a). Units are °C for MCSST, 10^{-6} sec^{-1} for divergence and Wm^{-2} for OLR. Also shown are the scatter maps of OLR vs divergence (b) and OLR vs MCSST (c).

Wm^{-2}), heavy clouds block the solar radiation decreasing the SST and converging winds develop at the sea surface so that the SST is cooling also partly due to evaporation. However, since the SST is still above its threshold temperature, with the support of wind convergence at the surface and divergence at 200 mb, the convection continues to develop and remains strong. Once the SST drops below its critical temperature (in July to August), the wind divergence alone (dynamic factor) is not able to support the convection, therefore it collapses rapidly. Since the solar radiation is still relatively strong and there is less cloud cover than previously, SST recovers slightly (about 0.5 to 1°C), reaching its second maximum near October. The pattern of divergence aloft does not permit development of convection at this time.

This analysis shows that neither the SST nor wind convergence at the surface are in themselves sufficient to generate and maintain deep convection. Instead this analysis points to the critical role played by the upper divergence field at 200 mb. Taking 1984 as an example, it is noticed that in May the upper divergence increases as the convection develops. In September/October convection is low despite the SST being warmer than 28°C. However, upper divergence is also low at this time. Alternatively in December/January, the upper divergence is high but the convection is low in response to low values of SST.

It is obvious from this analysis, that the relationship between SST and convection is not as straightforward as proposed by earlier studies (Bjerknes, 1969; Rowntree, 1972; Julian and Chervin, 1978). They argued that high SST will result in enhanced surface evaporation, and thus provide the latent heat which would increase atmospheric instability. Through these dynamic processes, the high SST would enhance atmospheric convection. This theory has been modified by recent studies (Ramage, 1977; Gill and Rasmusson, 1983; Gadgil *et al.*, 1984; Graham and Barnett, 1987; Weare, 1987) who found that the SST-convection correlation breaks down above 27-28°C. The results from this study point to firstly the importance of upper level

a)

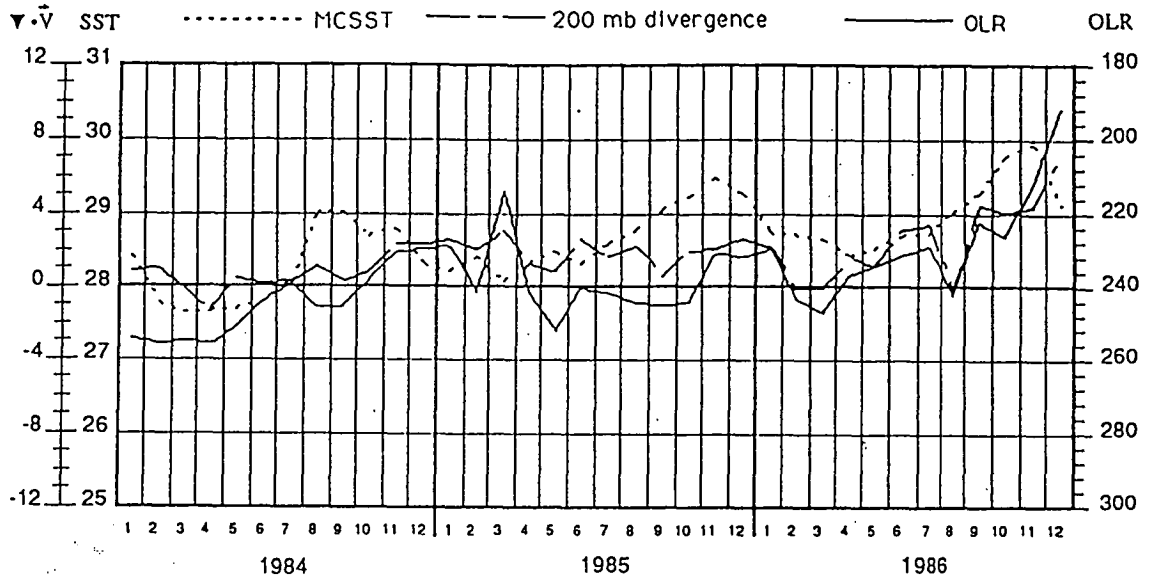

Monthly OLR, MCSST and 200 mb divergence during 1984 - 86 in the region of MPA.

b)

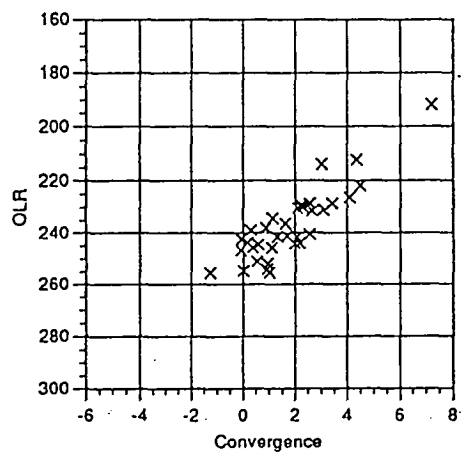

Monthly OLR vs convergence during 1984 - 86 in the region of MPA

c)

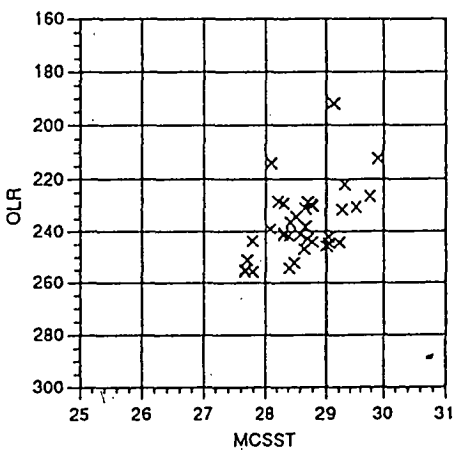

Monthly OLR vs MCSST during 1984 - 86 in the region of MPA

Figure 6.9 As of Figure 6.8 except for the region of MPA.

divergence in maintaining convection; and secondly the continuing importance of SST in initiating and maintaining convection.

b) The Mid-Pacific area (MPA) and the Southeast Indian Ocean (SEI)

The see-saw feature in SST between the mid-Pacific and the Southeast Indian Ocean has already been discussed in Chapter 4. Detailed monthly time series of SST, OLR and the 200 mb wind divergence are presented in this section (Figure 6.9 a). It may be noticed that all three time series in the mid-Pacific show increasing trends from 1984 to 1986. For monthly SST, the annual maxima were 29°C in 1984, 29.5°C in 1985 and 30°C in 1986. The 200 mb divergence in 1984 was very weak, less than 10^{-6} sec^{-1}, about 2×10^{-6} sec^{-1} in 1985, and reached values greater than 4×10^{-6} sec^{-1} from September 1986 onward. The scatter diagram of OLR vs 200 mb wind divergence (Figure 6.9 b) shows a clear linear relationship between the two variables. However, while the warming trend of SST provides greater chances for convection to develop, the scatter map of OLR vs SST shows little evidence of a direct linear relationship between the two. Again, deep convection must be supported by upper level divergence in this region, as found in the Bay of Bengal.

The scenario in the Southeast Indian Ocean is very different from that in the mid-Pacific (Figure 6.10a). The monthly SSTs in SEI are well below 26°C, so that the OLR are all above 240 Wm^{-2}. That is to say, there is no significant convection. This relationship between OLR and convergence field is also not well established. While convergence varies from -3 to 5×10^{-6} sec^{-1}, the OLRs only slightly varies around 260 Wm^{-2} (Figure 6.10b). This poor relationship is due to the fact that OLR is no longer a good indicator of convection when OLR is greater than 250 Wm^{-2}.

The cooling process of the sea surface in the Indian Ocean is very obvious. The annual minima are 21.8°C in 1984, 21.3°C in 1985 and 20.5°C in 1986. This is in contrast to the warming trend of SST in MPA. On the other hand, while the convection in the mid-Pacific increases with SST, the OLR in the Indian Ocean does not suggest a

a)

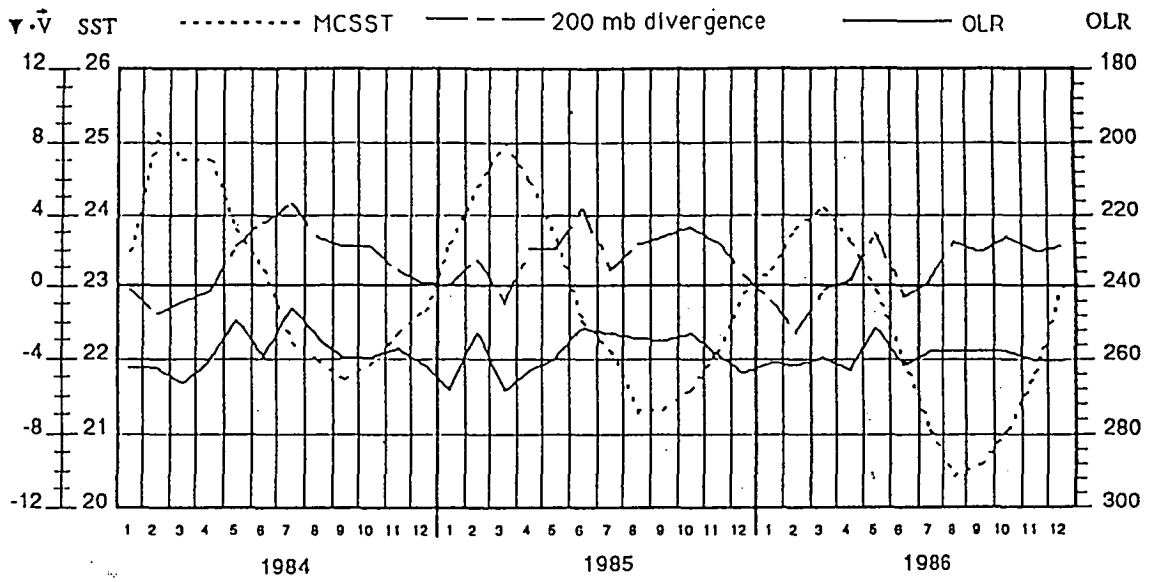

Monthly OLR, MCSST and 200 mb divergence during 1984 - 86 in the region of SEI.

b)

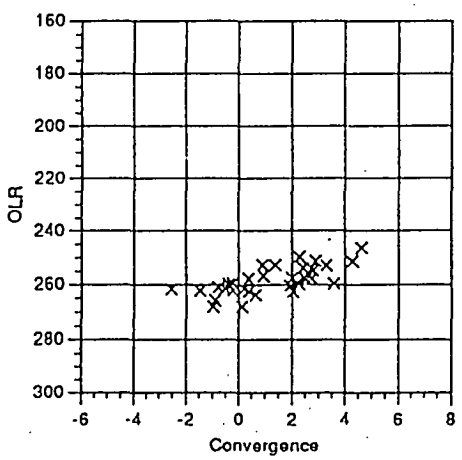

Monthly OLR vs convergence during 1984 - 86 in the region of SEI

c)

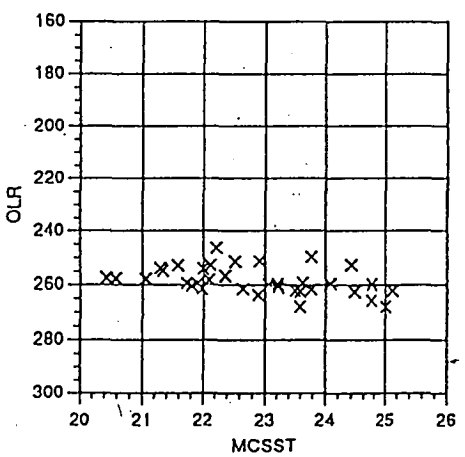

Monthly OLR vs MCSST during 1984 - 86 in the region of SEI

Figure 6.10 As of Figure 6.8 except for the region of SEI.

significant local weakening of convection with lower SSTs. This is due to the fact that convection seldom occurs when SSTs are below 27.5°C (Graham and Barnett, (1987)

c) The Arafura Sea (ARF) and the Caroline Sea (CRL)

The annual cycles of convection, SST and 200 mb wind convergence in the Arafura sea are all in phase (Figure 6.11). They all reach their maxima around December-January, and their minima in July-August, following the solar movement. There is also some warming of the SST in these three years. The December SSTs are 29.1°C in 1984, 30.1°C in 1985 and above 30.5°C in 1986. On the other hand, convection does not show any obvious increasing trend.

The situation in the Caroline Sea (Figure 6.12) shows that the annual cycles of these three variables are not as marked as those in the Arafura Sea. Nevertheless, the convection and 200 mb wind divergence reach their annual highs from June to September at the same time as these two variables in the Afafura Sea reach their annual low. This pattern suggests existence of a localized cell with convection over the Caroline Sea and subsidence over the Arafura Sea which will be further examined in section 6.4.4.

6.4.3 Conceptual Model

An examination of the Bay of Bengal data has led to the development of a conceptual model of convection which highlights the relationship between SST, OLR and upper divergence. To examine the model further, four regions in the band from 7.5°N to 20°N were selected. Each region represents a sector of 15° longitude by 12.5° latitude. To simplify matters, these regions have been selected in a narrow zonal band, therefore the annual course of solar radiation is the same in all regions. Similarly, the SST shows the same annual cycle. Data have been obtained by averaging the field of OLR, SST, and 200 mb and 850 mb wind divergence for each of these four regions on a monthly basis. Thus each field contains 36 values (3 years × 12 months).

a)

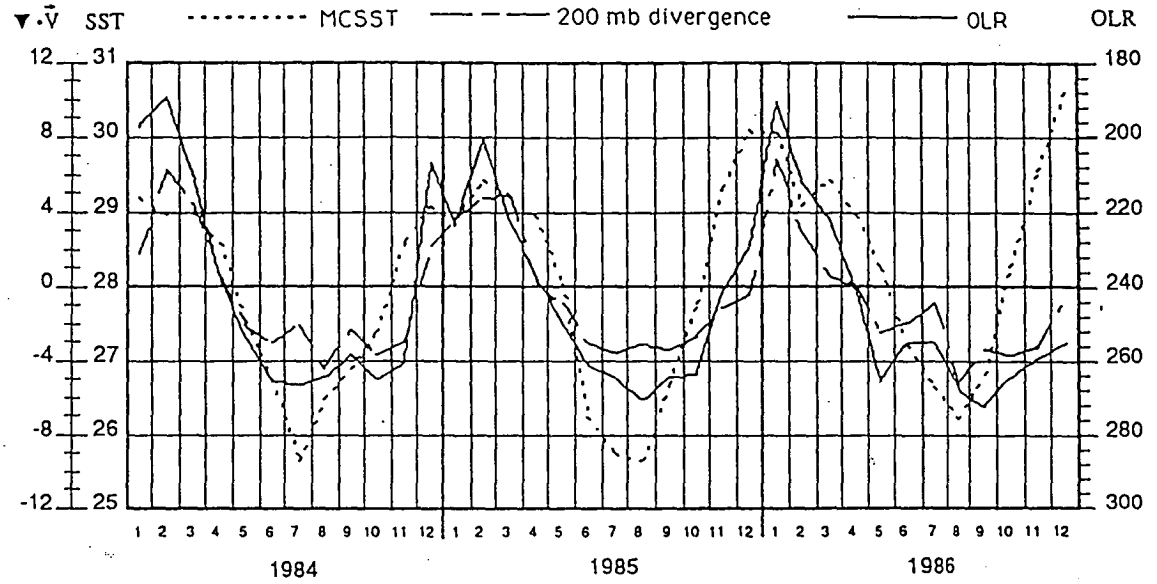

Figure 6.11 Monthly OLR, MCSST and 200 mb divergence during 1984 - 86 in the region of ARF.

b)

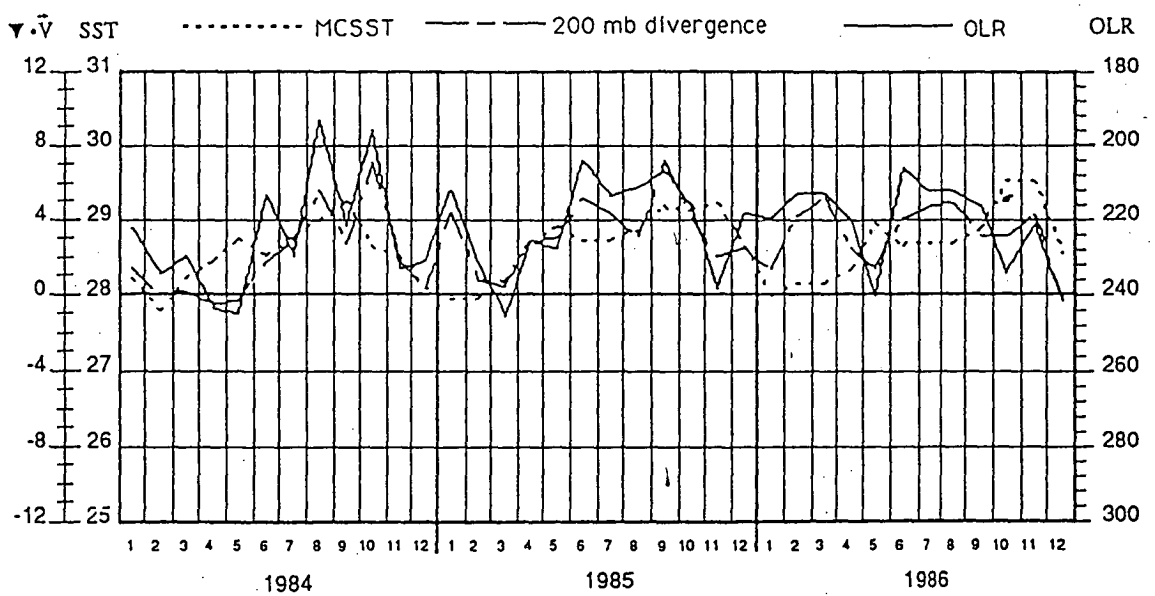

Figure 6.12 Monthly OLR, MCSST and 200 mb divergence during 1984 - 86 in the region of CRL.

Superimposed on the annual cycles is a secondary annual maximum and minimum. These features make it possible to classify five stages according to the behaviours of the SST. They are as follows:

1) The SST warmer than 27.5°C to its annual maximum;

2) From its annual maximum to its second minimum;

3) From its second minimum to its second maximum;

4) From its second maximum to a temperature equal to or warmer than 27.5°C;

5) Cooler than 27.5°C.

The scatter map of monthly SST and OLR for the four areas are shown in Figure 6.13a. It is very clear that below 27.5°C, convection seldom occurs. Once SST is warmer than 27.5°C, SST and OLR do not show any obvious relationship. This is similar to the observation by Graham and Barnett (1987). However, these data can be partitioned into the various convection stages as described above. To illustrate the process better, only the mean and the standard deviation (in SST and convection) during the five stages are plotted in the diagram (Figure 6.13b). In addition, to enhance the understanding of the temporal features of these five stages, the mean values and standard deviations of monthly differences from adjacent months are also shown in Figure 6.13c. To highlight the features at different stages, a composite cycle of convection is constructed. The averaged values of OLR, SST, wind divergences of both 200 mb and 850 mb levels at the end of each stage are calculated and presented in Figure 6.13b. The composite is a representation of 12 convection cycles (3 years times 4 regions). Areas with values of OLR larger than 240 Wm^{-2} (and SST cooler than 27.5°C and negative divergence) are shaded to indicate nonsensitive values to strong convection. Examining this diagram with the OLR/SST comparison (Figure 6.13 a, b, and c), the following important features of the five stages can be described:

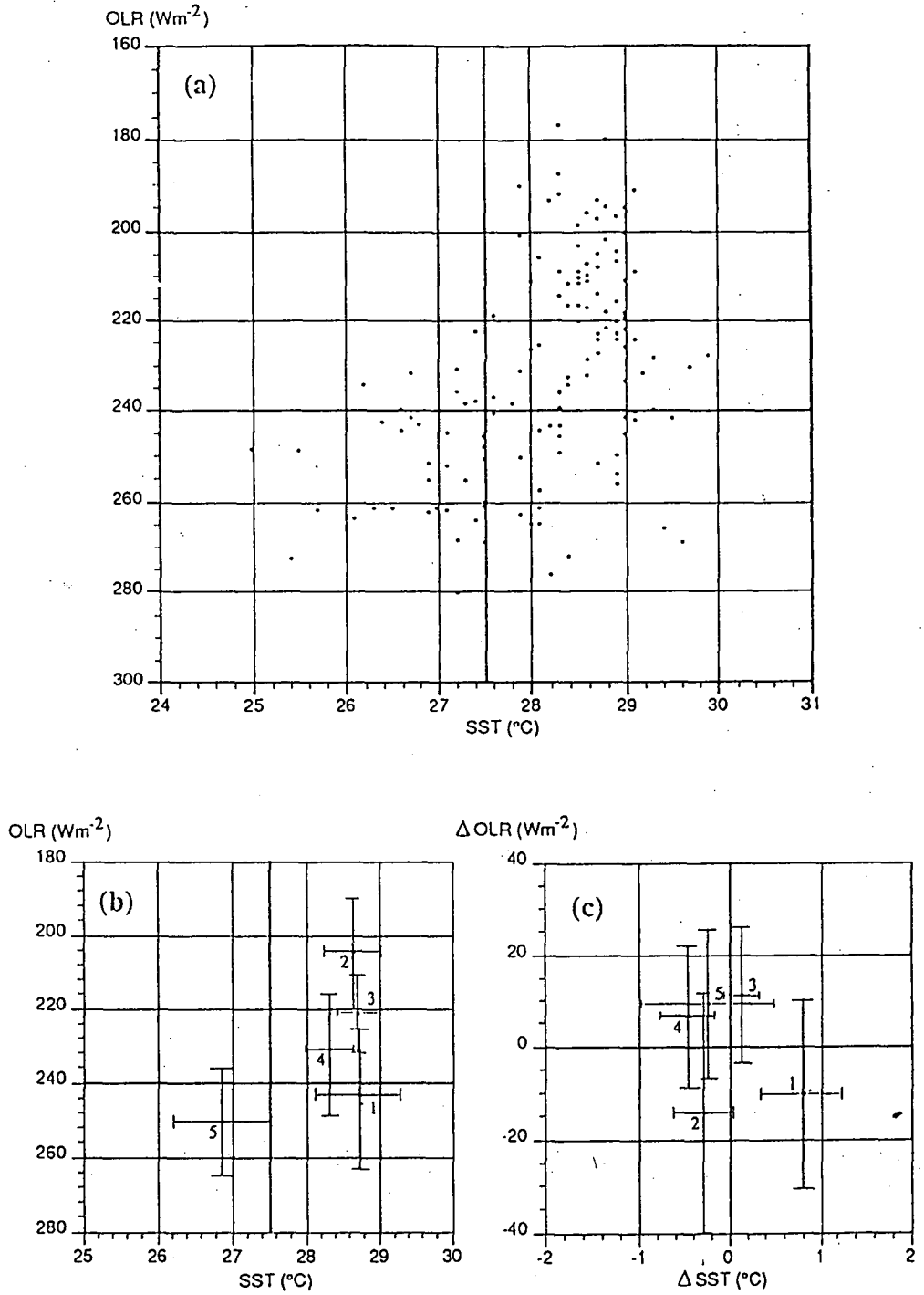

Figure 6.13 Scatter map of monthly OLR vs SST in 1984-86 (a). The mean values of SST and OLR in the five convection stages (denoted by number, see context for detail) are plotted while the corresponding standard deviations are represented by error bars (b). The mean values and standard deviations of monthly differences from adjacent months are shown in (c). Using (b) and (c), the five convection stages are clearly featured. A composite annual cycles related to the five stages of convection is in (d). See context for the construction of the composit cycle.

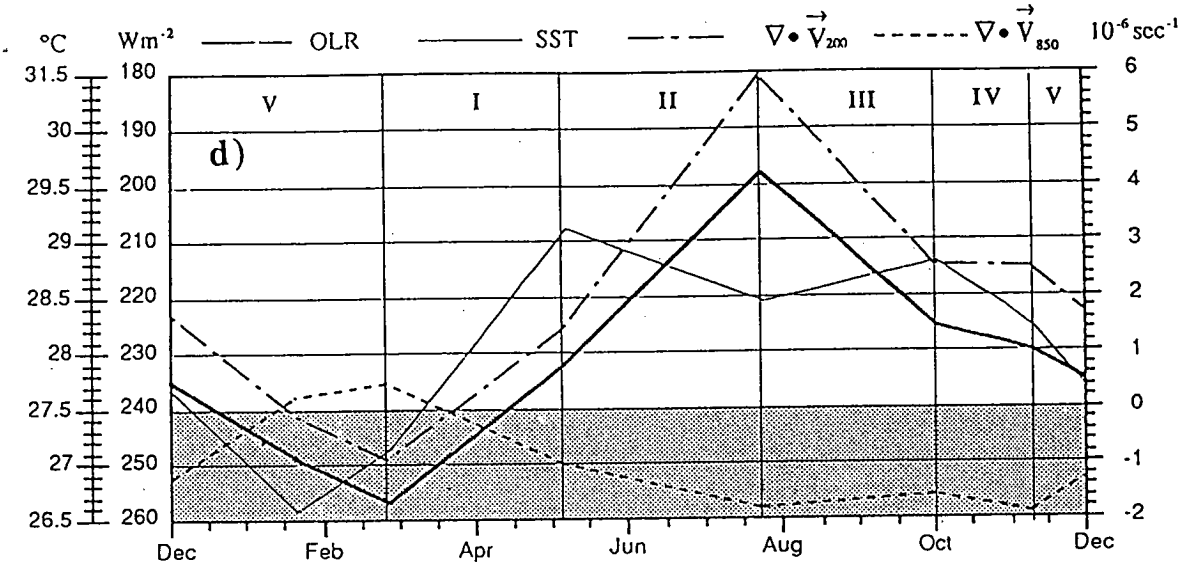

Figure 6.13 (Continued).

(I) Initial stage: SST exceeds 27.5°C and deep convection starts to occur but is not well developed. The average SST is 28.7°C and the OLR is 244 Wm^{-2}. Since the wind divergence aloft is not strong enough, convection does not always occur. At the end of the initial stage, the SST reaches its annual maximum, averaged at 29.2°C, while the averaged OLR is only 233 Wm^{-2} (Figure 6.13d). The whole stage usually occurs from April to May and lasts for 2.3 months.

(II) Fully developed stage: The 200 mb wind divergence increases rapidly at the end of the initial stage from 1.5×10^{-6} sec^{-1} to 6×10^{-6} sec^{-1}. This process intensifies the convection and it reaches its strongest intensity (OLR, 198 Wm^{-2}). On average, the SST in stage 2 decreased slightly, but the convection has increased in the mean to 205 Wm^{-2}. Due to blocking of solar radiation by heavy clouds and evaporative cooling by convergent wind at the surface (Meyers *et al.*, 1986) the SST decreases. At the end of this period, the SST reaches its second annual minimum, averaged at 28.45°C, and the average OLR is 198 Wm^{-2}. More interestingly, it is noticed that most annual maxima of convection happen at the time when SSTs reach their second annual minima. The averaged annual minimum OLR is 194 Wm^{-2}, not significantly different from the averaged OLR (198 Wm^{-2}) at the time of the SST second annual minimum. This second stage of convection usually occurs from June to August, lasting about 2.5 months at average. This stage points to the importance of cloud blocking in lowering the SSTs and the role of the upper divergence in maintaining the convection.

(III) Weakening stage: Convection starts to weaken once the SST has reached its relative minimum. Due to a lessening cloud cover and an increase in solar radiation, the SST warms up slightly. The averaged warming rate is 0.15°C per month while OLR increases at 11 Wm^{-2} per month (Figure 6.13c). At the end of this stage, the averaged SST is 28.81°C, about 0.4°C warmer than its previous relative low and the average OLR is 225 Wm^{-2}.

(IV) Collapsing stage: This is a relatively short period with an average duration of 1.3 months occurring around November. Since the solar radiation decreases and the Asian Winter Monsoon develops, the SST decreases at a rate of -0.45° per month. The OLR, on the other hand, continues its previous increasing trend at the rate of 7 Wm^{-2}.

(V) Idle stage: The SST is now below 27.5°C. Convection is not very active at this stage. The averaged OLR is about 250 Wm^{-2}. This stage is relatively long (about 3.6 months) lasting from December to March.

From the above analysis, it can be seen that the relationship between convection and SST is quite complex. While warmer SST (greater than 27.5°C) is a necessary condition for convection, it is not a sufficient condition for convection to develop. There is an interesting feed-back mechanism between the two variables which play different roles at different stages. It is also noticed that the minimum OLR (maximum convection) is in agreement with the second annual minimum of SST. This is in contrast to the usual perception that minimum OLR would coincide with the maximum SST.

There are a few interesting features in the composite convection cycle. Firstly, most of the variables show annual cycles, especially for the OLR and 200 mb wind divergence. These two variables show very good agreement both in the amplitude of the variation and in the phase. On the other hand, while the wind divergence at 850 mb level does show generally good agreement with OLR, these two variables are not as well linearly correlated in stage II and III. This suggests that while the 850 mb wind field is important in initiating the convection, the 200 mb wind field may play a more dominant role in the whole convection process.

Secondly, while the annual cycle dominates the SST variation, there is a superimposed second annual maximum and minimum. This might be partly due to the solar movement passing the region twice a year. However, the timing of the second minimum is in August when the solar zenith at noon should be close to zero.

Therefore, the explanation to this minimum by the solar movement is far from satisfactory. Evaporative cooling by the strongest surface winds (Meyers *et al.*, 1986) and cloud blocking of solar radiation are likely explanations for preventing any further increases in the SSTs.

Thirdly, in contrast to 200 mb wind divergence, the SST does not keep in phase with OLR variations very well. However, close examination finds that there is a tendency for SST to lead the OLR in the initiating, collapsing and idle stages. This suggests that SST is very important in providing a "warm background" and in generating an initial forcing (or instability) for large scale convection. After the initial development of the convection, the dynamics of the atmosphere (especially at higher level, e.g. 200 mb wind divergence) are more important in accelerating and maintaining convection. Again, a falling SST will initiate and lead to the collapse of convection.

Finally, the 200 mb and 850 mb divergences are well timed and opposite in phase. This certainly supports the accuracy of the calculation of divergence. It is also expected from the dynamical point of view.

6.4.4 Local circular cells related to ITCZ and SPCZ

6.4.4.1 General features of localized cells

As discussed in the Chapter 5, a narrow zone of subsidence at 200 mb level occurs north of Australia during the southern winter and spring. Close examination of the monthly wind divergence field has revealed some further evidence of these localized convergence centres. There is a tendency for pairing in the divergence and convergence cells at the 200 mb wind field. An examination of the 200 mb wind divergence field reveals that this cell-like behaviour is a feature of both the ITCZ and the SPCZ. In this section various characteristics of these cells are presented and related to other variables.

Given the nature of the cells, a strict set of guidelines must be followed if meaningful data is to be derived. In the rest of this section, both convergence and divergence centres refer exclusively to the 200 mb wind field.

a) Firstly the analysis is restricted to tropical regions bounded by latitudes 20°S and 20°N. In the case of the Tasman Sea, the latitude limit is expanded to 30°S poleward to include centres related to the SPCZ. Within this region only convergence and divergence centres greater than a threshold of $\pm 4 \times 10^{-6}$ sec^{-1} are considered in the analysis.

b) An examination of the regions of convergence and divergence over the 36 months indicated that there are preferred regions where these cells are located. This consideration has led to the partitioning of three regions along a zonal band. These are: the mid-Indian Ocean (70°E-100°E), the Banda Sea (100°E - 145°E) and the Coral Sea (145°E - 180°E). Figure 6.14 shows a typical distribution of these cells.

c) In some cases a divergence centre was not accompanied by a convergence centre in the same region. Data under these conditions were not included in the analysis. However it must be pointed out that this condition represented only a small fraction of the total number of cases (5%).

d) In the case that more than two divergence (or convergence) centres exist in one region as denoted by b), only the pair with the largest intensity and smallest separation are considered. Again these conditions existed in only a small percentage of the total cases (17%).

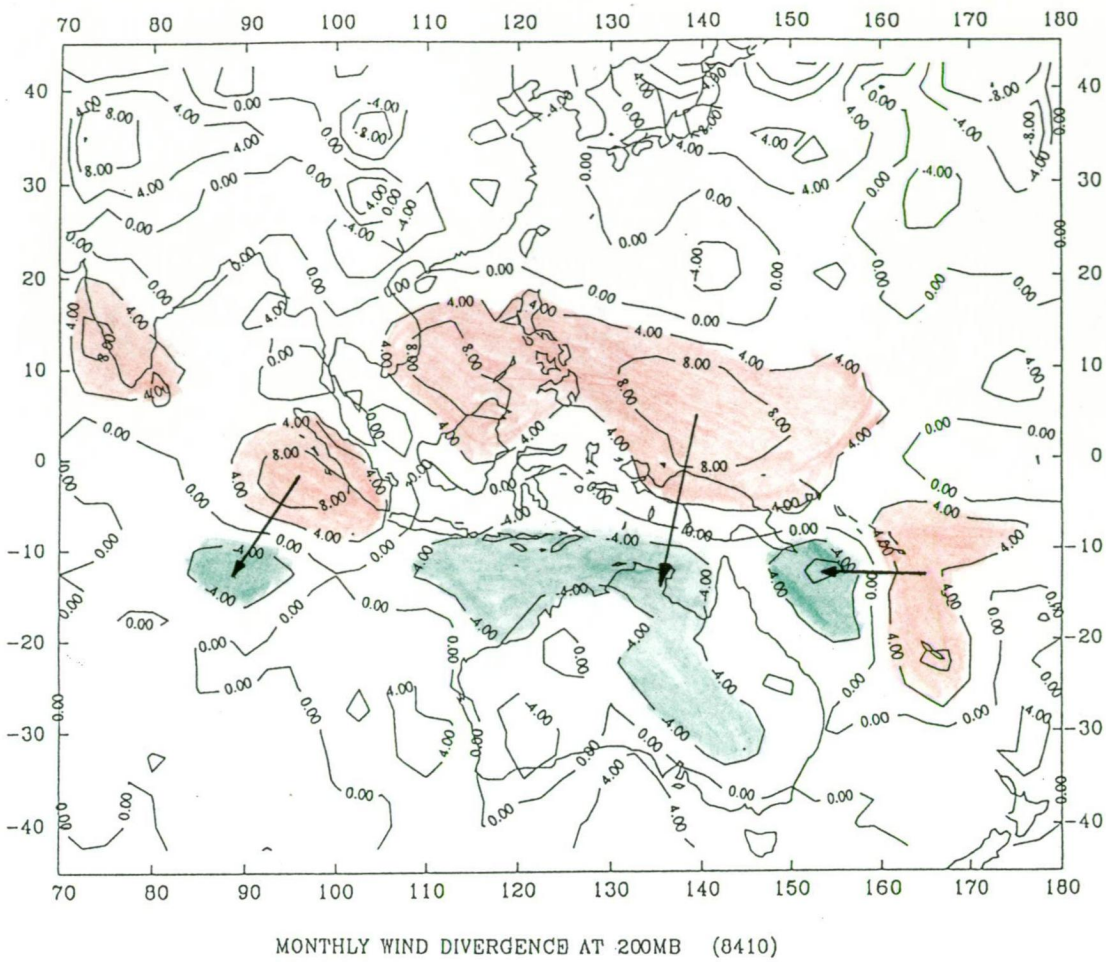

Figure 6.14 Example of localized circulation cells in the equatorial Indian Ocean, the Banda Sea, and the Coral Sea shown on monthly 200 mb wind divergence map. Areas shaded in red denote upper level divergence centre ($> 4 \times 10^{-6}$ sec^{-1}), and areas in green denote convergence centres ($< -4 \times 10^{-6}$ sec^{-1}).

Following these rules, three sets of the parameters related to both convergence and divergence centres in all of these three regions were measured to provide a basic data set. The intensity is determined by the value of the central contour lines. The basic unit of area is a 2.5 degree by 2.5 degree bin that the $\pm 4 \times 10^{-6}$ sec^{-1} contour line occupies. The area size of the both the convergence or divergence centres are therefore measured by the number of bins and divided into five categories: very small (VS, 5-14 bins), small (S, 15-34 bins), medium (M, 35-54 bins), large (L, 55-85 bins) and very large (VL, more than 85 bins).

The distance between paired cells, gradient of divergence between the paired cells and the orientation of the convergent centres related to its paired divergent centre were calculated in the analysis. Since these paired cells are all located near the Equator, the spatial distance covered by 1° latitude or 1° longitude differ only by a few percent (at the equator one degree equals 110 km). For simplicity in the calculation, distances are therefore calculated in units of "degrees", irregardless of whether they are latitudinal or longitudinal degrees. Gradients of paired cells are calculated in terms of difference between intensities of divergent and convergent cells (in units of 10^{-6} sec^{-1}) divided by distance in degrees. The orientation is measured clockwise starting from 0° when the convergence centre is located north of the corresponding divergence centre.

The frequency distribution of divergence gradients (Figure 6.15a) shows that a majority of the gradients occur between the values of 0.5×10^{-6} sec^{-1} $degree^{-1}$ to 1×10^{-6} sec^{-1} $degree^{-1}$. Furthermore, all three regions exhibit the same behaviours. In terms of distance, the peaks in the cells are between 10-19 degrees (Figure 6.15b). This distance is considerably smaller than the maximum distance scale (>35 degrees) of each of the subregions.

Figure 6.15c shows that there is a preferred orientation in the location of the convergence centres. In most cases they are located in a south to southwest sector relative to the divergence centres. This orientation, in the absence of a Coriolis force

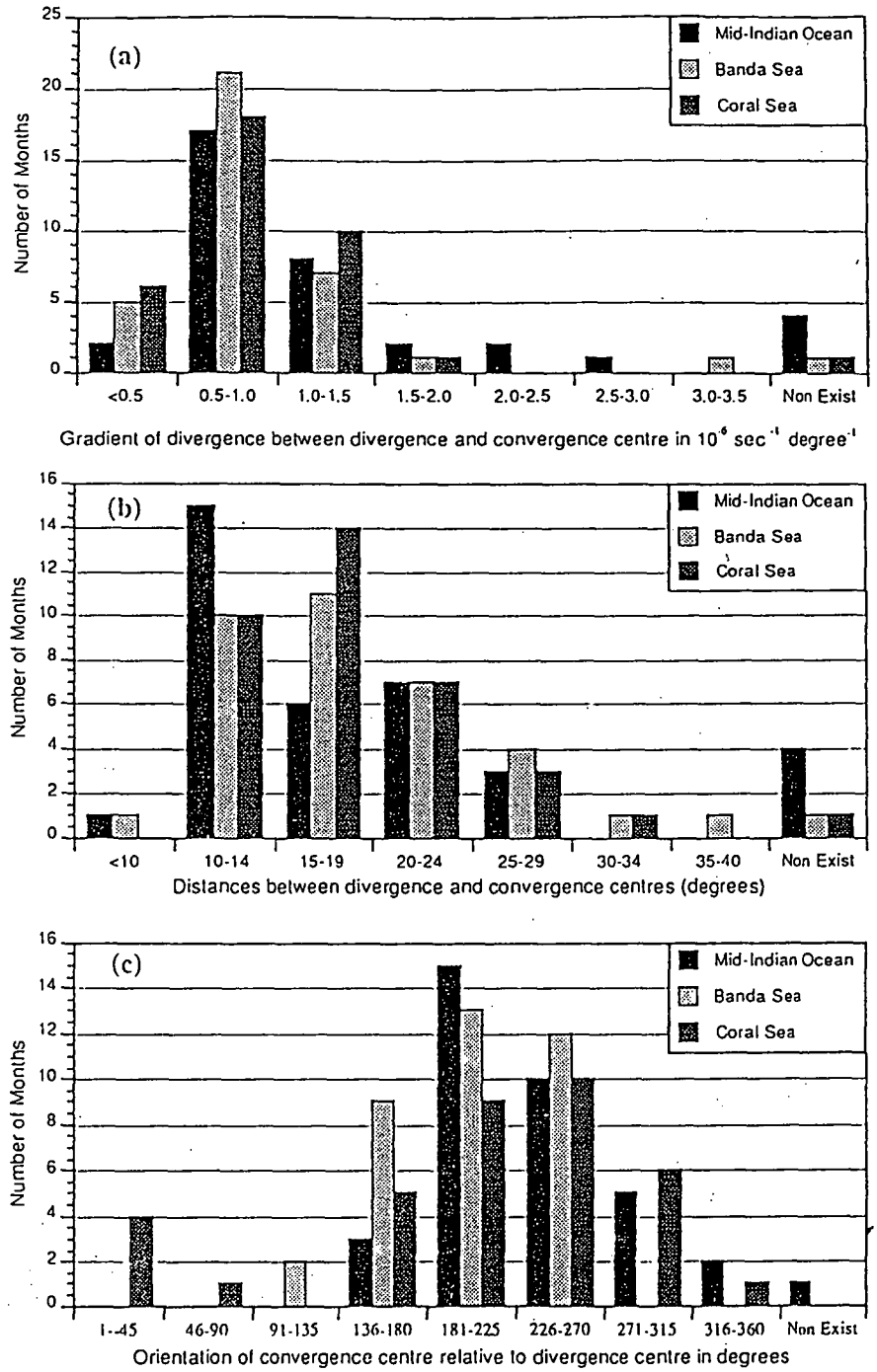

Figure 6.15 Frequency distributions of gradients of divergence in units of 10^{-6} sec^{-1} $degree^{-1}$ (a); distance in degrees (b); and orientation (c) related to localized cells in the three regions: the mid-Indian Ocean, the Banda Sea and the Coral Sea. The orientation (ranged from 0° to 360°) is measured clockwise starting from 0° when the convergence centre is located north of the corresponding divergence centre.

close to the equator, implies that surface southwesterly winds play an important role in maintaining these cells.

6.4.4.2 Interannual features

The gradients of divergence cells in the three study regions will be further discussed in this section, focusing on their interannual features. The time series of these gradients are smoothed using a 3-months running average.

a) The mid-Indian Ocean.

There is a strong peak in the time series of gradient in the mid-Indian Ocean (Figure 6.16a). The background value seems to be less than 1×10^{-6} sec^{-1} $degree^{-1}$. From the end of 1985 to the beginning of 1986, the values increased markedly and ranged from 1.5 to 2.5,. Checking the contour maps for the corresponding period (see Appendix), it was observed that there was a very strong and stable divergence centre existing at 95°E near the Equator (see Figure 6.14). This is a very interesting feature considering that this centre exhibited a seasonal shift from 10°S in the southern summer to 10°N in the southern winter in the time period previous to this. An examination of the SST and OLR fields failed to show any obvious anomalies during the same time period. During this time of the year the SST is above 28°C and the OLR is usually below 220 Wm^{-2}. Although it would be expected that the anomalously strong convection should be observed at this time in the area, a close look at the time series of OLR in this region did not confirm the expectation. It is therefore possible that below a certain value of OLR, the relationship between OLR and the 200 mb divergence field is no longer linear (see Figure 6.8).

b) Banda Sea

The time series of the gradients in divergence in Banda Sea area has not shown any anomalous features except a peak near the end of 1986 (Figure 6.17a). An examination of the original data set demonstrated that this peak resulted from an abnormal pair of

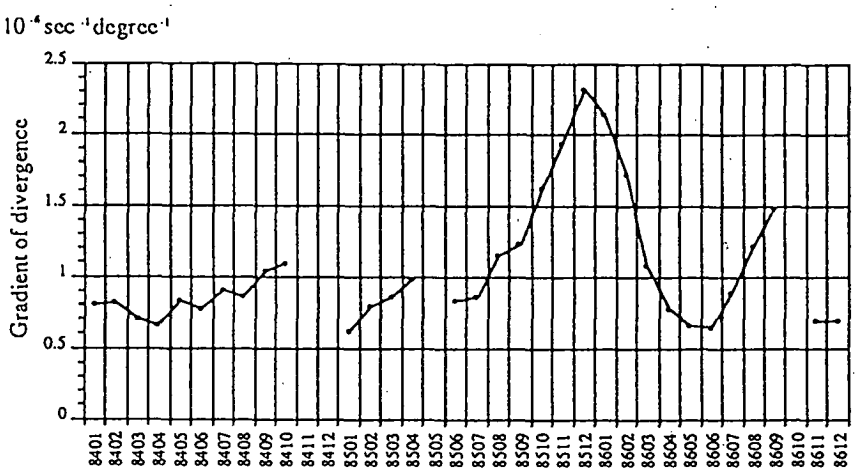

Figure 6.16 Time series of 3-month running average of gradient of divergence in units of 10^{-6} sec^{-1} $degree^{-1}$ in the mid-Indian Ocean.

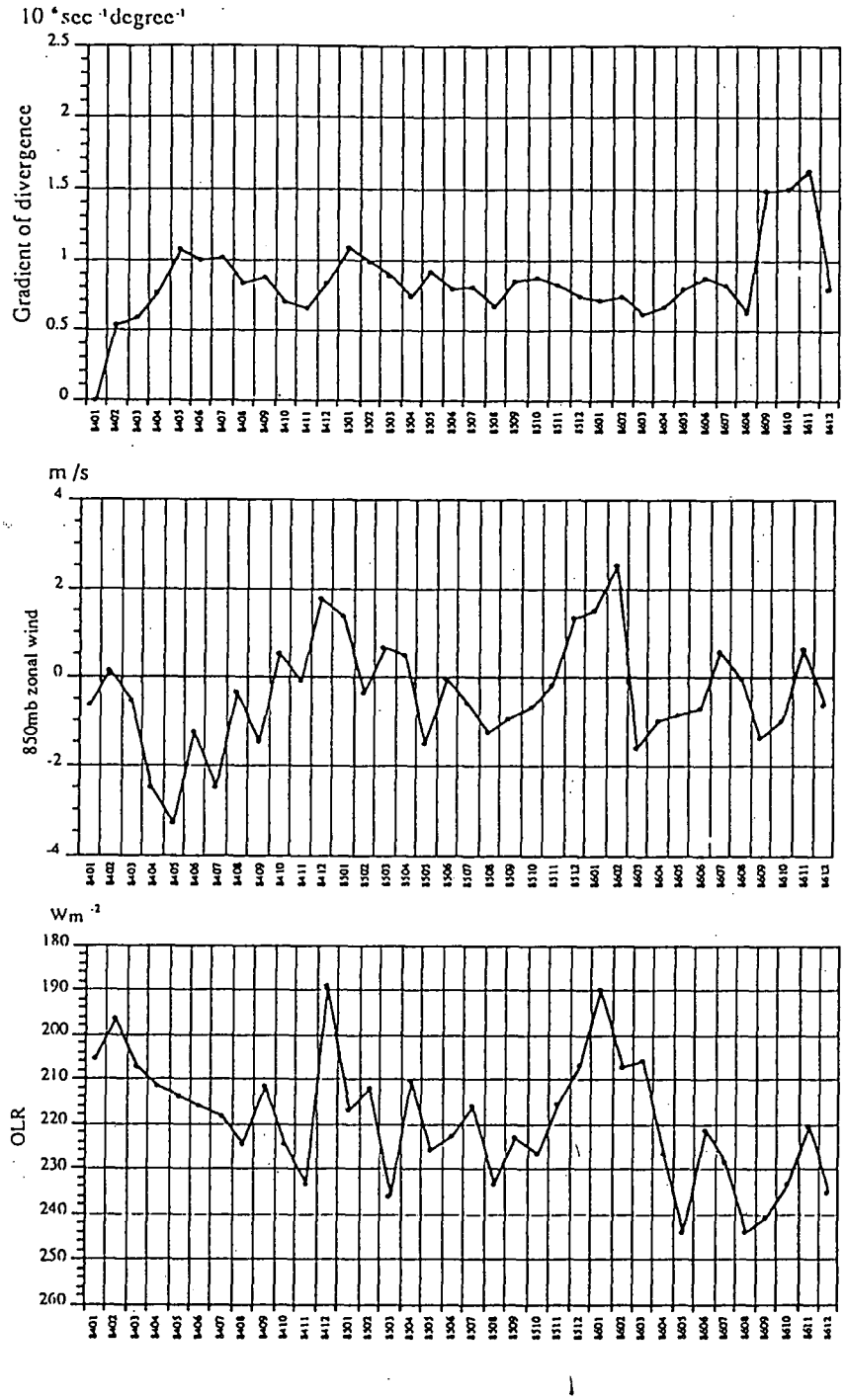

Figure 6.17 The same as Figure 6.16 except for the Banda Sea area (a). The monthly zonal wind at the 850 mb in the same area is shown in (b) and the OLR is shown in (c). Notice the weakening trend of easterly in m/s in (b) and the intensifying trend of OLR in Wm^{-2} in (c).

cells in October 1986. This feature will not be further discussed since it occurred only in one month.

A detailed examination of the wind field in this region has revealed that there is a strong buildup of westerlies at 850 mb in the three year period (Figure 6.17b). Convection in this area, represented by OLR, shows a weakening trend (Figure 6.17c). This is consistent with our knowledge that prior and during ENSO events, the convection centre moves eastward from Indonesia to the the mid-Pacific. Applying this concept to the time series, it is not surprising to see that convection in the Banda sea area weakens prior to the 1986 ENSO event.

c) Coral Sea

The time series of gradient of divergence in the Coral Sea shows a relatively high value in the middle of 1986 (Figure 6.18a). The wind fields, at the 200 mb and 850 mb levels, both show temporal trends. The southerly at 850 mb increases its strength gradually in the three years, especially in 1986 (Figure 6.18b). This time series reaches its peak in June 1986, approximately one month after the peak in the gradients of the divergence field. These two graphs suggest that the two paired centres were aligned in a meridional fashion and intensified in May/June 1986. A similar observation of increasing southerly wind component as a precursor to an ENSO event has been reported by Meyers *et al.* (1986). At the same time, the northerly at 200 mb increases towards the end 1986 (Figure 6.18c). At this time the convection centre in the Coral Sea area moved towards the dateline and therefore decreased the magnitude of the gradient, since the two centres were now further apart. However, whilst the gradients decrease, the intensity of the convection increased and this largely explains the increasing northerly component wind at 200 mb.

This intensified circulation is therefore represented well by the gradient of divergence in this region. On the other hand, it is also well represented by the convection in this area. Figure 6.18d shows a clearly increasing trend of convection in the mid-Pacific near the

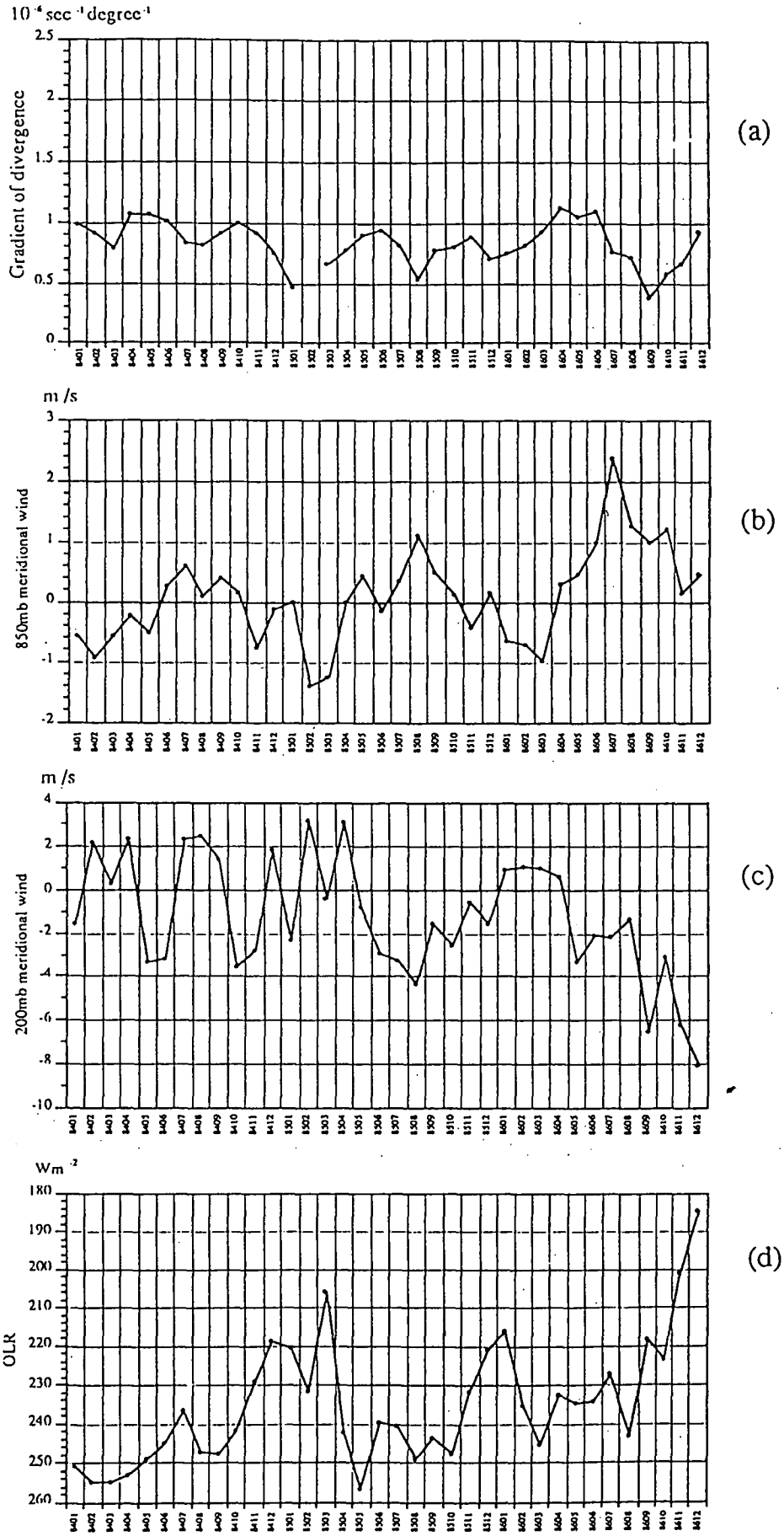

Figure 6.18 Time series of 3-month running average of gradient of divergence in units of 10^{-6} sec^{-1} $degree^{-1}$ in the Coral Sea (a). The monthly meridional wind at the 850 mb is shown in (b), the 200 mb meridional wind in (c) and OLR in (d).

dateline at the onset of the 1986/87 ENSO event. This observation is consistent with the results described in section 6.2 and by other ENSO studies (Rasmusson and Carpenter, 1982).

6.5 Summary

To give a comprehensive summary of this chapter, several important features of convection will be presented here.

a) Convection shows marked annual seasonal variation. Just before the out-break of the Indian Monsoon during May, convection in the tropical areas reaches its annual minimum. From June to July, the convection near the Bay of Bengal sharply increases to its annual maximum with a centre located along the 15°N zone. It then expands eastward to the south China sea and the western Pacific in August. From September onwards, the slightly contracting and weakening central convection zone moves southeastward to the north of Australia. It reaches its most eastward location in February and March with the centre located near 10°S. Convection then starts to dissipate while moving northwestward. Its weakest season is around May, when the centre is located near the Equator. These observations are very similar to those reported by Meehl (1987).

b) Several studies have shown that SST near 27.5-28°C is a threshold for the development of convection, this result is further confirmed in this study. In addition, it has been found that the value of 35 mm of low level precipitable water also covers the areas which exhibit large scale convection. This implies that the 35 mm low level precipitable water (surface to 700 mb) may also be a "necessary" condition for the development of convection.

c) The detailed examination of convection in the Bay of Bengal has initiated a conceptual model regarding the relationship between OLR, SST and 200 mb wind divergence field. The annual course of OLR can be divided into five stages, according

to the behaviour of SST. In the initial stage the SST increases from its threshold of 27.5°C to its annual maximum. While SSTs increase, the convection also intensifies. However, since the wind divergence at 200 mb is still not very strong, the convection has not reached its annual maximum although the SST reaches its maximum at the end of this stage.

In the fully developed stage, the SST drops slightly down due to heavy clouds and evaporative cooling. However, with the support of wind divergence at 200 mb and convergence at 850mb, convection continues to intensify and reaches its annual maximum when SSTs reach their annual second minimum. In the weakening stage, after the relative minimum of SST, convection starts to decrease and the SST increases to a second maximum slightly. The collapsing stage occurs as the SST reduces once again, following the southward shift of solar radiation. The convection, along with the wind divergence, is also weakening. In the idle stage the SST drops below the threshold of 27.5°C and there is no longer any strong convection.

The classification of convection into various stages clarifies the relationship between SST, OLR and divergence, even above the 27.5°C SST threshold. An important result of this work is that the annual maximum of convection coincides not with the annual maximum of SST, but with the second annual minimum. The locations of convection centres generally follow that of high SST centres, with a lag about 1-2 months. In the area eastward from Indonesia, at a specific time, the convection centres are generally located west of high SST centres. In addition, the wind divergence at upper levels in the Indian Ocean (associated with the Indian Summer Monsoon) may play more important roles in accelerating and maintaining convection than that in the western Pacific (associated with the Australian Monsoon). This is in turn may due to the fact that the Indian Monsoon is much stronger than the Australian Monsoon.

d) The localized divergence cells are also analysed to provide some further spatial structure of convection. There is a tendency for paired cells of convergence and

divergence centres to exist in preferred areas and with preferred relative orientations. The convergence centres tend to be located south to southwest of its corresponding divergence centre. This implies the presence of some southerly or southwesterly surface inflow into the convergence centre (i.e. convection centre). This inflow is obviously important in maintaining these cells.

Several interesting features were observed in the convection field as a precursor to the 1986/87 ENSO event. The SST rose towards the end of 1986 in the equatorial region near the dateline. This same region also experienced a decrease in OLR (increased convection) at the same time. A region of relatively high OLR (low convection) gradually expanded in the Banda Sea area from May 1986 onward and did not decrease as would have been expected from the data in previous years. Accompanying this feature, an anomalously strong southerly wind at 850 mb also occurred in the Coral Sea area, reaching a peak in July 1986. This confirms the observation by Harrison (1984) that prior to the 1982-83 ENSO event, there was a very strong southerly anomaly in the Tasman Sea area. Following this feature a strong 200 mb northerly wind occurs and reaches its maximum at the end of 1986. It is suggested here that these processes heralded the arrival of an ENSO event.

Chapter 7. Summary and Discussion

A series of comprehensive data sets including SST, wind, OLR and precipitable water during 1984-86 have been used and analysed in this study. Their results have been summarized in the previous corresponding chapters. Some important conclusions and related discussions are addressed in this chapter.

7.1 Interesting features revealed in this study

1. Operational MCSST data provides regular and informative SST measurements for meteorological and oceanographic studies. The comparisons have indicated an RMSD of about 0.7 °C for daily values and 0.5°C for monthly values. These satellite-derived SST measurements can generally detect the real variation of SST, and thus can be used to monitor the field of sea surface temperature. They are quite appropriate for calculating the monthly average values in combination with ship-of-opportunity data, and provide reasonably good estimates for short time-scales of weeks to months.

2. The ATRA wind analysis provide very useful data to monitor wind variations for the study area. Comparisons of wind data from the ATRA analysis to the ground-truth data show the former is highly representative of real variations. The spatial coherences between 200 mb wind divergence, 850 mb wind convergence and OLR have further confirmed the validity of ATRA wind analysis from the dynamical perspective. It should be noted, however, that predicted directions of surface wind in the ATRA analysis may be seriously in error in coastal regions and when wind speeds are small (<4 ms^{-1}), but are usually within 10° of the measured value when wind speeds are high.

3. The annual cycle of SST shows very small amplitudes in equatorial regions, but the phase are in opposition. The discontinuity in phase angle in the Malaysian-Papua New

Guinea region serves to partition the areas influenced by the Asian Winter Monsoon, and the Indian and Australian Monsoon systems.

The results of the EOF analyses indicate a see-saw in the SST anomalies between the middle equatorial Pacific and the eastern Indian Ocean. The time series corresponding to this pattern shows a linear interannual trend which is observed as a build-up of positive SST anomalies in the western Pacific and negative SST anomalies in the eastern Indian Ocean. The intensified convection has also been shown following the increasing of SST in the tropical area near the dateline.

4. The analysis of the three-year wind data set has shown similar seasonal means to those found in earlier studies. Generally speaking, the seasonal means of the zonal and meridional wind components at 850 and 200 mb are similar to long term climate studies, although the zonal winds in the tropical Indian Ocean were noted to be stronger in this data set. This feature might also explain the stronger low level convergence east of New Guinea and in the tropical Indian Ocean obtained in this study. In addition, the convergence zone east of the Philippines has not been reported by other studies, for example, that of Rasmusson and Carpenter (1982). It is however, important to keep in mind that the data sets used in the comparison are not identical since Rasmusson and Carpenter used surface observations as opposed to the 850 mb data used in this study.

Harmonic analysis techniques were applied to analyse the annual, semi-annual, 30-65 day and 10-30 day cycles. A strong annual cycle was found in the northern hemisphere, with maxima being obtained in the monsoon region. The contribution to the total variance by the semiannual cycle is much smaller, with the exception of the zonal wind at 200 mb. A strong amplitude is obtained with the 30-65 day oscillation, in good agreement with earlier studies relating wind and OLR at this frequency. However, some interesting features have also been found in the propagation of the intraseasonal oscillations of the zonal wind. These propagation features need to be

studied in more detail. At shorter time scales (10-30 days) a strong mid-latitude signal was found, which is clearly related to synoptic events.

5. The following features of convection were documented:

a) Convection in the study area shows a marked seasonal variation. It reaches its annual minimum just before the out-break of the Indian Monsoon during May. An annual maximum is reached near the Bay of Bengal during June to July. It then expands eastward to the South China Sea and the western Pacific in August. From September onwards, the slightly contracting and weakening central convection zone moves southeastward to the north of Australia. It reaches its most eastward location in February and March with the centre located near 10°S. Convection then starts to dissipate and become weakest around May, when the centre is located near the Equator. The annual course is very similar to those reported by Meehl (1987).

b) The results obtained here confirm that SST near 27.5-28°C is a threshold which must be exceeded for convection to develop. It has also been found that large scale convection develops only within areas with LLPW values greater than 35 mm. This implies that this level of precipitable water vapour may also be a "necessary" condition for the development of convection.

c) A conceptual model of convection has been presented to examine the relationship between OLR, SST and wind divergence fields at 200 mb and 850 mb levels, based on a zonal band along the Bay of Bengal (Figure 6.7). The annual course of SST can be divided into five stages, when convection shows different responses (the initiating, fully developing, weakening, collapsing and idle stages). With this classification of convection, the relationships among the variables are much clear, even above the 27.5°C SST threshold. This model suggests that while SST is important in providing a "warm background" and in initiating convection, the upper level wind divergence is more important in accelerating and maintaining convection. It also explains why the annual maximum of convection does not coincide with the annual maximum of SST,

but instead with the second annual minimum. The model has also suggested possible effects of evaporation and cloud blocking of solar radiation to the cooling of sea surface.

By examining the spatial patterns of SST and OLR, it has been noticed that the locations of convection centres generally follow those of high SST centres, with a lag of about 1-2 months; and in the area eastward from Indonesia, at a specific time, the convection centres are generally located west of warm SST centres.

d) The localized divergence cells at 200 mb level are also analysed to document the spatial structure of convection. There is a tendency for paired cells of convergence and divergence to exist in preferred areas with preferred relative orientations. The convergence centres tend to locate south to southwest of their corresponding divergence centres. This implies that at the surface, there are some southerly or southwesterly inflow into the surface convergence centre (i.e. the convection centre). This inflow is obviously important in maintaining these cells.

e) A few precursors to the 1986/87 ENSO event have been documented in this study. The sea surface warmed up gradually towards the end of 1986 in the equatorial region near the dateline, along with a gradual intensification of convection. A region of relatively weak convection gradually expanded in the Banda Sea area from May 1986 onward. An anomalously strong southerly wind at 850 mb developed in the Coral Sea area and reached a peak in July 1986. At 200 mb level, a strong northerly wind occurred which reached its maximum at the end of 1986. All of these anomalies described here suggested arrival of an ENSO event.

7.2 Discussions

There are a few areas which need to be further addressed in future studies.

1. This study has not looked deeply into the short-term variations (less than a month) of SST, wind and other convection-related processes. Even though many past studies

have focused on the short term variations of individual variables, like wind and OLR (Knutson and Weickmann, 1987), only a few recent studies have examined simultaneously a number of variables (Steiner and Khalsa, 1987; Weickmann and Khalsa, 1990). It is expected that by simultaneous examination of these variables, especially by incorporating the daily (or weekly) OLR data and upper level wind field, some subtle connections between them will be further revealed. This study established a climatological background for further study of the short term variation.

2. It has been shown that wind divergences and OLR are linearly correlated on a monthly basis. By using daily or weekly OLR data, some further insights into the temporal relationship between these two fields should be revealed. It would be interesting to see if wind divergences do play a controlling role during the fully developed, weakening and collapsing stages of convection as in the conceptual model. Cross-spectral analysis will help to reveal their temporal relationships.

3. The conceptual model suggests an effective link between evaporation and cloud blocking of solar radiation and cooling of sea surface. It would be interesting to incorporate estimates of air/sea heat fluxes, like latent heat flux and incoming solar radiation, in future studies. Further, insights into the sources and mechanisms of convection would be gained by calculating the horizontal water vapour transfer using wind and precipitable water data.

4. This study mainly focuses on the convection process in tropical areas, and the conceptual model is built on the analysis of SST, wind and OLR in the tropical region near 10°N. It would be interesting to study how these variables interact over other tropical areas. It is also important to see whether the dynamics of convection suggested by the conceptual model can be found over other areas. In addition, it would be interesting to study how convection over tropical areas relate to extra-tropical systems.

5. The data used in this study covers the period of 1984-86, lying between the 1982/83 ENSO and the 1986/87 ENSO events. To gain a fuller understanding of the

convection process and the modifications which occur during ENSO events, it would be necessary to extend the study period to 1988.

Bibliography

Anderson, J. R., D. E. Stevens, and P. R. Julian, 1984: Temporal variations of the tropical 40-50 day oscillation . *Mon. Wea. Rev.*, **112**, 2431-2438.

Anderson, R. K., and V. J. Oliver, 1970: Some examples of use of synchronous satellite pictures for studying changes in tropical cloudiness. Extended Abstracts: *Symposium on Tropical Meteorology*, 2-11 June, 1970, University of Hawaii, Honolulu, Hawaii.

Ardanuy, P. E., and H. L. Kyle, 1986: El Nino and outgoing longwave radiation: observations from Nimbus-7 ERB. *Mon. Wea. Rev.*, **114**, 415-433.

Ardanuy, P. E., H. L. Kyle, and H. D. Chang, 1987: Evolution of the Southern Oscillation as observed by the Nimbus-7 ERB experiment. *Mon. Wea. Rev.*, **115**, 2615-2625.

Arkin, P. A., 1982: The relationship between interannual variability in the 200 mb tropical wind field and the Southern Oscillation. *Mon. Wea. Rev.*, **110**, 808-823.

Barnett, T. P., 1977: The principal time and space scales of the Pacific trade wind field. *J. Atmos. Sci.*, **34**, 221-235.

Barnett, T. P., 1981: Statistical relations between ocean and atmosphere fluctuations in the tropical Pacific. *Meteorol. Mag.*, **11**, 1043-1058.

Barnett, T. P., 1983: Interaction of the monsoon and Pacific tradewind system at interannual time scales. Part I: the equatorial zone. *Mon. Wea. Rev.*, **111**, 756-773.

Barnett, T. P., 1984a: Prediction o f the El Nino of 1982-83. *Mon. Wea. Rev.*, **112**, 1403-1407.

Barnett, T. P., 1984b: Interaction of the monsoon and Pacific tradewind system at interannual time scales. Part II: the tropical band. *Mon. Wea. Rev.*, **112**, 2380-2387.

Barnett, T. P., 1984c: Interaction of the monsoon and Pacific tradewind system at interannual time scales. Part III: a partial anatomy of the Southern Oscillation. *Mon. Wea. Rev.*, **112**, 2388-2400.

Barry, R. G., and R. J. Chorley, 1987: *Atmosphere, Weather and Climate.* Methuen, London, 460 pp.

Barton, I. J., 1985: Transmission model and ground-truth investigation of satellite-derived sea surface temperatures. *J. Climate and Appl. Meteor.*, **24**, 508-516.

Bellanger, M., 1984: *Digital Processing of Signals: Theory and Practice.* John Wiley & Sons, New York.

Bernstein, R. L., 1982: Sea surface temperature estimation using the NOAA 6 satellite Advanced Very High Resolution Radiometer. *J. Geophys. Res.*, **87**, 9455-9465.

Bernstein, R. L., and D. B. Chelton, 1985: Large-scale sea surface temperature variability from satellite and shipboard measurements. *J. Geophys. Res.*, **90**, 11619-11630.

Bjerknes, J., 1966: A possible response of the atmospheric Hadley circulation to equatorial anomalies of ocean temperature. *Tellus*, **18**, 820-829.

Bjerknes, J., 1969: Atmospheric teleconnections from the equatorial Pacific. *Mon. Wea. Rev.*, **97**, 163-172.

Bjerknes, J., 1972: Large-scale atmospheric response to the 1964-65 Pacific equatorial warming. *J. Phys. Oceanogr.*, **2**, 212-217.

Brooks, C. E. P., and H. W. Brady, 1921: The clash of the trades in the Pacific. *Quart. J. Roy. Meteor. Soc.*, **47**, 1-13.

Brown, O. B., J. W. Brown, and R. H. Evans, 1985: Calibration of advanced very high resolution radiometer infrared observations. *J. Geophys. Res.*, **90**, 11667-11677.

Busalacchi, A., and J. J. O'Brien, 1981: Interannual variability of the equatorial Pacific in the 1960's. *J. Geophys. Res.*, **86**, 10901-10907.

Cadet, D. L., 1983: Mean fields of precipitable water over the Indian Ocean during the 1979 summer monsoon from TIROS-N soundings and FGGE data. *Tellus*, **35B**, 329-345.

Cane, M. A., 1983: Oceanographic events during El Nino. *Science*, **222**, 1189-1195.

Cane, M. A., 1984: Modeling sea level during El Nino. *J. Phys. Oceanogr.*, **14**, 1864-1874.

Cane, M. A., S. E. Zebiak and S. C. Dolan, 1986: Experimental forecasts of El Nino. *Nature*, **321**, 827-832.

Chatfield, C., 1975: The analysis of time series: theory and practice. Chapman and Hall, London, 263 pp.

Church, J. A., G. R. Cresswell, and J. S. Godfrey, 1989: The Leeuwin Current. *Coastal and Estuarine Studies*, S. J. Neshyba, *et. al.* (eds), Springer-Verlag, New York.

Chen, T., 1985: Global water vapor flux and maintenance during FGGE. *Mon. Wea. Rev.*, **113**, 1801-1819.

Chen, T., 1987: 30-50 day oscillation of 200-mb temperature and 850-mb height during the 1979 northern summer. *Mon. Wea. Rev.*, **115**, 1589-1605.

Chen, T., and M. Yen, 1986: The 40-50 day oscillation of the low-Level monsoon circulation over the Indian Ocean. *Mon. Wea. Rev.*, **114**, 2550-2570.

Chervin, R. M., 1984: The influence of ocean surface temperature gradient and continentality on the Walker Circulation. part I: prescribed tropical changes. *Mon. Wea. Rev.*, **112**, 1510-1523.

Cogan, J. L., and J. H. Willand, 1976: Measurement of sea surface temperature by the NOAA 2 satellite satellite. *J. Appl. Meteorol.*, **15**, 173-180.

Cornejo-Garrido, A. G., and P. H. Stone, 1977: On the heat balance of the Walker Circulation. *J. Atmos. Sci.*, **34**, 1155-1162.

Crowe, P. R., 1951: The trade wind circulation of the world. *Trans. Pap. Inst. Brit. Geogr.*, **15**, 37-56.

Davidson, N. E., 1984: Short-term fluctuations in the Australian Monsoon during winter MONEX. *Mon. Wea. Rev.*, **112**, 1697-1708.

Davidson, N. E., and B. J. McAvaney, 1981: The ANMRC tropical analysis scheme. *Aust. Meteorol. Mag.*, **29**, 155-168.

Davidson, N. E., and J. Holland, 1987: A diagnostic analysis of two intense monsoon depressions over Australia. *Mon. Wea. Rev.*, **115**, 380-392.

Davidson, N. E., J. L. McBride, and B. J. McAvaney, 1983: The onset of the Australian monsoon during winter MONEX: synoptic aspects. *Mon. Wea. Rev.*, **111**, 496-516.

Davidson, N. E., J. L. McBride, and B. J. McAvaney, 1984: Divergent circulations during the onset of the 1978-79 Australian monsoon. *Mon. Wea. Rev.*, **112**, 1684-1696.

Egger, E., J., G. Meyers, and P. V. Wright, 1981: Pressure, wind and cloudiness in the tropical Pacific related to the Southern Oscillation. *Mon. Wea. Rev.*, **109**, 1139-1149.

Enfield, D. B., 1987: The intraseasonal oscillation in eastern Pacific sea levels: how is it forced?. *Meteorol. Mag.*, **17**, 1860-1876.

Fraedrich, K., 1988: El Nino/Southern Oscillation predictability. *Mon. Wea. Rev.*, **116**, 1001-1012.

Fu, C., H. F. Diaz, and J. O. Fletcher, 1986: Characteristics of the response of sea surface temperature in the central Pacific associated with warm episodes of the Southern Oscillation oscillation. *Mon. Wea. Rev.*, 114, 1716-1738.

Gadgil, S., P. V. Joseph, and N. V. Joshi, 1984: Ocean-atmosphere coupling over monsoon regions. *Nature*, **312**, 141-143.

Garcia, O., 1981: A comparison of two satellite rainfall estimations for GATE. *J. Appl. Meteor.*, **20**, 430-438.

Garcia, O., 1985: Atlas of highly reflective clouds for the global tropics: 1971-1983. Environ. Res. Lab., NOAA, Bounder, Colo., 365 pp.

Garcia, O., and M. Anderson, 1984: The pattern of convective activity in the tropical Pacific during the last three ENSO events, *Proceedings of the Eighth Annual Climate Diagnostics Workshop*, Downsview, Ontario, 122-128. NOAA, Rockville, Md.

Garcia, O., S. J. S. Khalsa, and E. J. Steiner, 1986: Atmospheric characteristics of the equatorial Pacific during the 1982-1983 El Nino, deduced from satellite and aircraft observations. *J. Geophys. Res.*, **91**, 13217-13231.

Gautier, C., 1986: Evolution of the net surface shortwave radiation over the Indian Ocean during summer MONEX. *Mon. Wea. Rev.*, **114**, 447-462.

Geisler, J. E., 1981: A linear model of the Walker Circulation. *J. Atmos. Sci.*, **38**, 1390-1400.

Gill, A.E., 1980: Some simple solutions for heat-induced tropical circulation. *Quart. J. Roy. Meteor. Soc.*, **106**, 447-462.

Gill, A. E., 1985: An overview of the dynamics of the tropical oceans and global atmosphere, *International Conference on the TOGA Scientific Programme*, WMO/TD No. 65.

Gill, A. E., and E. M. Rasmusson, 1983: The 1982-83 climate anomaly in the equatorial Pacific. *Nature*, **306**, 229-234.

Goldenberg, S. B., and J. J. O'Brien, 1981: Time and space variability of tropical Pacific wind stress. *Mon. Wea. Rev.*, **109**, 1190-1207.

Goswami, B. N., and J. Shukla, 1984: Quasi-periodic oscillations in a symmetric general circulation model. *J. Atmos. Sci.*, **41**, 20-37.

Graham, N. E., and T. P. Barnett, 1987: Sea surface temperature, surface wind divergence, and convection over tropical oceans. *Science*, **238**, 657-659.

Griffith, G. C., W. L. Woodley, P. G. Grube, D. W. Martin, J. Stout and D. N. Sikdar, 1978: Rain estimation from geosyschronous satellite imagery - visible and infrared studies. *Mon. Wea. Rev.*, **106**, 1153-1171.

Grose, W. L., W. T. Blackshear, and R. Turner, 1984: The response of a nonlinear, time-dependent, baroclinic model of the atmosphere to tropical thermal forcing. *Quart. J. R. Met. Soc.*, **110**, 981-1002.

Gruber, A., and A. F. Krueger, 1984: The status of the NOAA outgoing longwave radiation data set. *Bull. Amer. Metror. Soc.*, **65**, 958-962.

Gruber, A., and C. Watkins, 1982: Statistical assessment of the quality of TIROS-N and NOAA-6 satellite soundings. *Mon. Wea. Rev.*, **110**, 867-876.

Gruber, A., and J. S. Winston, 1978: Earth-atmosphere radiative heating based on NOAA scanning radiometer measurements. *Bull. Amer. Meteor. Soc.*, **59**, 1570-1573.

Gutzler, D. S., and D. E. Harrison, 1987: The structure and evolution of seasonal wind anomalies over the near-equatorial eastern Indian and western Pacific oceans. *Mon. Wea. Rev.*, **115**, 169-192.

Gutzler, D. S., and T. M. Wood, 1990: Structure of large-scale convective anomalies over tropical oceans. *J. Clim.*, **3**, 483-496.

Hamilton, K., and R. R. Garcia, 1986: El Nino/Southern Oscillation events and their associated midlatitude teleconnections 1531-1841. *Bull. Amer. Meteorol. Soc.*, **67**, 1354-1360.

Hamming, R. W., 1983: *Digital Filters.* Prentice-Hall, Inc., New Jersey, 257 pp.

Harrison, D. E., 1984: The appearance of sustained equatorial surface westerlies during the 1982 Pacific warm event. *Science*, **224**, 1099-1102.

Harrison, D. E., 1984: Where did the strong equatorial westerlies of the 1982 warm event begin?. *Trop. Ocean Atmos. Newslett.*, **24**, 17-18.

Harrison, D. E., 1987: Monthly mean island surface winds in the central tropical Pacific and El Nino events. *Mon. Wea. Rev.*, **115**, 3133-3145.

Harrison, D. E., and D. Gutzler, 1986: Variability of monthly averaged surface and 850 mb wind at tropical Pacific islands. *Mon. Wea. Rev.*, **114**, 285-294.

Harrison. D. E., and P. S. Schopf, 1984: Kelvin-wave induced anomalous advection and the onset of surface warming in El Nino events. *Mon. Wea. Rev.*, **112**, 923-933.

Hastenrath, S., and P. Lamb, 1979: *Climatic Atlas of the Indian Ocean. Part 1. Surface Circulation and Climate. Part 2. The Oceanic Heat Budget.* University of Wisconsin Press, 109 and 104 pp.

Hastenrath, S., and M. Wu, 1982: Oscillations of upper-air circulation and anomalies in the surface climate of the tropics. *Arch. Meteor. Geophys. Bioklim.*, **B-31**, 1-37.

Hayashi, Y., 1977: Space-Time power spectral analysis using the maximum entropy method. *J. Meteor. Soc. Japan*, **55**, 415-420.

Hayashi, Y., and A. Sumi, 1986: The 30-40 day oscillations simulated in an "aqua planet" model. *J. Atmos. Sci.*, **41**, 20-37.

Hayden, C. M., W. L. Smith, and H. M. Woolf, 1981: Determination of moisture from NOAA polar orbiting satellite sounding radiances. *J. Appl. Meteor.*, **20**, 450-466.

Heddinghaus, T. R., and A. R. Krueger, 1981: Annual and interannual variations in outgoing longwave radiation over the tropics. *Mon. Wea. Rev.*, **109**, 1208-1218.

Hellerman, S., and M. Rosenstein, 1983: Normal monthly windstress over the world ocean with error estimates. *J. Phys. Oceanogr.*, **13**, 1093-1104.

Hendon, H. H., 1988: A qualitative assessment of the Australian tropical region analyses. *Mon. Wea. Rev.*, **116**, 5-17.

Hohn, F. E., 1964: *Elementary Matrix Algebra.* Macmillan, New York, 395 pp.

Horel, J. D., 1982: On the annual cycle of the tropical Pacific atmosphere and ocean. *Mon. Wea. Rev.*, **110**, 1863-1878.

Horel, J. D., and A. G. Cornejo-Garrido, 1986: Convection along the coast of northern Peru during 1983: spatial and temporal variation of clouds and rainfall. *Mon. Wea. Rev.*, **114**, 2091-2105.

Horel, J. D., and J. M.Wallace, 1981: Planetary-Scale atmospheric phenomena associated with the Southern Oscillation. *Mon. Wea. Rev.*, **109**, 813-829.

Imbarlt, D., N. A. Scott, and A. Chedin, 1981: Multichannel radiometric determination of sea surface temperature: parameterization of the atmospheric correction. *J. Appl. Meteorol.*, **20**, 556-564.

Janowiak, U. E., A. F. Krueger, P. A. Arkin and A. Gruber, 1985: *Atlas of Outgoing Longwave Radiation Derived from NOAA Satellite Data*, NOAA Atlas No. 6, U.S. Dept. of Commerce, Silver Spring, MD, 44 pp.

Janowiak, J. E., C. F. Ropelewski, and M. S. Halpert, 1986: The precipitation anomaly classification: a method for monitoring regional precipitation deficiency and excess on a global scale. *J. Clim. Appl. Met.*, **25**, 565-574.

Japan Meteorology Agency, 1989: *Climatic Charts of Sea Surface Temperature of the Western North Pacific and the Global Ocean.* 77 pp.

Jenkins, G. M., and D. G. Watts, 1968: *Spectral Analysis and Its Applications*. Holden-Day, San Francisco, 525 pp.

Julian, P. R., 1984: Objective analysis in the tropics: a proposed scheme. *Mon. Wea. Rev.*, **112**, 1752-1767.

Julian, P. R., and R. M. Chervin, 1978: A study of the Southern Oscillation and Walker Circulation phenomenon. *Mon. Wea. Rev.*, **106**, 1433-1451.

Julian, P. R., and R. A. Madden, 1981: Comments on a paper by T. Yasunari, A quasi-stationary appearance of 30 to 40 day period in the cloudiness fluctuations during the summer monsoon over India. *J. Meteor. Soc. Japan*, **59**, 435-437.

Khalsa, S. J. S., 1983: The role of sea surface temperature in large-scale air-sea interaction. *Mon. Wea. Rev.*, **111**, 954-966.

Katz, E. J., P. Hisard, J. Verstraete, and S. L. Garzoli, 1986: Annual change of sea surface slope along the equator of the Atlantic Ocean in 1983 and 1984. *Progr. Oceanogr.*, **322**, 245-247.

Keen, R. A., 1984: Equatorial westerlies during the 1982-83 ENSO event. *Trop. Ocean Atmos. Newslett.*, **25**, 10-11.

Keen, R. A., 1987: Equatorial westerlies and the Southern Oscillation, in "*Proceedings of the U.S. TOGA Western Pacific Air-Sea Interaction Workshop*" (Editors: R. Lukas and P. Webster), UCAR, USTOGA 8, 207 pp.

Keenan, T. D., and L. R. Brody, 1988: Synoptic-scale modulation of convection during the Australian summer monsoon. Nature, 116, 71-85.

Kendrew, W. G., 1937: The Climates of the Continents, 3rd ed. Oxford University Press, 473 pp.

Keshavamurty, R. N., 1982: Response of the atmosphere to sea surface temperature anomalies over the equatorial Pacific and teleconnections of the Southern Oscillation. *J. Atmos. Sci.*, **39**, 1241-1259.

Keshavamurty, R. N., 1983: Southern Oscillation: Further studies with a GFDL general circulation model. *Mon. Wea. Rev.*, **111**, 1988-1997.

Kiladis, G. N., and H. van Loon, 1988: The Southern Oscillation. Part VII: meteorological anomalies over the Indian and Pacific sectors associated with the extremes of the oscillation. *Mon. Wea. Rev.*, 116, 120-136.

Kilonsky, B. J., and C. S. Ramage, 1976: A technique for estimating tropical open-ocean rainfall from satellite observations. *J. Appl. Meteor.*, **15**, 972-975.

Knutson, T. R., K. M. Weickmann, and J. E. Kutzbach, 1986: Global-scale intraseasonal oscillations of outgoing longwave radiation and 250 mb zonal wind during Northern Hemisphere summer. *Mon. Wea. Rev.*, **114**, 605-623.

Knutson, T. T., and K. M. Weickmann, 1987: 30-60 day atmospheric oscillations: composite life cycles of convection and circulation anomalies. *Mon. Wea. Rev.*, **115**, 1407-1436.

Koppen, W., 1923: *Die Klimate der Erde: Grundiss der Klimakunde.* Walter de Gruyter, Berlin, 369 pp.

Krishnamurti, T. N., and P. K. Jayakumar 1982: The 30-50 day mode at 850 mb during MONEX. *J. Atmos. Sci.*, **39**, 2088-2095.

Krishnamurti, T. N., P. K. Jayakumar, J. Sheng, N. Surgi and A. Kumar, 1985: Divergent circulations on the 30 to 50 day time scale. *J. Atmos. Sci.*, **42**, 364-375.

Krueger, A. F., and T. Gray, 1969: Long-term variations in equatorial circulation and rainfall. *Mon. Wea. Rev.*, **97**, 700-711.

Krueger, A. F., and J. S. Winston, 1974: A comparison of the flow over the tropics during two contrasting circulation regime. *J. Atmos. Sci.*, **23**, 40-63.

Lajoie, F. A., 1986: Effects of the upper flow asymmetry on the future direction of motion of tropical cyclones. *Mon. Wea. Rev.*, **114**, 1863-1875.

Lamb, P. J., R. A. Peppler, and S. Hastenrath, 1986: Interannual variability in the tropical Atlantic. *Progr. Oceanogr.*, 322, 238-240.

Lanzanete, J. R., 1984: A rotated eigenanalysis of the correlation between 700 mb heights and sea surface temperatures in the Pacific and Atlantic. *Mon. Wea. Rev.*, **112**, 2270-2280.

Lau, K. M., 1979: A numerical study of tropical large-Scale air-Sea interaction. *J. Atmos. Sci.*, **36**, 1467-1489.

Lau, K. M., 1981: Oscillations in a simple equatorial climate system. *J. Atmos. Sci.*, **38**, 248-261.

Lau, K. M., and P. H. Chan, 1985: Aspects of the 40-50 day oscillation during the northern winter as inferred from outgoing longwave radiation. *Mon. Wea. Rev.*, **113**, 1889-1909.

Lau, K. M., and P. H. Chan, 1986a: Aspects of the 40-50 day oscillation during the northern summer as inferred from outgoing longwave radiation. *Mon. Wea. Rev.*, **114**, 1354-1367.

Lau, K. M., and P. H. Chan, 1986b: The 40-50 day oscillation and the El Nino/Southern Oscillation: a new perspective. *Bull. Amer. Meteorol. Soc.*, **67**, 533-534.

Lau, K. M., and T. Phillips, 1986: Coherent fluctuations of extratropical geopotential height and tropical convection in intraseasonal time scales. *J. Atmos. Sci.*, **43**, 1164-1181.

Lau, K. M., G. J. Yang, and S. H. Sheng, 1988: Seasonal and intraseasonal climatology of summer monsoon rainfall east Asia. *Mon. Wea. Rev.*, **116**, 18-37.

Lau, K. M., 1981: Oscillations in a simple equatorial climate system. *J. Atmos. Sci.*, **38**, 248-261.

Lau, K. M., 1985: Elements of a stochastic-dynamical theory of the long-term variability of the El Nino/Southern Oscillation. *J. Atmos. Sci.*, **42**, 1552-1558.

Lau, K. M., and P. H. Chan, 1983: Short-Term climate variability and atmospheric teleconnections from satellite-Observed outgoing longwave radiation. part II: lagged correlations. *J. Atmos. Sci.*, **40**, 2751-2767.

Lau, N.C., and K. M. Lau, 1986: The structure and propagation of intraseasonal oscillations appearing in a GFDL GCM. *J. Atmos. Sci.*, **43**, 2023-2047.

Legeckis, R., 1986: A satellite time series of sea surface temperatures in the eastern equatorial Pacific Ocean, 1982-1986. *J. Geophys. Res.*, **91**, 12879-12886.

Levitus, S., 1982: *Climatological Atlas of the World Oceans*. NOAA Prof. Pap. 13, U.S. Government Printing Office, Washington, DC, 173 pp.

Levitus, S., 1987: A comparison of the annual cycle of two sea surface temperature climatologies of the world ocean. *J. Phys. Oceanogr.*, **17**, 197-214.

Levitus, S., and A. H. Oort, 1977: Global analysis of oceanographic data. *Bull. Amer. Meteor. Soc.*, **58**, 1270-1284.

Liebmann, L., B., 1987: Observed relationships between large-scale convection and the tropical circulation on subseasonal time scales during northern hemisphere winter. *J. Atmos. Sci.*, **44**, 2543-2561.

Liebmann B., and D. L. Hartmann, 1982: Interannual variations of outgoing IR associated with tropical circulation changes during 1974-78. J. Atmos. Sci., **39**, 1153-1162.

Lindstrom, E., R. Lukas, R. Fine, E. Firing, S. Godfrey, G. Meyers, and M. Tsuchiya, 1987: The western equatorial Pacific Ocean circulation study. *Progr. Oceanogr.*, **330**, 533-537.

Lindzen, R. S., and S. Nigam, 1987: On the role of sea surface temperature gradients in forcing low-level winds and convergence in the tropics. *J. Atmos. Sci.*, **44**, 2418-2436.

Liu, W. T., 1984: Determination of monthly mean humidity in the atmospheric surface layer over oceans from satellite data. *J. Phys. Oceanogr.*, **14**, 1451-1457.

Lockwood, J. G., 1974: *World Climatology: An environmental approach.* Arnold, London. 330 pp.

Lorenc, A. C., 1984: The evolution of planetary-Scale 200 mb divergent flow during the FGGE year. *Quart. J. R. Met. Soc.*, **110**, 427-441.

Love, G., 1985: Cross-equatorial influence of winter hemisphere subtropical cold surges. *Mon. Wea. Rev.*, **113**, 1487-1498.

Lukas, R., 1987: On the role of western Pacific air-sea interaction in the El Nino/Southern Oscillation phenomenon, in "*Proceedings of the U.S. TOGA western Pacific air-sea interaction workshop*" (Editors: R. Lukas and P. Webster), UCAR, USTOGA 8, 207 pp.

Lukas, R., and P. Webster (eds.), 1988: *Proceedings of the U.S. TOGA western Pacific air-sea interaction workshop,* Honolulu, Hawaii, 16-18 September 1987, USTOGA 8, 207 pp.

Luther, L., D. S., and D. Harrison, 1984: Observing long-period fluctuations of surface winds in the tropical Pacific: initial results from island data. *Mon. Wea. Rev.*, **112**, 285-302.

Madden, R. A., 1986: Seasonal variations of the 40-50 day oscillation in the tropics. *J. Atmos. Sci.*, **43**, 3138-3158.

Madden, R. A., and P. R. Julian, 1971: Detection of a 40-50 day oscillation in the zonal wind in the tropical Pacific. *J. Atmos. Sci.*, **28**, 702-708.

Madden, R. A., and P. R. Julian, 1972: Description of global-scale circulation cells in the tropics with a 40-50 day period. *J. Atmos. Sci.*, **29**, 1109-1123.

Martin, D. W., and W. D. Scherer, 1973: Review of satellite rainfall estimation methods. *Bull. Amer. Meteor. Soc.*, **54**, 661-674.

Mason, B. J., 1970: Future developments in meteorology: An outlook to the year 2000. *Quart. J. Roy. Met. Soc.*, **96**, 349-368

McBride, J. L., and N. Nicholls, 1983: Seasonal relationships between Australian rainfall and the Southern Oscillation. *Mon. Wea. Rev.*, **111**, 1998-2004.

McClain, E. P., W. G. Pichel, and C. C. Walton, 1985: Comparative performance of AVHRR-based multichannel sea surface temperatures. *J. Geophys. Res.*, **90**, 11587-11601.

McCreary, J. P., 1983: A model of tropical ocean-atmosphere interaction. *Mon. Wea. Rev.*, **111**, 370-387.

McCreary, J. P., and D. L. T. Anderson, 1984: A simple model of El Nino and the Southern Oscillation. *Mon. Wea. Rev.*, **112**, 934-946.

McPhaden, M. J., H. P. Freitag, S. P. Hayes, B. A. Taft, Z. Chen, and K. Wyrtki, 1987: The response of the equatorial Pacific Ocean to a westerly wind burst in may 1986, in "*Proceedings of the U.S. TOGA Western Pacific Air-Sea Interaction Workshop*" (Editors: R. Lukas and P. Webster), UCAR, USTOGA 8, 207 pp.

McWilliams, J. C., and P. R. Gent, 1978: A coupled air-sea model for the tropical Pacific. *J. Atmos. Sci.*, **35**, 962-989.

Meehl, G. A., 1987: The annual cycle and interannual variability in the tropical Pacific and Indian ocean regions. *Mon. Wea. Rev.*, **115**, 27-50.

Merle, J., 1983: Seasonal variability of subsurface thermal structure in the tropical Atlantic. *Hydrodynamics of the Equatorial Ocean*, Elsevier, 31-49.

Meyers, G., J. R. Donguy, and R. K. Reed, 1986: Evaporative cooling of the western equatorial Pacific Ocean by anomalous winds. *Nature*, **323**, 523-526.

Michael, K., 1989: *A Satellite-Based Study of Ocean-Atmosphere Heat Fluxes in the Vicility of John Brewer Reef, Queensland.* PhD Dissertation, University of Tasmania.

Michael, K., and M. Nunez, 1991: Derivation of ocean-atmosphere heat fluxes in a tropical environment using satellite and surface data, *Intl. J. Climatol.*, **11**, 559-575.

Morrissey, M. L., 1986a: *An Examination of the Measurability of Tropical Convection and Area Averaged Precipitation.* PhD Dissertation, University of Hawaii.

Morrissey, M. L., 1986b: A statistical analysis of the relationships among rainfall, outgoing longwave radiation and the moisture budget during January-March 1979. *Mon. Wea. Rev.*, **114**, 931-942.

Murakami, M., 1979: Large-scale aspects of deep convective activity over the GATE area. *Mon. Wea. Rev.*, **107**, 994-1013.

Murakami, M., 1983: Analysis of the deep convective activity over the Western Pacific and Southeast Asia. Part I: diurnal variation. *J. Meteor. Soc. Japan*, **61**, 60-75.

Murakami, T., 1980a: Temporal variations of satellite-observed outgoing longwave radiation over the winter monsoon region. Part I: long-period (15-30 day) oscillations. *Mon. Wea. Rev.*, **108**, 408-426.

Murakami, T., 1980b: Temporal variations of satellite-observed outgoing longwave radiation over the winter monsoon region. Part II: short-period (4-6 day) oscillations. *Mon. Wea. Rev.*, **108**, 427-444.

Murakami, M., 1983: Analysis of the deep convection activity over the western Pacific and Southeast Asia. Part I: Diurnal variation. *J. Meteor. Soc. Japan*, **61**, 60-76.

Murakami, T., 1987: Intraseasonal atmospheric teleconnection patterns during the northern hemisphere summer. *Mon. Wea. Rev.*, **115**, 2133-2154.

Murakami, T., L.-X. Chen, A. Xie and M. Shrestha, 1986: Eastward propagation of 30-60 day perturbations as revealed from outgoing longwave radiation data. *J. Atmos. Sci.*, **43**, 961-971.

Mysak, L. A., and G. J. Mertz, 1984: A 40-60 day oscillation in the source region of the Somali Current during 1976. *J. Geophys. Res.*, **89**, 711-715.

Namias, J., 1985: New evidence for relationships between north Pacific atmospheric circulation and El Nino. *Trop. Ocean Atmos. Newslett.*, 2-3.

Neelin, J. D., and I. M. Held, 1987: Modeling tropical convergence based on the moist static energy budget. *Mon. Wea. Rev.*, **115**, 3-12.

Nicholls, N., 1987: The use of canonical correlation to study teleconnections. *Mon. Wea. Rev.*, **115**, 393-399.

Nicholls, N., 1989: Sea surface temperatures and Australian winter rainfall. *J. Clim.*, **2**, 965-973.

North, G. R., and T. L. Bell, 1982: Sampling errors in the estimation of empirical orthogonal functions. *Mon. Wea. Rev.*, **110**, 699-706.

Palmer, T. N., 1986: Influence of the Atlantic, Pacific and Indian oceans on Sahel rainfall. *Progr. Oceanogr.*, **322**, 251-253.

Palmer, T. N., and D. A. Mansfield, 1984: Response of two atmospheric general circulation models to sea-surface temperature anomalies in the tropical East and West Pacific. *Nature*, **310**, 483-485.

Pazan, S. E., and G. Meyers, 1982: Interannual fluctuations of the tropical Pacific wind field and the Southern Oscillation. *Mon. Wea. Rev.*, **110**, 587-600.

Philander, S. G. H., 1983: El Nino Southern Oscillation phenomena. *Nature*, **302**, 295-301.

Philander, S. G. H., 1986: Unusual conditions in the tropical Atlantic Ocean in 1984. *Progr. Oceanogr.*, **322**, 236-238.

Philander, S. G. H., 1990: *El Nino, La Nina, and the Southern Oscillation*, Academic Press, San Diego, 293 pp.

Philander, S. G. H., and A. D. Siegel, 1985: Simulation of El Nino of 1982-1983. *Proc. 16th Int. Liege Colloq. on Ocean Hydrodynamics*. J. Nihoul, Ed., Elsevier Oceanography Series, Amsterdam, 767 pp.

Philander, S. G. H., E. Yamagata and P. C. Pacanowski, 1984: Unstable air-sea interactions in the tropics. *J. Atmos. Sci.*, **41**, 604-613.

Priestley, M. B., 1981: *Spectral Analysis and Time Series*, Volume 1, Academic Press, New York, 653 pp.

Prohaska, J. T., 1976: A technique for analyzing the linear relationships between two meteorological fields. *Mon. Wea. Rev.*, **104**, 1345-1353.

Quinn, W. H., and W. V. Burt, 1972: Use of the Southern Oscillation in weather prediction. *J. Appl. Meteor.*, **11**, 616-628.

Ramage, C. S., 1968: Role of a tropical maritime continent in the atmospheric circulation. *Mon. Wea. Rev.*, **96**, 365-370.

Ramage, C. S., 1977: Sea surface temperature and local weather. *Mon. Wea. Rev.*, **105**, 540-544.

Ramage, C. S., 1985: El Nino variability and tropical cyclones. *Trop. Ocean Atmos. Newslett.*, , 3-4.

Ramage, C. S., and A. M. Hori, 1981: Meteorological aspects of the El Nino. *Mon. Wea. Rev.*, **109**, 1827-1835.

Rasmusson, E. M., and J. M. Wallace, 1983: Meteorological aspects of the El Nino/Southern Oscillation. *Science*, **222**, 1195-1202.

Rasmusson, E. M., and T. H. Carpenter, 1982: Variations in tropical sea surface temperature and surface wind fields associated with the Southern Oscillation/El Nino. *Mon. Wea. Rev.*, **110**, 354-384.

Reiter, E. R., 1978: Long-term wind variability in the tropical Pacific, its possible causes and effects. *Mon. Wea. Rev.*, **106**, 324-330.

Reverdin, G., D. L. Cadet, and D. Gutzler, 1986 : Interannual displacements of convection and surface circulation over the equatorial Indian Ocean. *Quart. J. R. Met. Soc.*, **112**, 43-67.

Reynolds, R. W., 1982: *A Monthly Averaged Climatology of Sea Surface Temperatures.* NOAA Tech. Rep. NWS31, Washington, DC, 35 pp.

Reynolds, R. W., 1983: A comparison of sea surface temperature climatologies. *J. Clim. Applied. Meteor.*, **22**, 447-459.

Reynolds, R. W., 1988: A real-time global sea surface temperature analysis. *J. Clim.*, **1**, 75-86.

Richards, F., and P. Arkin, 1981: On the relationship between satellite-Observeed cloud cover and precipitation. *Mon. Wea. Rev.*, **109**, 1081-1093.

Richman, M. B., 1981: Obliquely rotated principal components: an improved meteorological map typing technique?. *J. Appl. Meteorol.*, **20**, 1145-1159.

Riehl, H., 1979: *Climate and Weather in the Tropics*, Academic Press, London, 611 pp.

Rinne, J., and S. Jarvenoja, 1986: A rapid method of computing empirical orthogonal functions from a large dataset. *Mon. Wea. Rev.*, **114**, 2571-2577.

Robinson, M., 1976: *Atlas of North Pacific Ocean Monthly Mean Temperatures and Mean Salinities of the Surface Layer.* Naval Oceanogr. Off., Ref. Publ. 2, Washington, DC, 194 pp.

Robinson, M., R. A. Bauer and E. H. Schroeder, 1979: *Atlas of North Atlantic-Indian Ocean Monthly Mean Temperatures and Mean Salinities of the Surface Layer.* Naval Oceanogr. Off., Ref. Publ. 18, Washington, DC, 234 pp.

Roemmich, D., and B. Cornuelle, 1987: Digitization and calibration of the expendable bathythermograph. *Deep Sea Res.*, **34A**, 299-307.

Ropelewski, C. F., and M. S. Halpert, 1987: Global and regional scale precipitation patterns associated with the El Nino/Southern Oscillation. *Mon. Wea. Rev.*, **115**, 1606-1626.

Ropelewski, C. F., and P. D. Jones, 1987: An extension of the Tahiti-Darwin Southern Oscillation index. *Mon. Wea. Rev.*, **115**, 2161-2165.

Rosenlof, K. H., and D. E. Stevens, 1986: The Walker Circulation with observed zonal winds, a mean Hadley cell, and cumulus friction. Mon. Wea. Rev., 43, 449-467.

Rowntree, P. R., 1972: The influence of tropical east Pacific Ocean temperature on the atmosphere. *Q. J. R. Meteor. Soc.*, **98**, 290-321.

Sadler, J. C., 1975: *The Upper Tropospheric Circulation over the Global Tropics.* Rep. UH-MET 75-05, Dept. meteor., University of Hawaii, 35 pp.

Sadler, J. C., 1980: Comments on "A study of the Southern Oscillation and Walker Circulation phenomenon." *Mon. Wea. Rev.*, **108**, 825-828.

Sadler, J. C., M. A. Lander, A. M. Hori, and L. K. Oda, 1987a: *Tropical Marine Climate Atlas. Vol. I: Indian Ocean and Atlantic Ocean.* NOAA/TOGA/EPOCS, UHMET 87-01. University of Hawaii, 51 pp.

Sadler, J. C., M. A. Lander, A. M. Hori, and L. K. Oda, 1987b: *Tropical Marine Climate Atlas. Vol. II: Pacific Ocean.* NOAA/TOGA/EPOCS, UHMET 87-02. University of Hawaii, 27 pp.

Sangster, W. E., : A method of representing the horizontal pressure force without reduction of station pressures to sea level. *J. Meteor.*, **17**, 166-176.

Schott, T. B., J. C. Chan, and R. L. Elsberry, 1987: Further applications of empirical orthogonal functions of wind fields for tropical cyclone motion studies. *Mon. Wea. Rev.*, **115**, 1225-1237.

Shukla, J., and K. R. Saha, 1974: Computation of non-divergent streamfunction and irrotational velocity potential from the observed winds. *Mon. Wea. Rev.*, **102**, 419-425.

Shukla, J., and J. M. Wallace, 1983: Numerical simulation of the atmospheric response to equatorial Pacific sea surface temperature anomalies. *J. Atmos. Sci.*, **40**, 1613-1630.

Smith, W. L., and H. M. Woolf, 1976: The use of eigenvectors of statistical covariance matrices for interpreting satellite sounding radiometer observations. *J. Atmos. Sci.*, **33**, 1127-1140.

Smith, W. L., H. M. Woolf, C. M. Hayden, D. Q. Wark, and L. M. McMillin, 1979: The TIROS-N operational vertical sounder. *Bull. Am. Meteor. Soc.*, **60**, 1177-1187

Smith, W. L., 1966: Note on the relationship between total precipitable water and surface dew point point. *J. Appl. Meteorol.*, **5**, 726-727.

Smith, W. L., P. K. Rao, R. Koffler, and R. Curtis, 1970: The determination of sea-surface temperature from satellite high resolution infrared window radiation measurements. *Mon. Wea. Rev.*, **98**, 604-611.

Smith, W., H. M., Woolf, C. Hayden, D. Wark, and, and L. McMillin, 1979: The TIROS-N operational vertical sounder. *Bull. Amer. Meteorol. Soc.*, **60**, 1177-1187.

Steiner, E. J., 1985: Low-level moisture and convection in the tropical Pacific. *Trop. Ocean Atmos. Newslett.*, **30**, 5-7.

Steiner, E. J., 1987: The relationship of low-level winds and moisture to convection in the tropical Pacific, *Mon. Wea. Rev.*, **115**, 744-749.

Steiner, E. J., and S. J. S. Khalsa, 1987: Sea surface temperature, low-level moisture, and convection in the tropical Pacific, 1982-1985. *J. Geophys. Res.*, **92**, 14217-14224.

Stephens, J. J., and K. W. Johnson, 1978: Rotational and divergent wind potentials. *Mon. Wea. Rev.*, **106**, 1452-1457.

Stevenson, J. W., and P. P. Niiler, 1983: Upper ocean heat budget during the Hawaii-to-Tahiti shuttle experiment. *J. Phys. Oceanogr.*, **13**, 1894-1907.

Stone, P. H., and R. M. Chervin, 1984: The influence of ocean surface temperature gradient and continentality on the Walker Circulation circulation. part II: prescribed global changes. *Mon. Wea. Rev.*, **112**, 1524- 1534.

Strong, A. E., 1986: Monitoring El Nino using satellite based sea surface temperatures. *Ocean-Air Interactions*, **1**, 11-28.

Strong, A. E., and E. P. McClain, 1984: Improved ocean surface temperatures from space-comparisons with drifting buoys. *Bull. Amer. Meteorol. Soc.*, **65**, 138-142.

Strong, A. E., and J. A. Pritchard, 1980: Regular monthly mean temperatures on earth's oceans from satellites. *Bull. Amer. Meteor. Soc.*, **61**, 553-559.

Susskind, J., and J. Rosenfield, 1984: Remote sensing of weather and climate parameters from HIRS2/MSU on TIROS-N. *J. Geophys. Res.*, **89**, 4677-4697.

Tarbell, T. C., and T. T. Warner, 1981: An example of the initialization of the divergent wind component in a mesoscale numerical weather prediction model. *Mon. Wea. Rev.*, **109**, 77-95.

Tchernia, P., 1980: *Descriptive Regional Oceanography.* Pergamon Press, 248 pp.

Trenberth, K. E., 1976: Spatial and temporal variations of the Southern Oscillation. *Mon. Wea. Rev.*, **102**, 639-653.

Trenberth, K. E., 1984: Signal versus noise in the Southern Oscillation. *Mon. Wea. Rev.*, **112**, 326-332.

Trenberth, K. E., 1987: The zonal mean westerlies over the southern hemisphere. *Mon. Wea. Rev.*, **115**, 1528-1533.

Trewartha, G. T., 1937: *Introduction to Weather and Climate.* McGraw-Hill, 535 pp.

Troup, A. J., 1965: The Southern Oscillation'. *Quart. J. R. Met. Soc.*, **91**, 490-506.

van Loon, H. , 1984: The Southern Oscillation. Part III: Associations with the trades and with the trough in the westerlies of the south Pacific Ocean. *Mon. Wea. Rev.*, **112**, 947-954.

van Loon, H., and R. L. Jenne, 1969: The half-yearly oscillations in the tropics of the Southern Hemisphere. *J. Atmos. Sci.*, **26**, 218-232.

van Loon, H., and R. L. Jenne, 1970: On the half-yearly oscillations in the tropics. *Tellus*, **22**, 391-398.

van Loon, H., and D. J. Shea, 1985: The Southern Oscillation oscillation. part IV: the precursors south of 15°S to the extremes of the oscillation oscillation. *Mon. Wea. Rev.*, **113**, 2063-2074.

van Loon, H., and J. C. Rogers, 1981: Remarks on the circulation over the southern hemisphere in FGGE and on its relation to the phases of the Southern Oscillation. *Mon. Wea. Rev.*, **109**, 2255-2559.

van Loon, H., and J. C. Rogers, 1981: The Southern Oscillation. part II: associations with changes in the middle troposphere in the northern winter. *Mon. Wea. Rev.*, **109**, 1163-1168.

van Loon, H., and R. A. Madden, 1981: The Southern Oscillation. part I: global associations with pressure and temperature in northern winter. *Mon. Wea. Rev.*, **109**, 1150-1162.

Walker, G. T., 1923: Correlation in seasonal variations of weather. III. A preliminary study of world weather. Mem. Ind. Met. Dept., 24, 75-131.

Walker, G. T., 1924: Correlation in seasonal variations of weather. IX. A further study of world weather. Mem. Ind. Met. Dept., 24, 275-332.

Weare, B. C., 1977: Empirical orthogonal analysis of Atlantic Ocean surface temperatures. *Quart. J. Roy. Meteor. Soc.*, **103**, 467-478.

Weare, B. C., 1979: A statistical study of the relationships between ocean surface temperatures and the Indian monsoon. *J. Atmos. Sci.*, **36**, 2279-2291.

Weare, B. C., 1984: Interannual moisture variation near the surface of the tropical Pacific Ocean. Science, 110, 489-504.

Weare, B. C., 1986: A comparison of shallow water model results for three estimates of a composite El Nino forcing. Mon. Wea. Rev., 43, 162-170.

Weare, B. C., 1987: Relationships between monthly precipitation and SST variations in the tropical Pacific region. *Mon. Wea. Rev.*, **115**, 2687-2698.

Weare, B. C., and J. S. Nasstrom, 1982: Examples of extended empirical orthogonal function analysis. *Mon. Wea. Rev.*, **110**, 481-485.

Weare, B. C., A. R. Navato and R. E. Newell, 1976: Empirical orthogonal analysis of Pacific sea surface temperatures. *J. Phys.Oceanogr.*, **6**, 671-678

Weare, B. C., and P. T. Strub, 1981: Annual mean atmospheric statistics at the surface of the tropical Pacific Ocean. *Mon. Wea. Rev.*, **109**, 1002-1012.

Webster, P. J., 1981: Mechanisms determining the atmospheric response to sea surface temperature anomalies. *J. Atmos. Sci.*, **38**, 554-571.

Weickmann, K. M., 1983: Intraseasonal circulation and outgoing longwave radiation modes during Northern Hemisphere winter. *Mon. Wea. Rev.*, **111**, 1838-1858.

Weickmann, K. M., and S. J. S. Khalsa, 1990: The shift of convection from the Indian Ocean to the western Pacific Ocean during a 30-60 day oscillation. *Mon. Wea. Rev.*, **118**, 964-978.

Weickmann, K. M., G. R. Lussky and J. E. Kutzbach, 1985: Intraseasonal (30-60 day) fluctuations of outgoing longwave radiation and 250 mb streamfunction during northern winter. *Mon. Wea. Rev.*, **113**, 941-961.

Weisberg, R. H., and C. Colin, 1986: Equatorial Atlantic Ocean temperature and current variations during 1983 and 1984. *Progr. Oceanogr.*, **322**, 240-243.

Wells, N. C., 1979: The effect of a tropical sea surface temperature anomaly in a coupled ocean-atmosphere model. *J. Geophys. Res.*, **84**, 4985-4997.

Whetton, P. H., 1986: *A Synoptic Climatological Analysis of Victorian Rainfall Variability*. PhD dissertation, Dept. of Meteorology, University of Melbourne.

White, W. B., and G. Meyers, 1982: Space/time statistics of short-term climatic variability in the western north Pacific. *J. Geophys. Res.*, **87**, 1979-1989.

White, W. B., G. A. Meyers, J. R. Donguy, and S. E. Pazan, 1985: Short-term climatic variability in the thermal structure of the Pacific Ocean during 1979-82. *Meteor. Mag.*, **15**, 917-935.

Winston, J. S., A. Gruber, T. I. Gray, Jr., M. S. Varnadore, C. L. Earnest, and L. P. Mannello, 1979: *Earth-Atmosphere Radiation Budget Analysis Derived from NOAA Satellite Data*, June 1974-February 1978, Vols. 1 and 2, NOAA, U.S. Dept. of Commerce, 34 pp.

Winston, J. S., and A. F. Krueger, 1977: Diagnosis of the satellite-observed radiative heating in relation to the summer monsoon. *Pure Appl. Geophys.*, **115**, 1131-1144.

World Meteorological Organization, 1985: *Scientific Plan for the Tropical Ocean and Global Atmosphere Programme.* WCRP-3, September, WMO/ICSW/IOC/SCOR, Geneva, 147 pp.

Wyrtki, K., 1965: The annual and semiannual variation of sea surface temperature in the North Pacific Ocean. *Limnol. Oceanogr.*, **10**, 307-313.

Wyrtki, K., 1974: Sea level and seasonal fluctuations of the equatorial currents in the western Pacific Ocean. J. Phys. Oceanogr., 4, 91-103.

Wyrtki, K., 1975: El Nino - The dynamic response of the equatorial Pacific Ocean to atmospheric forcing. *J. Phys. Oceanogr.*, **5**, 572-584.

Wyrtki, K., and G. Meyers, 1975a: The trade wind field over the Pacific Ocean. Part I. The mean field and the mean annual variation. Rep. HIG-75-1. Hawaii Inst. Geophys., University of Hawaii, 26 pp.

Wyrtki, K., and G. Meyers, 1975b: The trade wind field over the Pacific Ocean. Part II. Bimonthly fields of wind stress: 1950 to 1972. Rep. HIG-75-2. Hawaii Inst. Geophys., University of Hawaii, 16 pp.

Wyrtki, K., and G. Meyers, 1976: The trade wind field over the Pacific Ocean. *J. Appl. Meteorol.*, **15**, 698-704.

Wyrtki, K., 1979: The response of sea level topography to the 1976 El Nino. *J. Phys. Oceanogr.*, **9**, 1223-1231.

Wyrtki, K., 1982: Eddies in the Pacific North Equatorial Current. *J. Phys. Oceanogr.*, **12**, 746-749.

Yasunari, T., 1980: A quasi-stationary appearance of 30-40 day period in the cloudiness fluctuations during the summer monsoon over India. *J. Meteor. Soc. Japan*, **58**, 225-229.

Yasunari, T., 1981: Structure of an Indian summer monsoon system with around 40-day period. *J. Meteor. Soc. Japan*, **59**, 336-354.

Yasunari, T., 1985: Zonally propagating modes of the global eastwest circulation associated with the Southern Oscillation. *J. Meteor. Soc. Japan*, **63**, 1013-1029.

Zebiak, S. E., 1982: A simple atmospheric model of relevance to El Nino. *J. Atmos. Sci.*, **39**, 2017-2027.

Zebiak, S. E., 1986: Atmospheric convergence feedback in a simple model for El Nino. *Mon. Wea. Rev.*, **114**, 1263-1271.

Zebiak, S. E., and M. A. Cane, 1987: A model El Nino-Southern Oscillation. *Mon. Wea. Rev.*, **115**, 2262-2278.

APPENDIX

Monthly Mean of Sea Surface Temperature, Outgoing Longwave Radiation,Wind Divergences at 200 mb and 850 mb in 1984-86

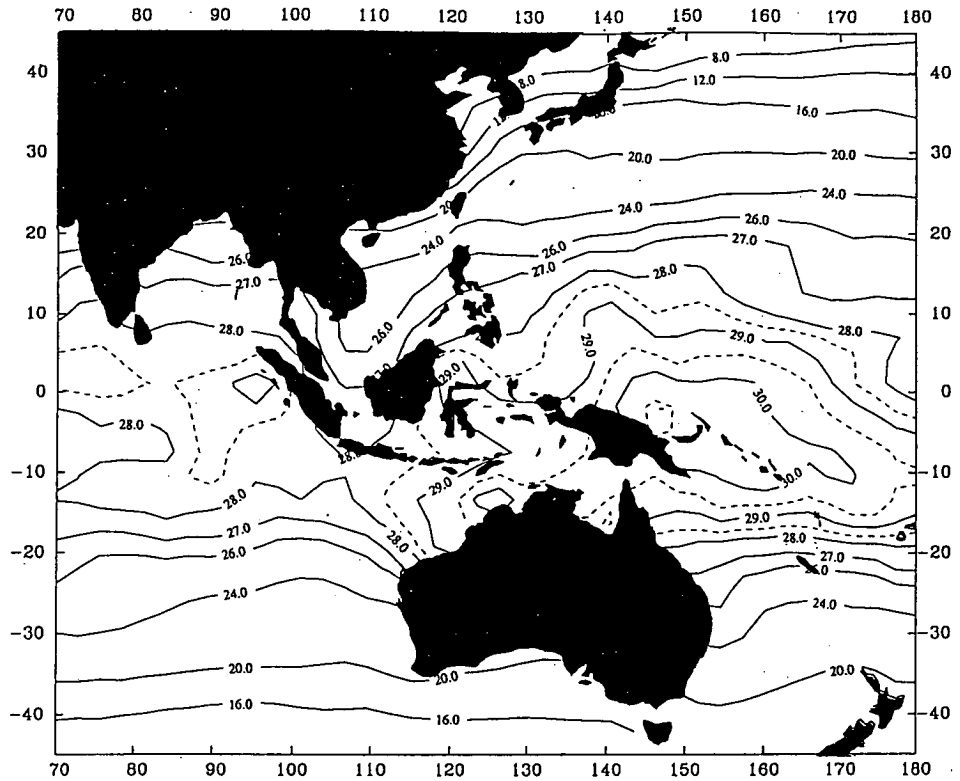

REYNOLDS BLENDED MONTHLY SST (8401)

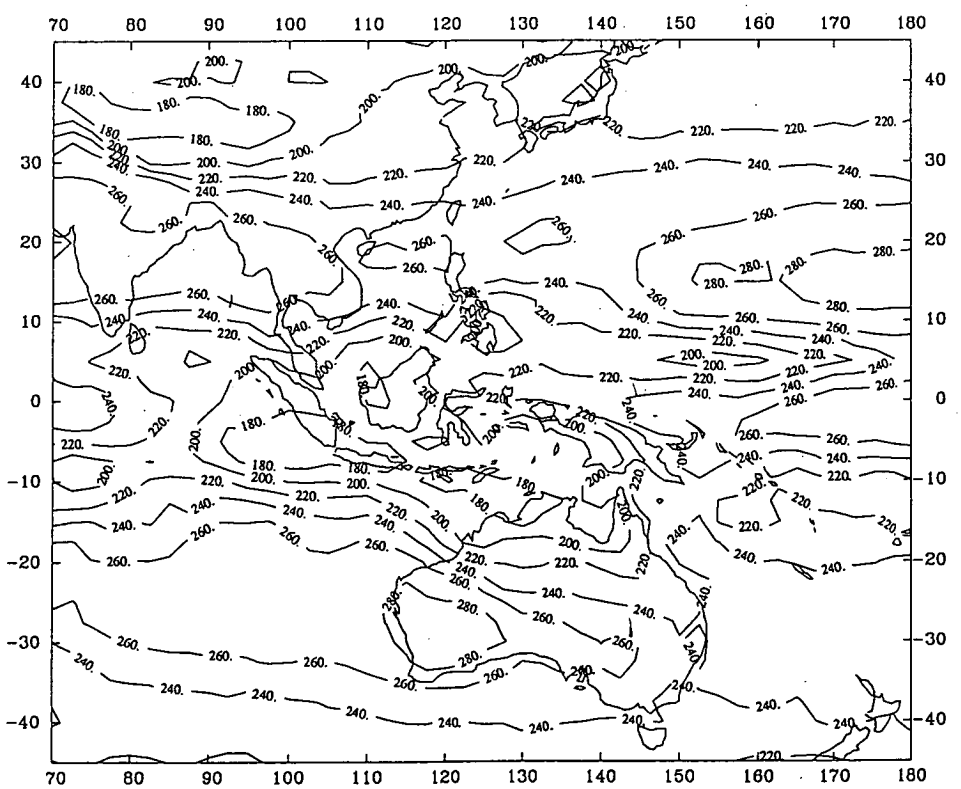

MONTHLY OLR (8401) (UNIT W/M*M)

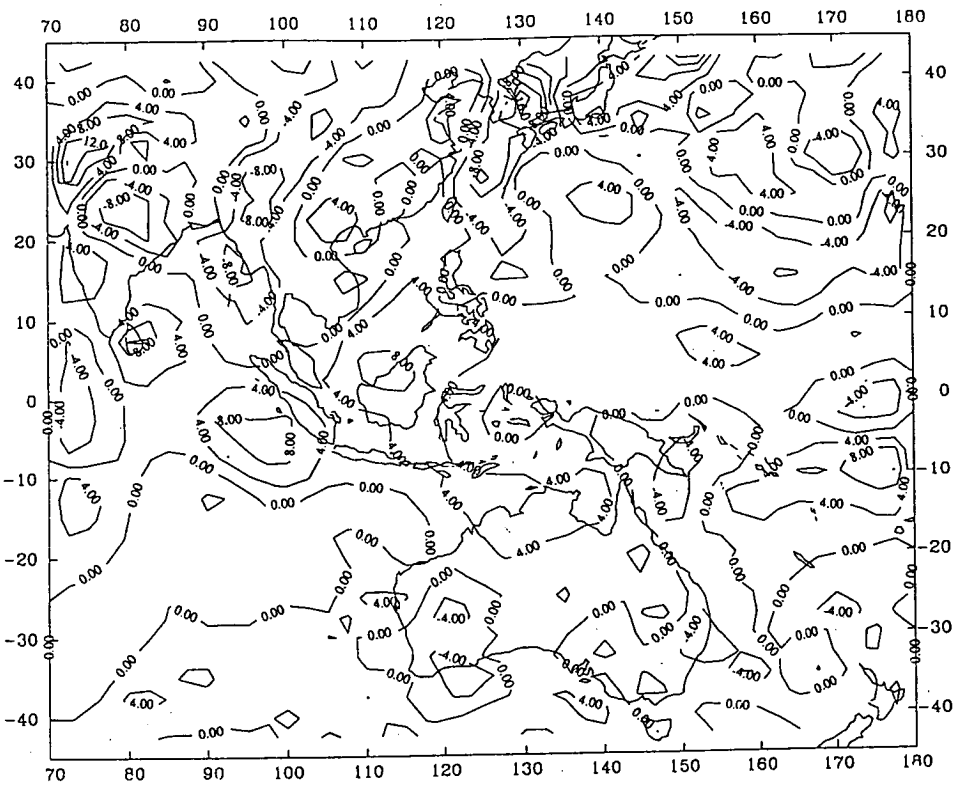

MONTHLY WIND DIVERGENCE AT 200MB (8401)

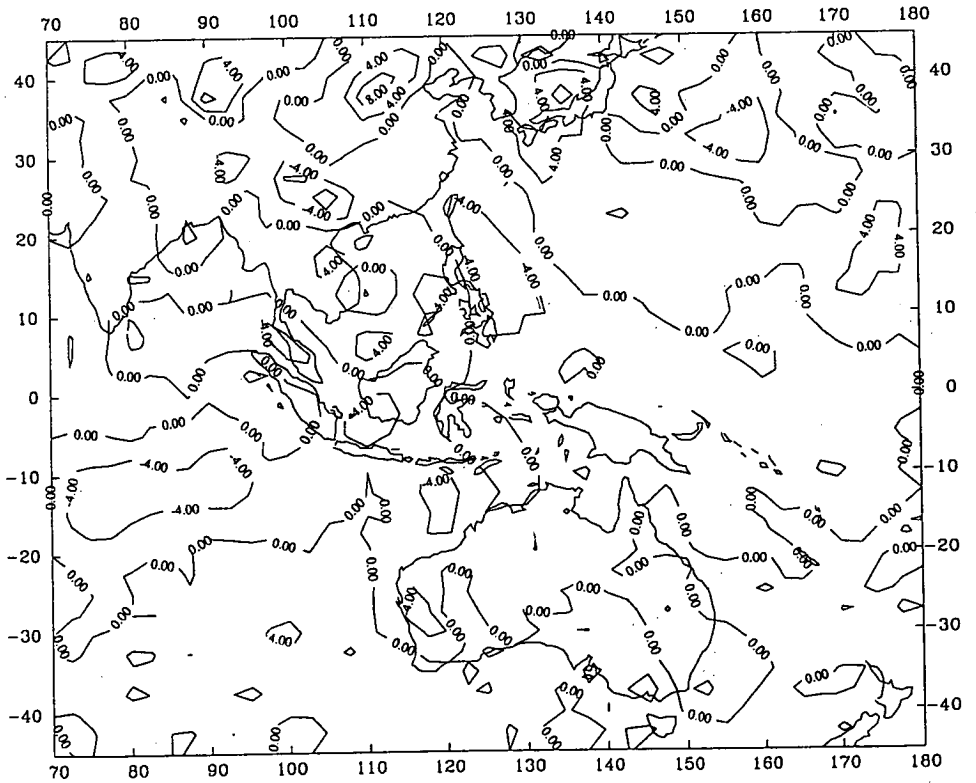

MONTHLY WIND DIVERGENCE AT 850MB (8401)

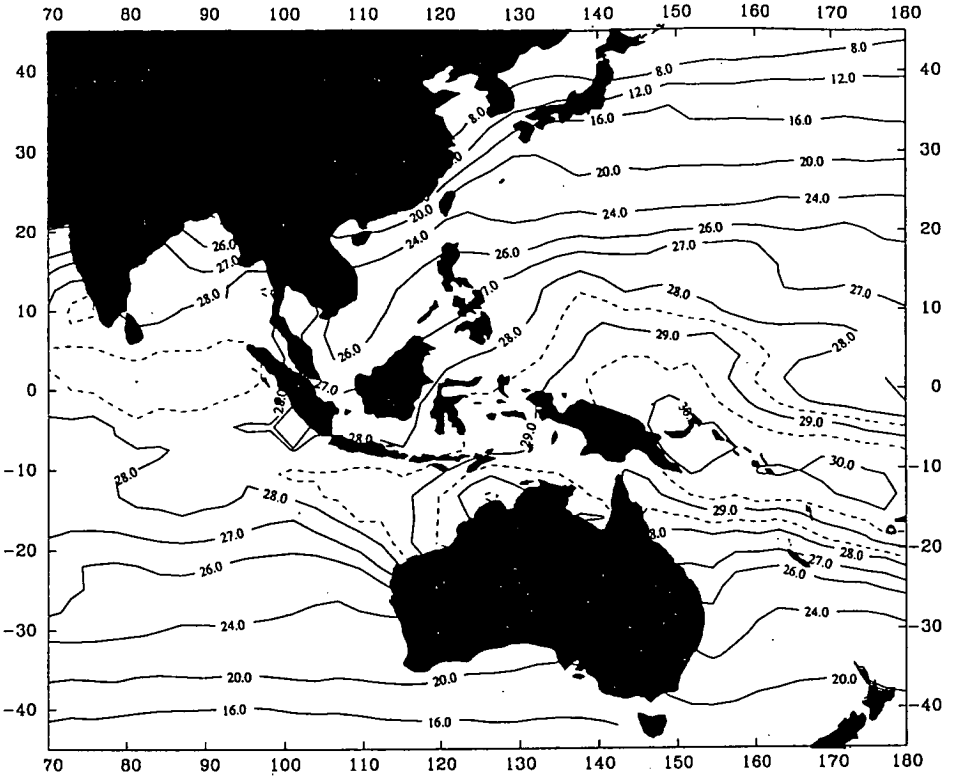

REYNOLDS BLENDED MONTHLY SST (8402)

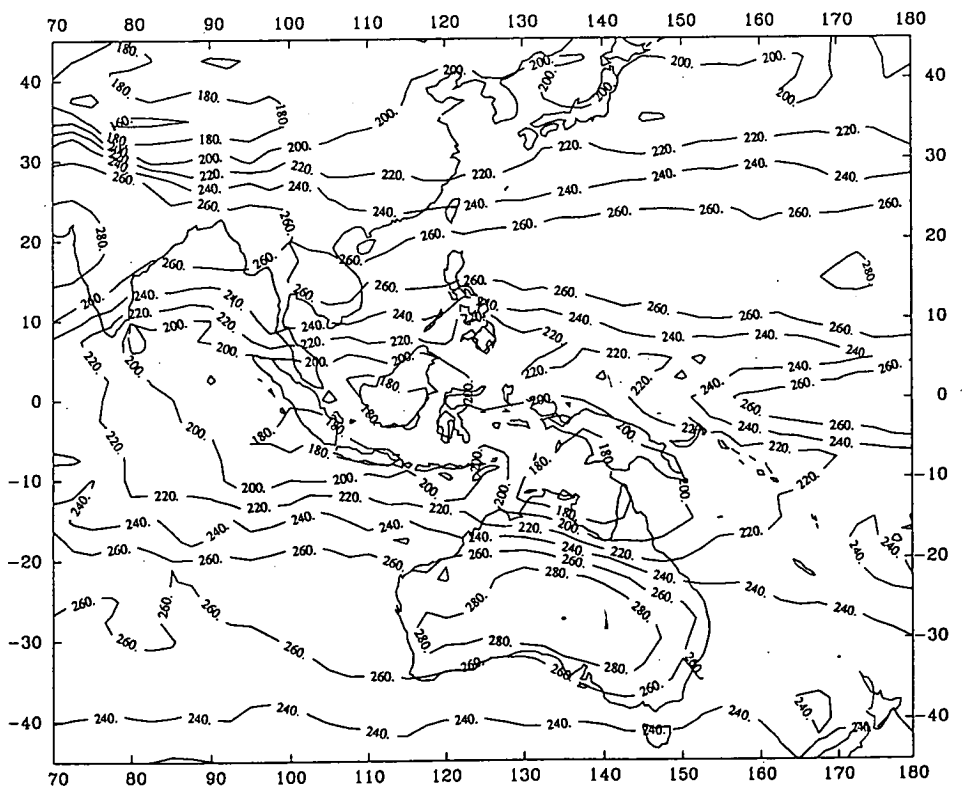

MONTHLY OLR (8402) (UNIT W/M*M)

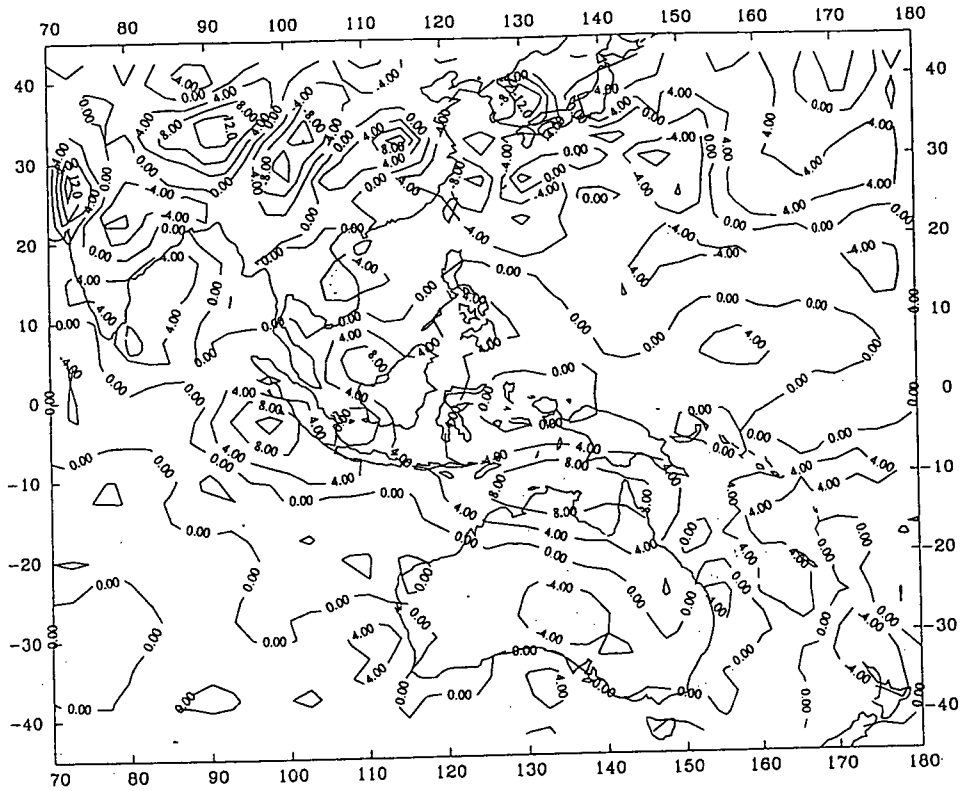

MONTHLY WIND DIVERGENCE AT 200MB (8402)

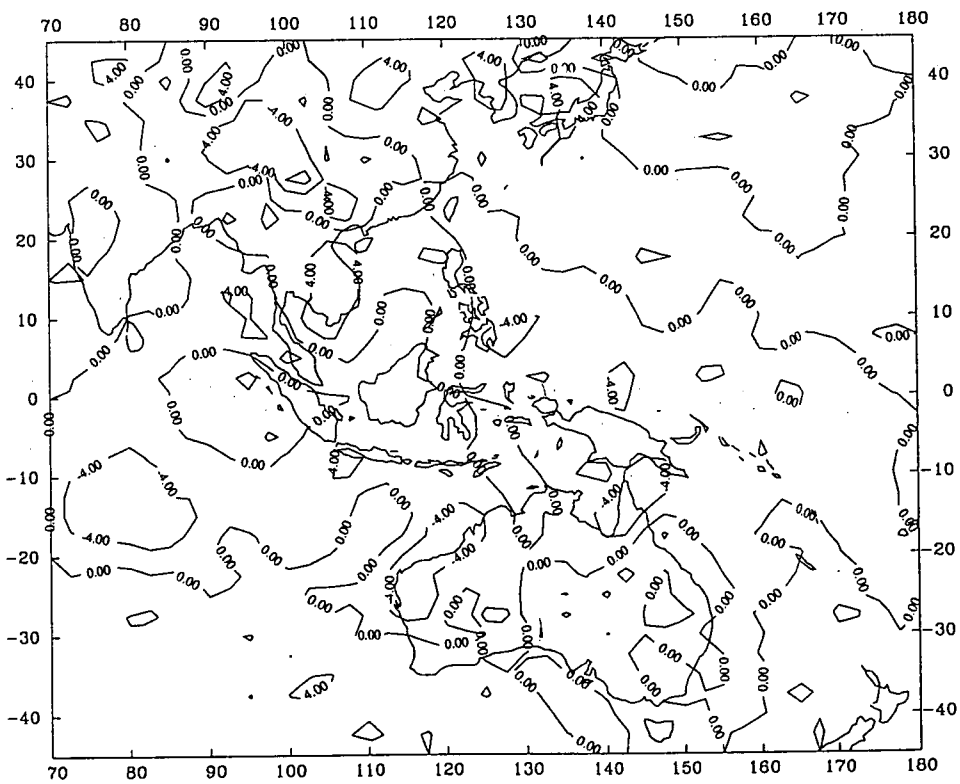

MONTHLY WIND DIVERGENCE AT 850MB (8402)

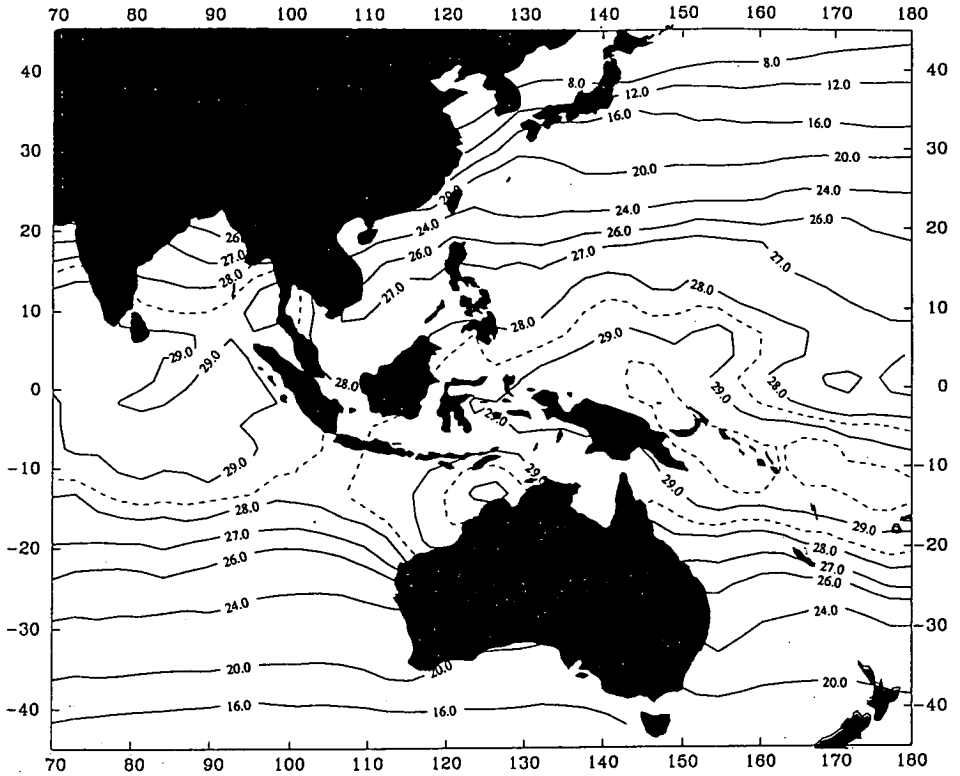

REYNOLDS BLENDED MONTHLY SST (8403)

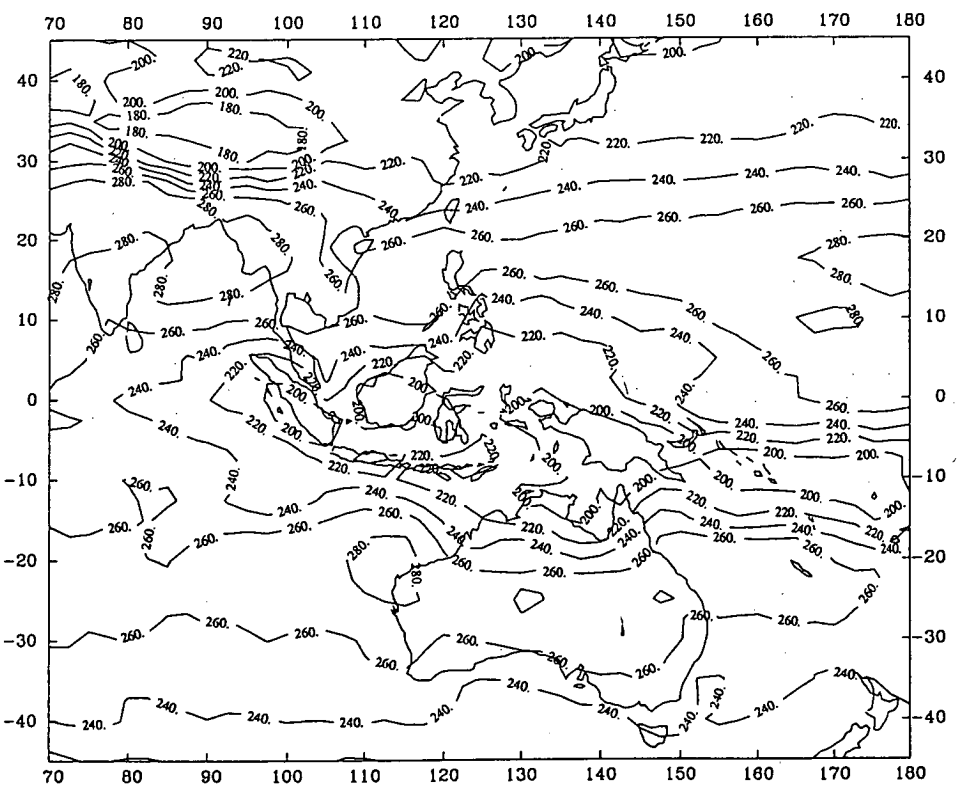

MONTHLY OLR (8403) (UNIT W/M*M)

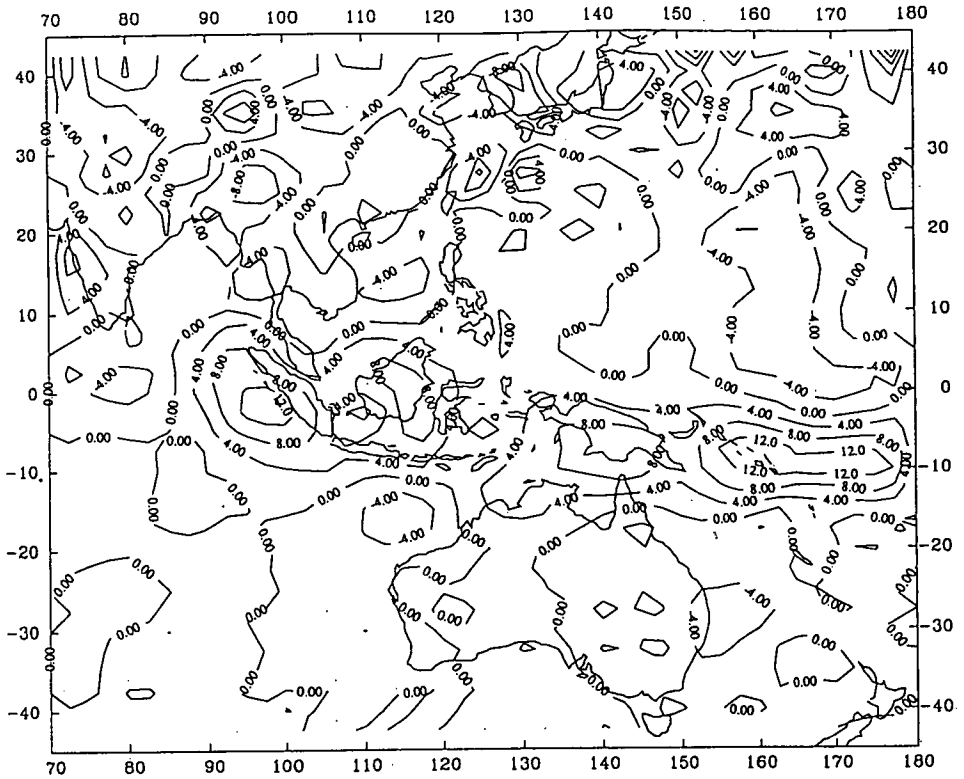

MONTHLY WIND DIVERGENCE AT 200MB (8403)

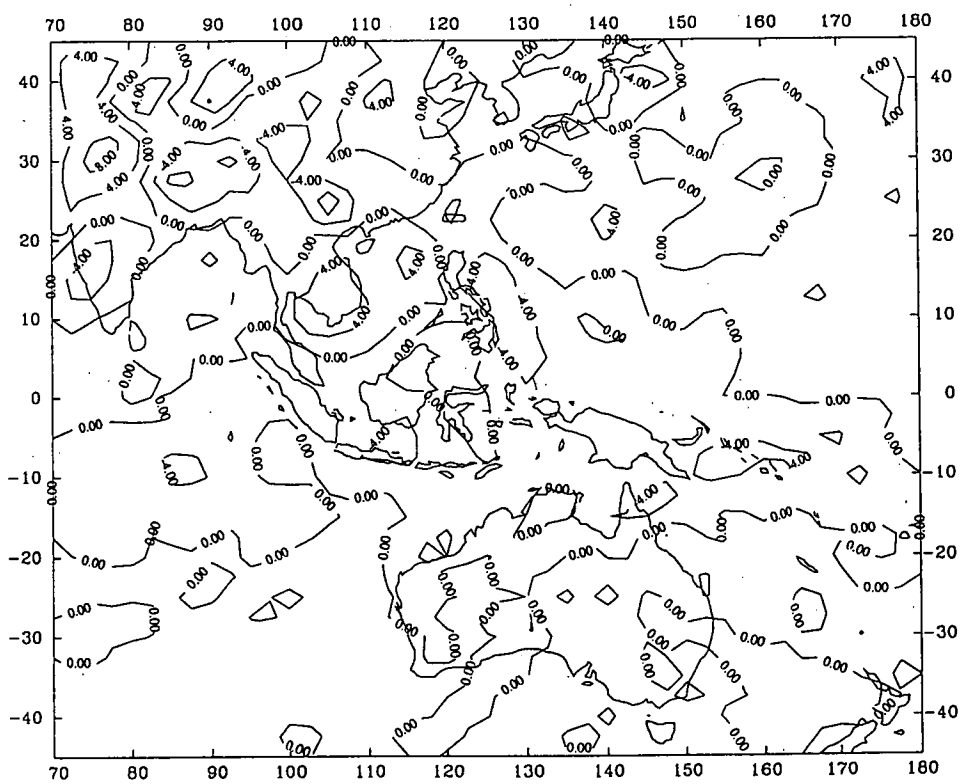

MONTHLY WIND DIVERGENCE AT 850MB (8403)

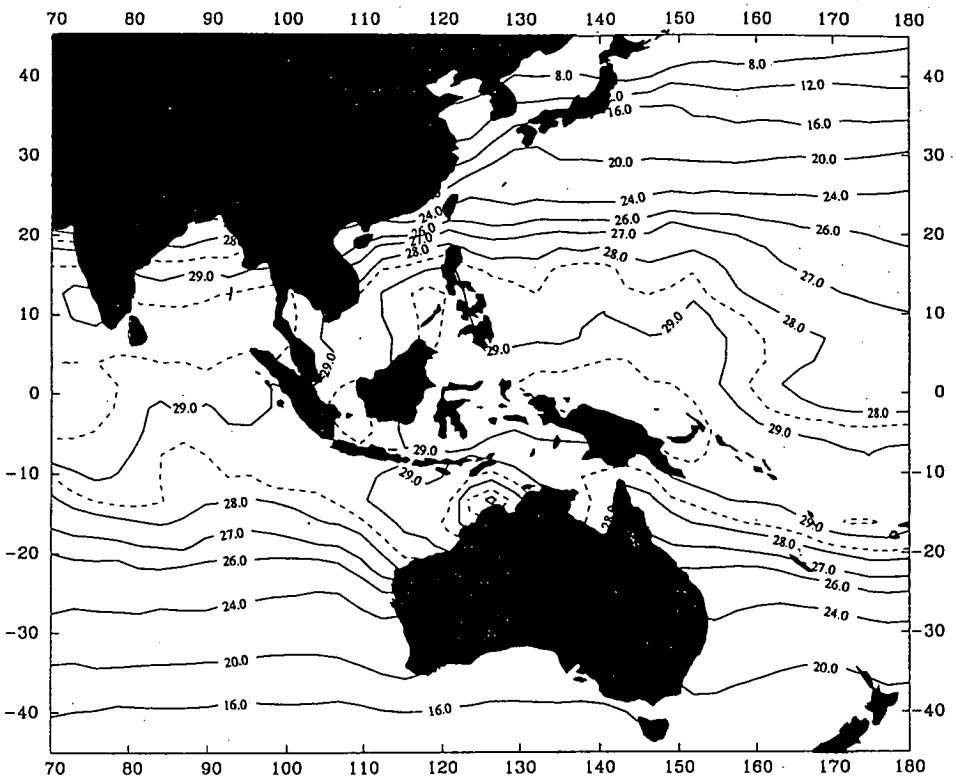

REYNOLDS BLENDED MONTHLY SST (8404)

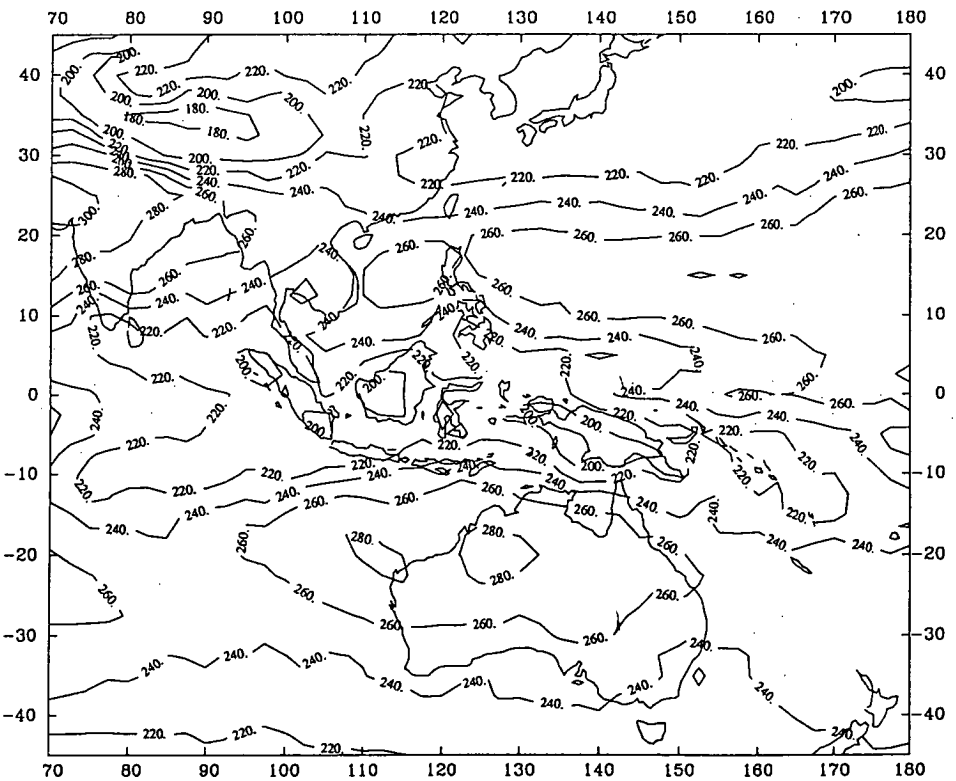

MONTHLY OLR (8404) (UNIT W/M*M)

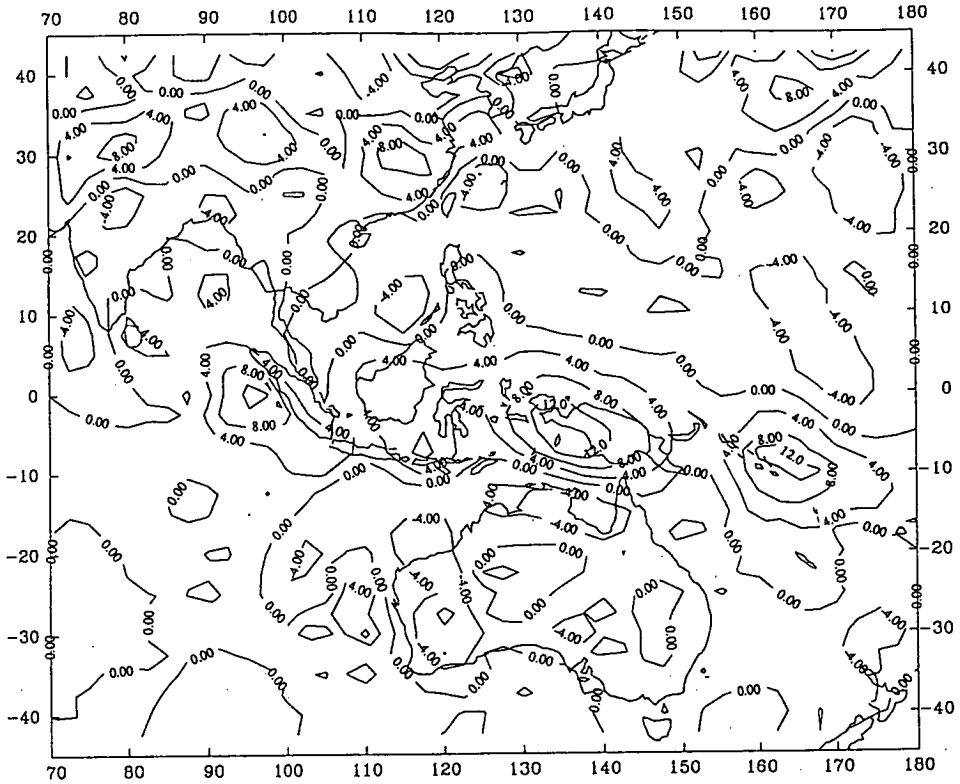

MONTHLY WIND DIVERGENCE AT 200MB (8404)

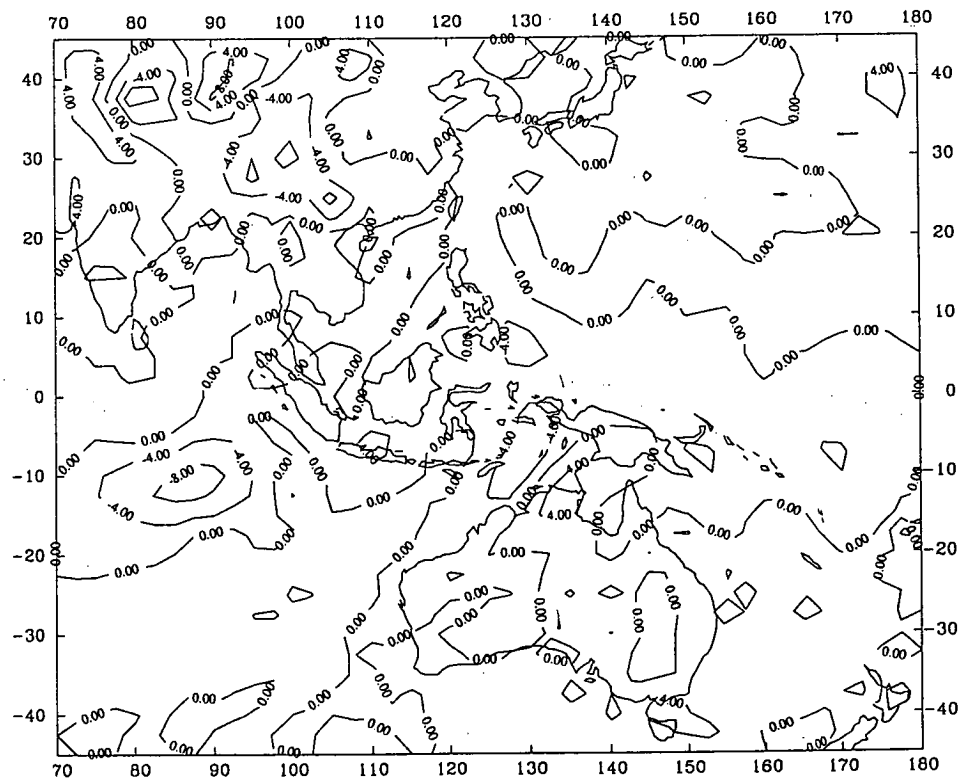

MONTHLY WIND DIVERGENCE AT 850MB (8404)

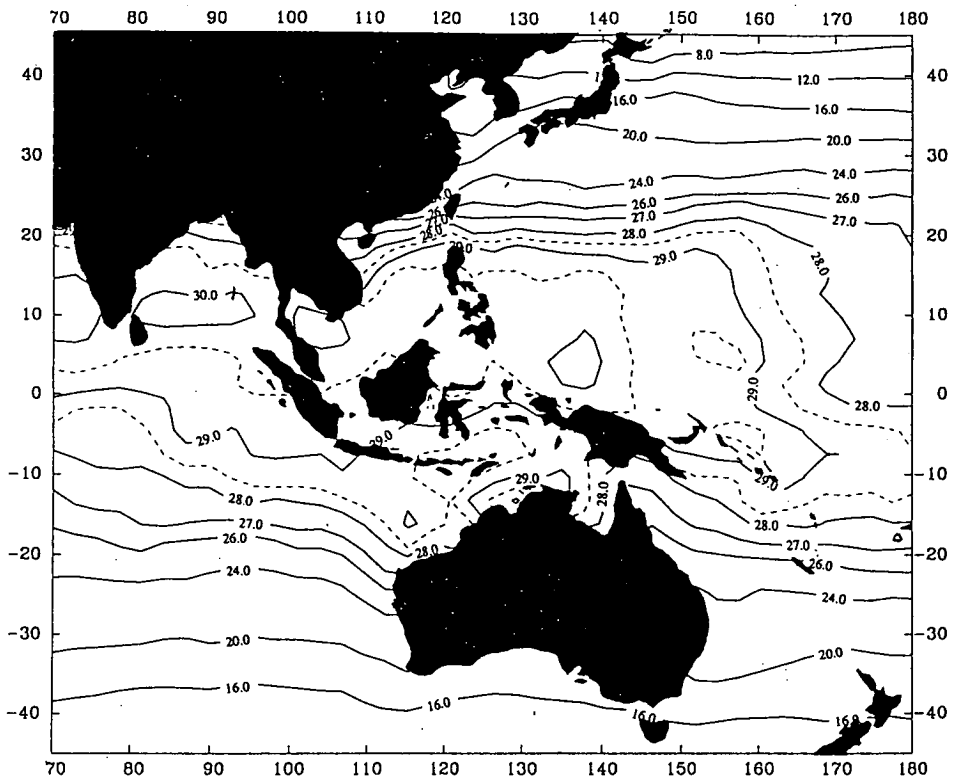

REYNOLDS BLENDED MONTHLY SST (8405)

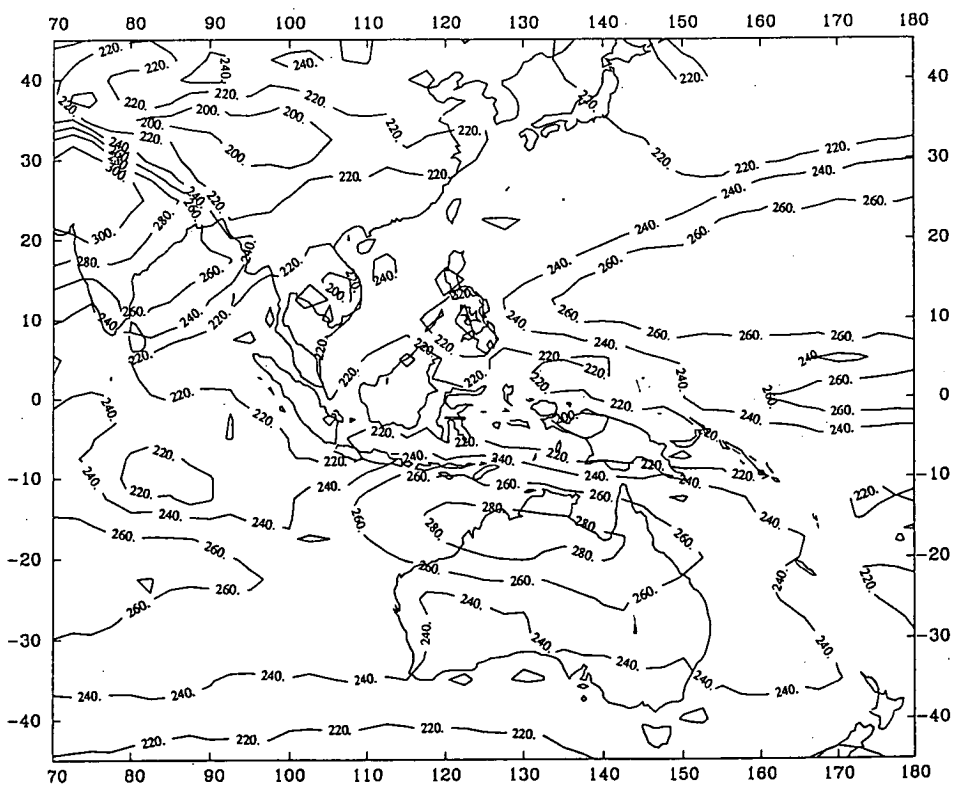

MONTHLY OLR (8405) (UNIT W/M*M)

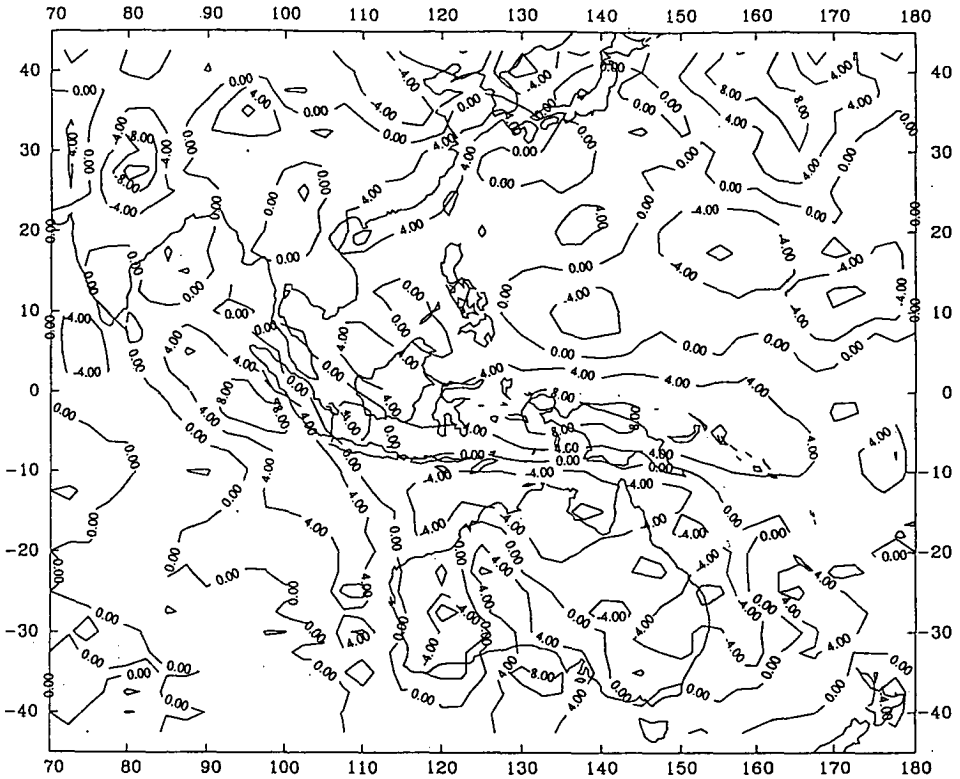

MONTHLY WIND DIVERGENCE AT 200MB (8405)

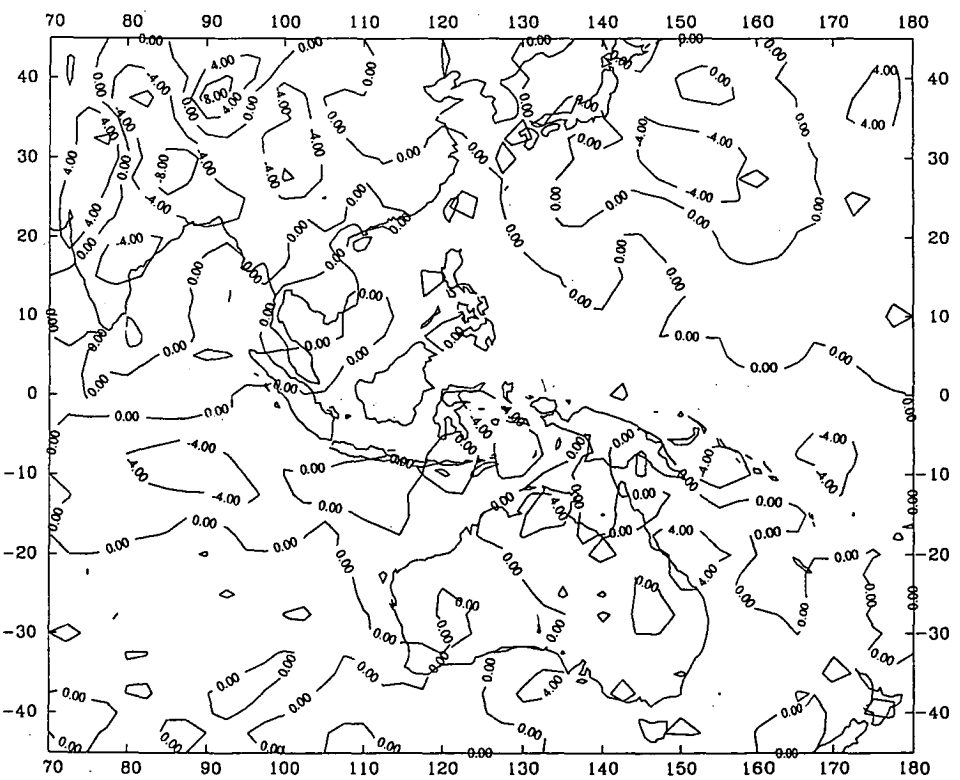

MONTHLY WIND DIVERGENCE AT 850MB (8405)

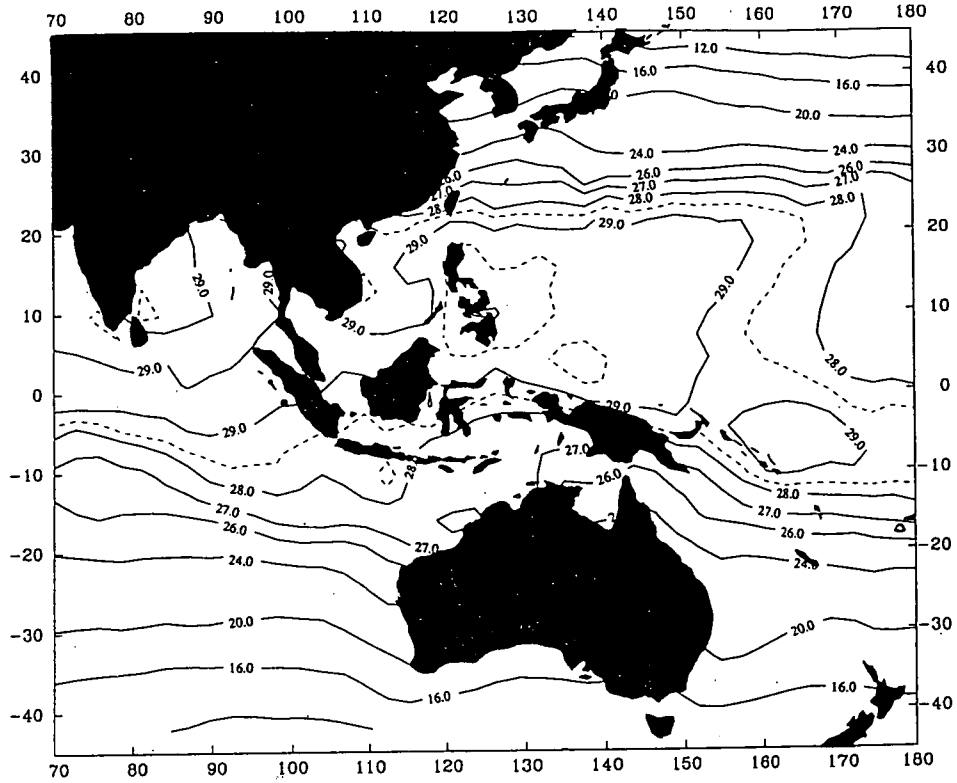

REYNOLDS BLENDED MONTHLY SST (8406)

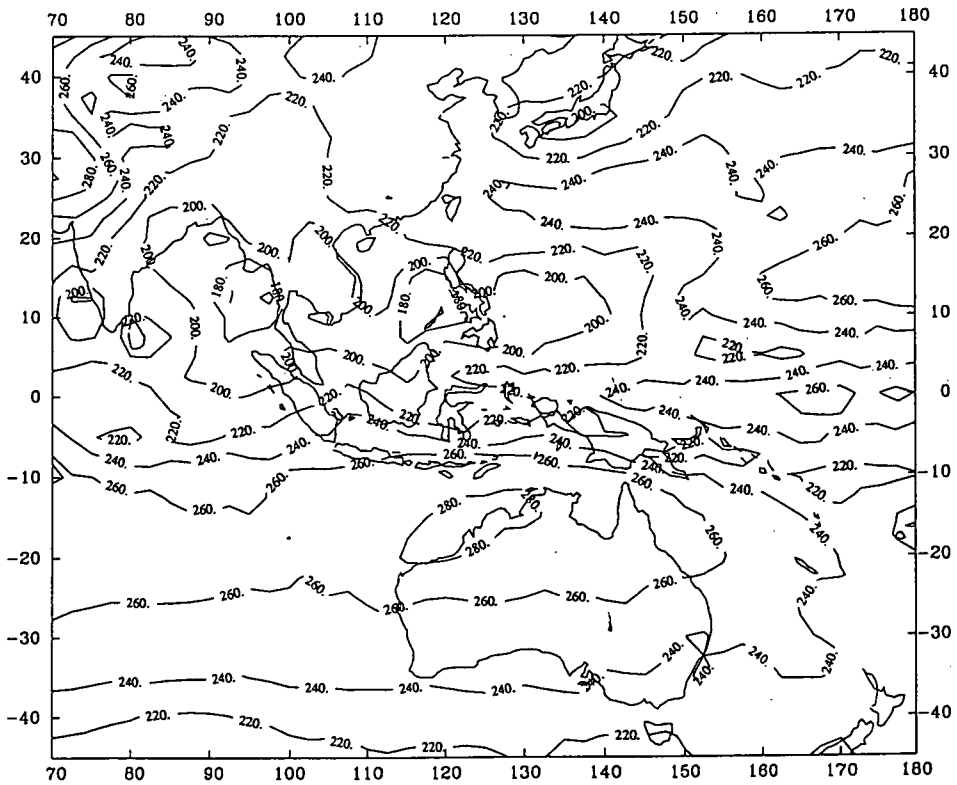

MONTHLY OLR (8406) (UNIT W/M*M)

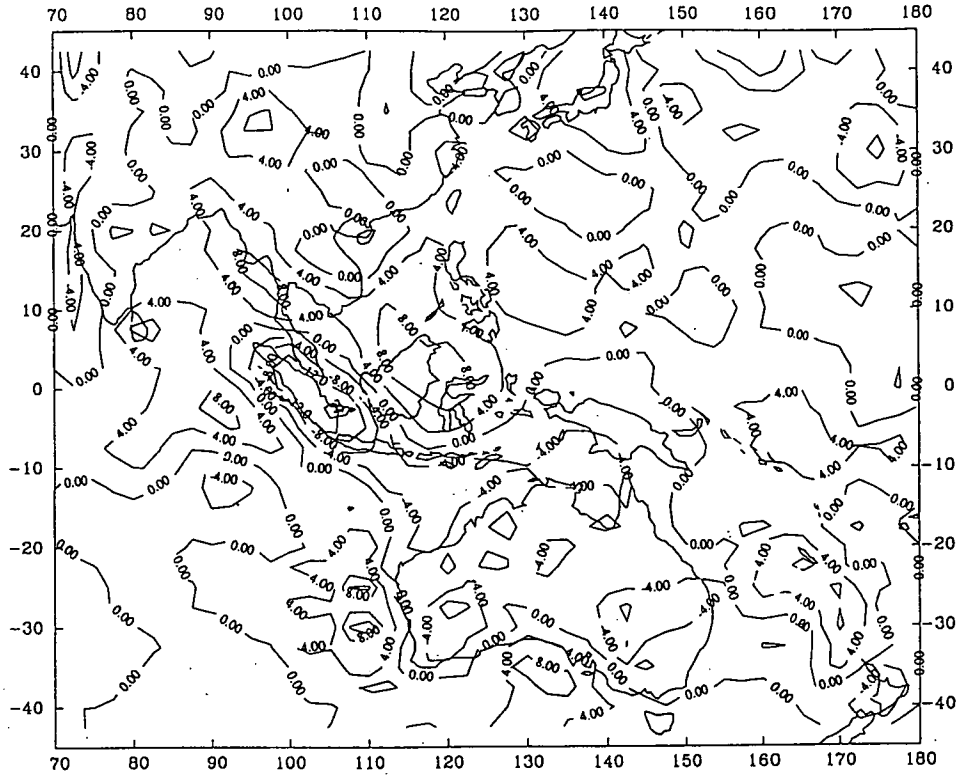

MONTHLY WIND DIVERGENCE AT 200MB (8406)

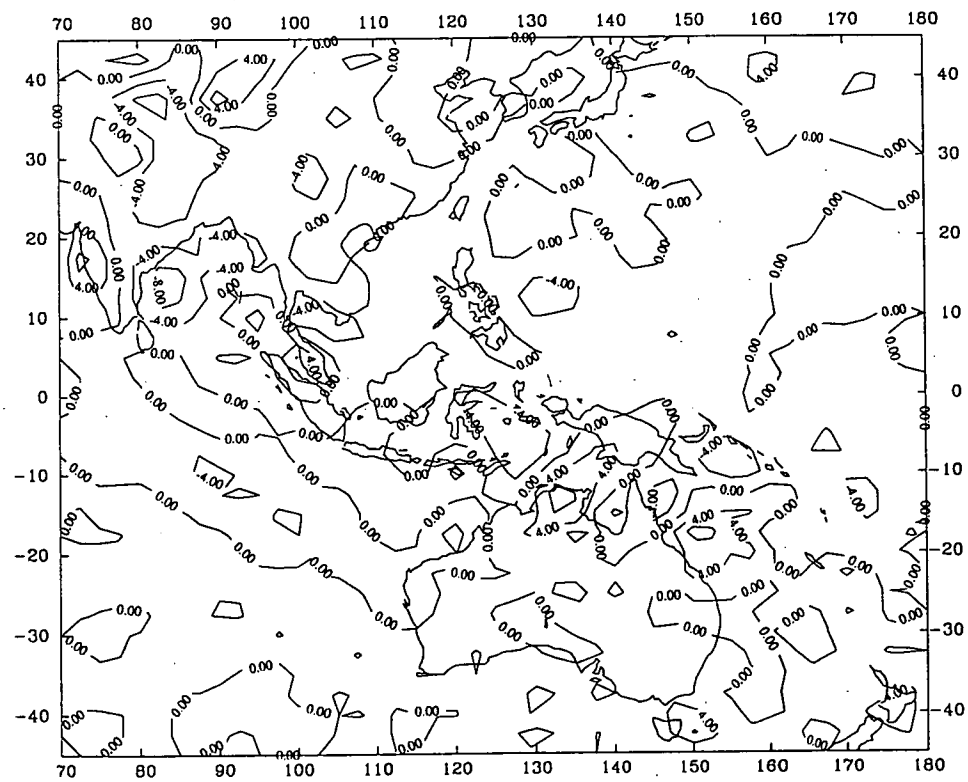

MONTHLY WIND DIVERGENCE AT 850MB (8406)

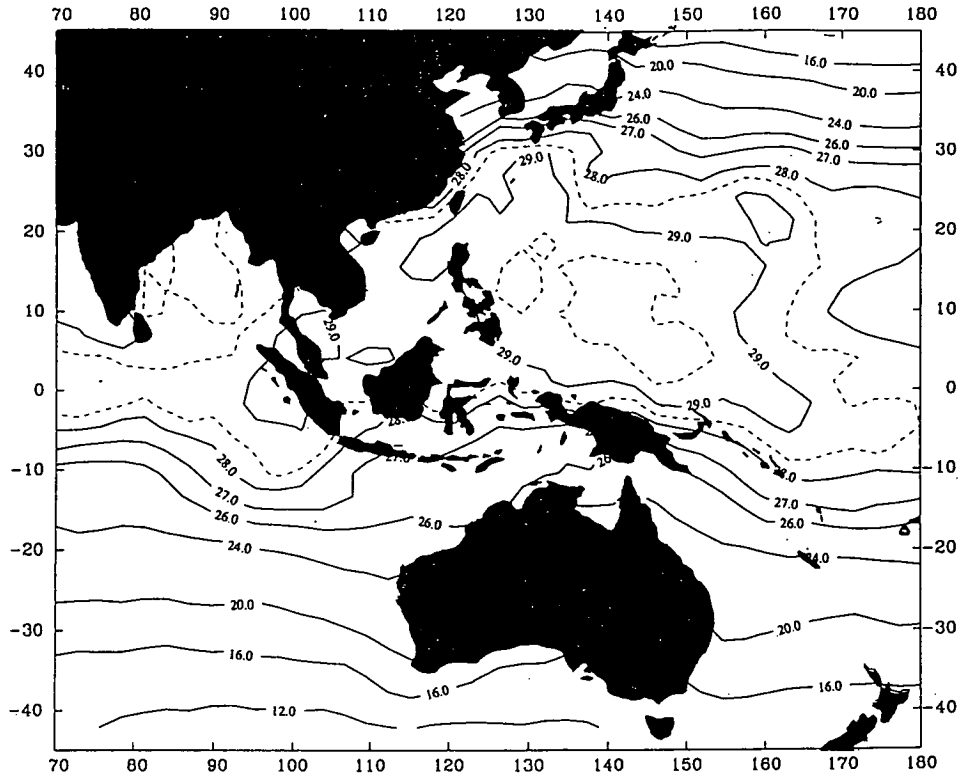

REYNOLDS BLENDED MONTHLY SST (8407)

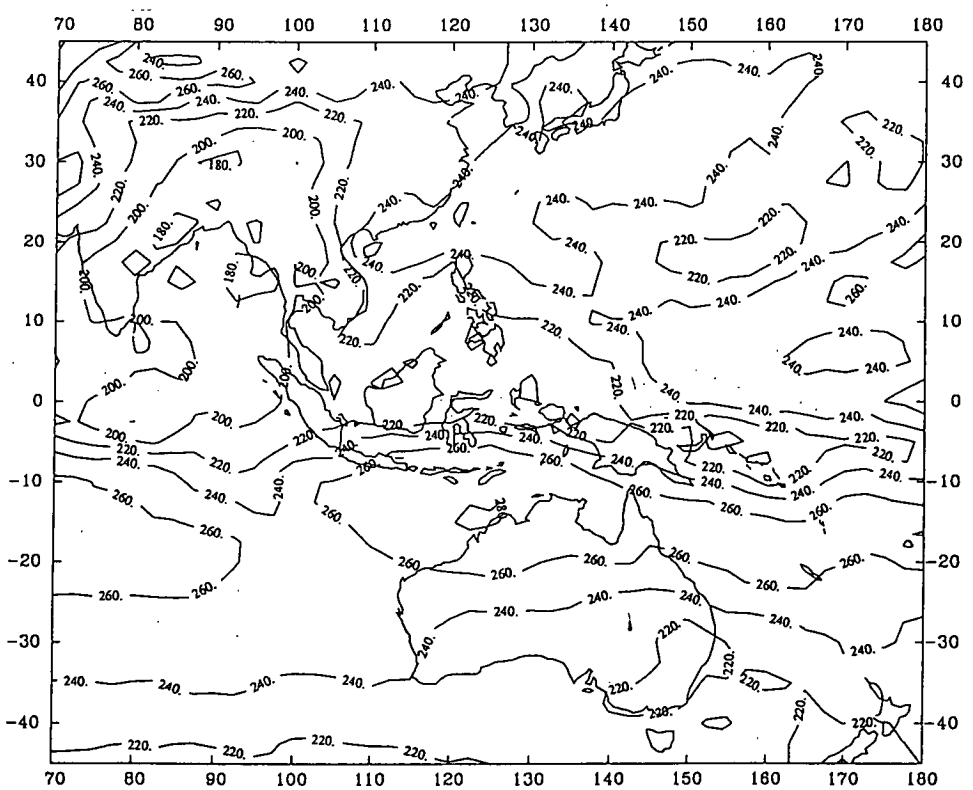

MONTHLY OLR (8407) (UNIT W/M*M)

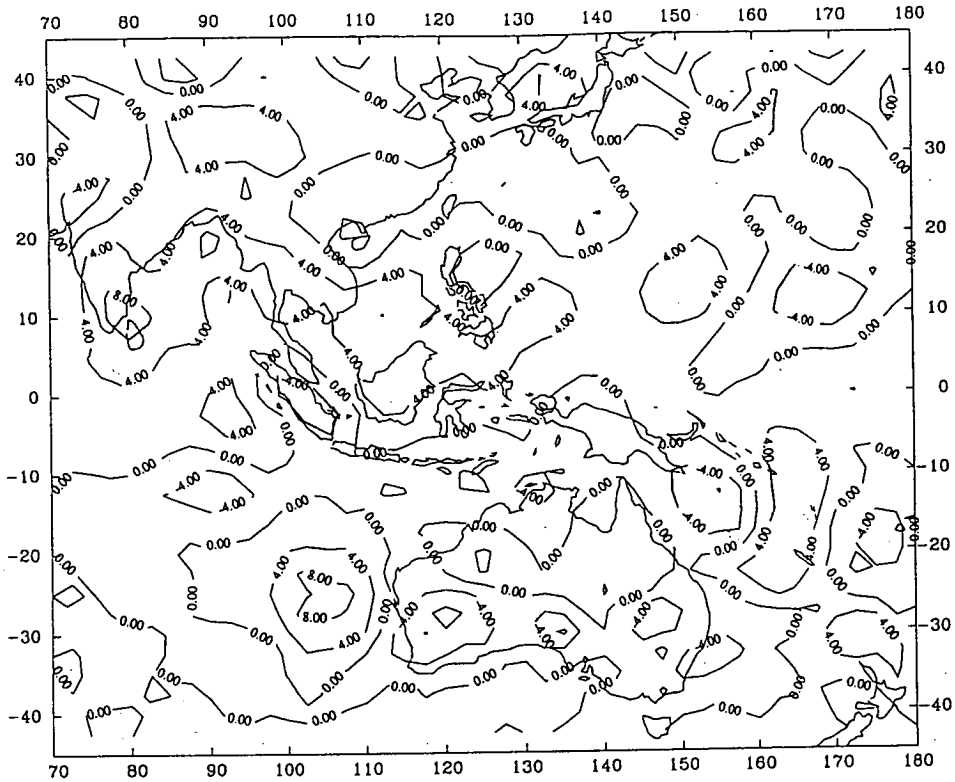

MONTHLY WIND DIVERGENCE AT 200MB (8407)

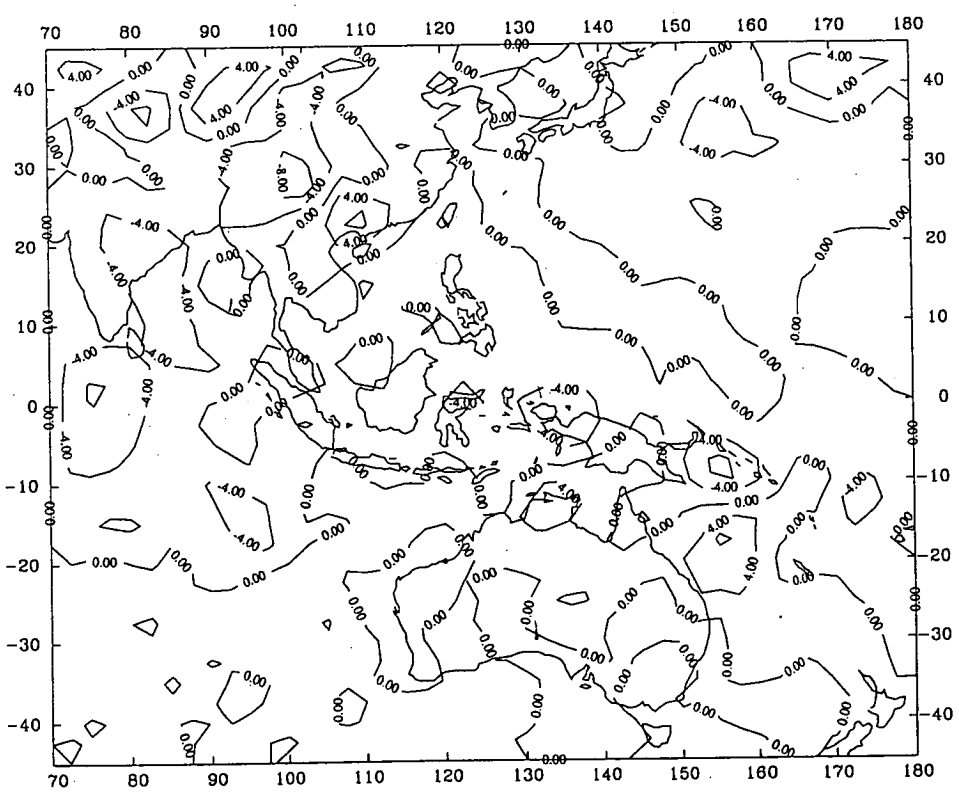

MONTHLY WIND DIVERGENCE AT 850MB (8407)

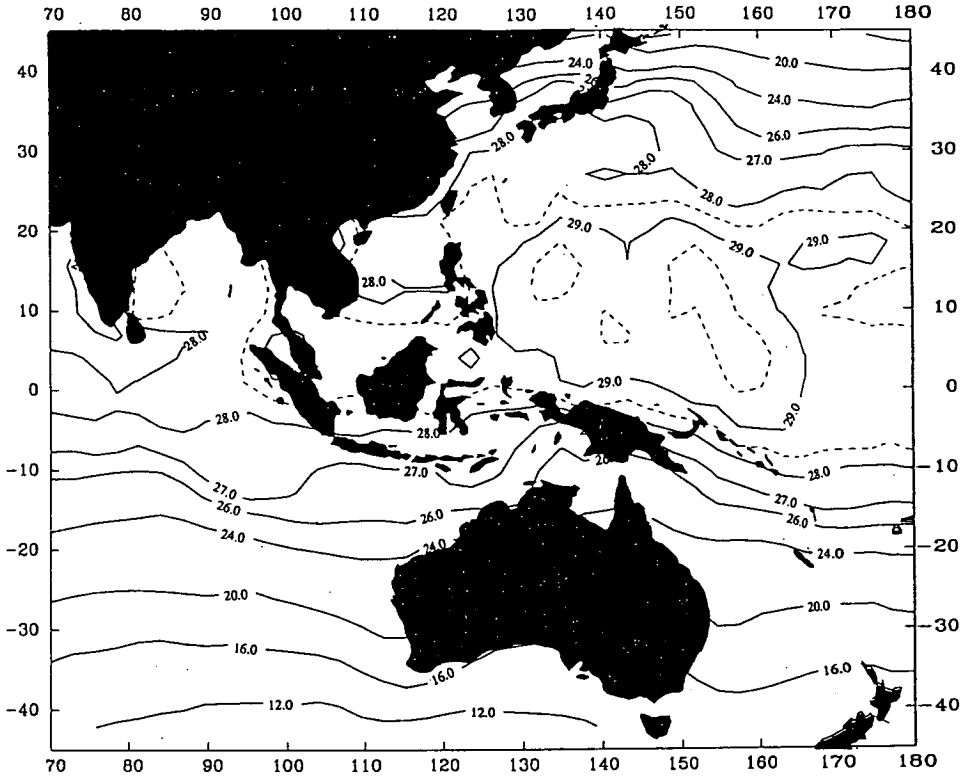

REYNOLDS BLENDED MONTHLY SST (8408)

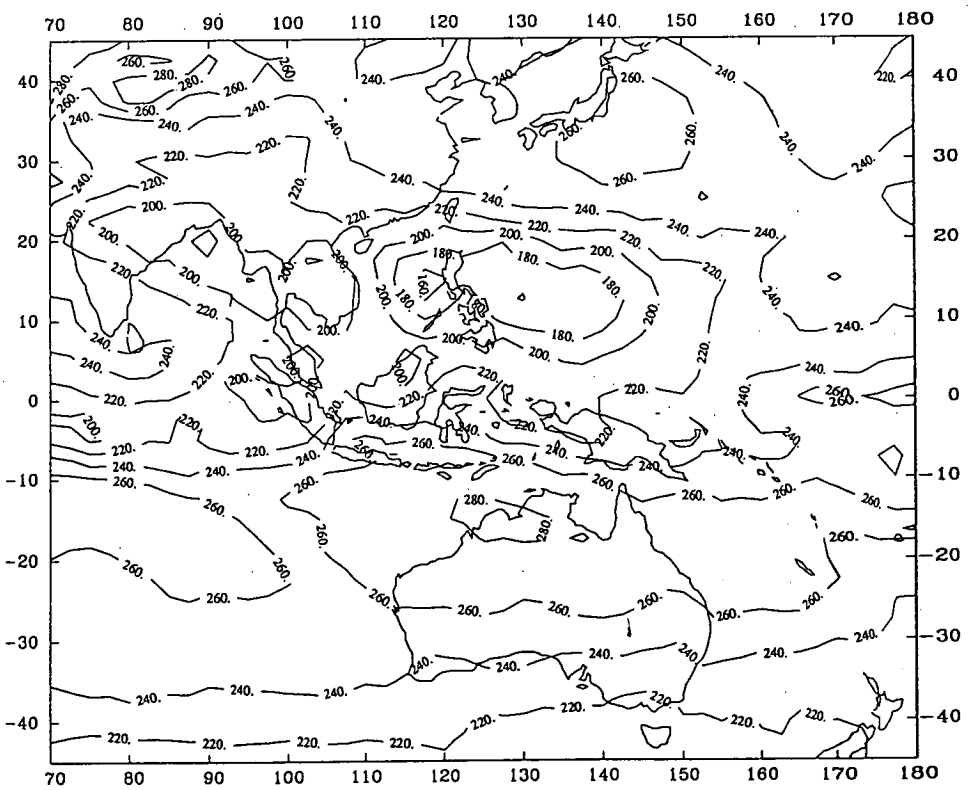

MONTHLY OLR (8408) (UNIT W/M*M)

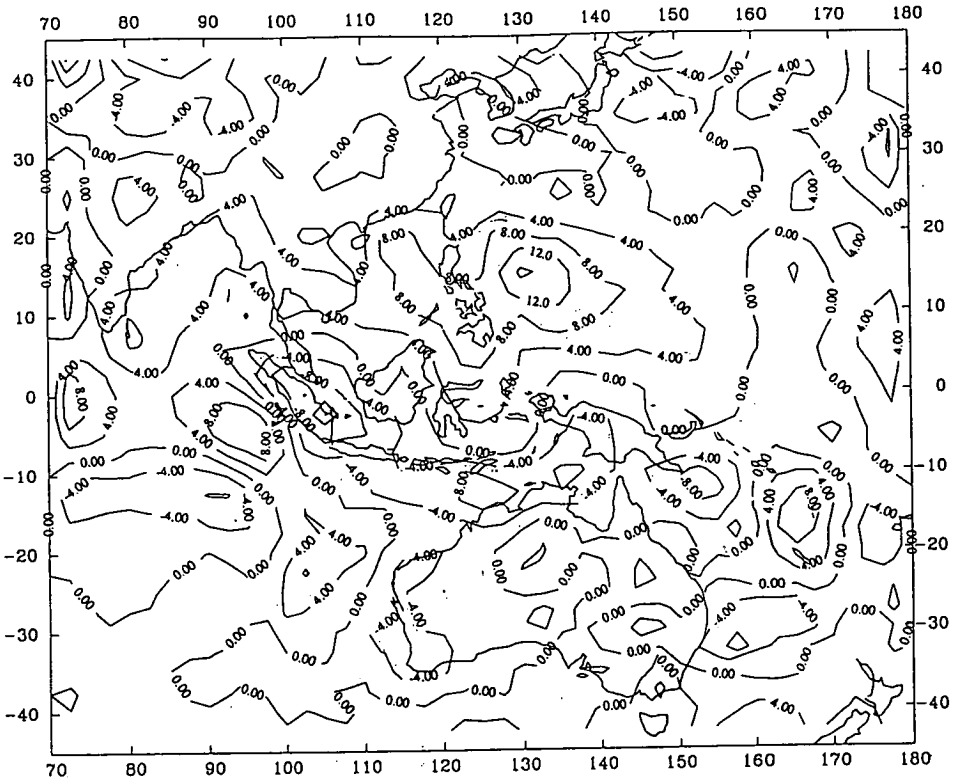

MONTHLY WIND DIVERGENCE AT 200MB (8408)

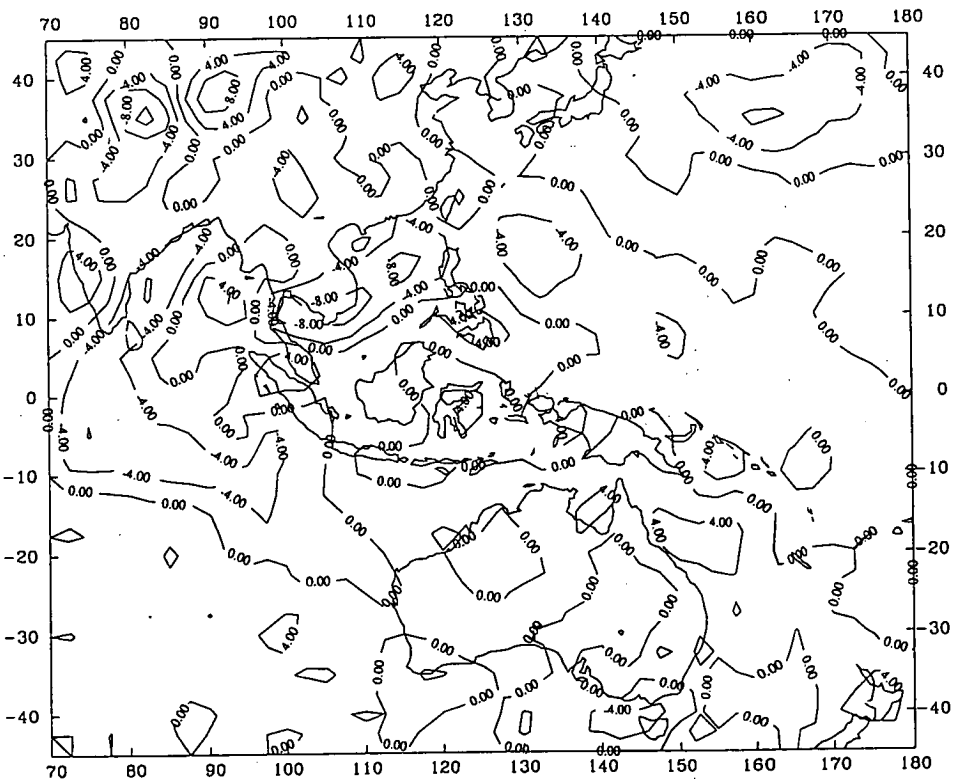

MONTHLY WIND DIVERGENCE AT 850MB (8408)

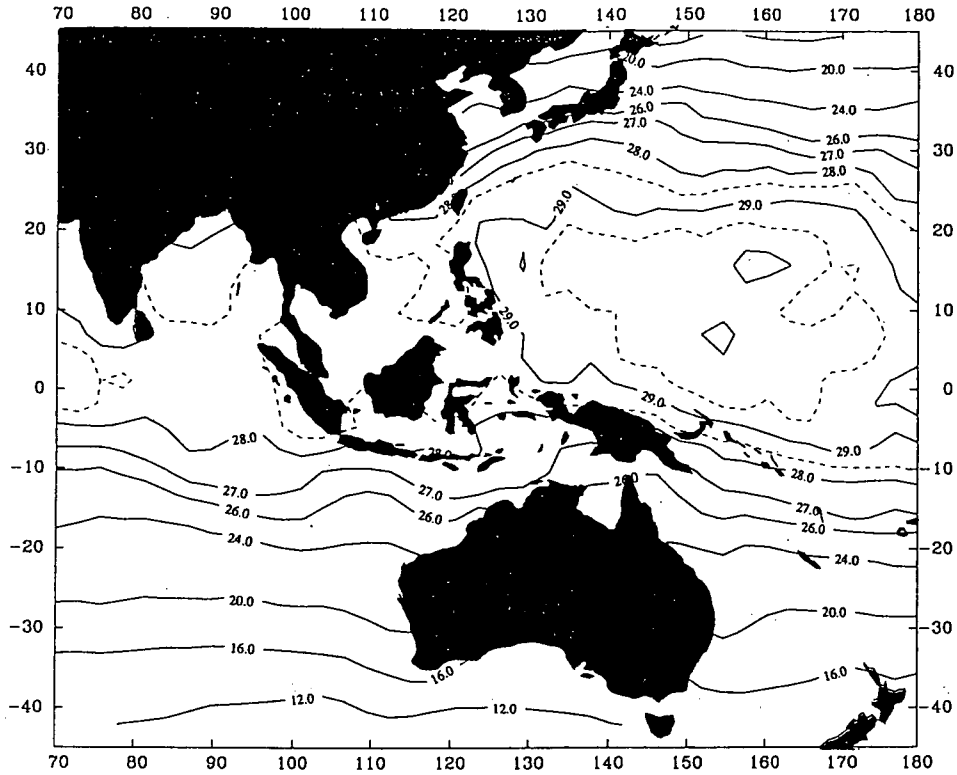

REYNOLDS BLENDED MONTHLY SST (8409)

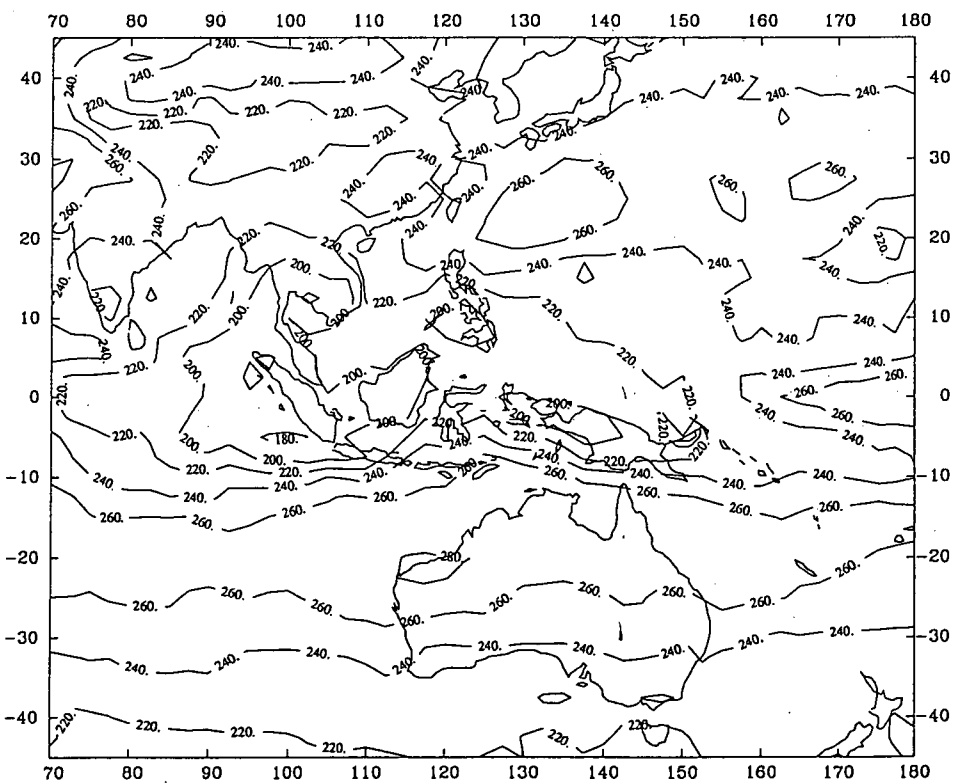

MONTHLY OLR (8409) (UNIT W/M*M)

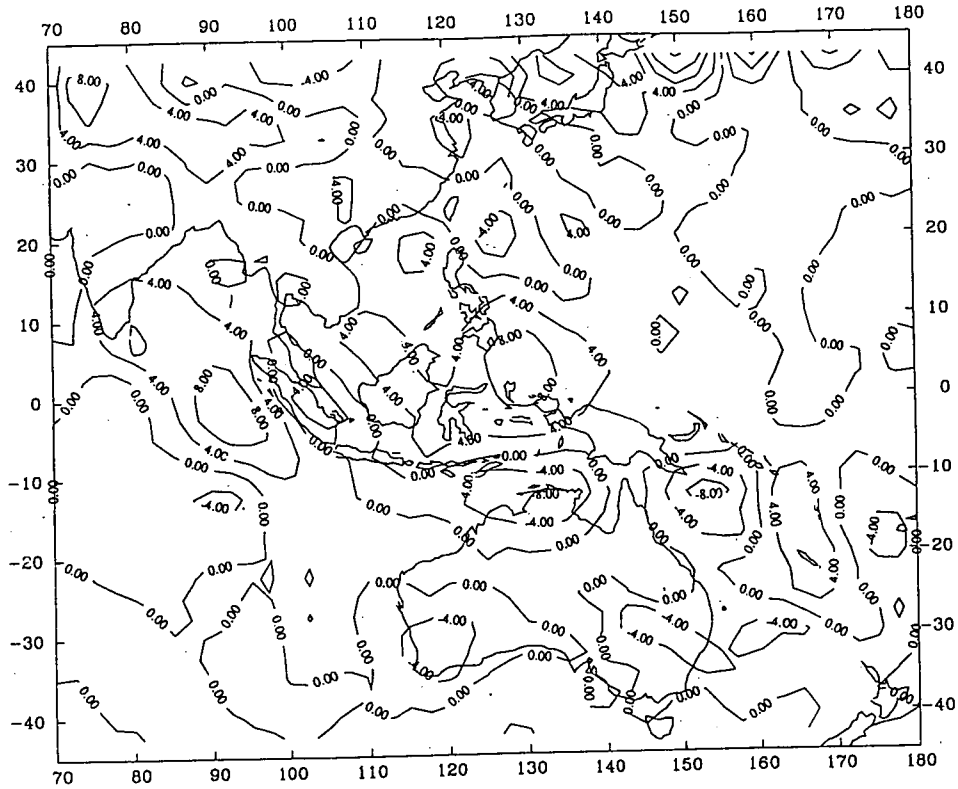

MONTHLY WIND DIVERGENCE AT 200MB (8409)

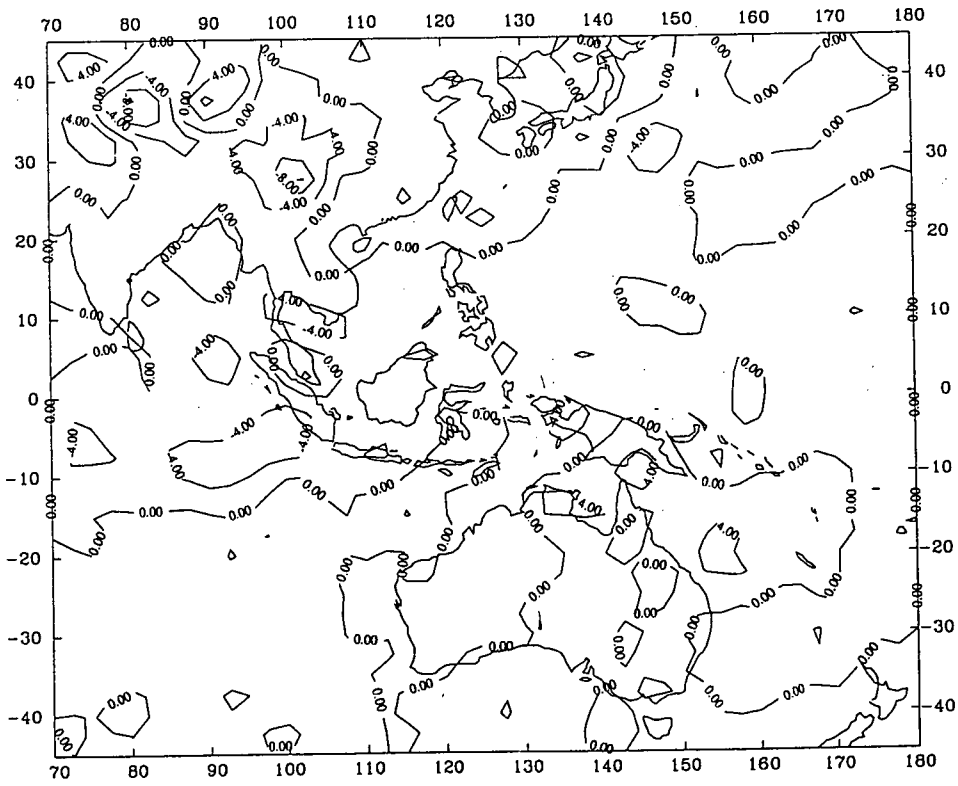

MONTHLY WIND DIVERGENCE AT 850MB (8409)

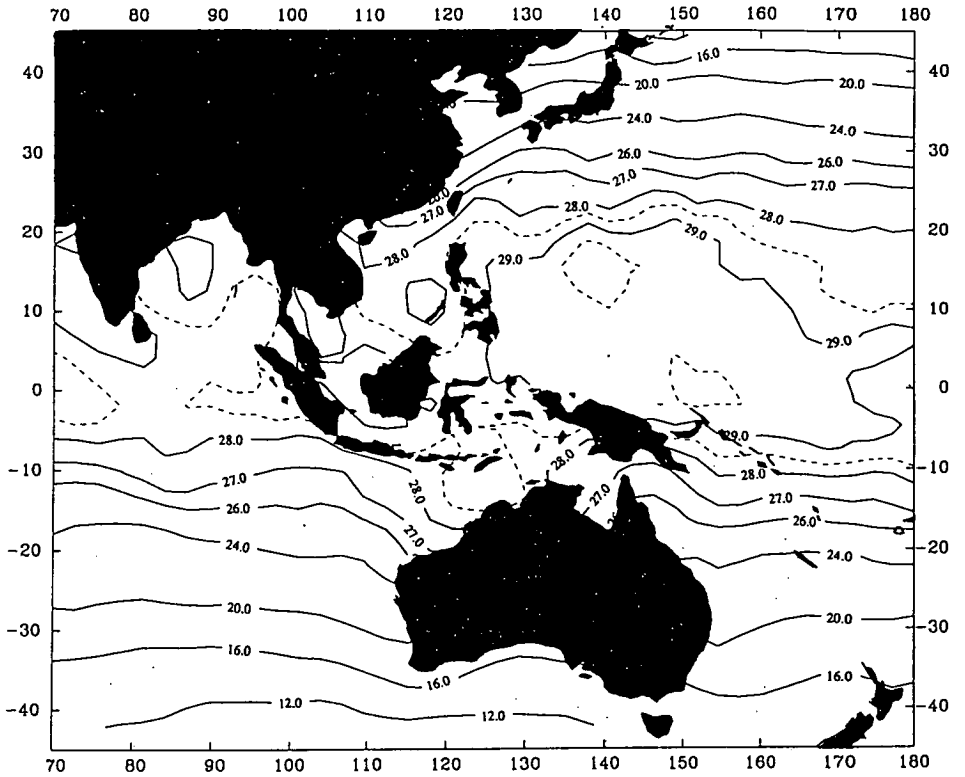

REYNOLDS BLENDED MONTHLY SST (8410)

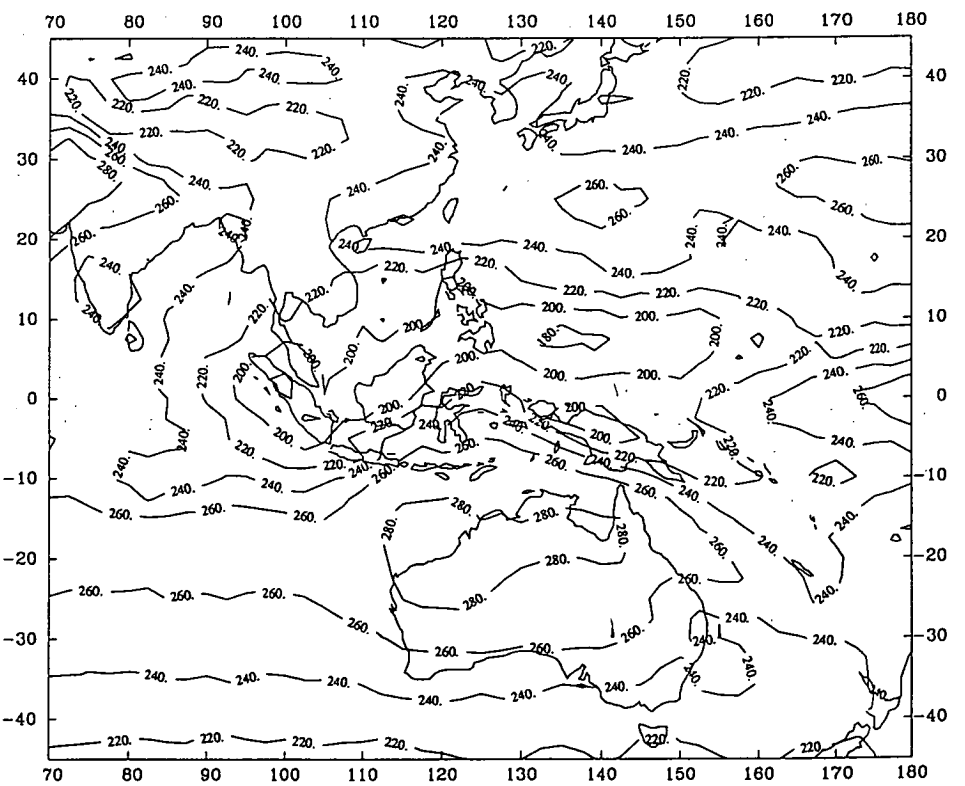

MONTHLY OLR (8410) (UNIT W/M*M)

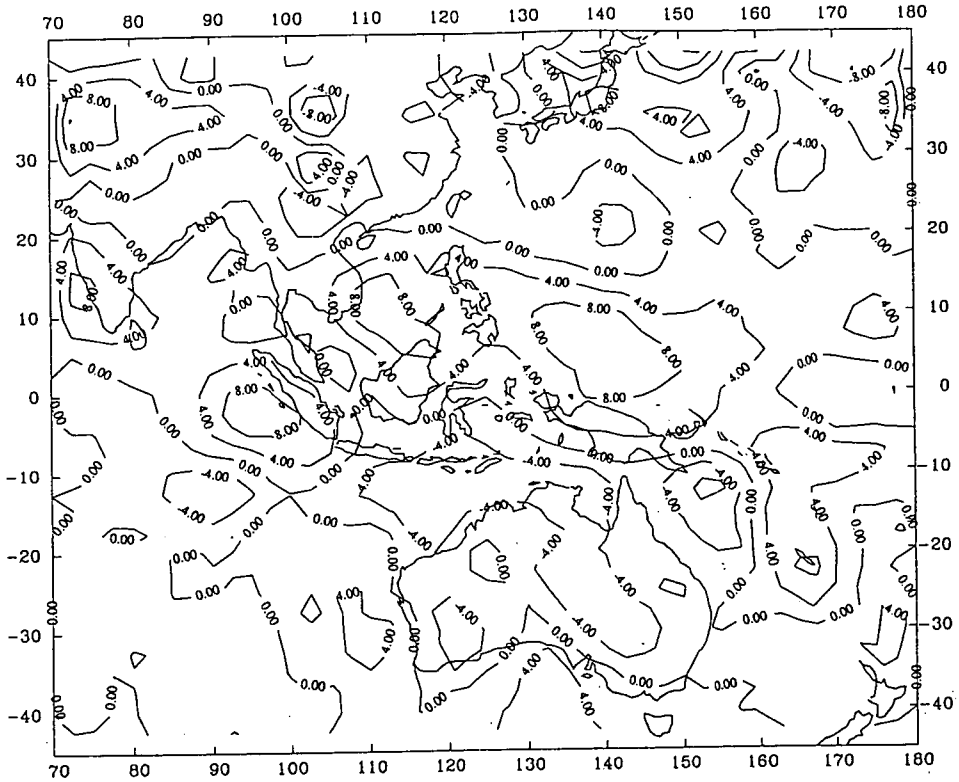

MONTHLY WIND DIVERGENCE AT 200MB (8410)

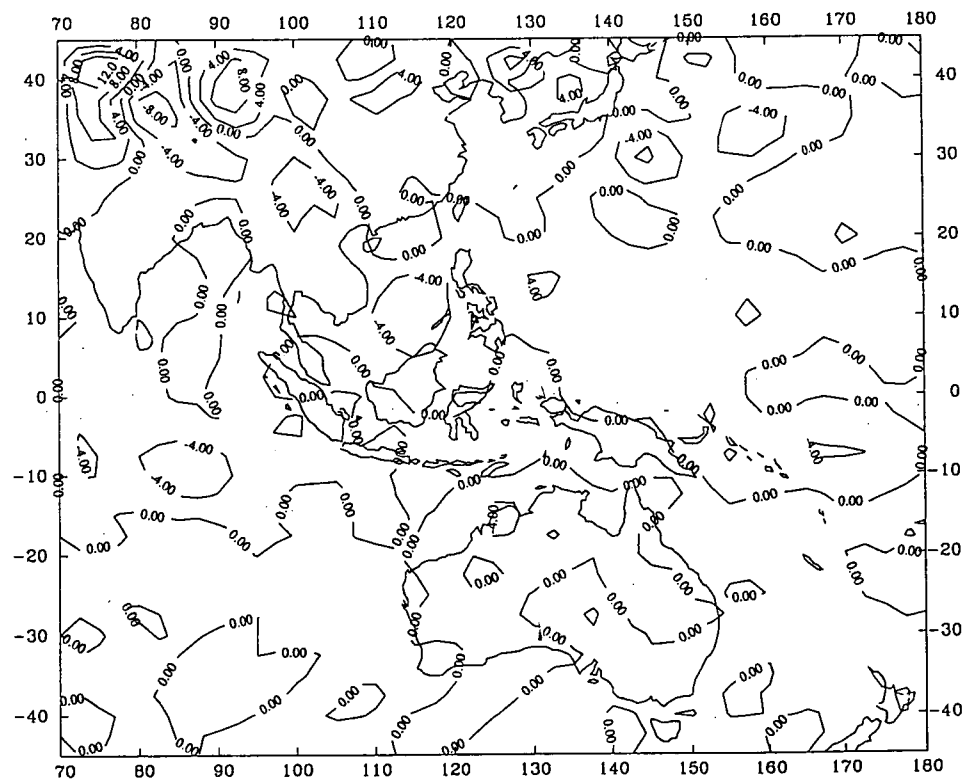

MONTHLY WIND DIVERGENCE AT 850MB (8410)

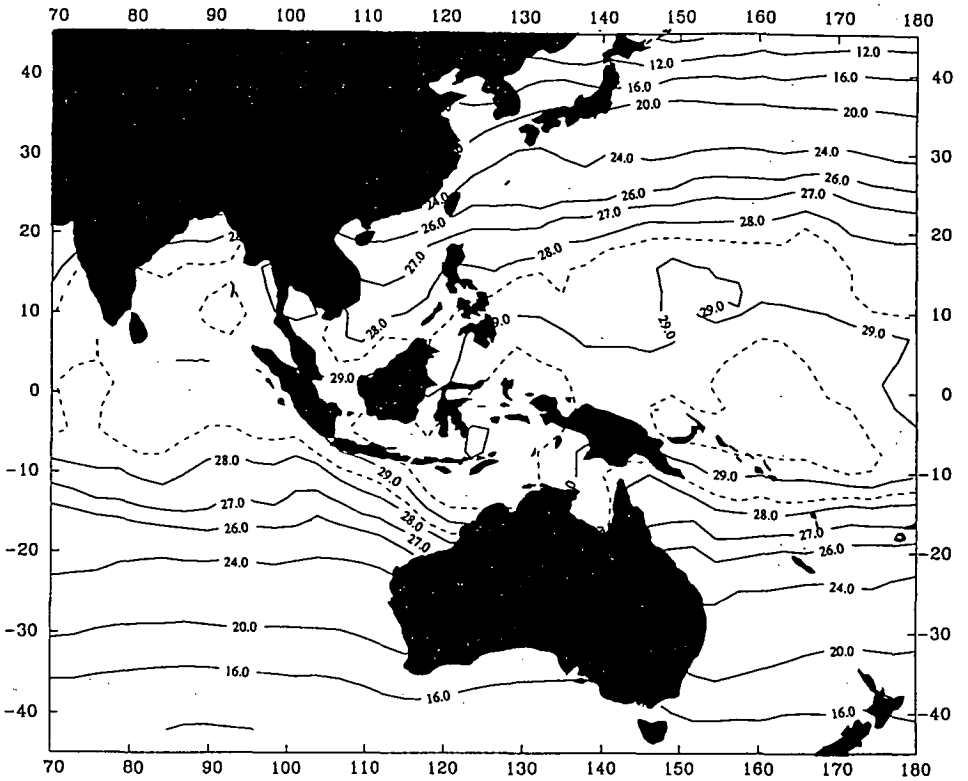

REYNOLDS BLENDED MONTHLY SST (8411)

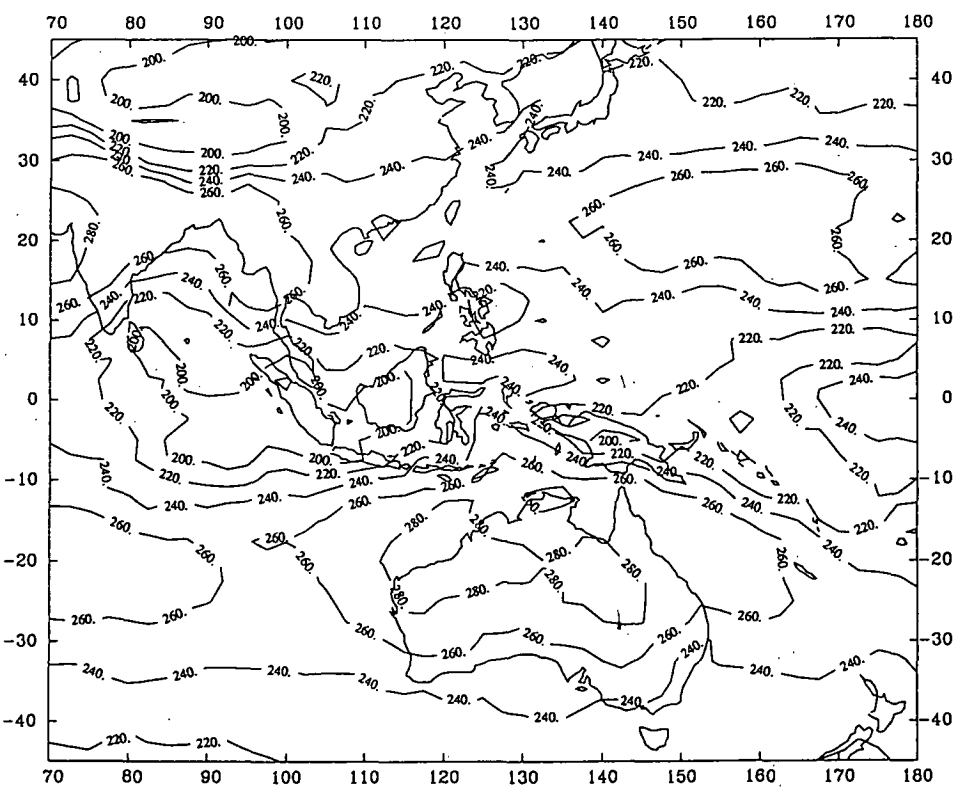

MONTHLY OLR (8411) (UNIT W/M*M)

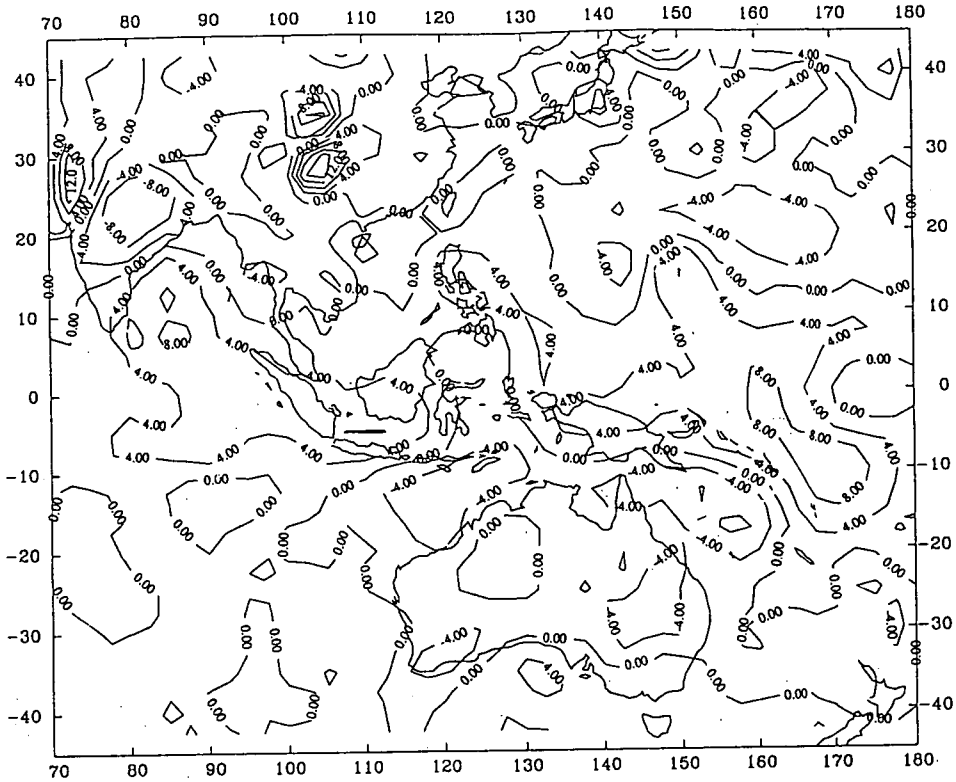

MONTHLY WIND DIVERGENCE AT 200MB (8411)

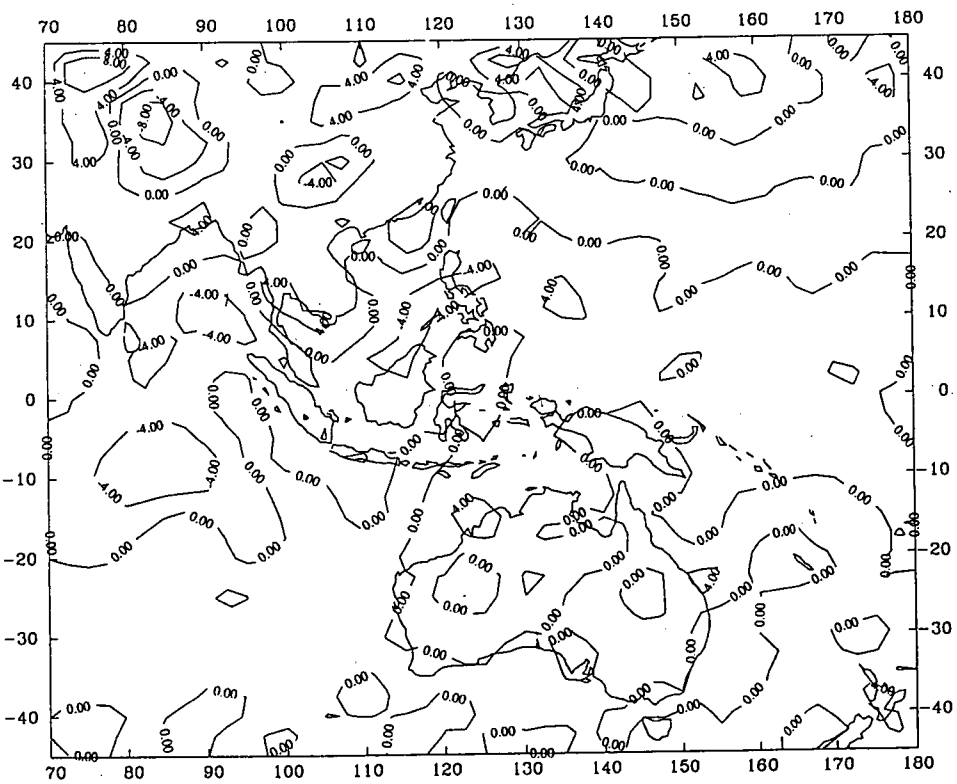

MONTHLY WIND DIVERGENCE AT 850MB (8411)

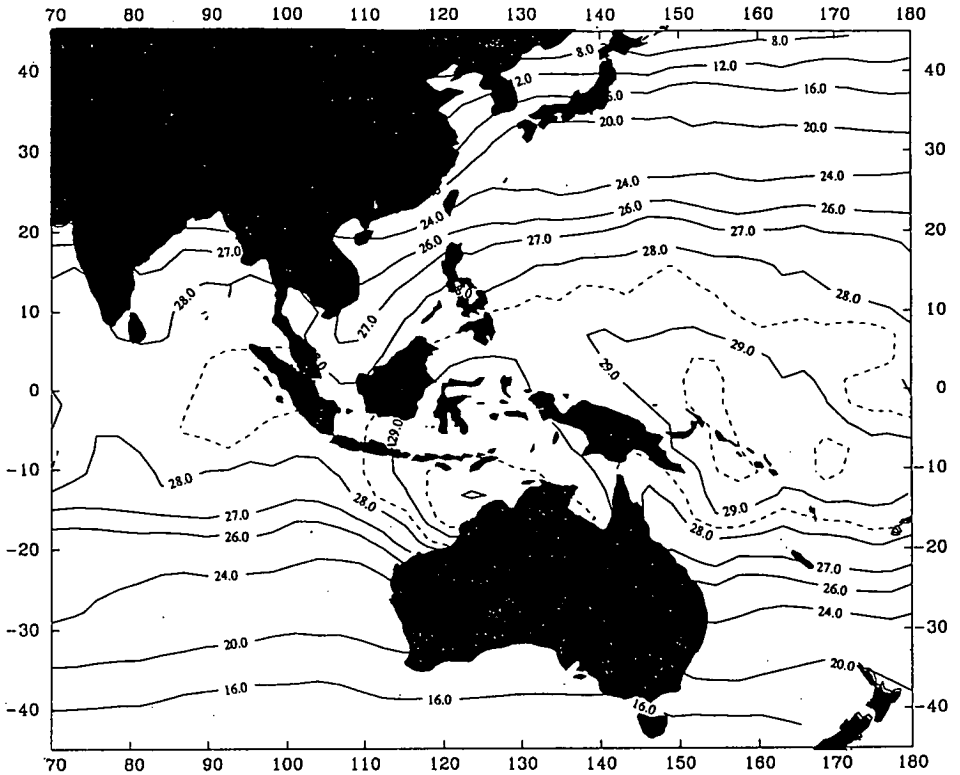

REYNOLDS BLENDED MONTHLY SST (8412)

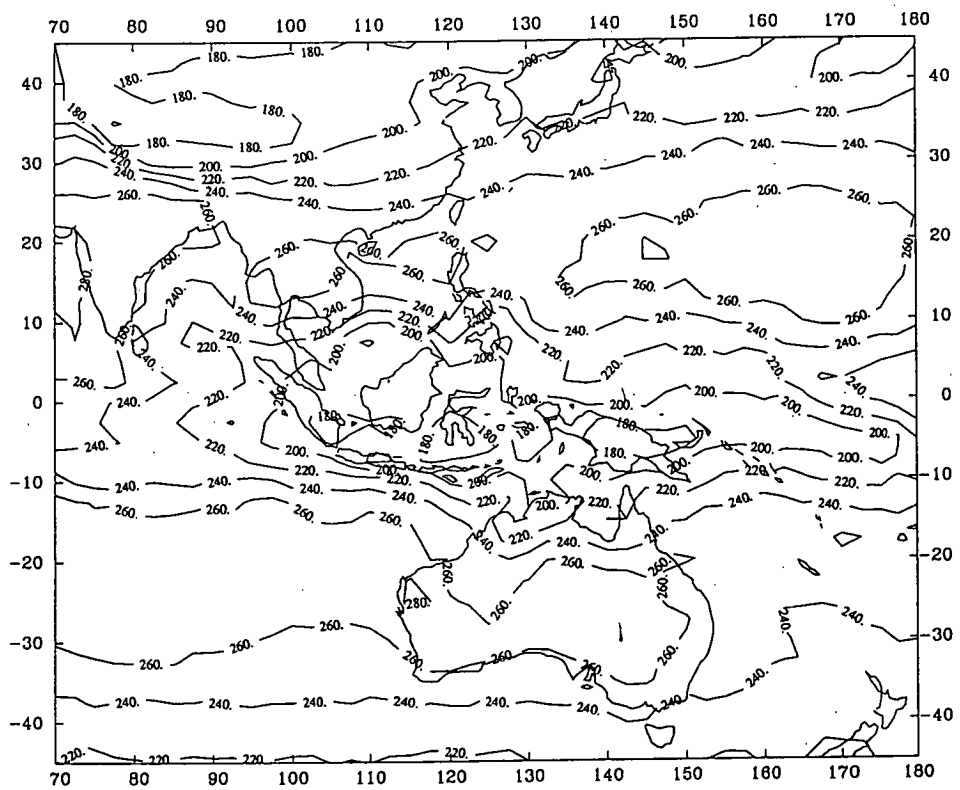

MONTHLY OLR (8412) (UNIT W/M*M)

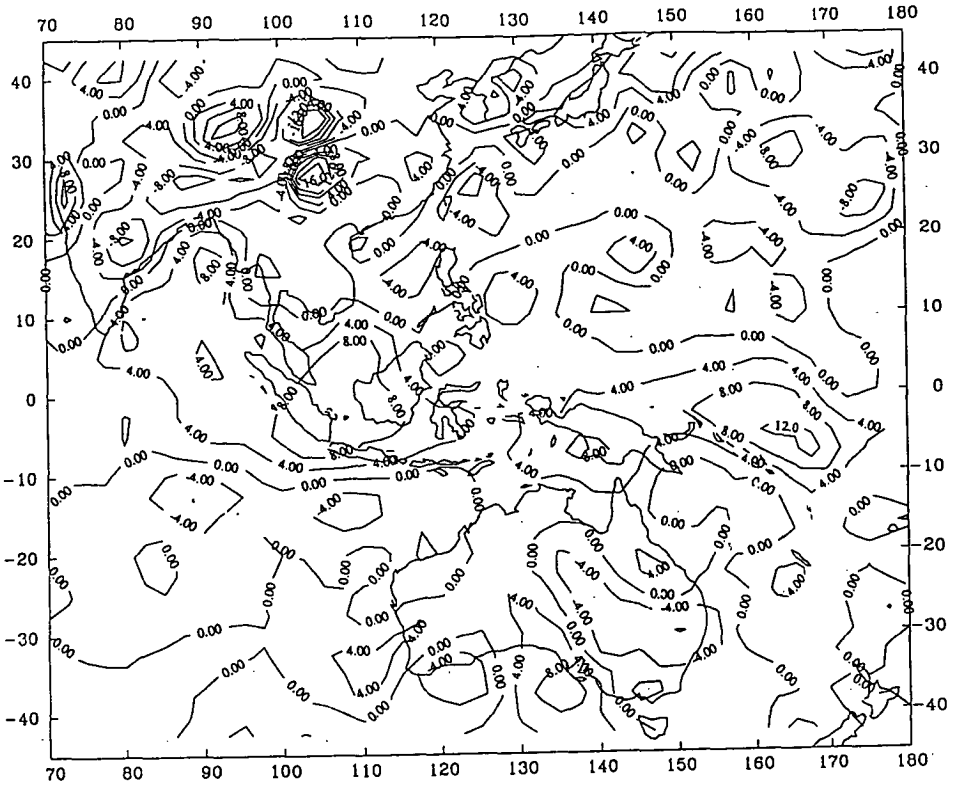

MONTHLY WIND DIVERGENCE AT 200MB (8412)

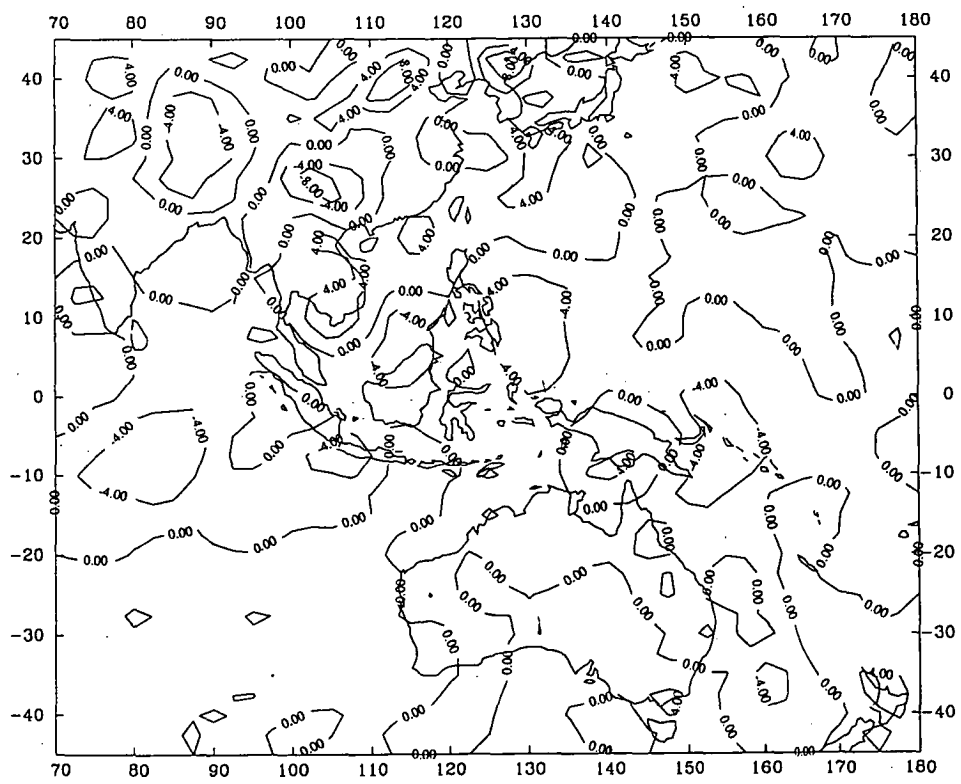

MONTHLY WIND DIVERGENCE AT 850MB (8412)

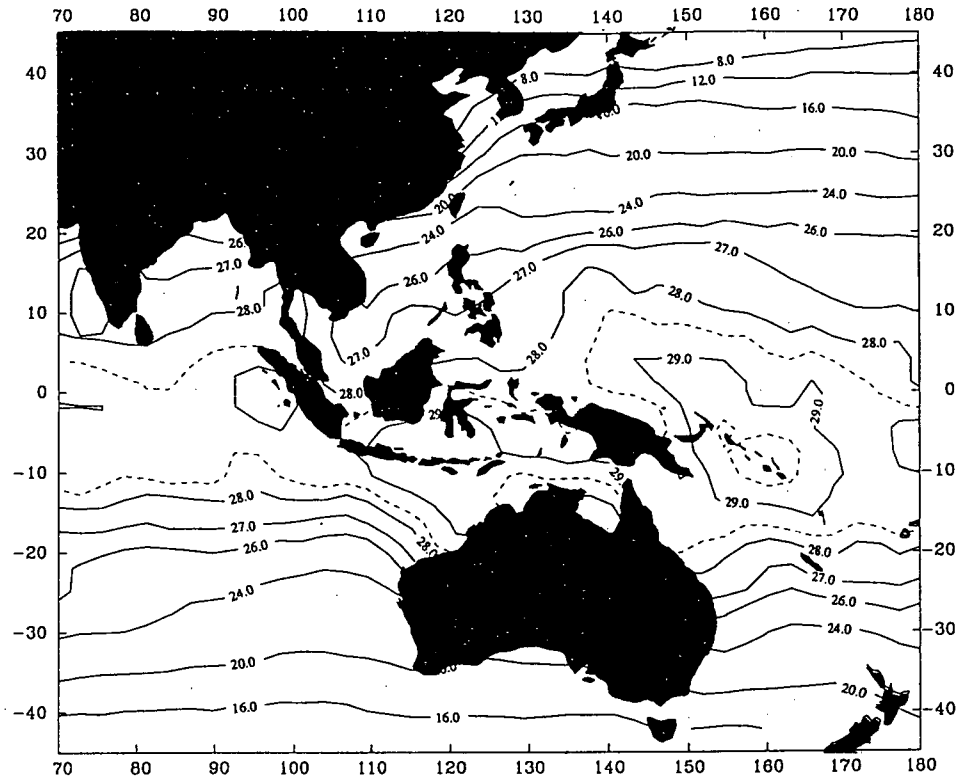

REYNOLDS BLENDED MONTHLY SST (8501)

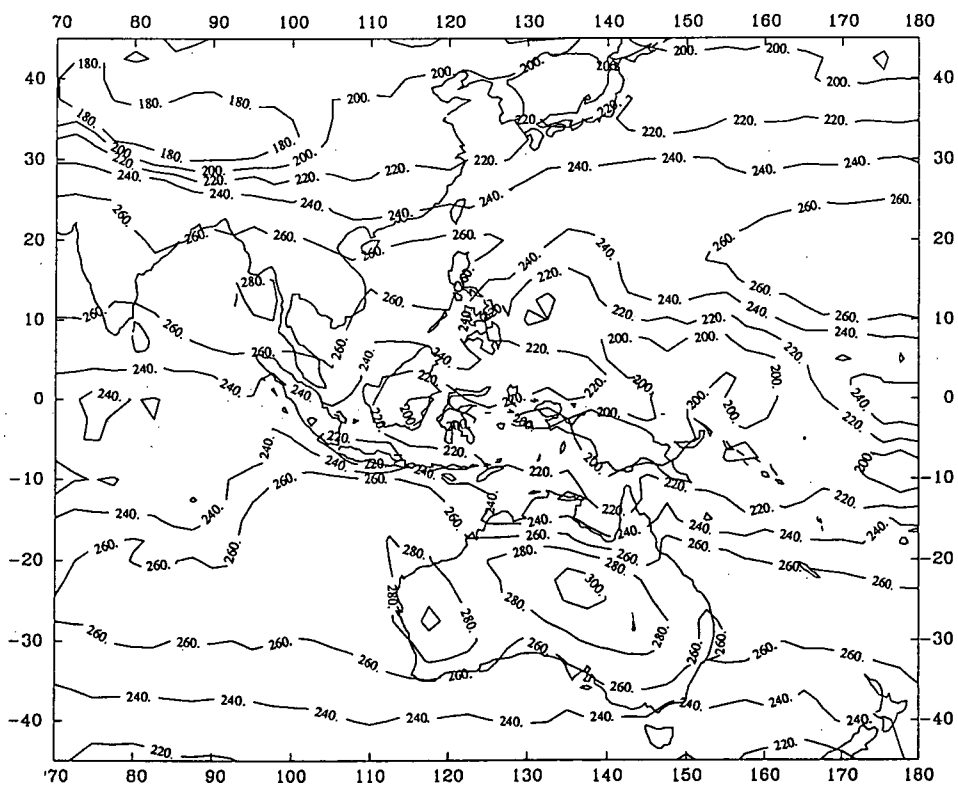

MONTHLY OLR (8501) (UNIT W/M*M)

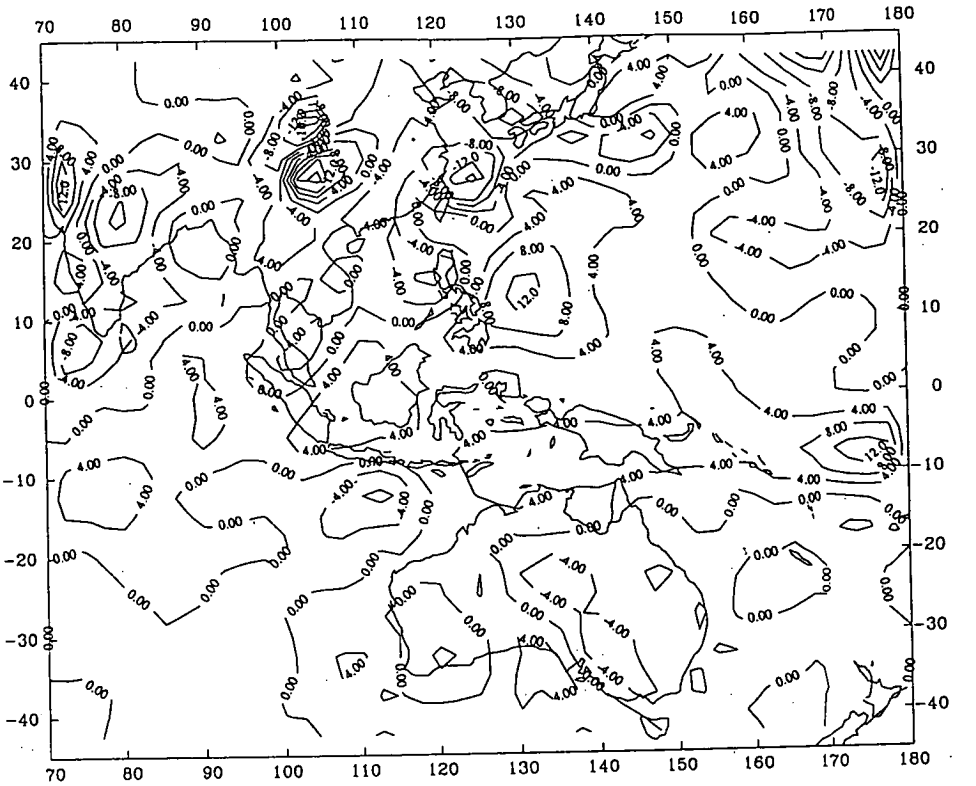

MONTHLY WIND DIVERGENCE AT 200MB (8501)

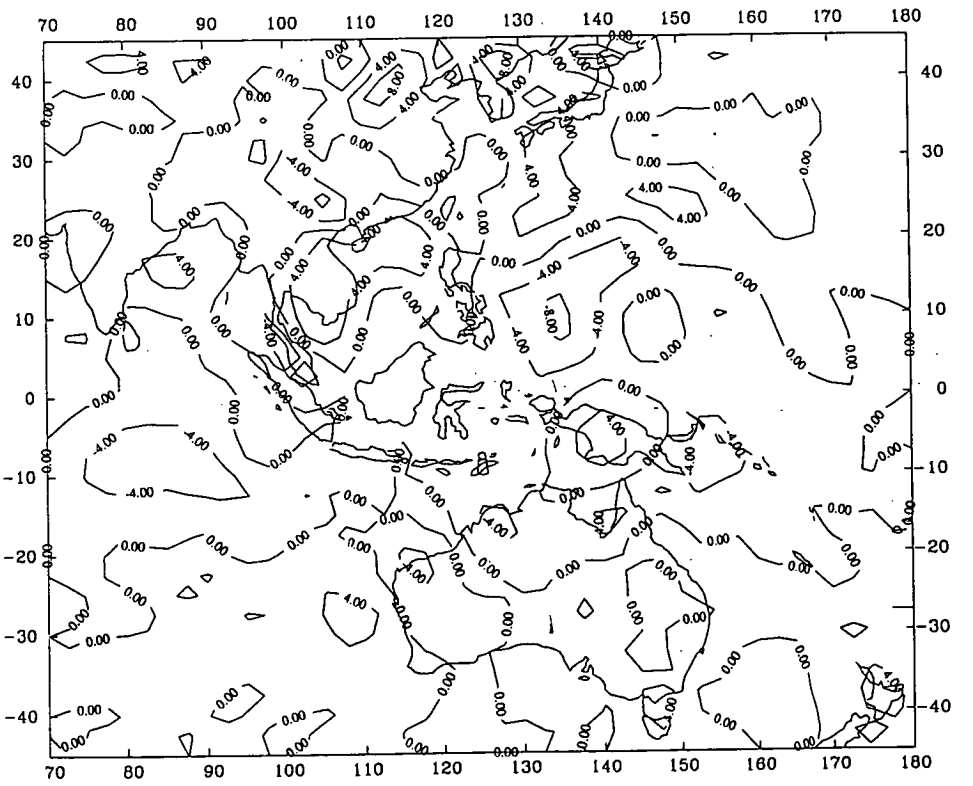

MONTHLY WIND DIVERGENCE AT 850MB (8501)

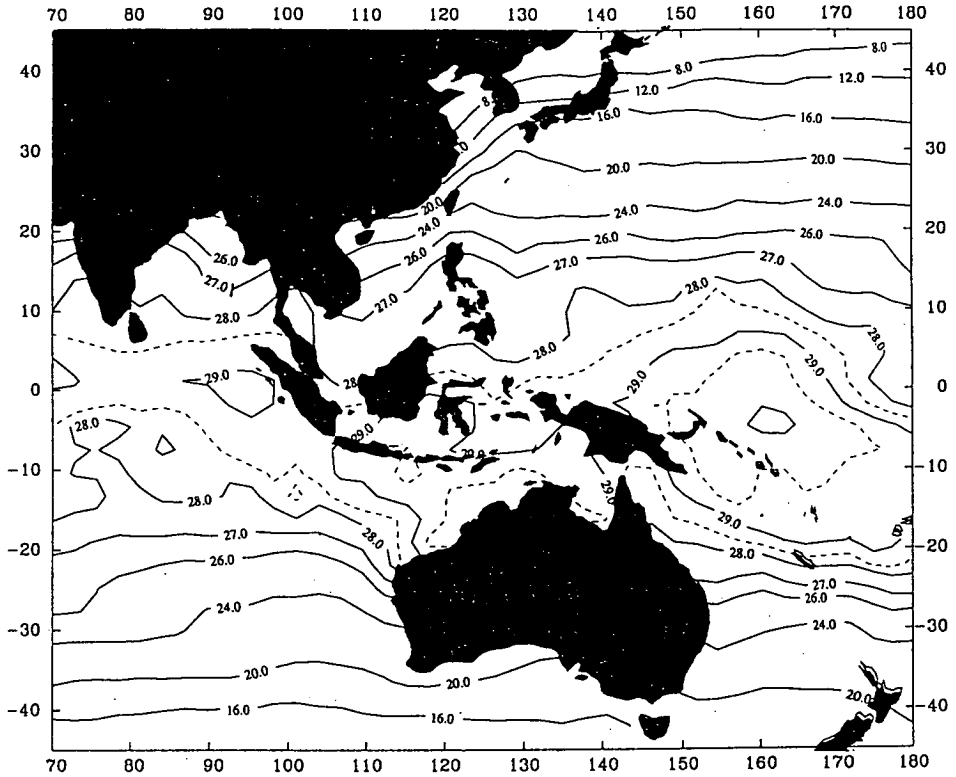

REYNOLDS BLENDED MONTHLY SST (8502)

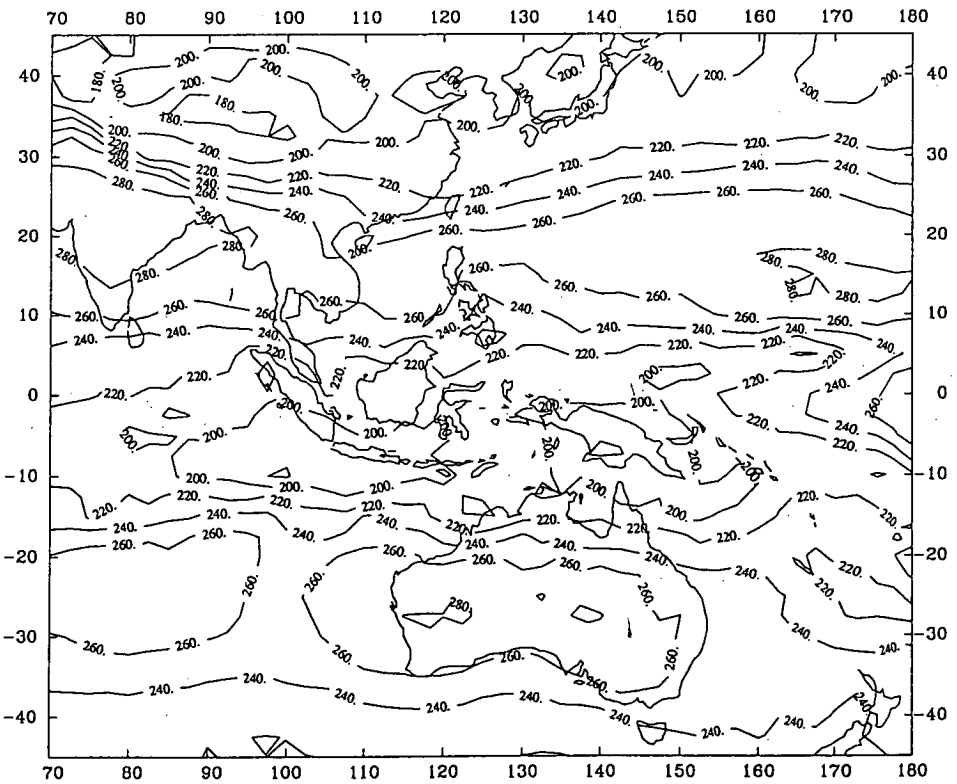

MONTHLY OLR (8502) (UNIT W/M*M)

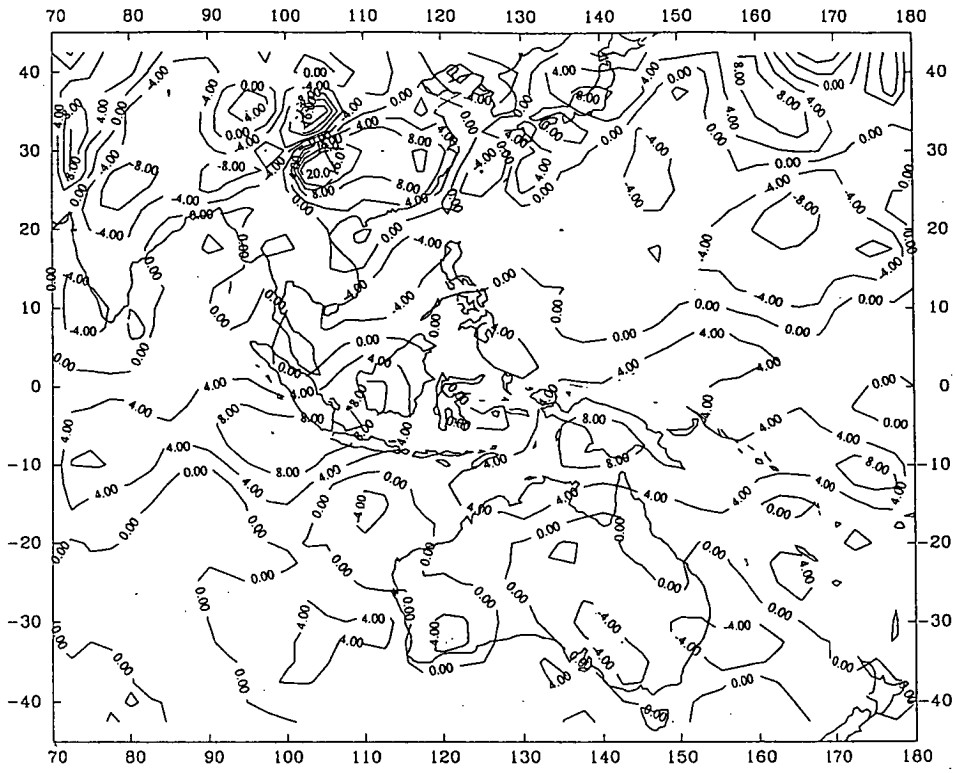

MONTHLY WIND DIVERGENCE AT 200MB (8502)

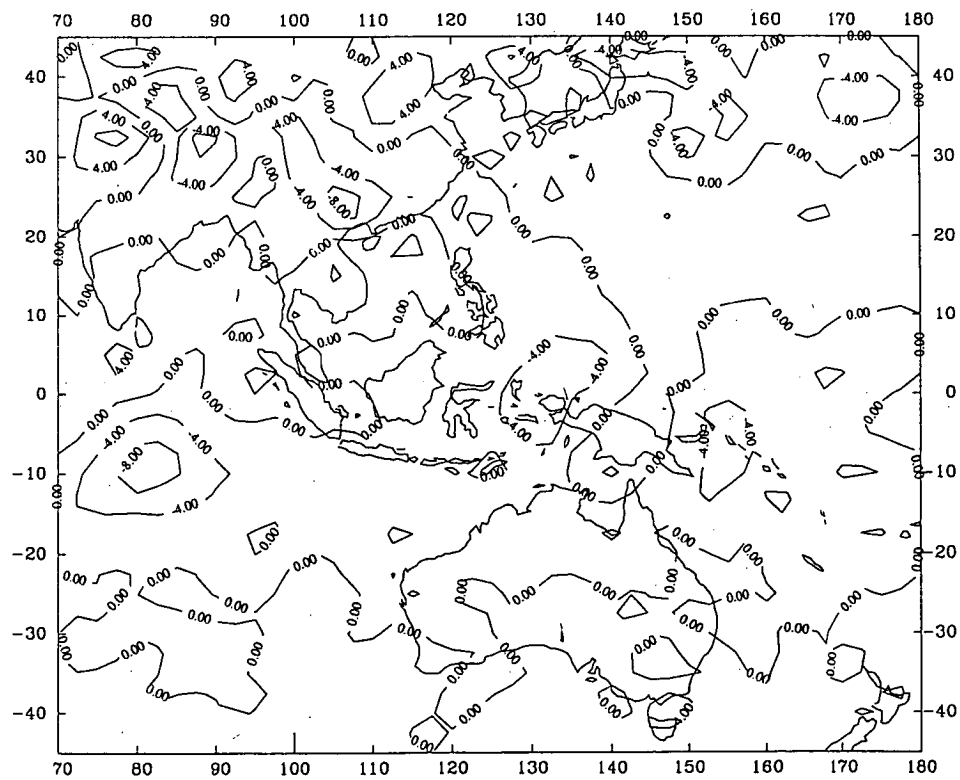

MONTHLY WIND DIVERGENCE AT 850MB (8502)

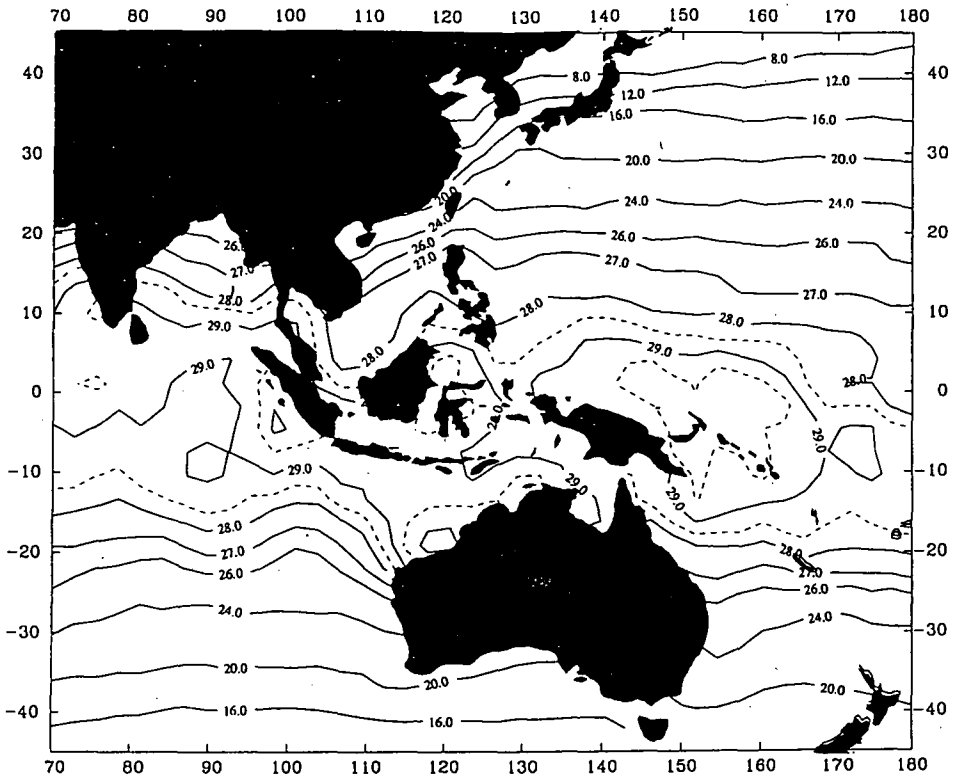

REYNOLDS BLENDED MONTHLY SST (8503)

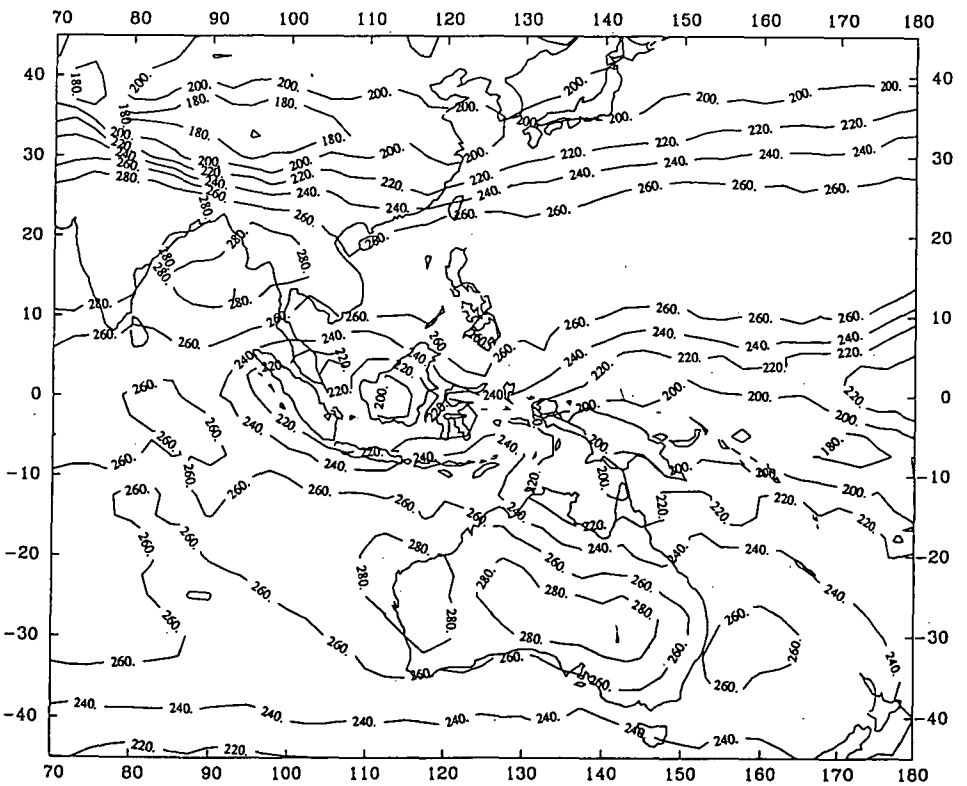

MONTHLY OLR (8503) (UNIT W/M*M)

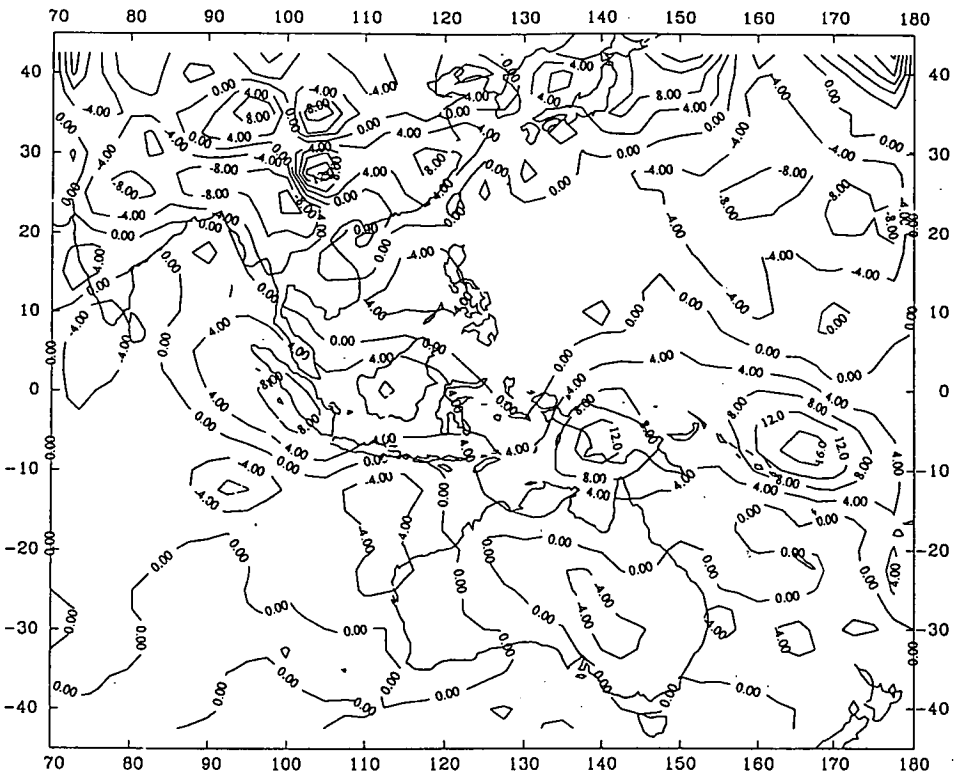

MONTHLY WIND DIVERGENCE AT 200MB (8503)

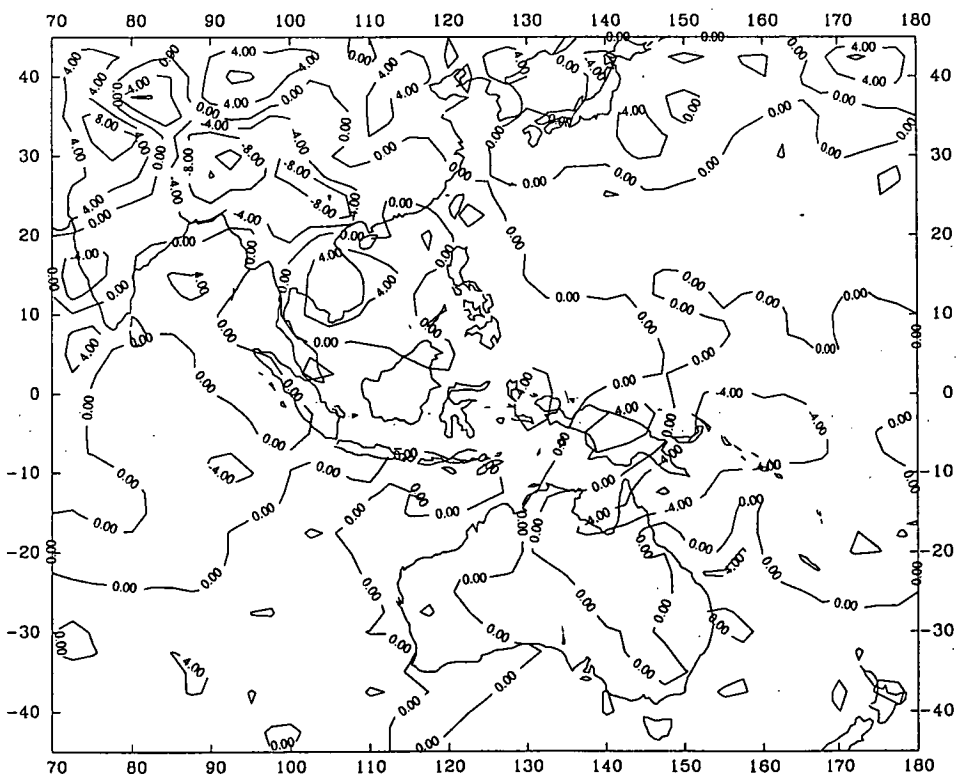

MONTHLY WIND DIVERGENCE AT 850MB (8503)

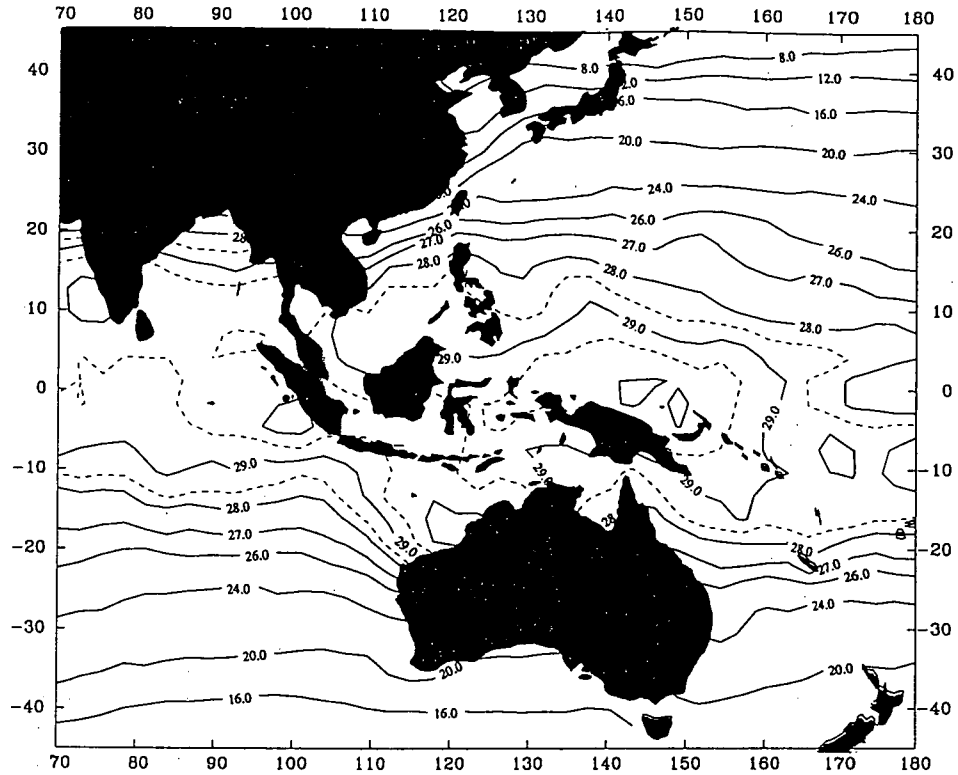

REYNOLDS BLENDED MONTHLY SST (8504)

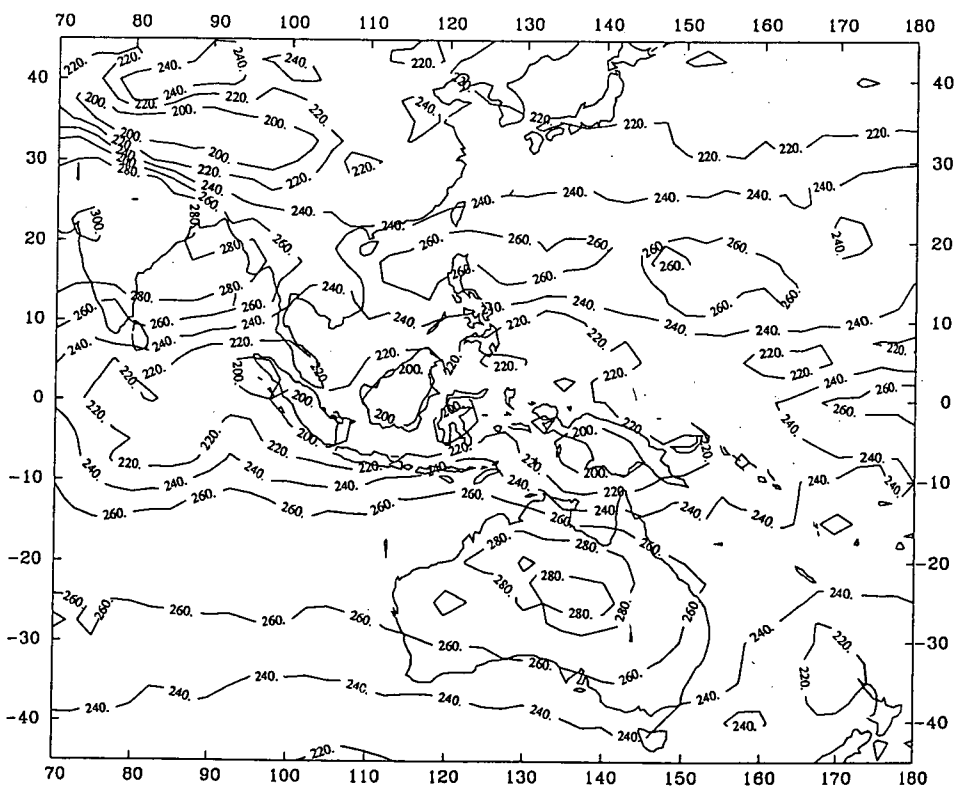

MONTHLY OLR (8504) (UNIT W/M*M)

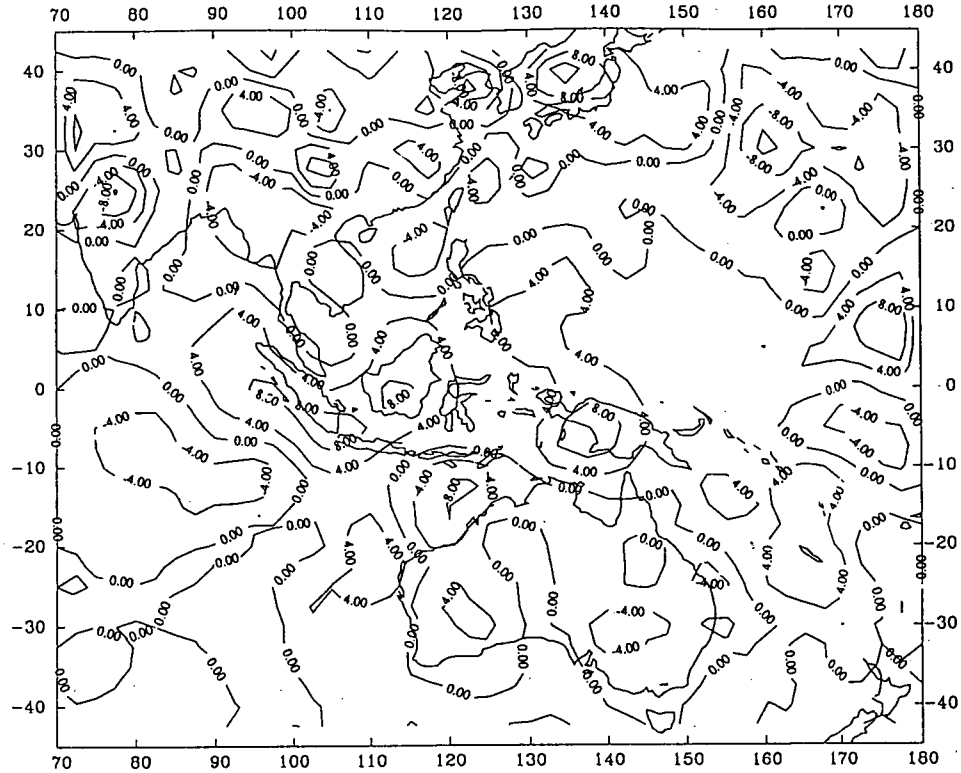

MONTHLY WIND DIVERGENCE AT 200MB (8504)

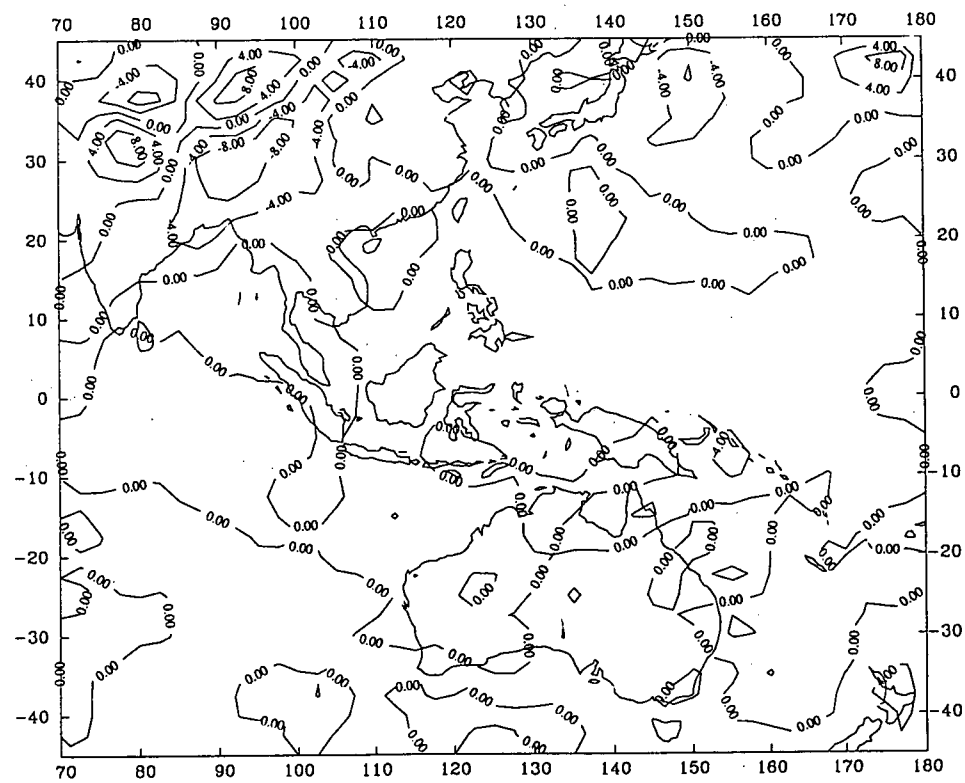

MONTHLY WIND DIVERGENCE AT 850MB (8504)

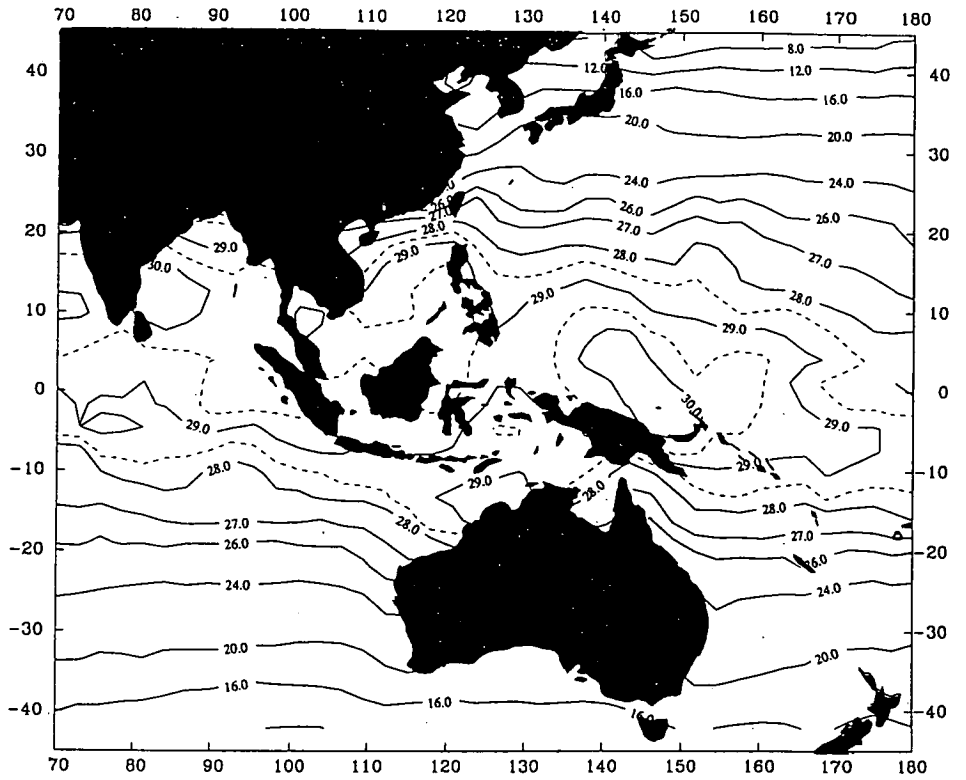

REYNOLDS BLENDED MONTHLY SST (8505)

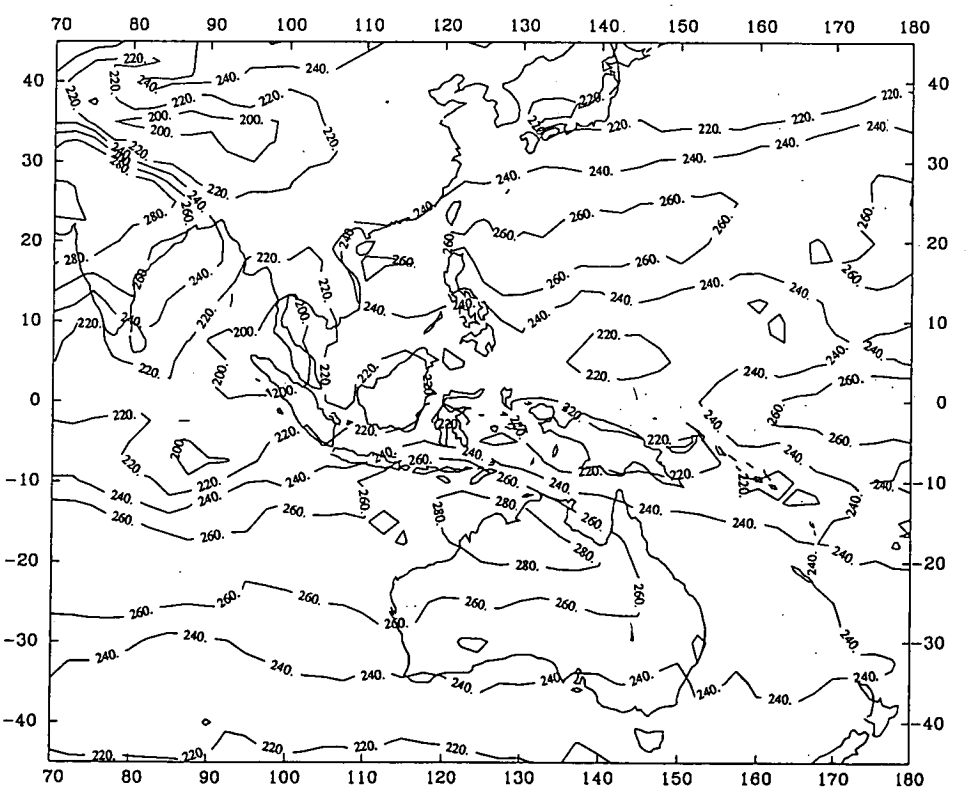

MONTHLY OLR (8505) (UNIT: W/M*M)

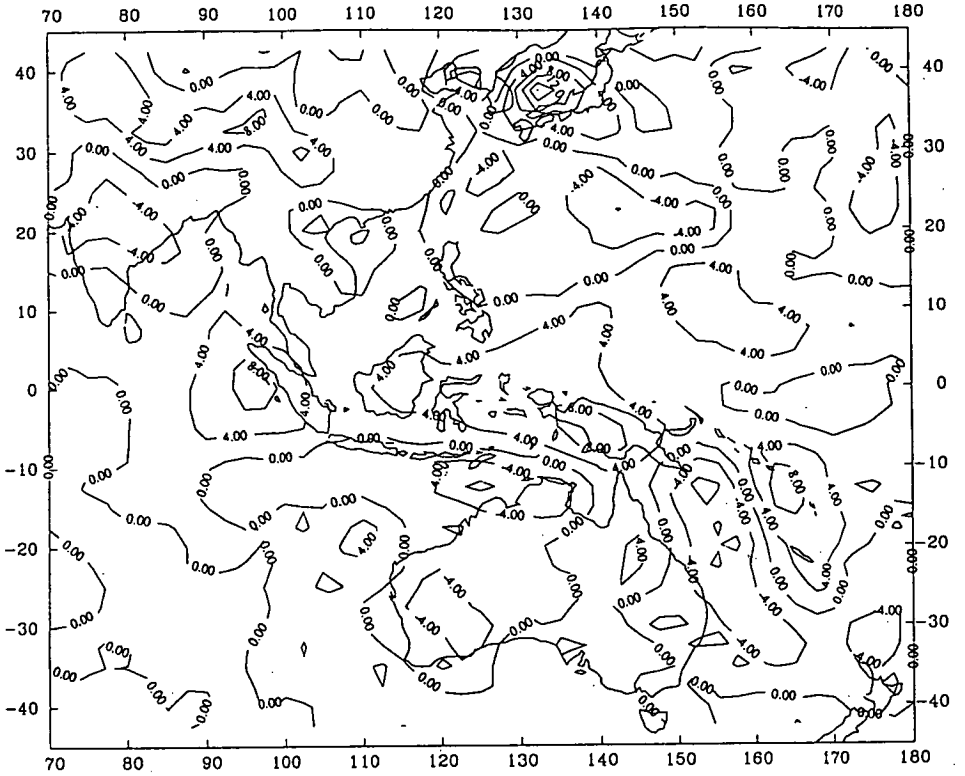

MONTHLY WIND DIVERGENCE AT 200MB (8505)

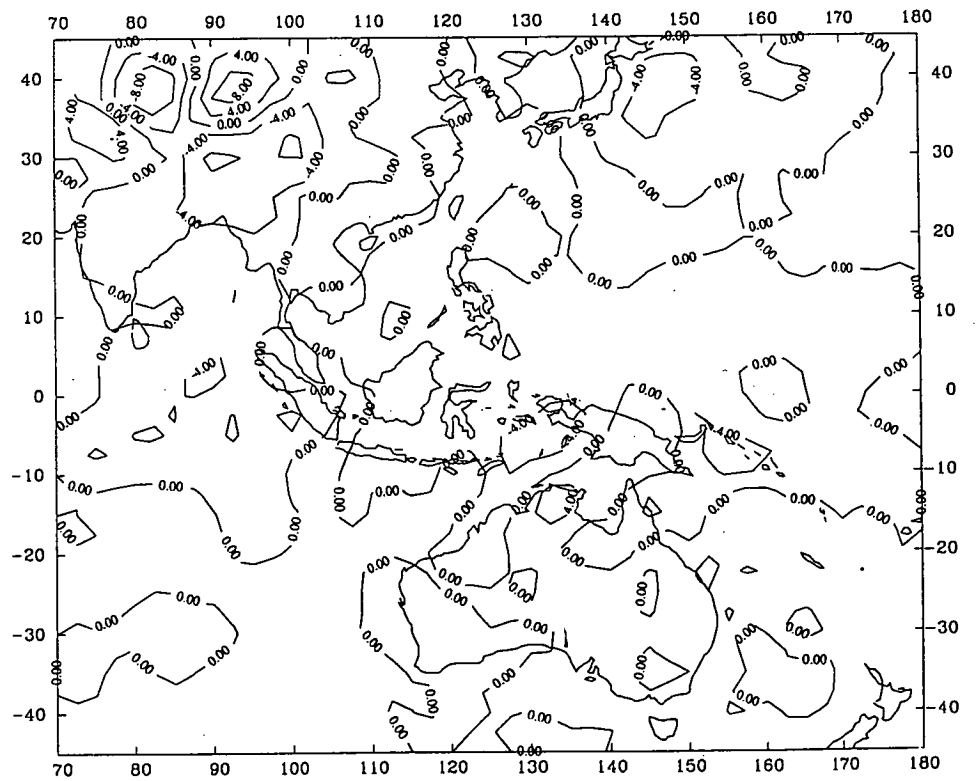

MONTHLY WIND DIVERGENCE AT 850MB (8505)

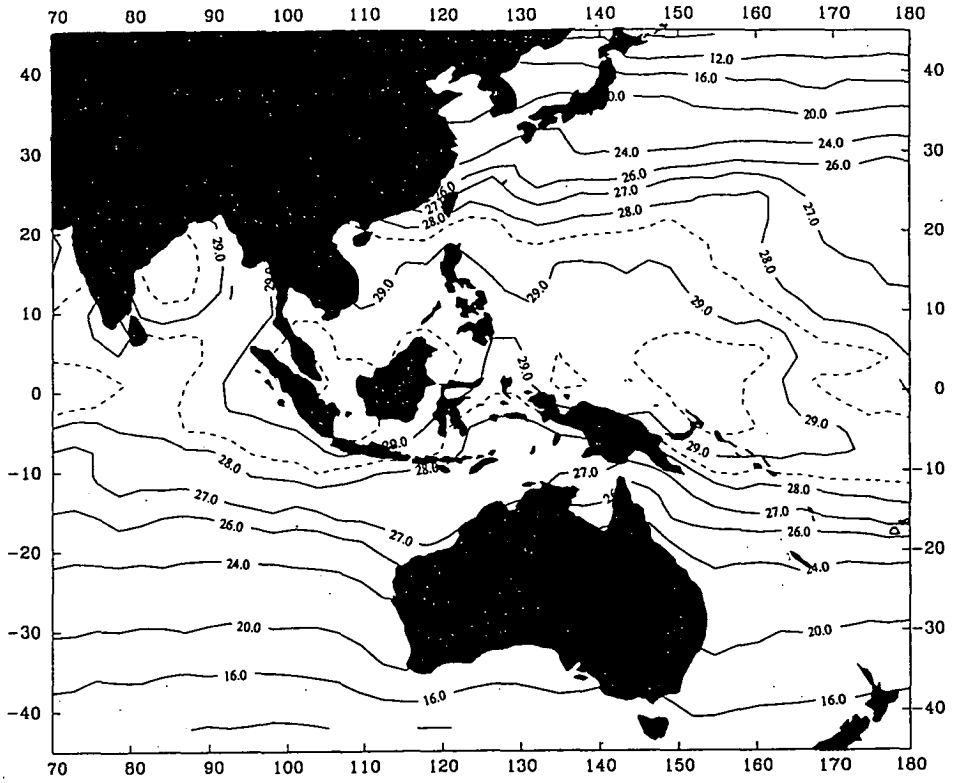

REYNOLDS BLENDED MONTHLY SST (8506)

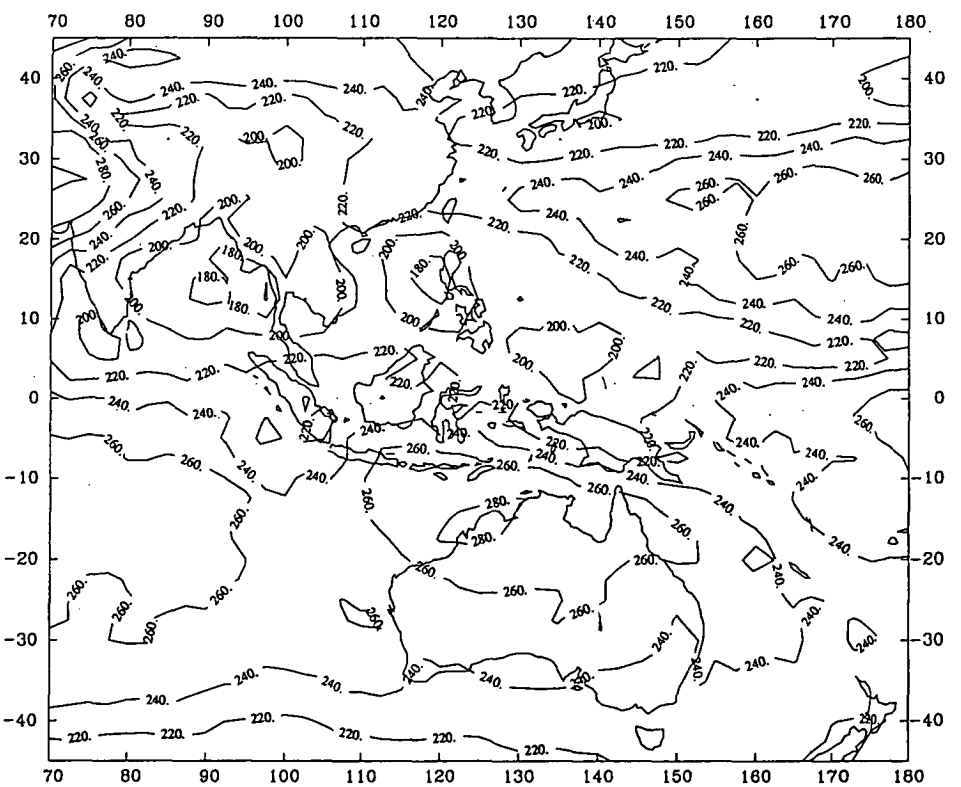

MONTHLY OLR (8506) (UNIT W/M*M)

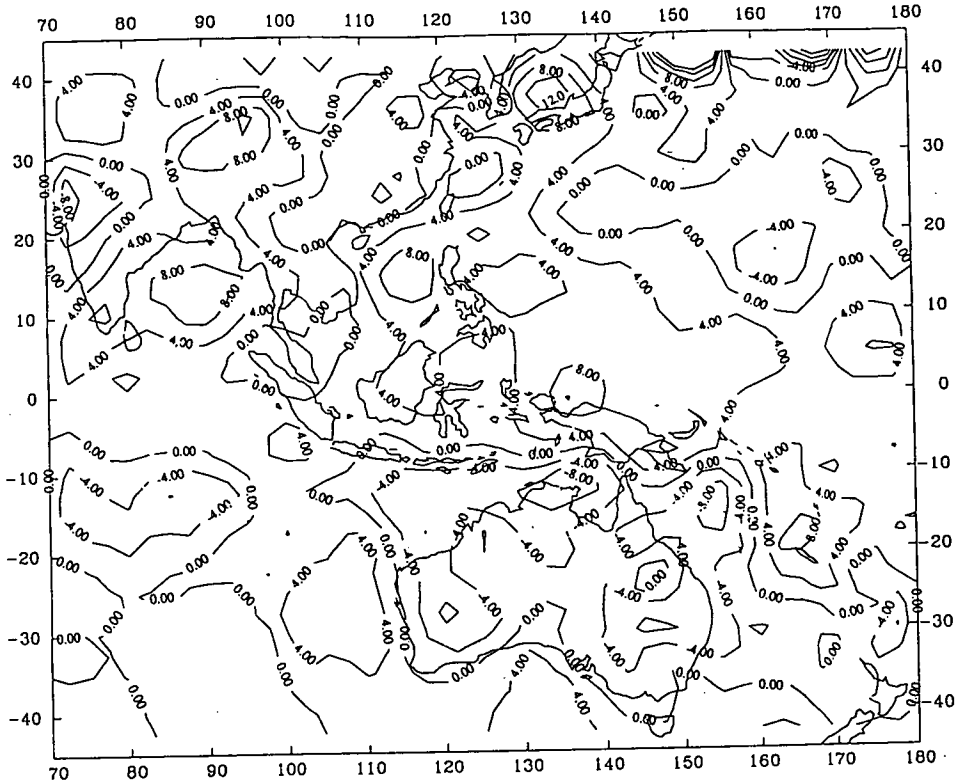

MONTHLY WIND DIVERGENCE AT 200MB (8506)

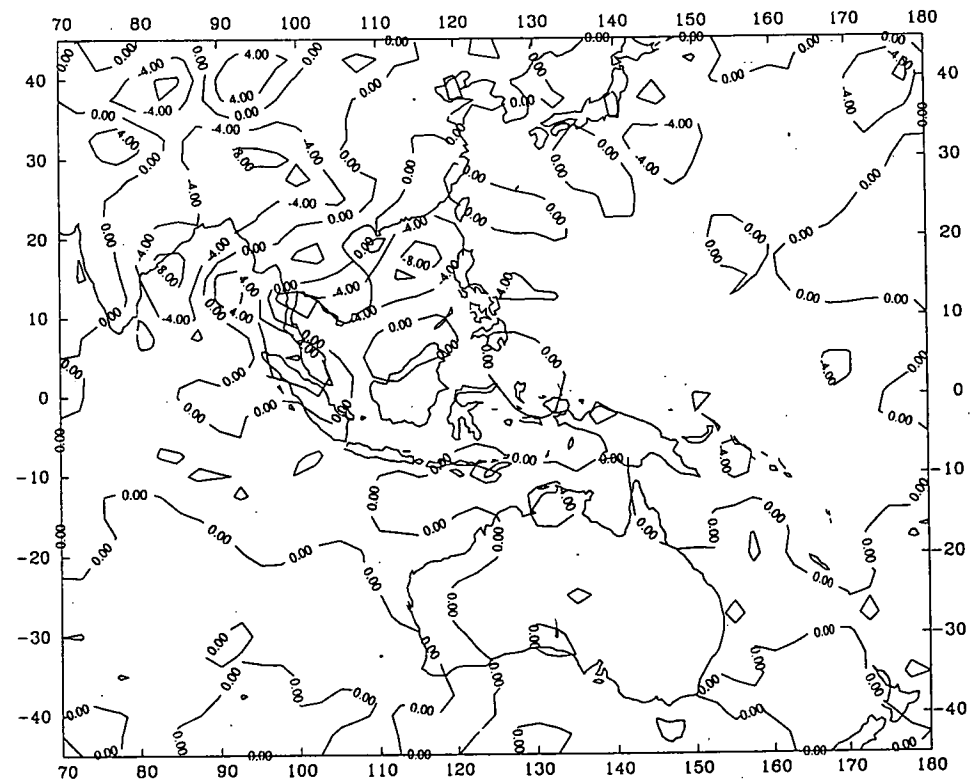

MONTHLY WIND DIVERGENCE AT 850MB (8506)

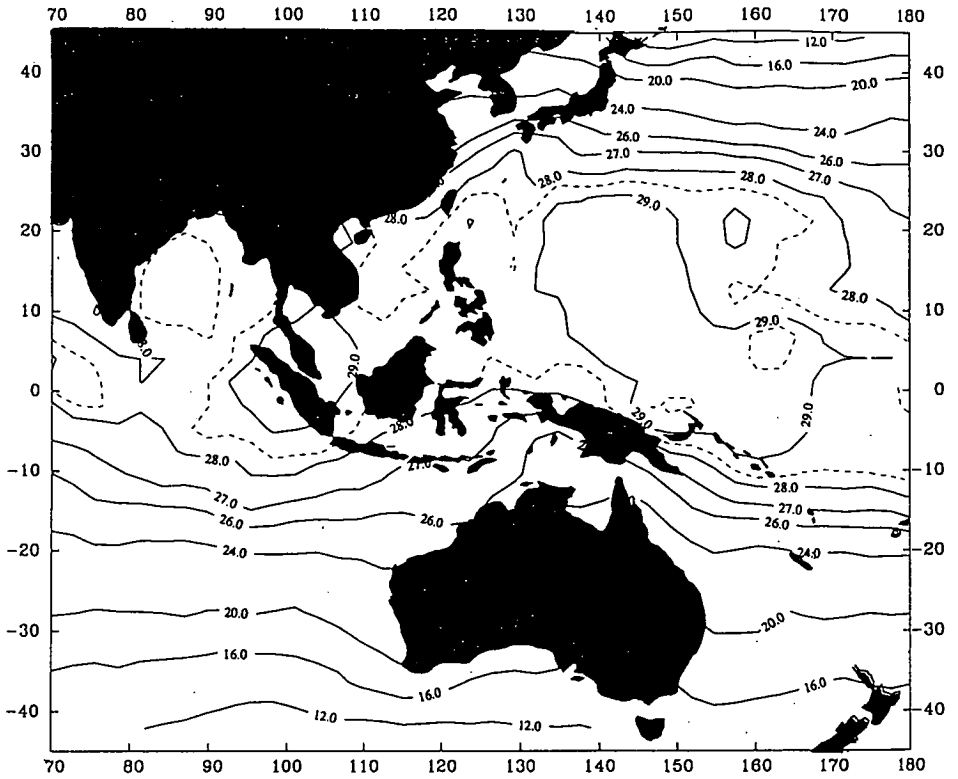

REYNOLDS BLENDED MONTHLY SST (8507)

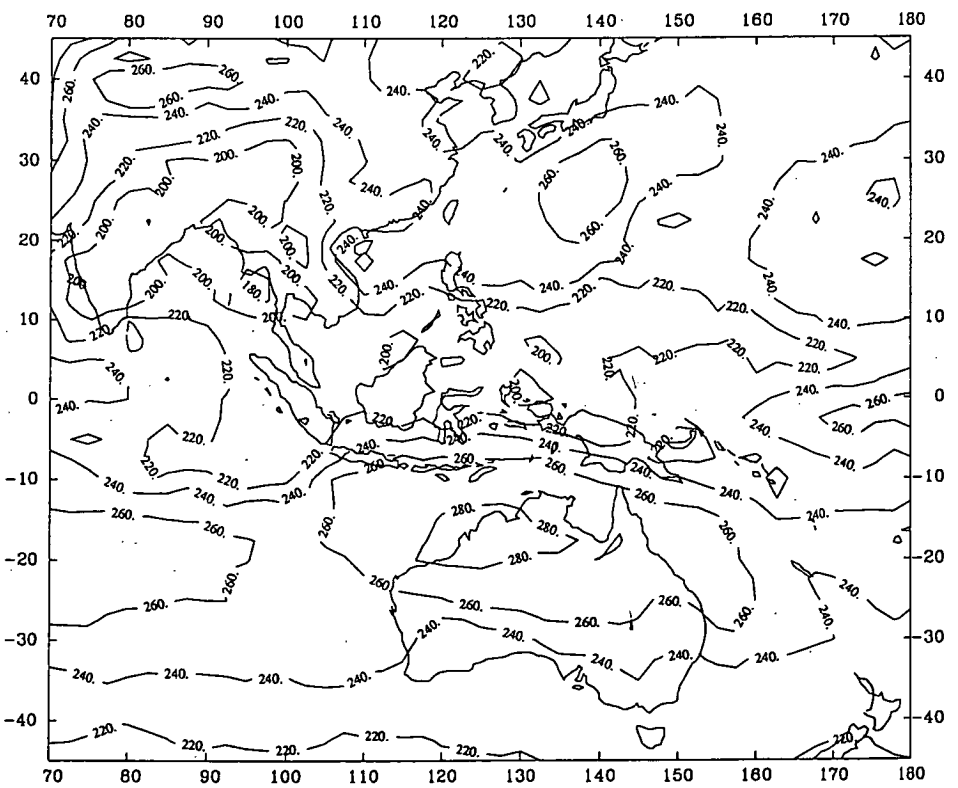

MONTHLY OLR (8507) (UNIT W/M*M)

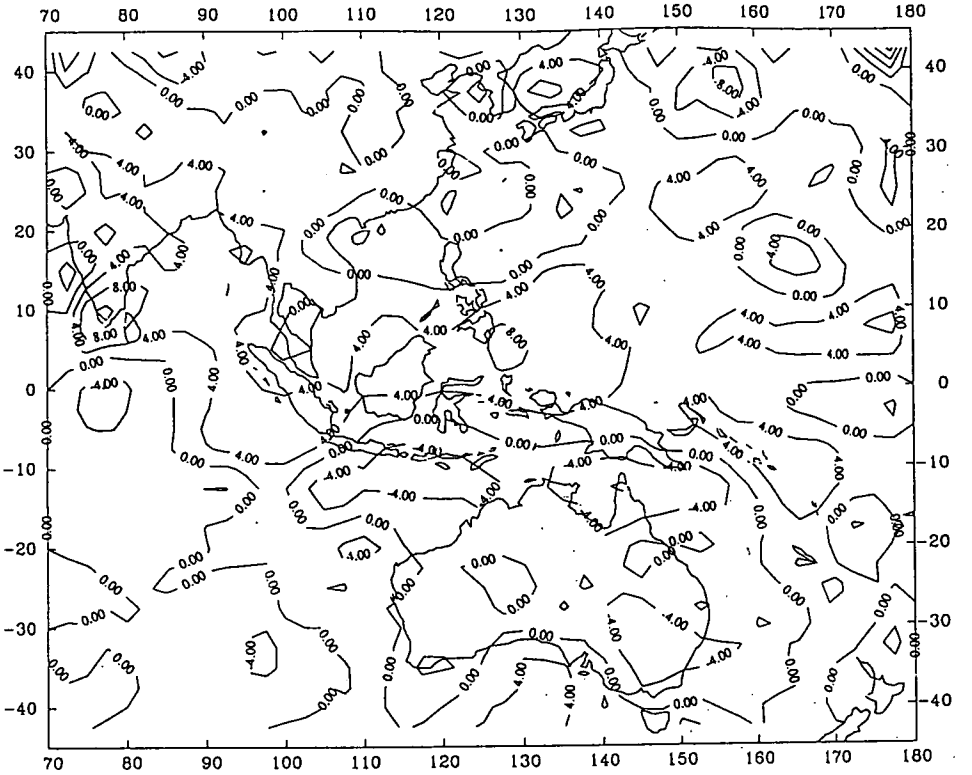

MONTHLY WIND DIVERGENCE AT 200MB (8507)

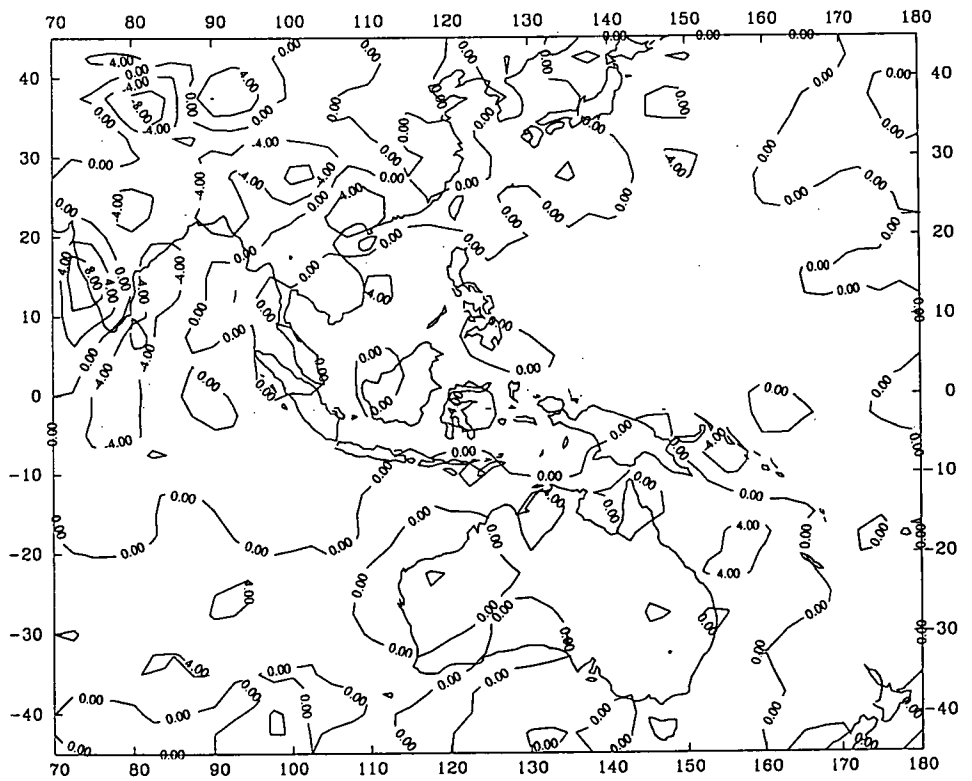

MONTHLY WIND DIVERGENCE AT 850MB (8507)

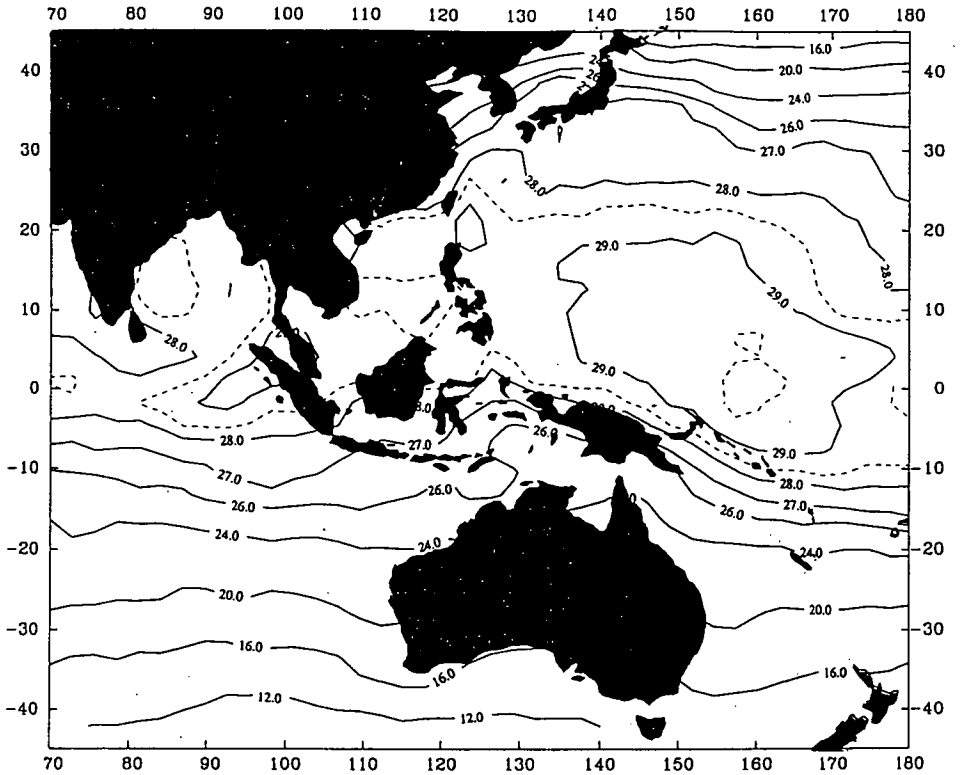

REYNOLDS BLENDED MONTHLY SST (8508)

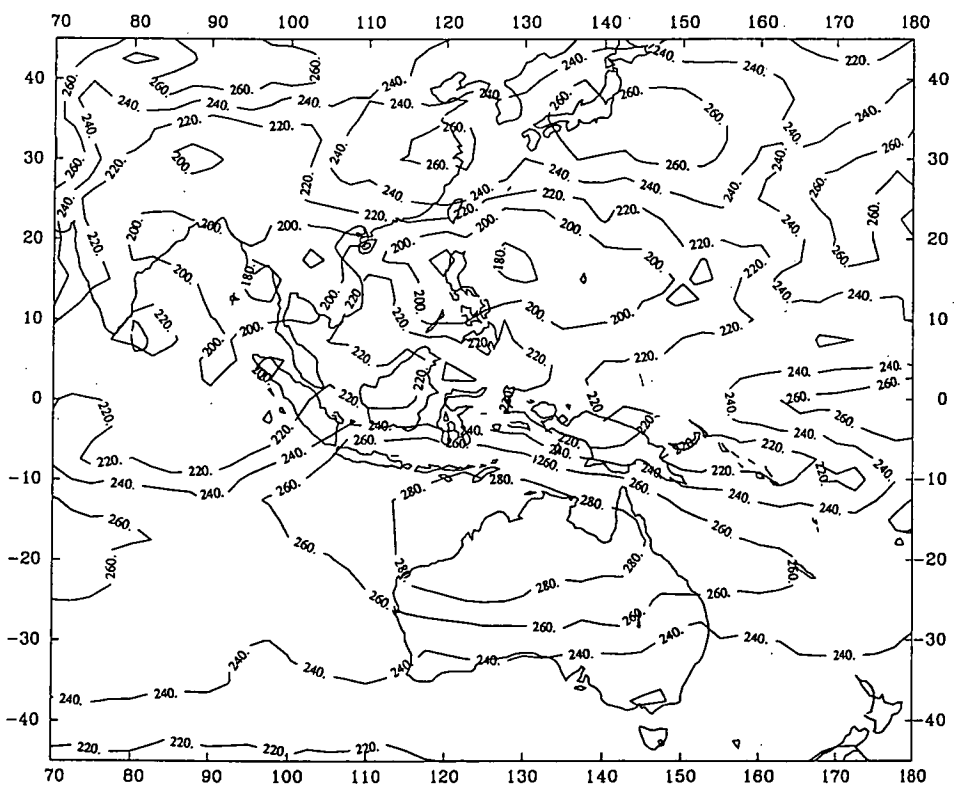

MONTHLY OLR (8508) (UNIT W/M*M)

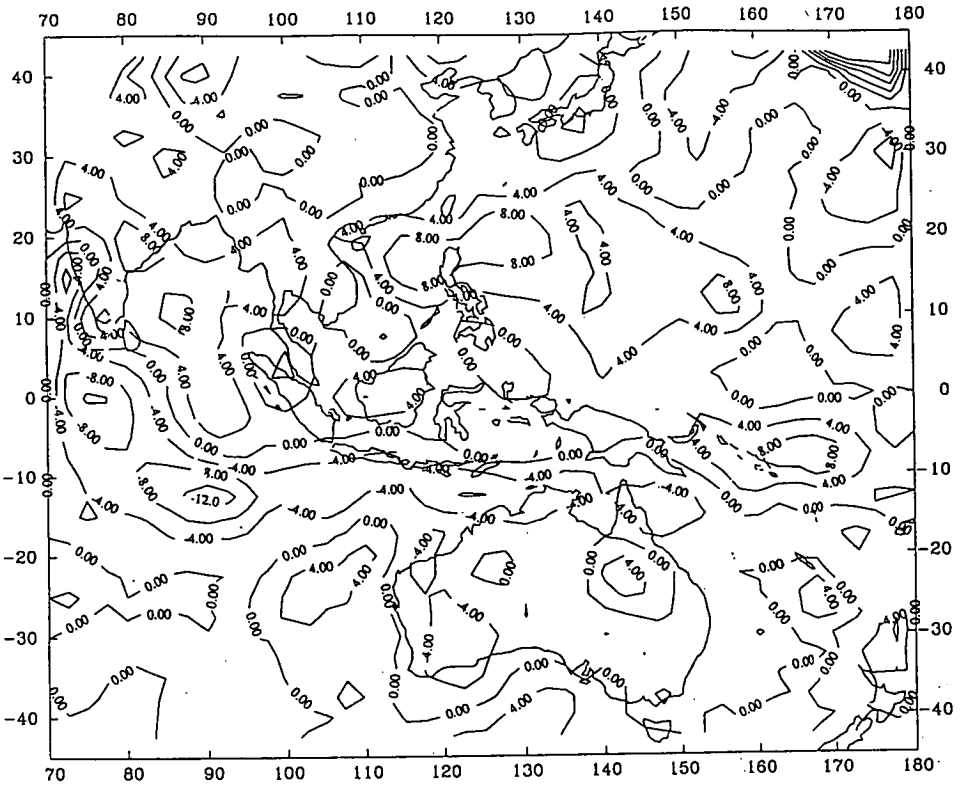

MONTHLY WIND DIVERGENCE AT 200MB (8508)

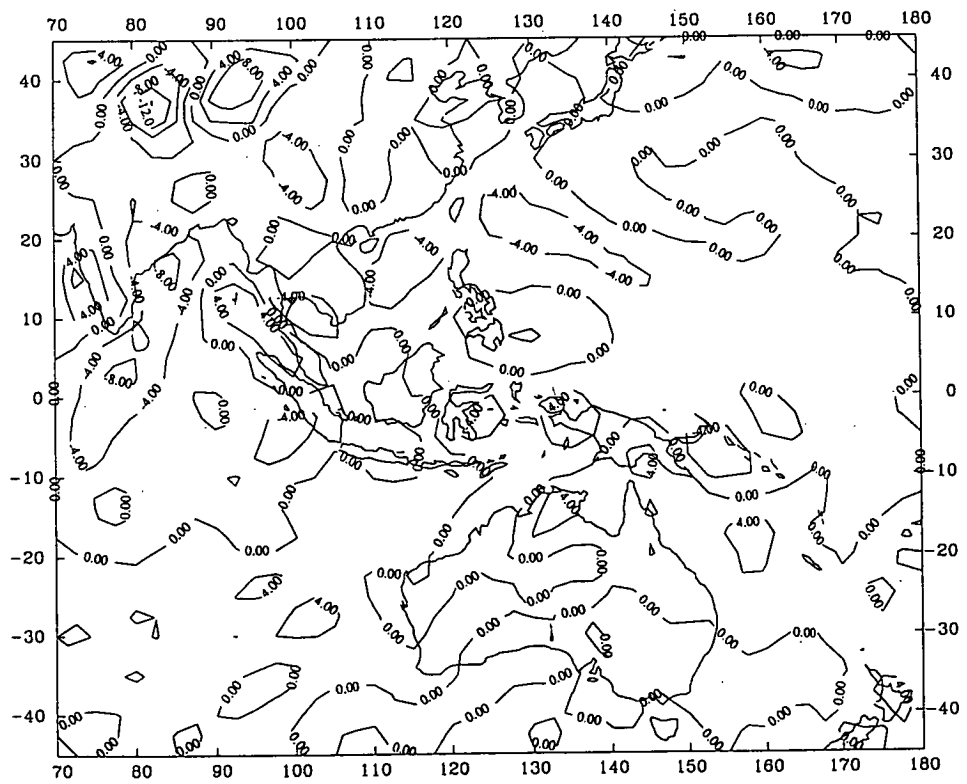

MONTHLY WIND DIVERGENCE AT 850MB (8508)

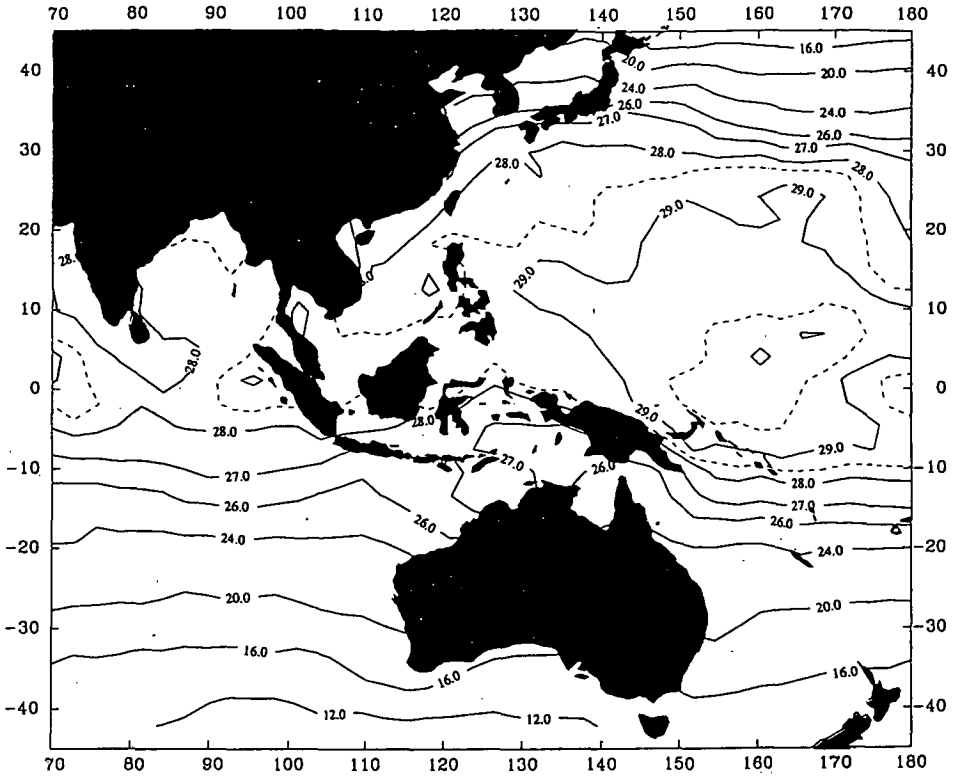

REYNOLDS BLENDED MONTHLY SST (8509)

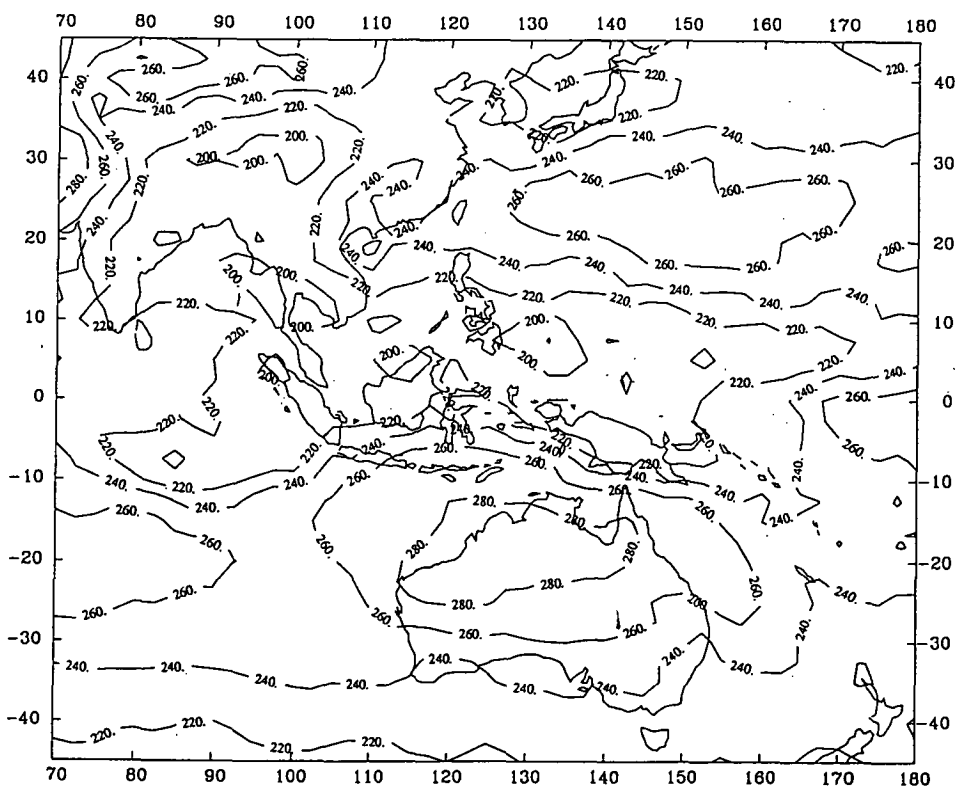

MONTHLY OLR (8509) (UNIT W/M*M)

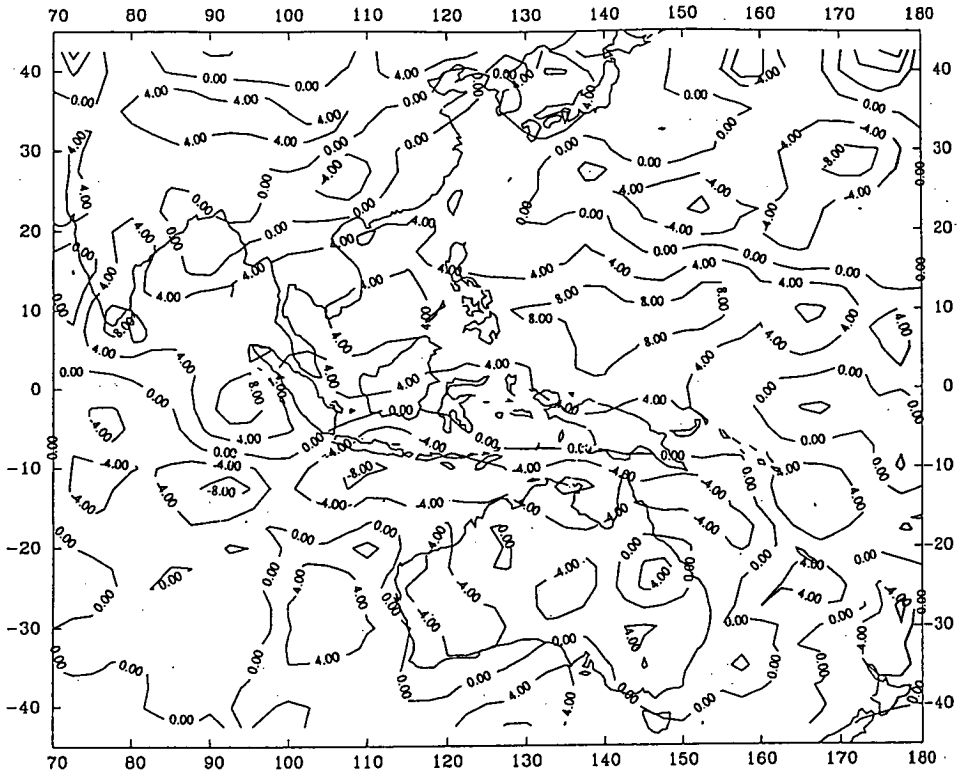

MONTHLY WIND DIVERGENCE AT 200MB (8509)

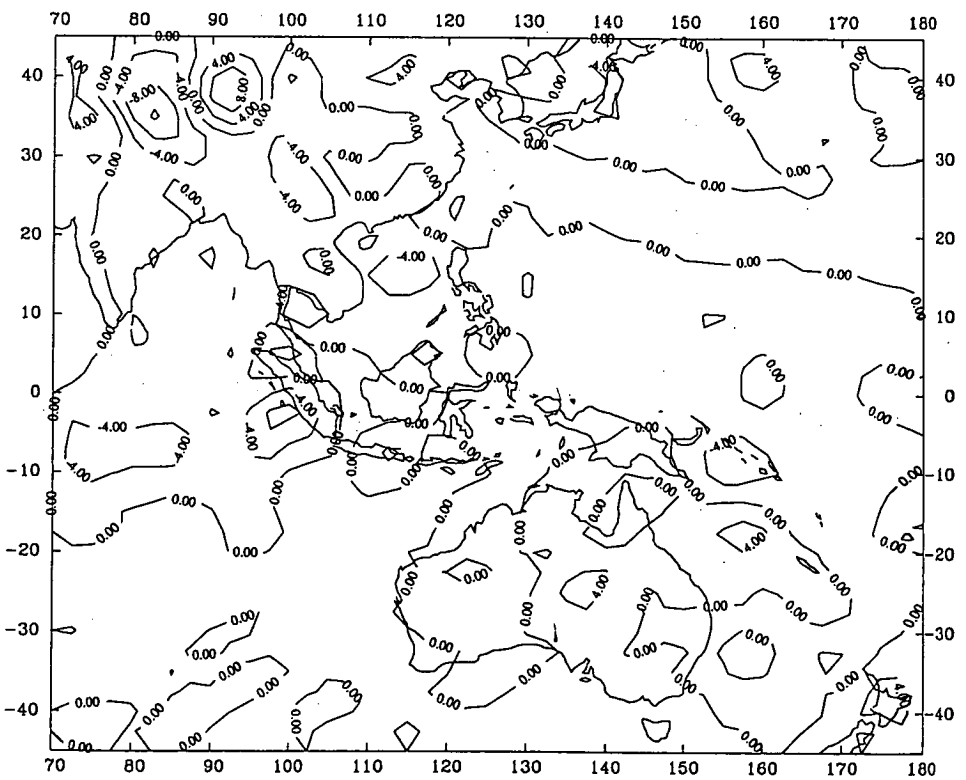

MONTHLY WIND DIVERGENCE AT 850MB (8509)

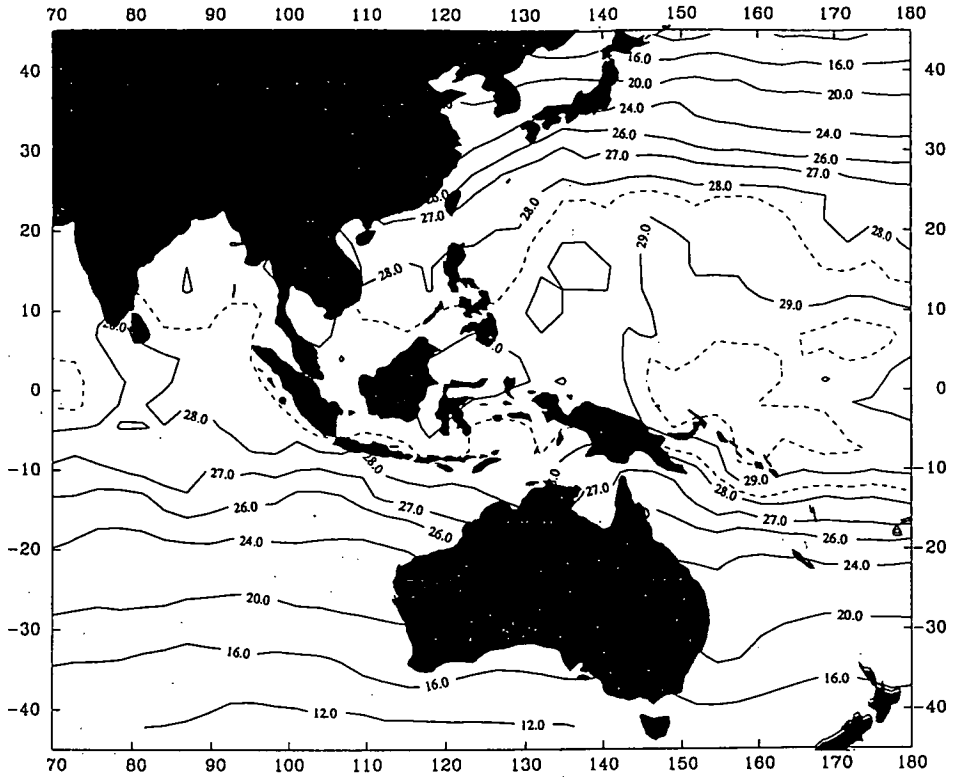

REYNOLDS BLENDED MONTHLY SST (8510)

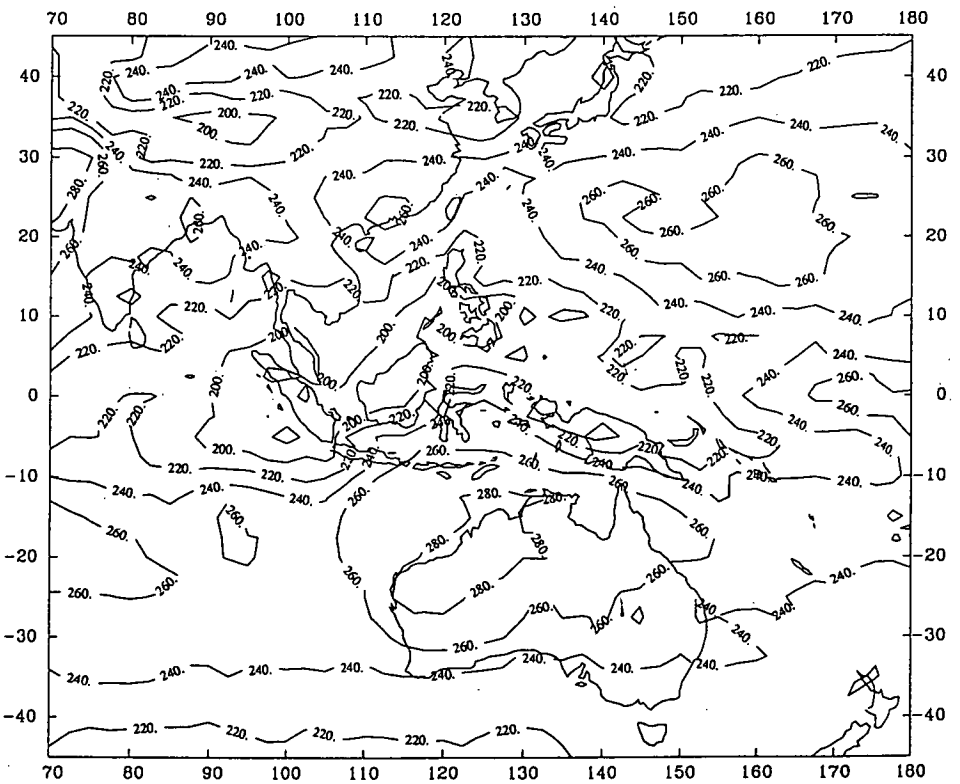

MONTHLY OLR (8510) (UNIT W/M*M)

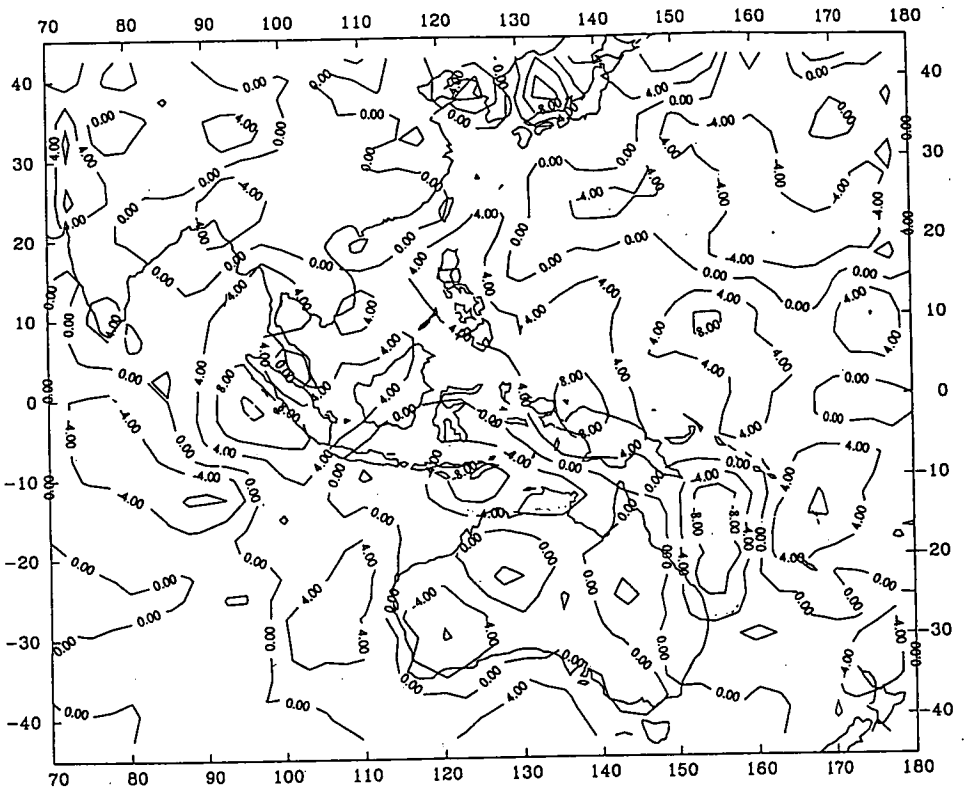

MONTHLY WIND DIVERGENCE AT 200MB (8510)

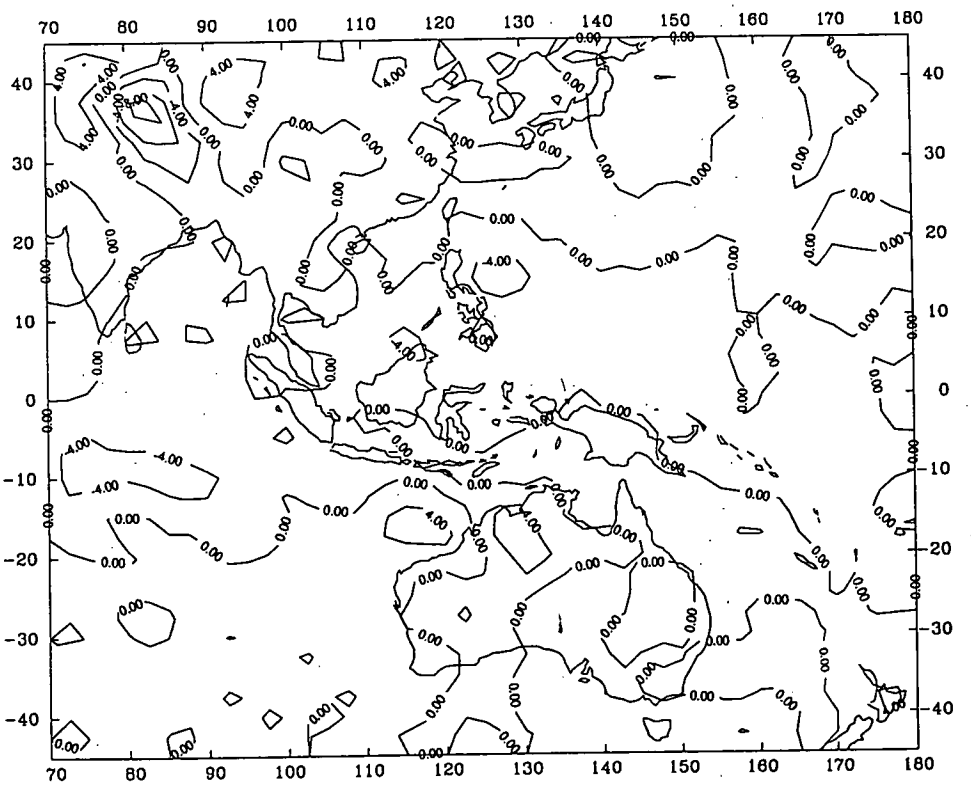

MONTHLY WIND DIVERGENCE AT 850MB (8510)

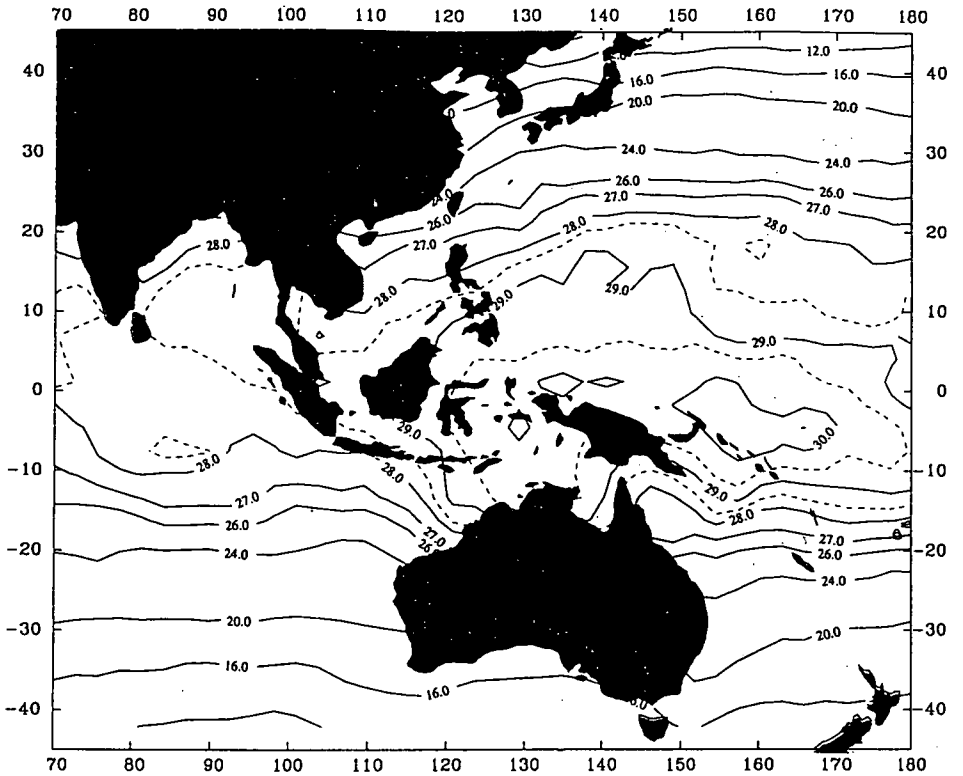

REYNOLDS BLENDED MONTHLY SST (8511)

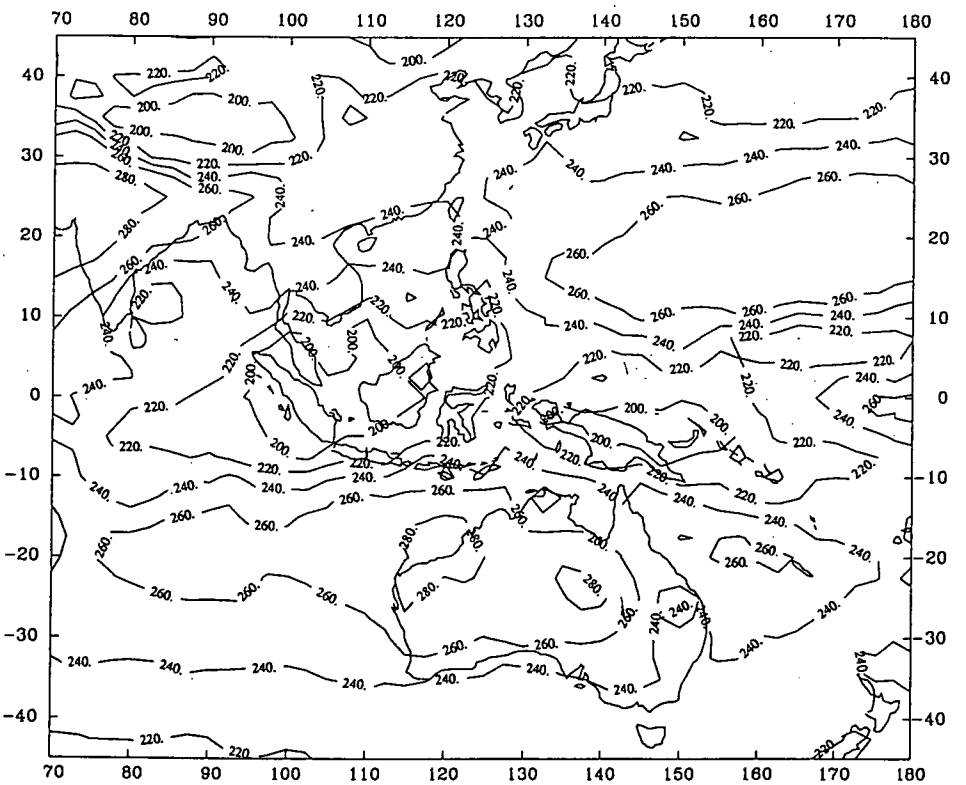

MONTHLY OLR (8511) (UNIT W/M*M)

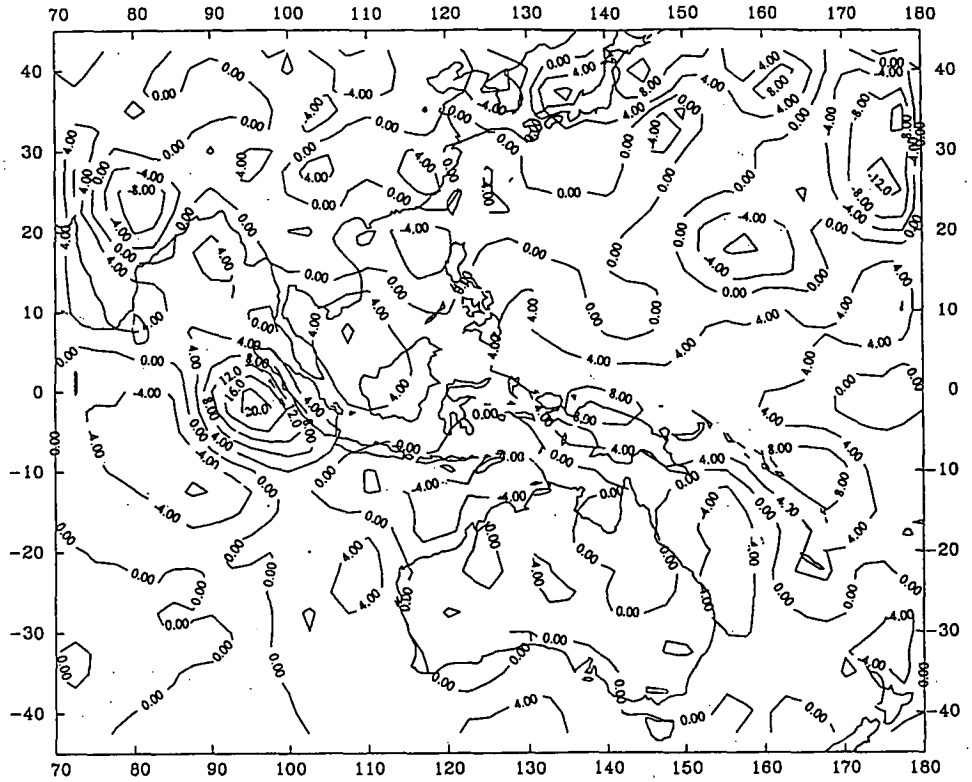

MONTHLY WIND DIVERGENCE AT 200MB (8511)

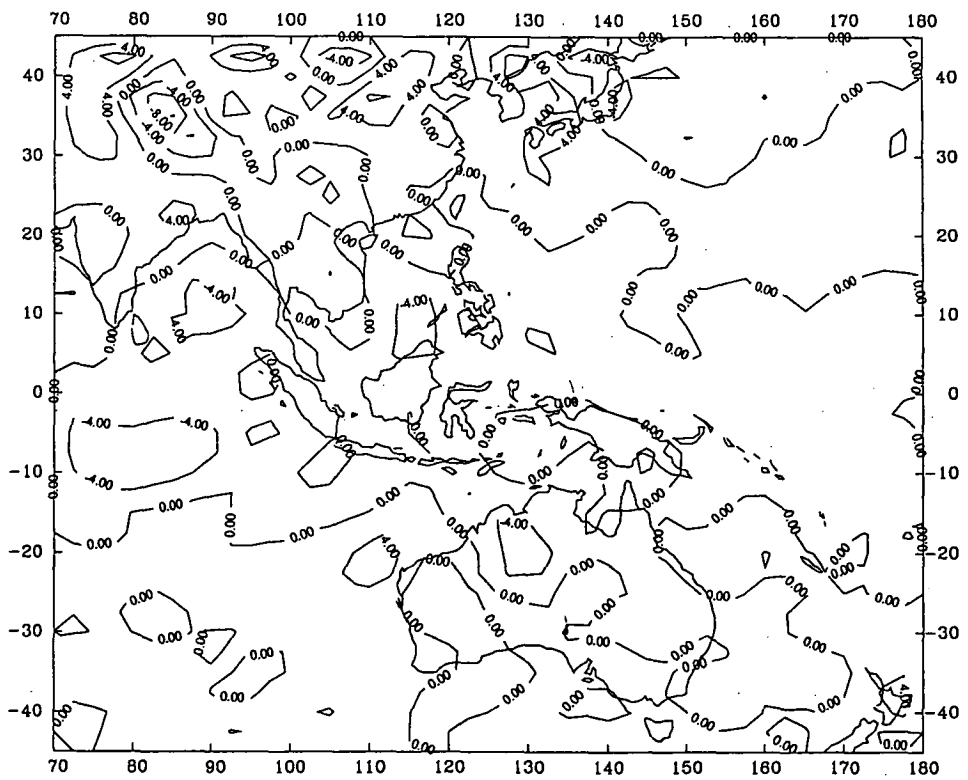

MONTHLY WIND DIVERGENCE AT 850MB (8511)

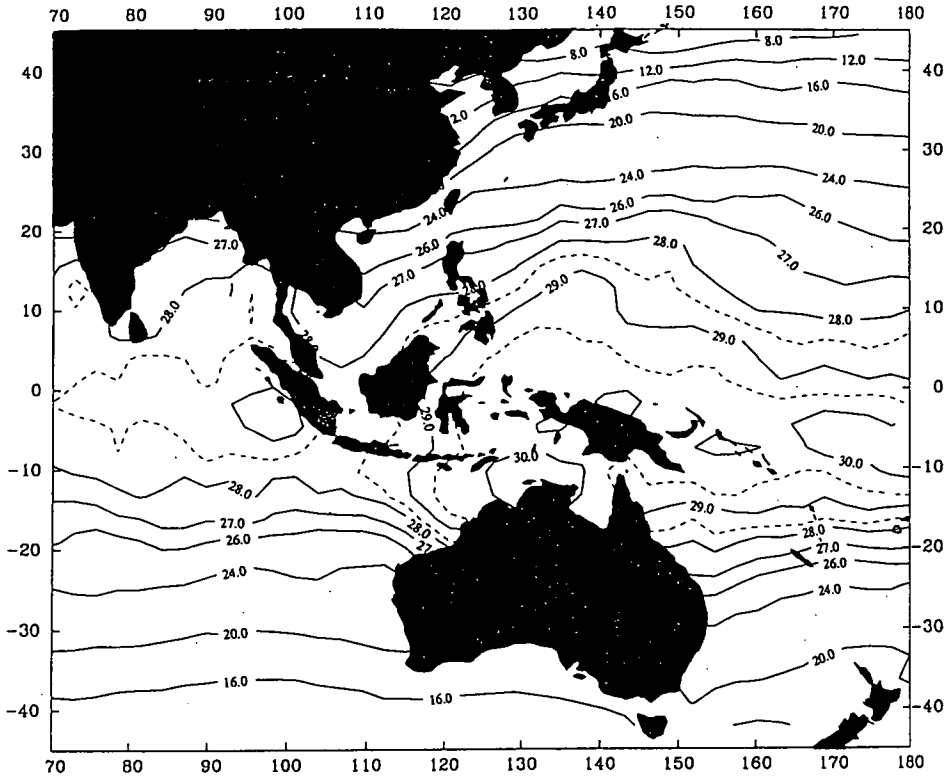

REYNOLDS BLENDED MONTHLY SST (8512)

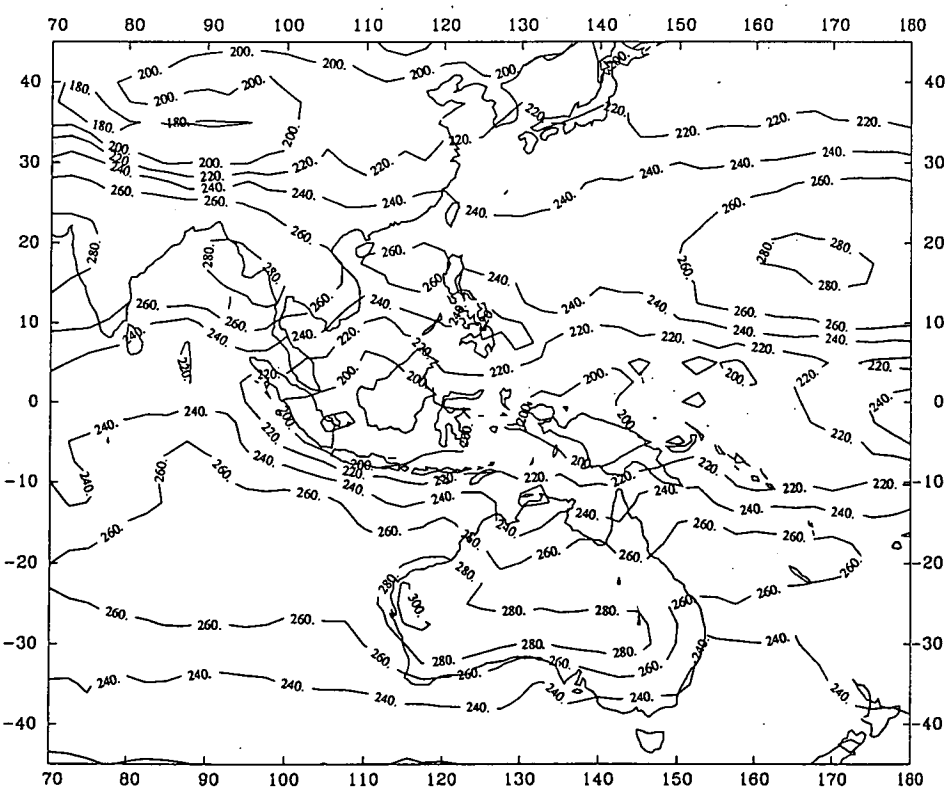

MONTHLY OLR (8512) (UNIT W/M*M)

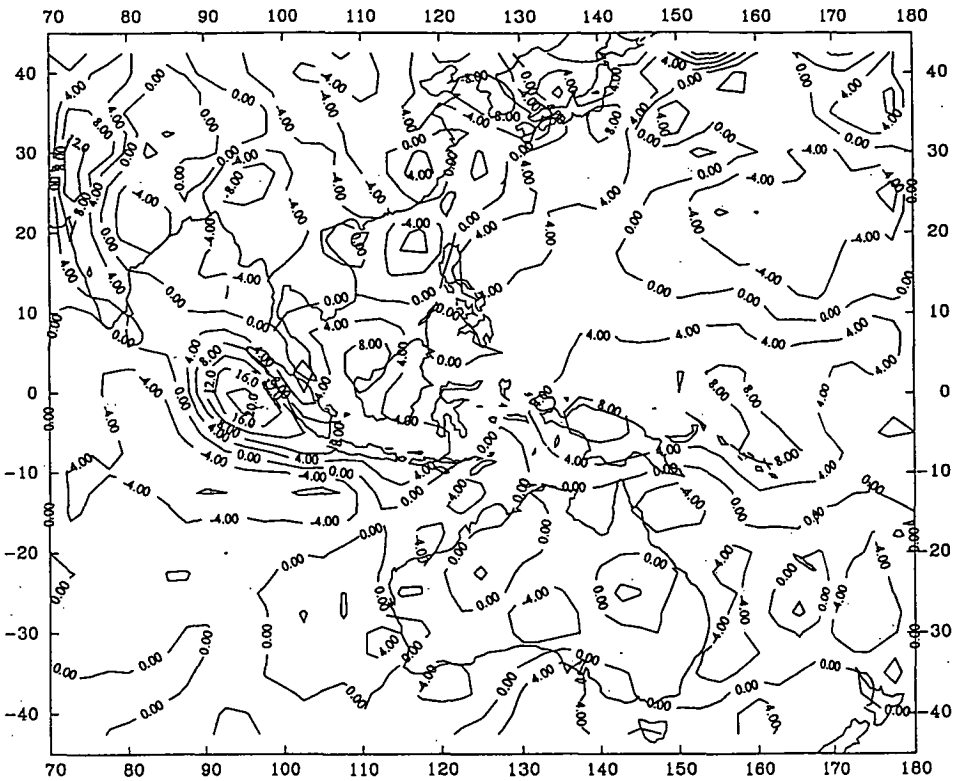

MONTHLY WIND DIVERGENCE AT 200MB (8512)

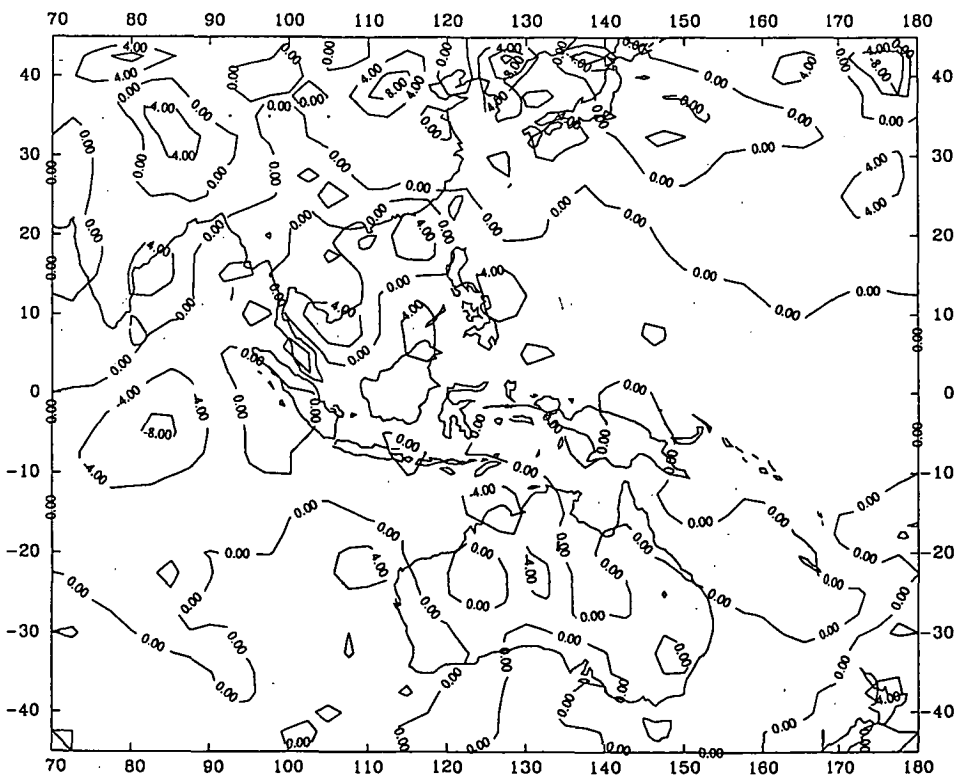

MONTHLY WIND DIVERGENCE AT 850MB (8512)

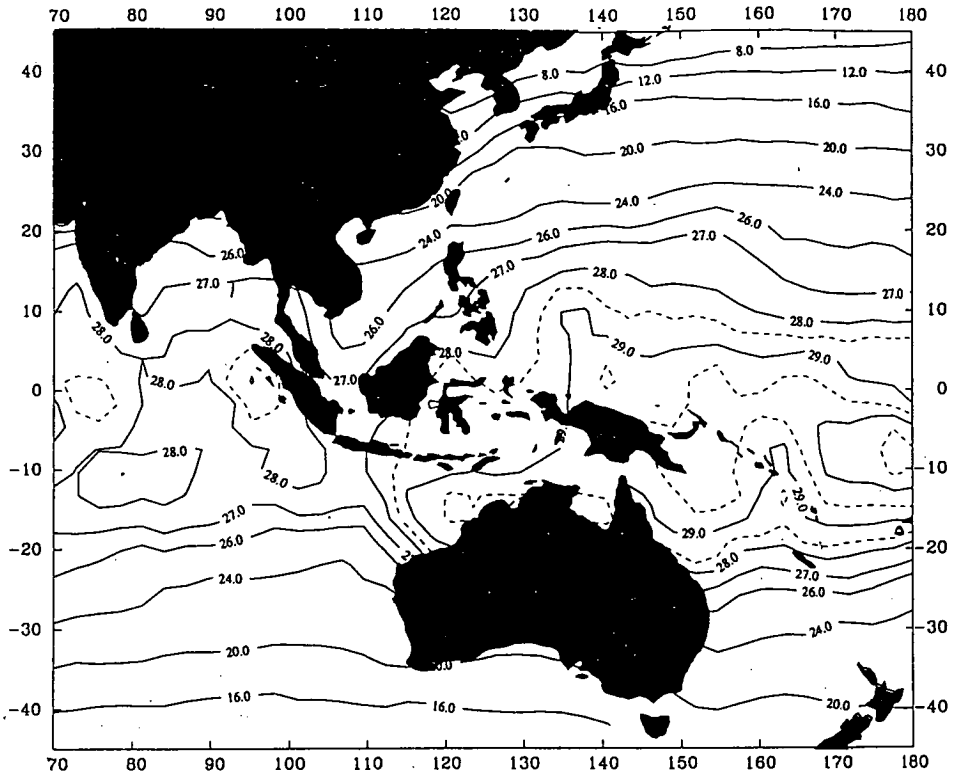

REYNOLDS BLENDED MONTHLY SST (8601)

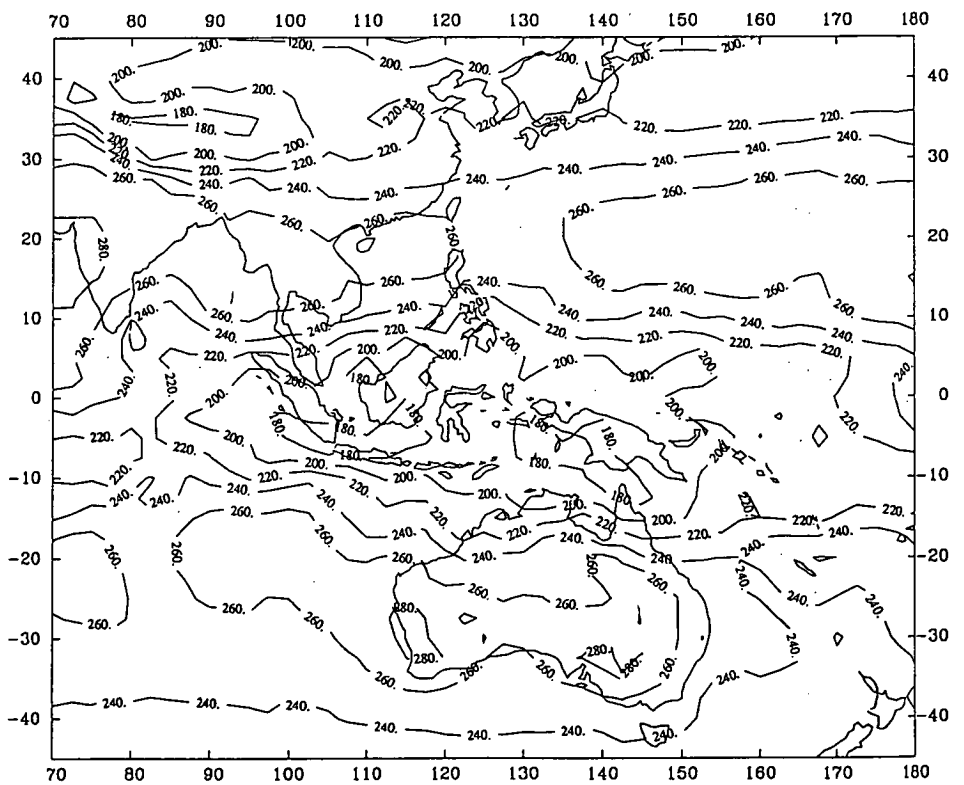

MONTHLY OLR (8601) (UNIT W/M*M)

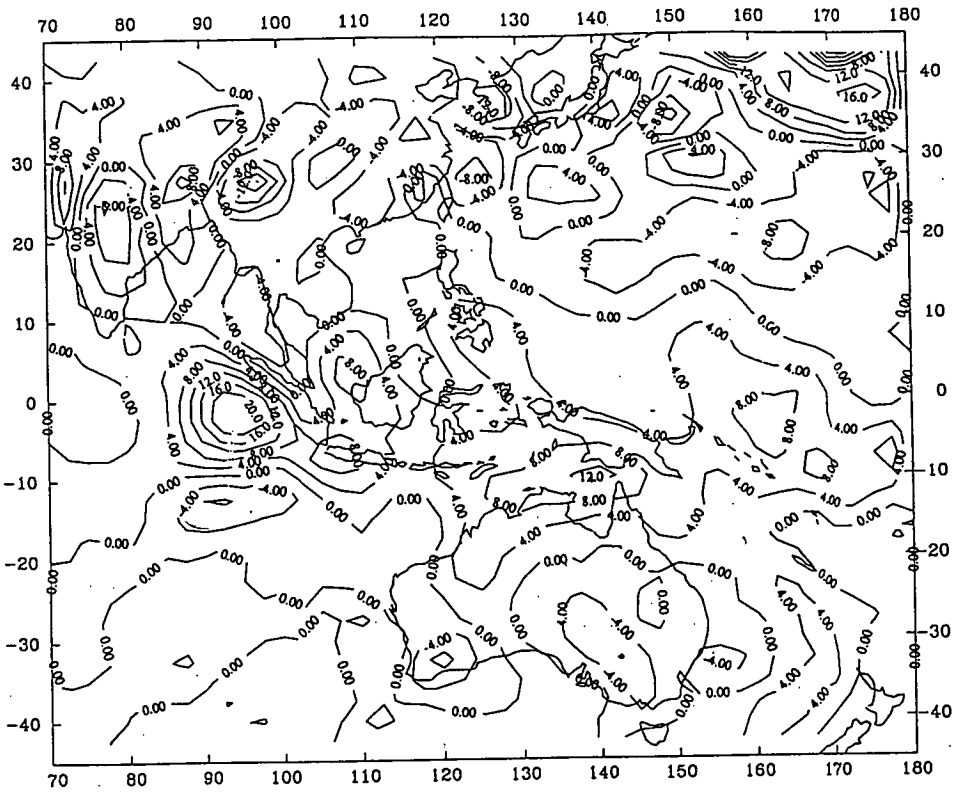

MONTHLY WIND DIVERGENCE AT 200MB (8601)

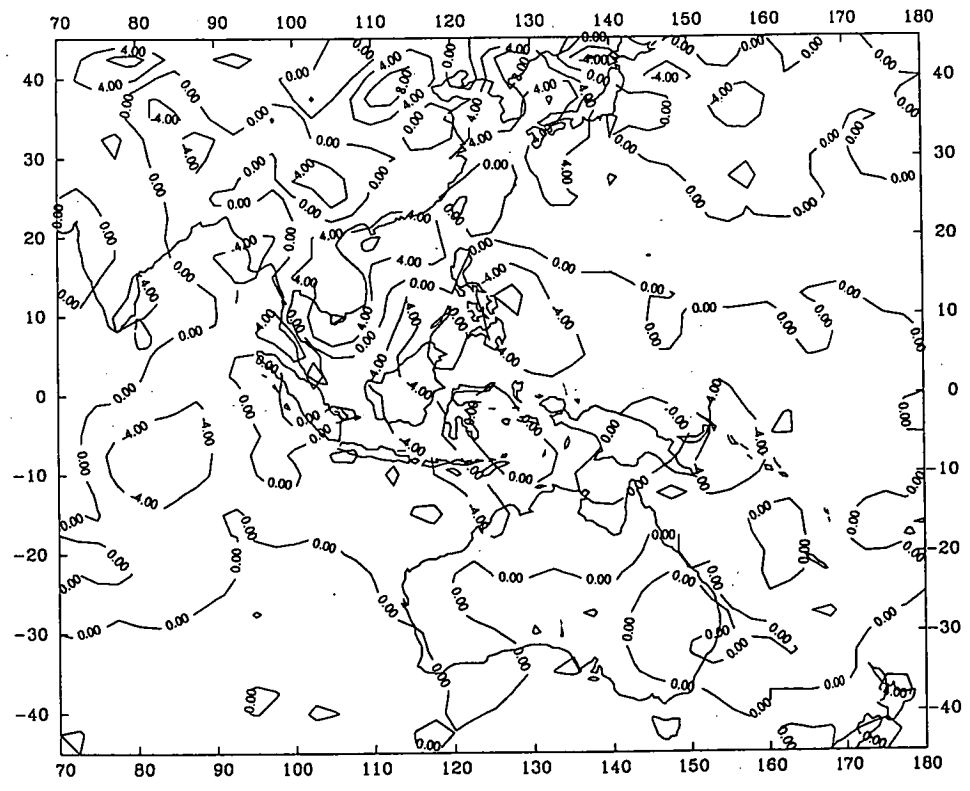

MONTHLY WIND DIVERGENCE AT 850MB (8601)

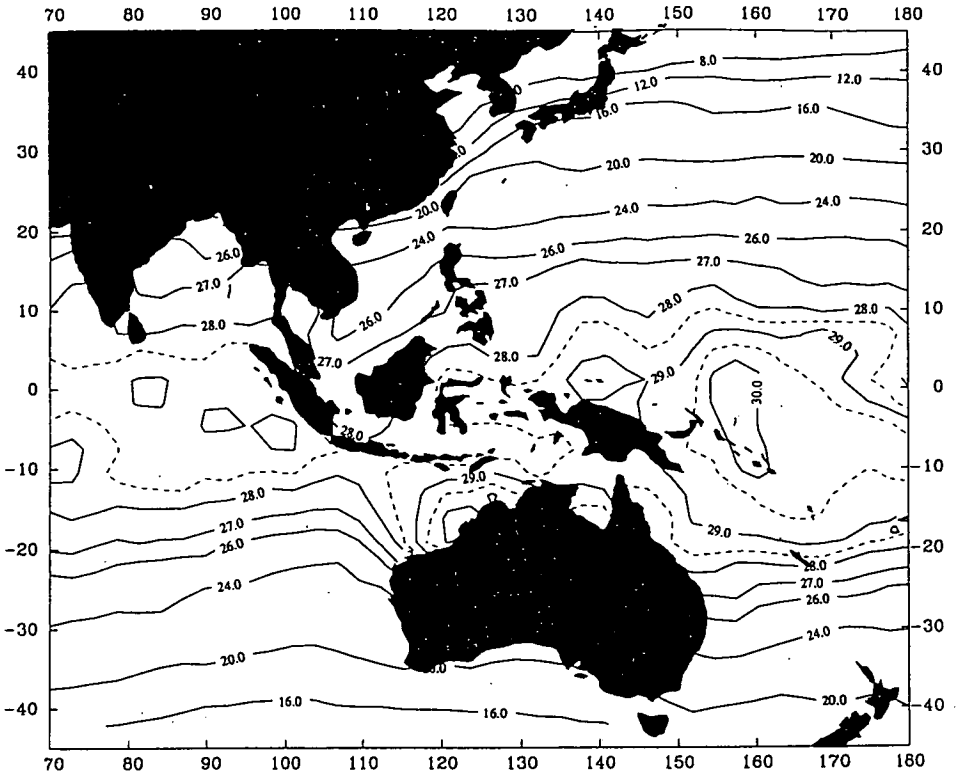

REYNOLDS BLENDED MONTHLY SST (8602)

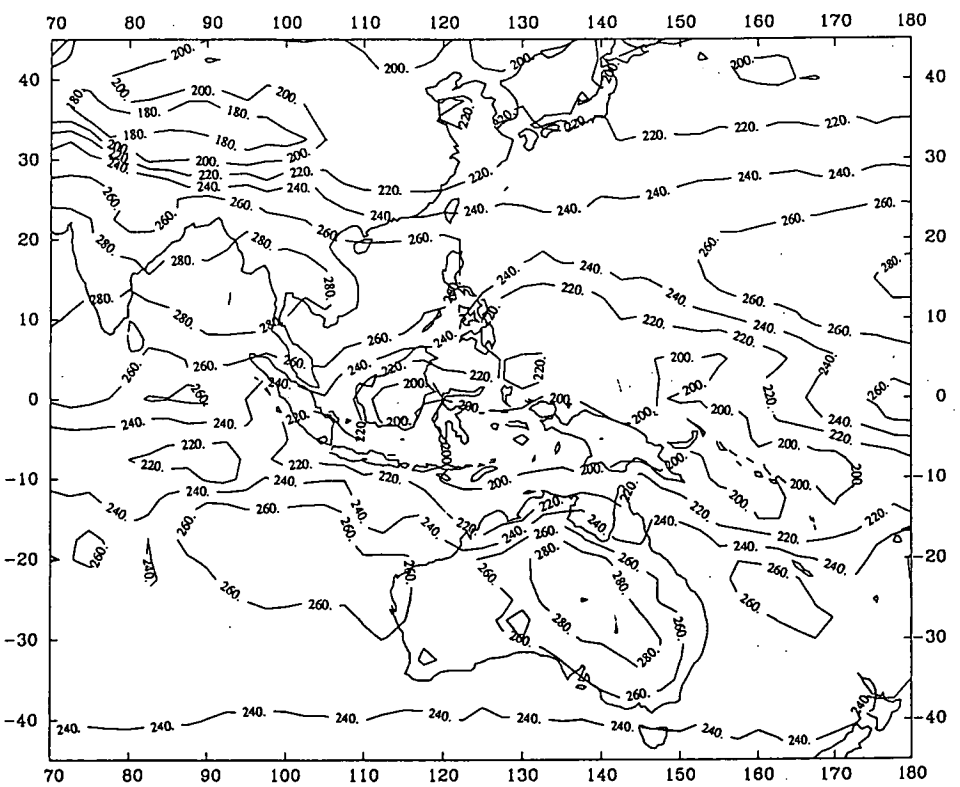

MONTHLY OLR (8602) (UNIT W/M*M)

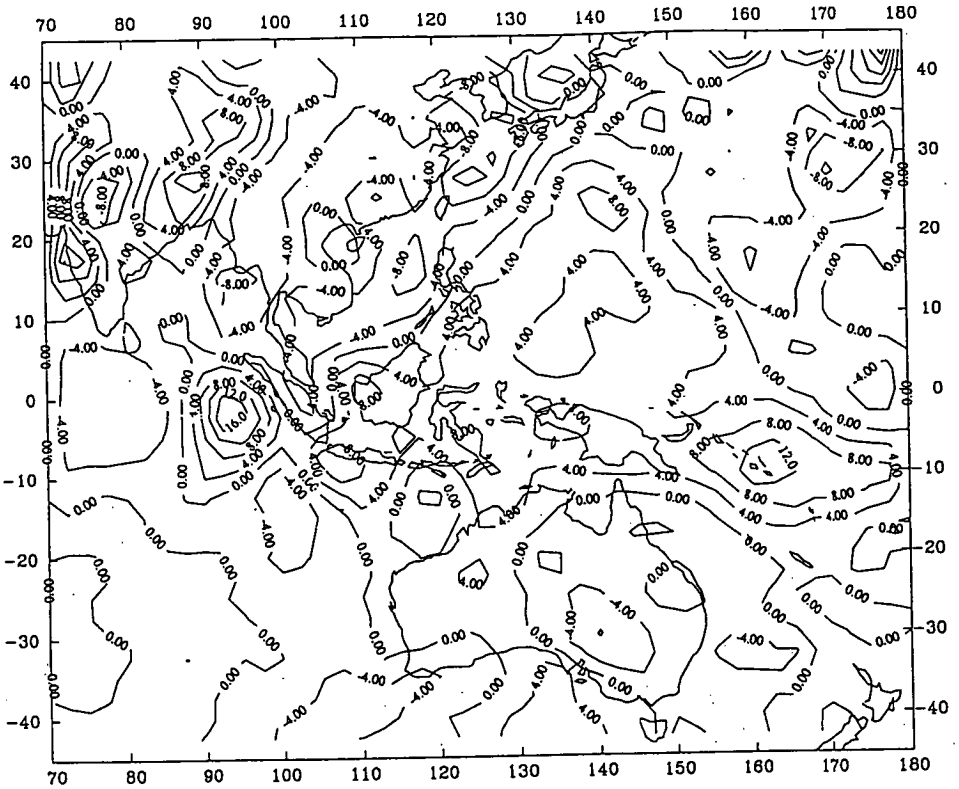

MONTHLY WIND DIVERGENCE AT 200MB (8602)

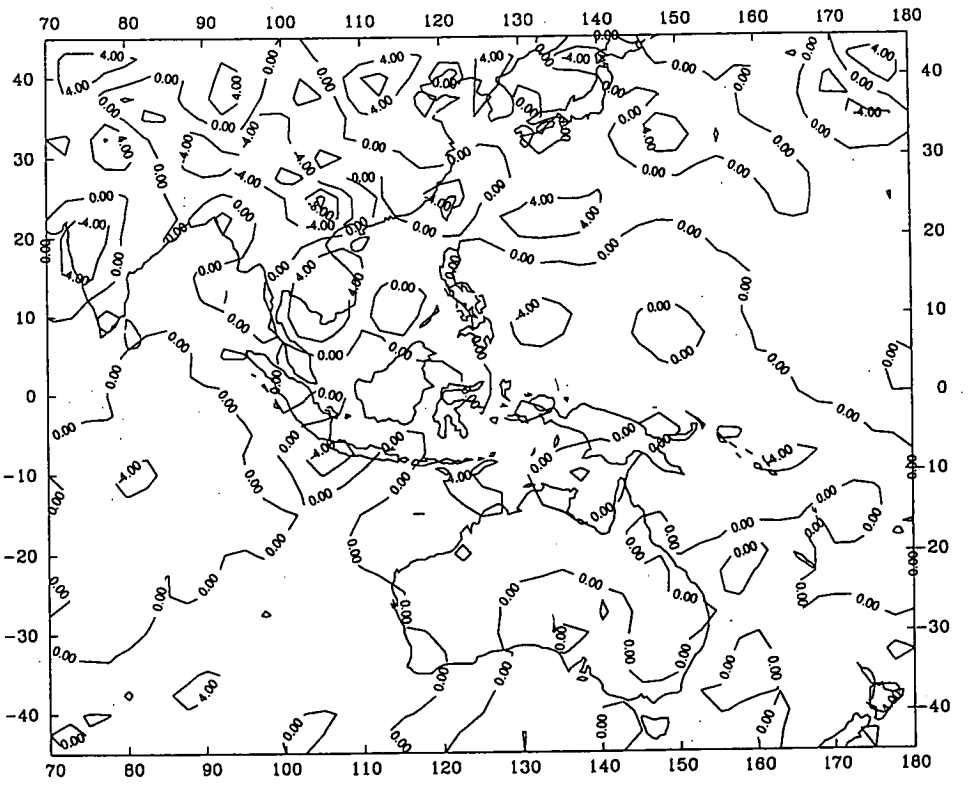

MONTHLY WIND DIVERGENCE AT 850MB (8602)

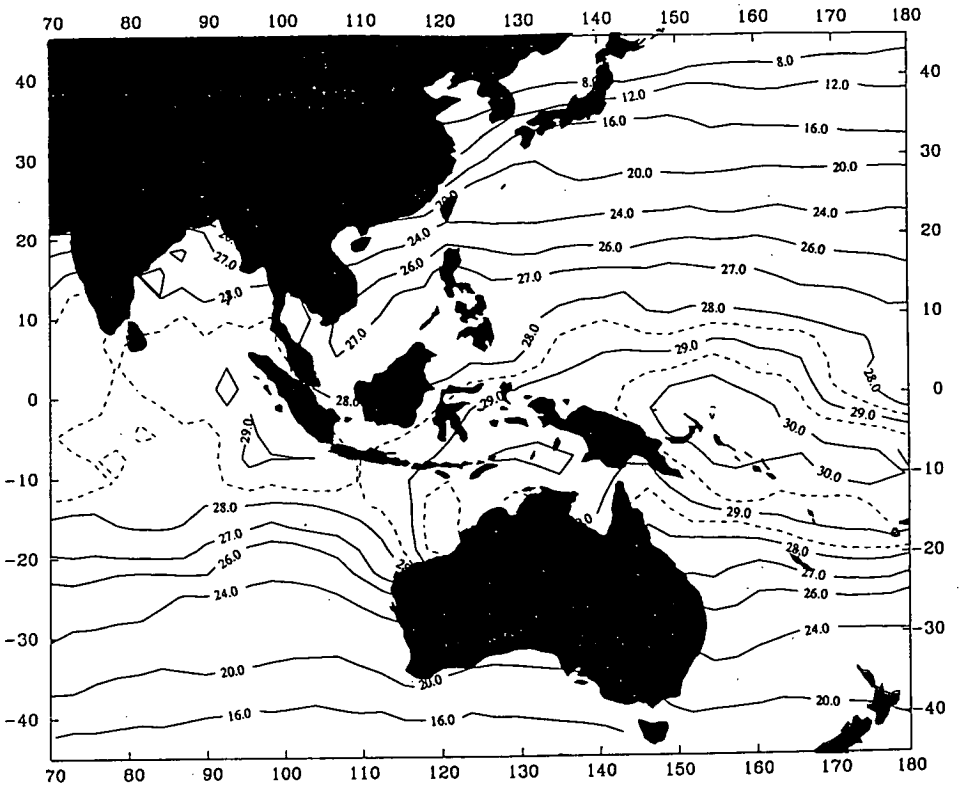

REYNOLDS BLENDED MONTHLY SST (8603)

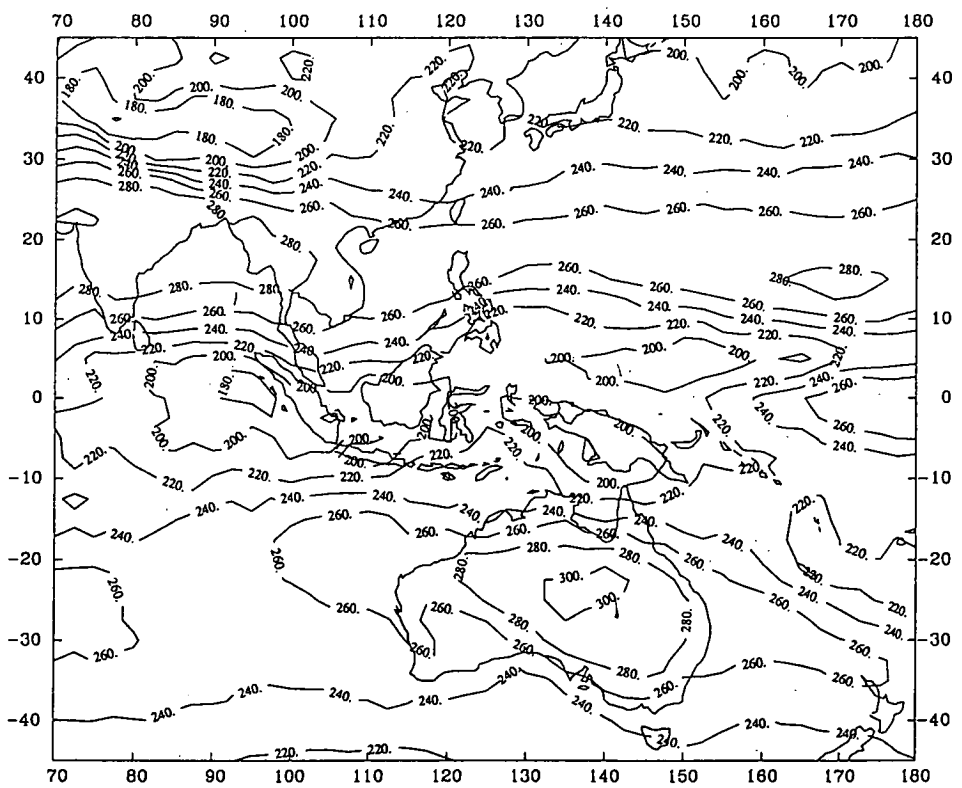

MONTHLY OLR (8603) (UNIT W/M*M)

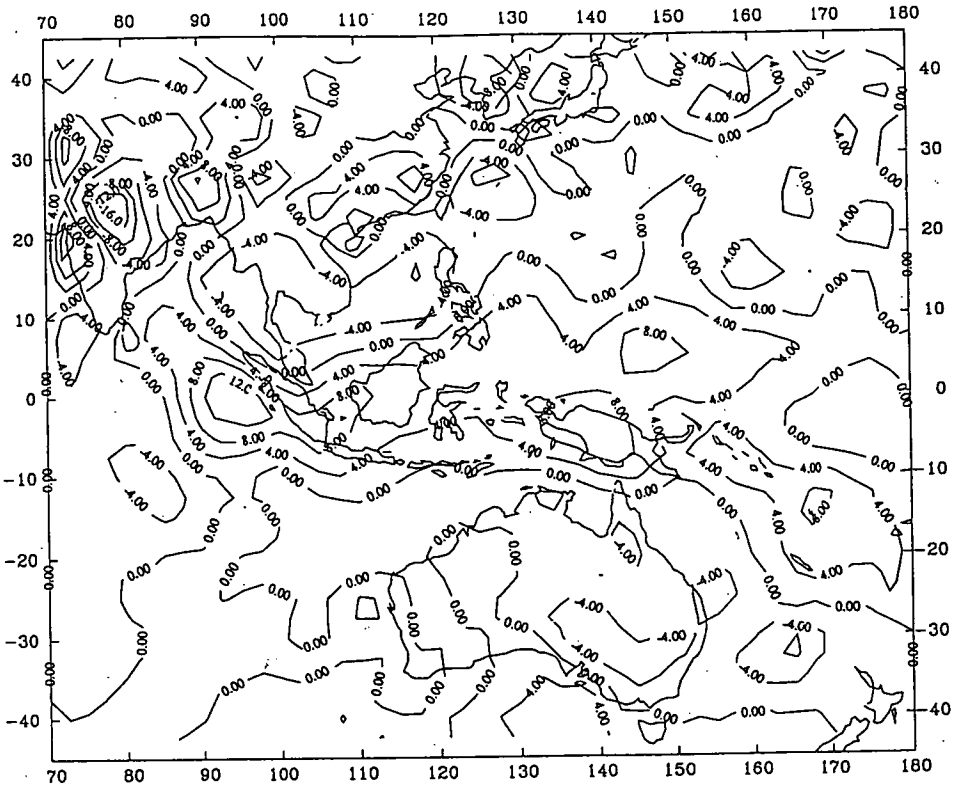

MONTHLY WIND DIVERGENCE AT 200MB (8603)

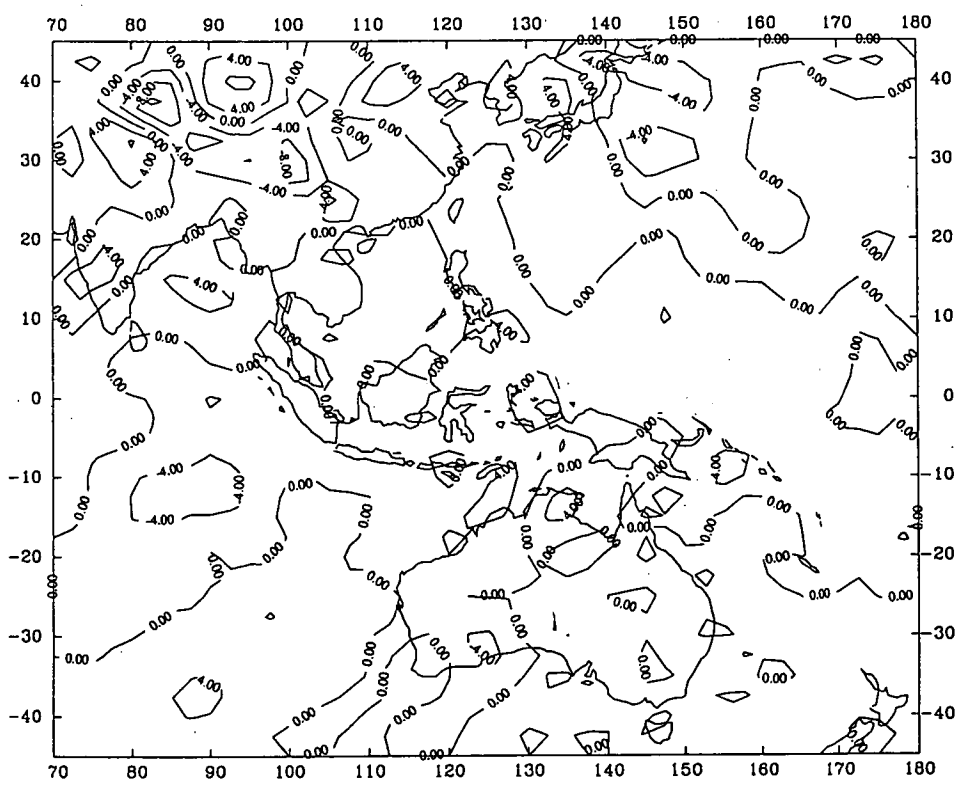

MONTHLY WIND DIVERGENCE AT 850MB (8603)

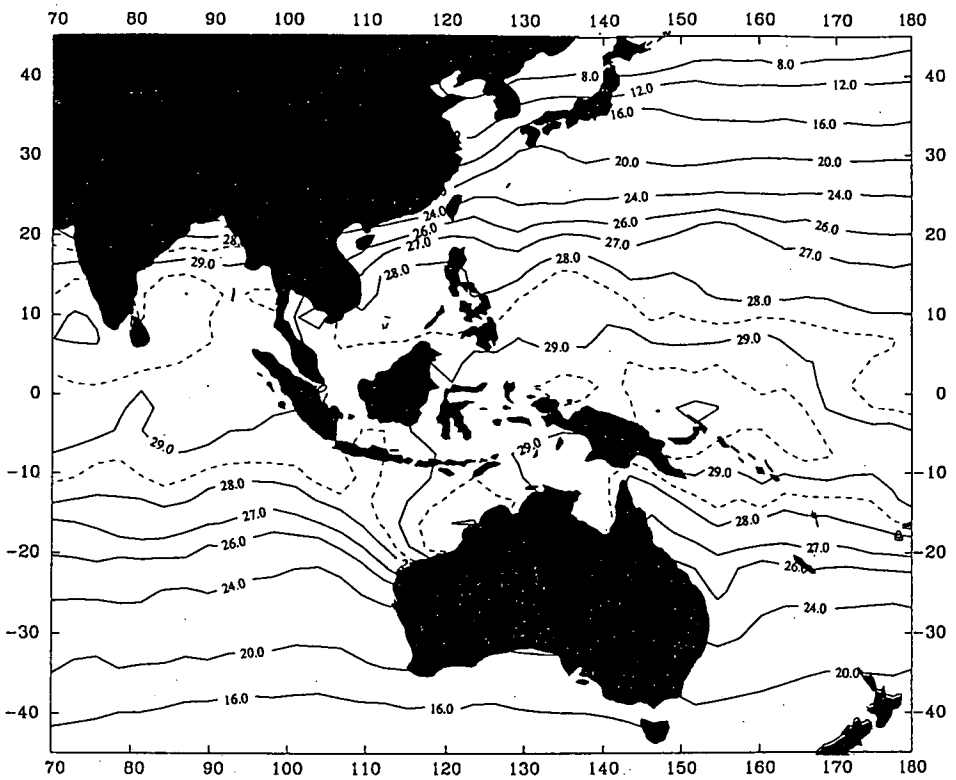

REYNOLDS BLENDED MONTHLY SST (8604)

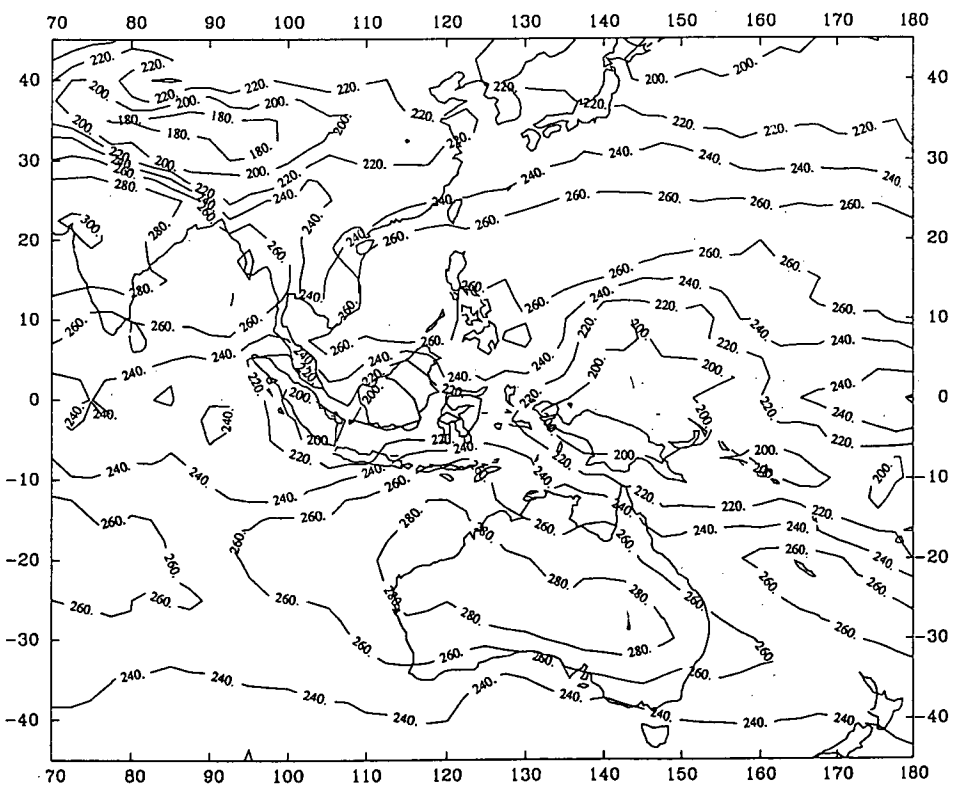

MONTHLY OLR (8604) (UNIT W/M*M)

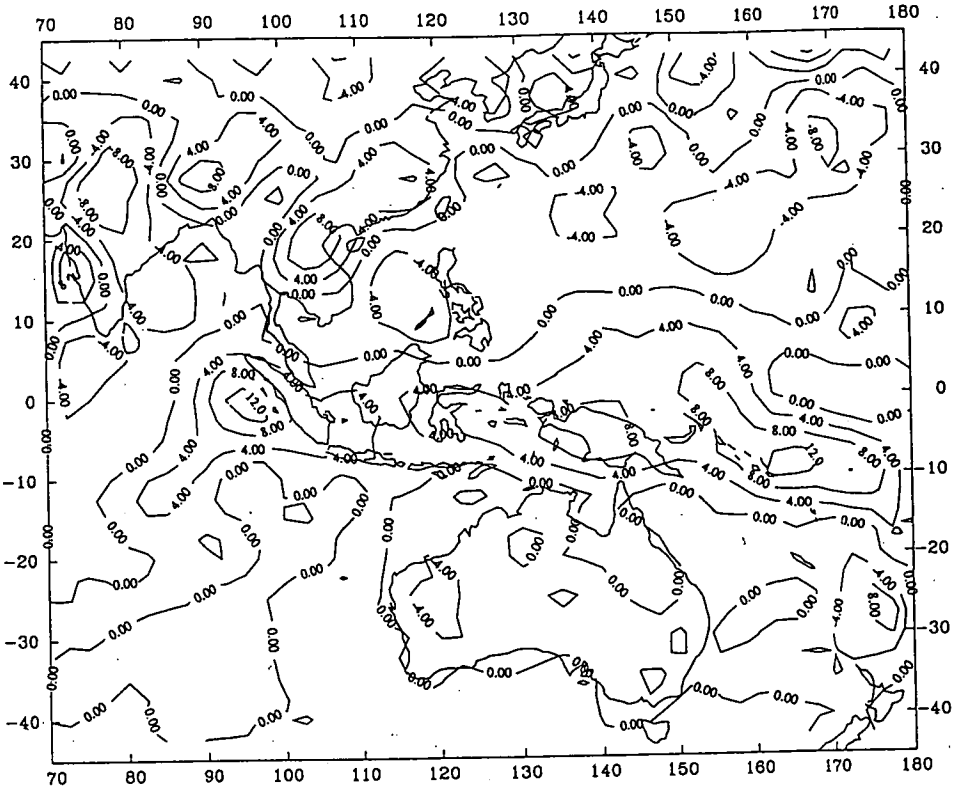

MONTHLY WIND DIVERGENCE AT 200MB (8604)

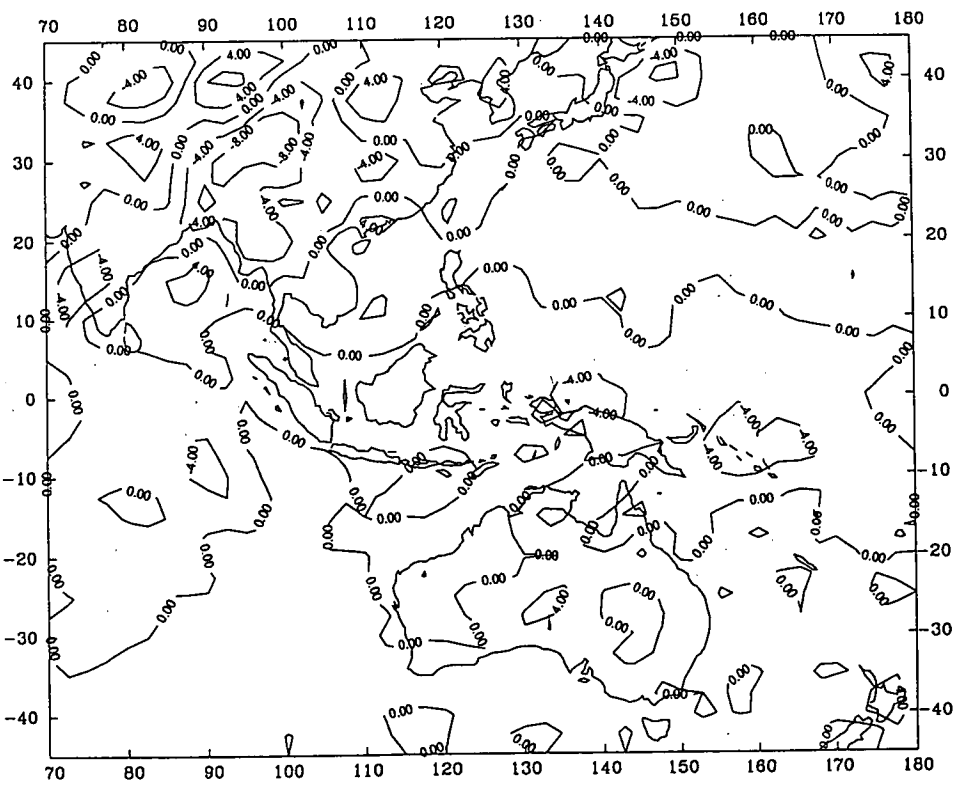

MONTHLY WIND DIVERGENCE AT 850MB (8604)

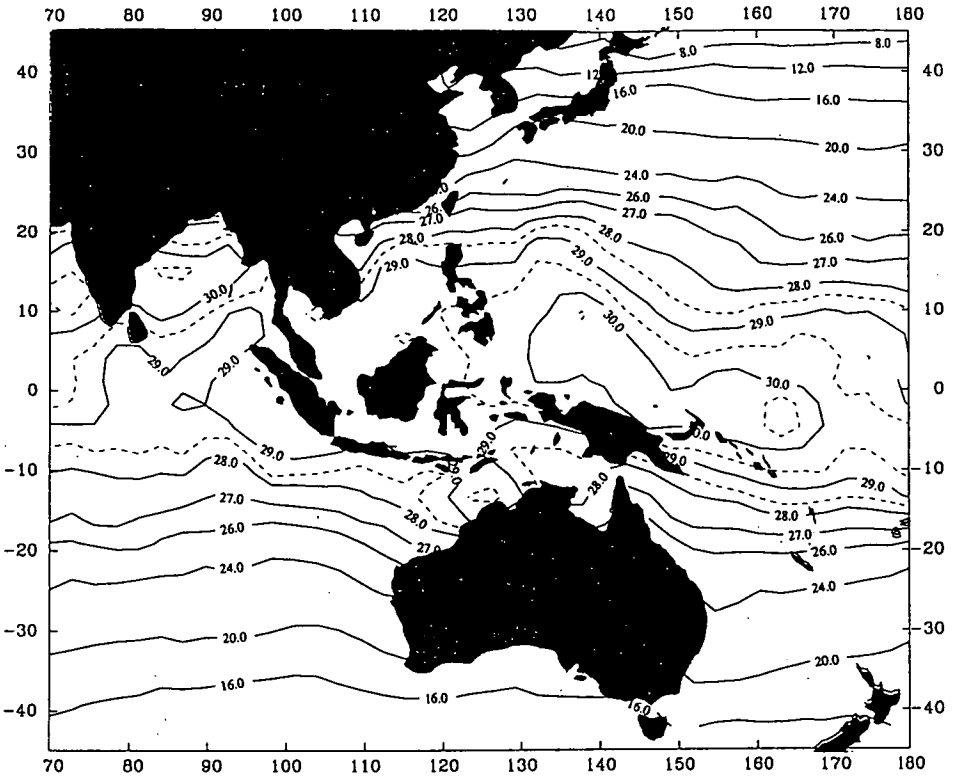

REYNOLDS BLENDED MONTHLY SST (8605)

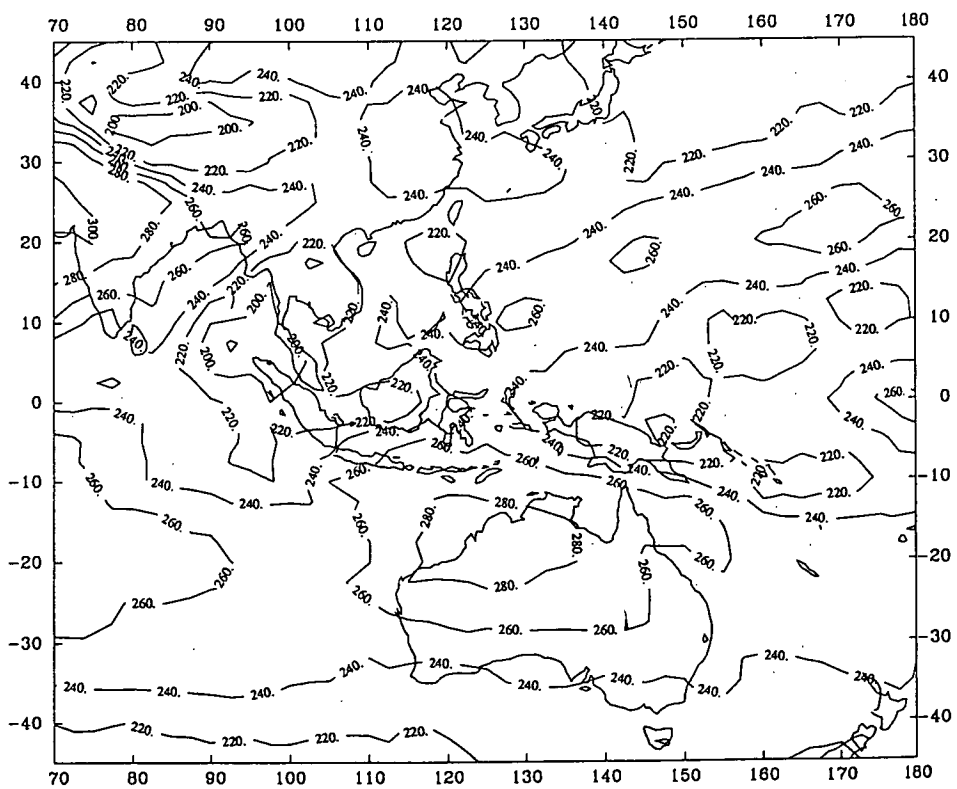

MONTHLY OLR (8605) (UNIT W/M*M)

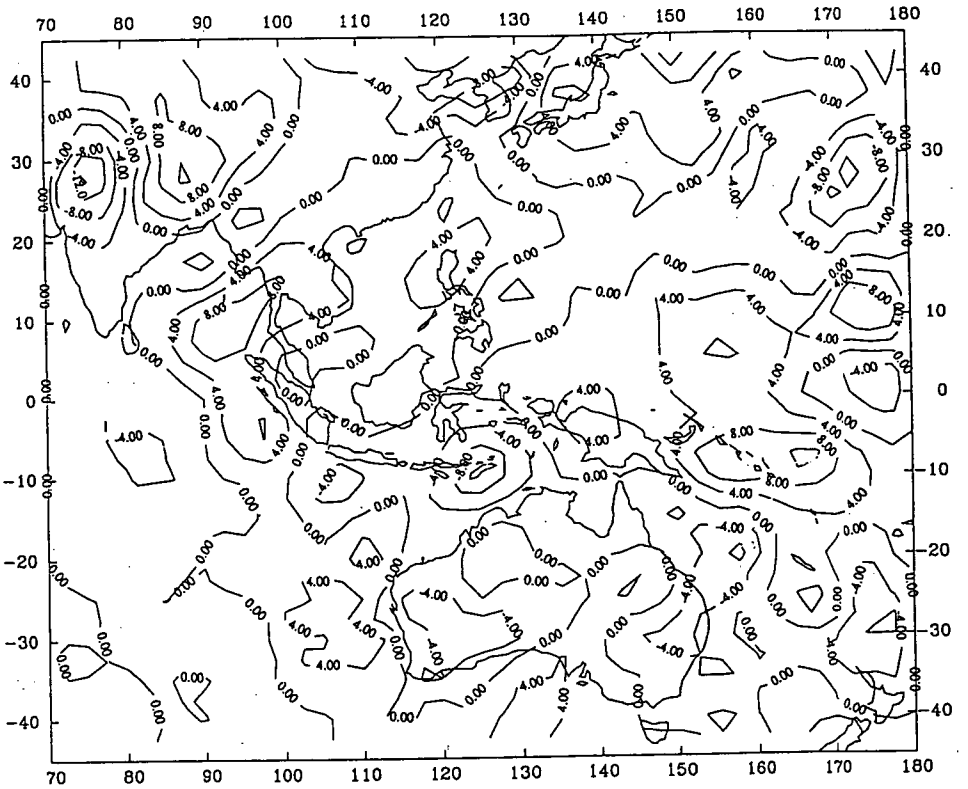

MONTHLY WIND DIVERGENCE AT 200MB (8605)

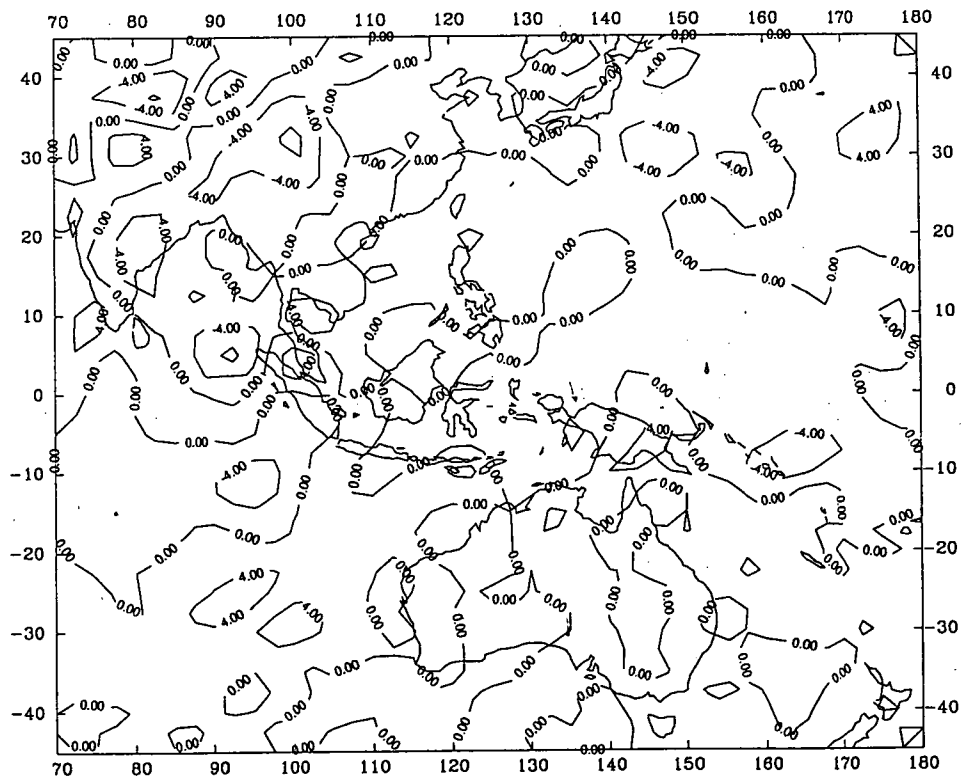

MONTHLY WIND DIVERGENCE AT 850MB (8605)

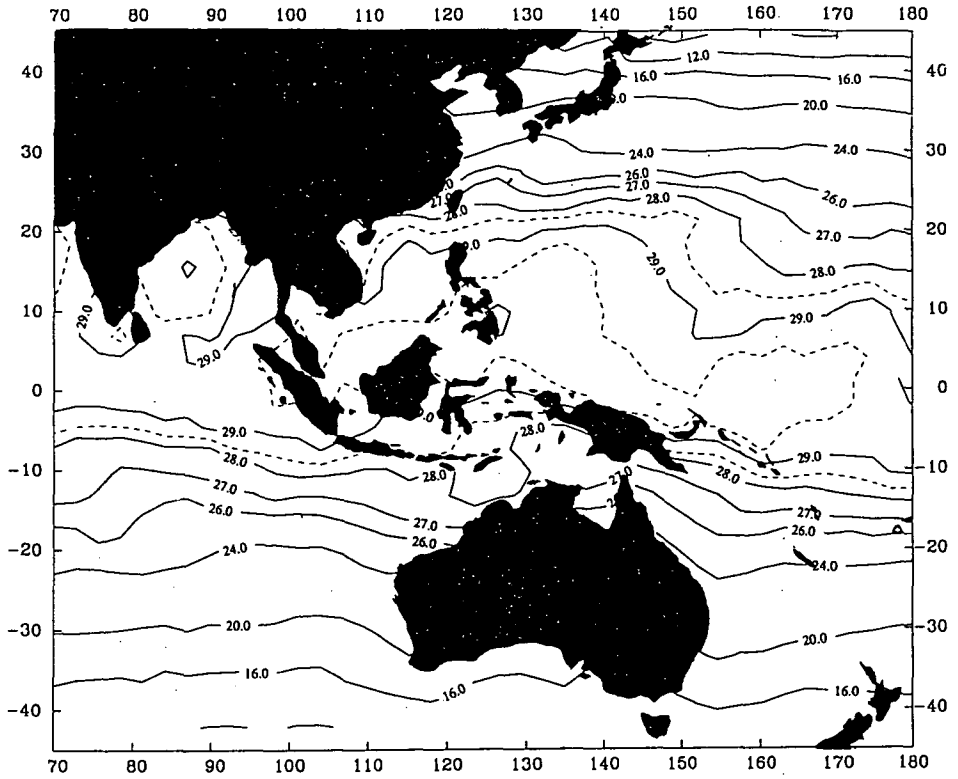

REYNOLDS BLENDED MONTHLY SST (8606)

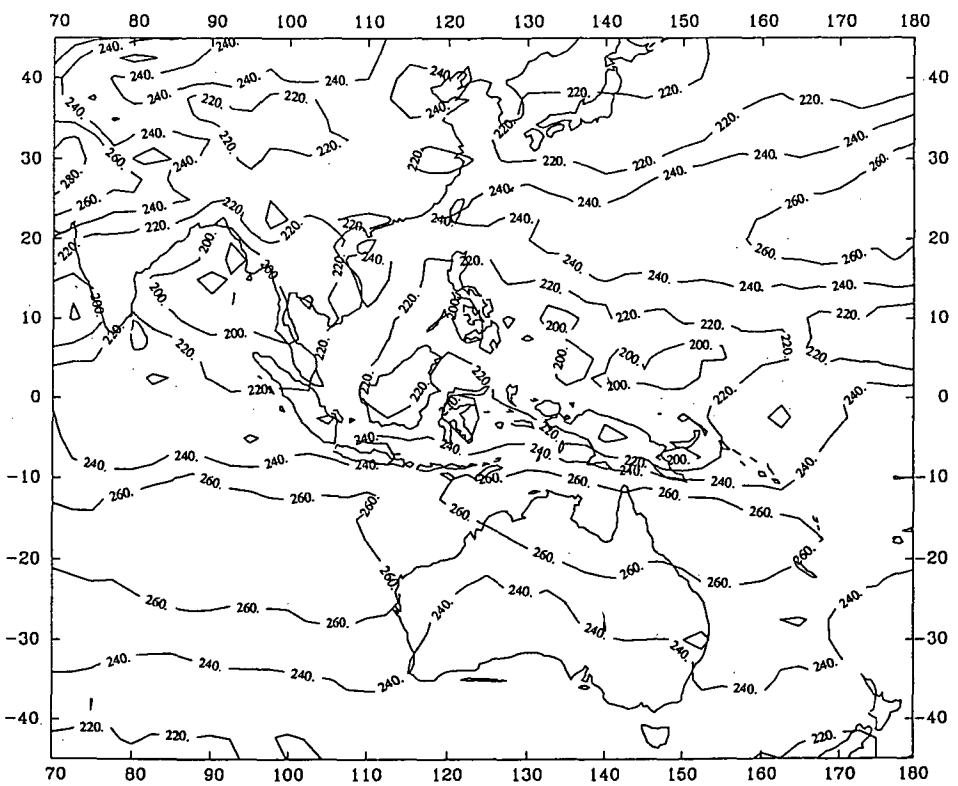

MONTHLY OLR (8606) (UNIT W/M*M)

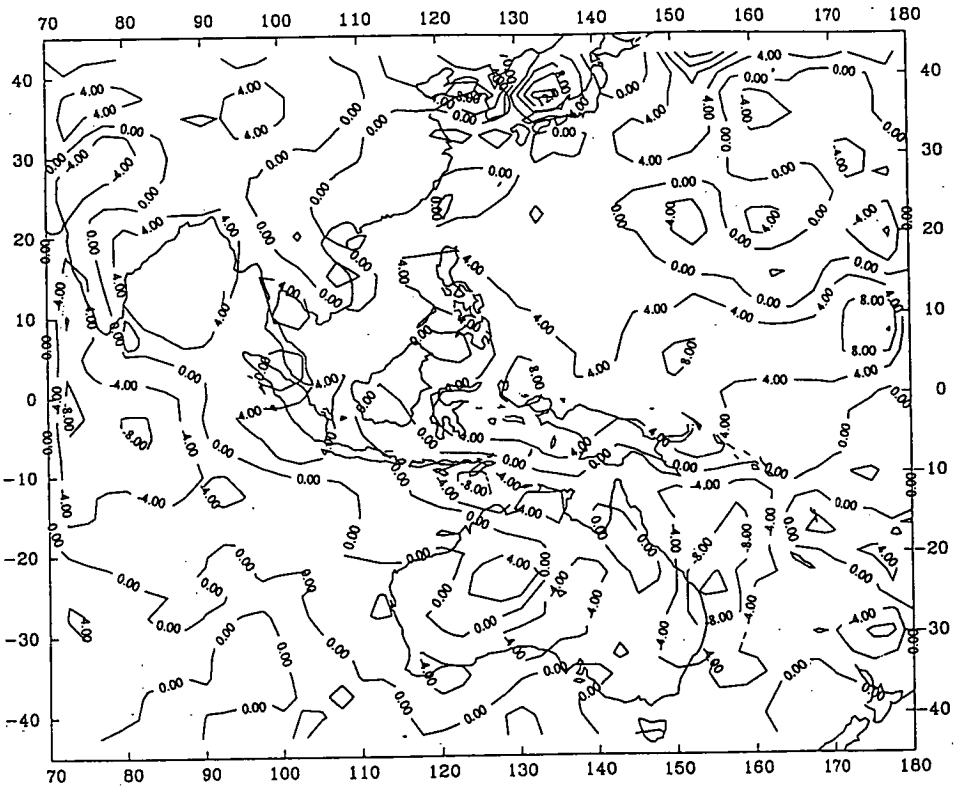

MONTHLY WIND DIVERGENCE AT 200MB (8606)

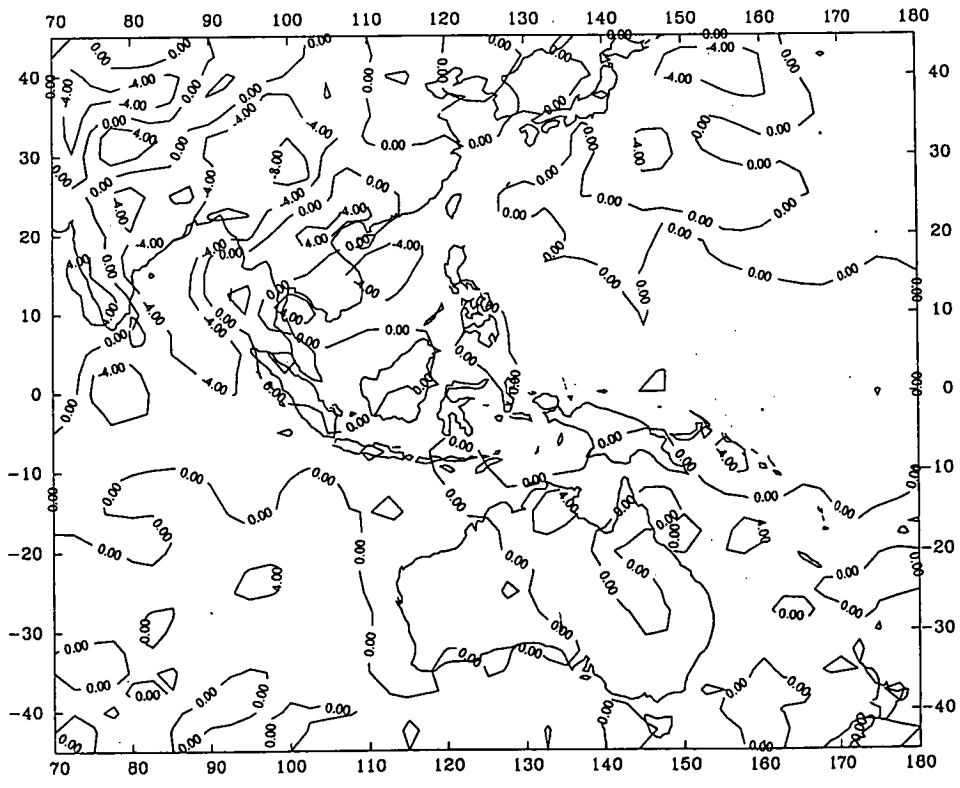

MONTHLY WIND DIVERGENCE AT 850MB (8606)

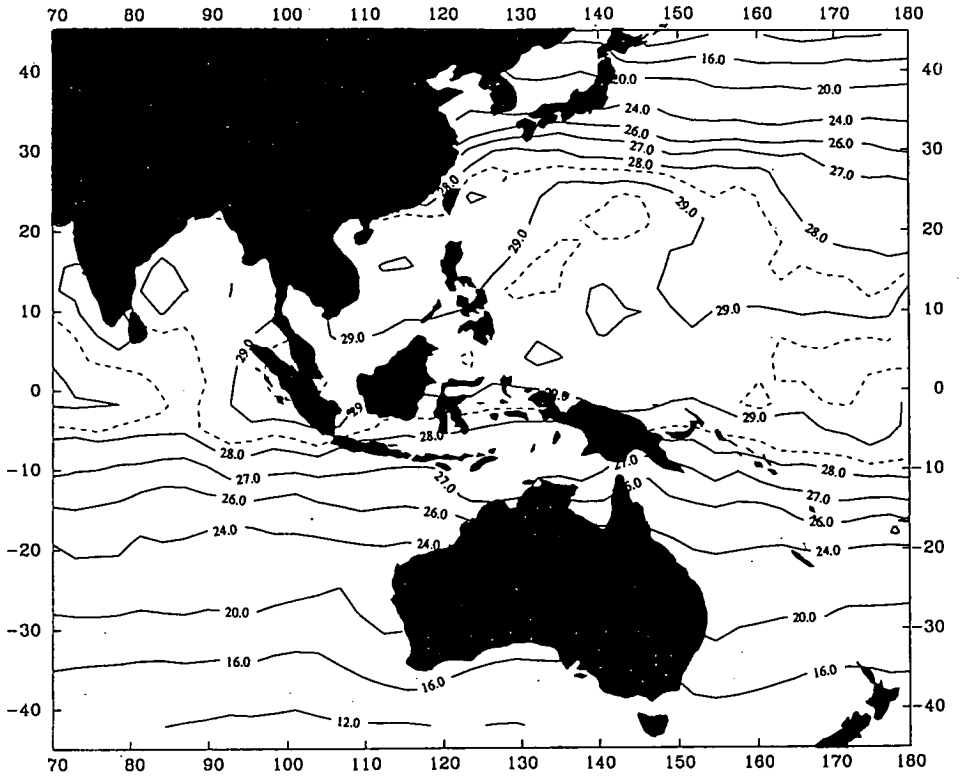

REYNOLDS BLENDED MONTHLY SST (8607)

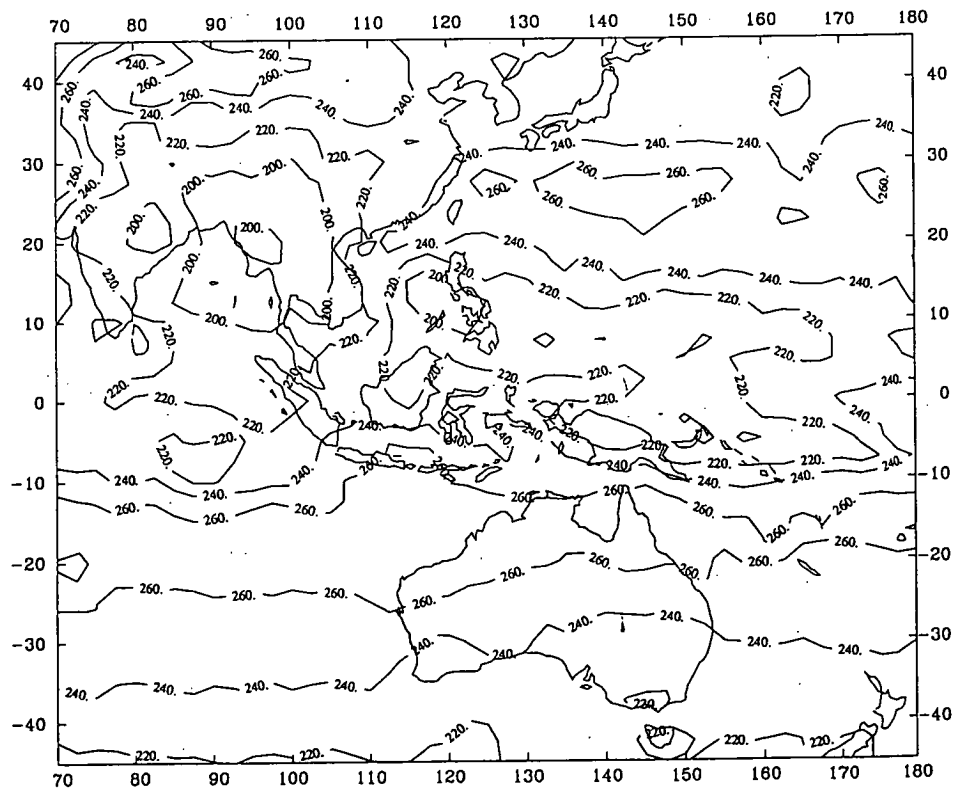

MONTHLY OLR (8607) (UNIT W/M*M)

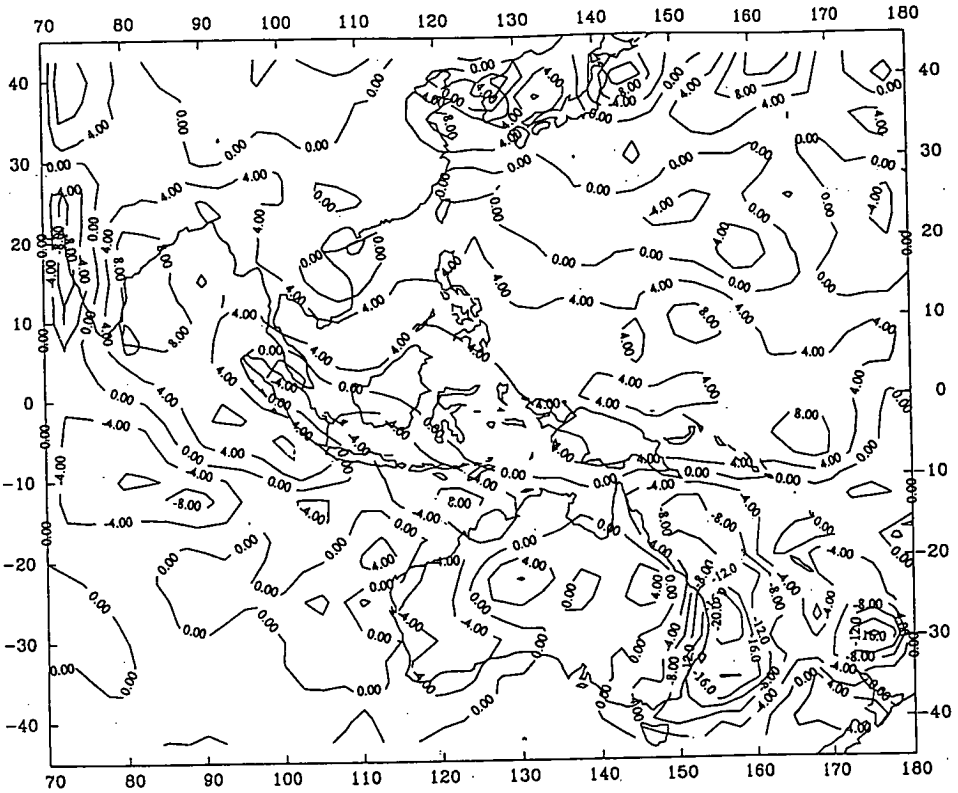

MONTHLY WIND DIVERGENCE AT 200MB (8607)

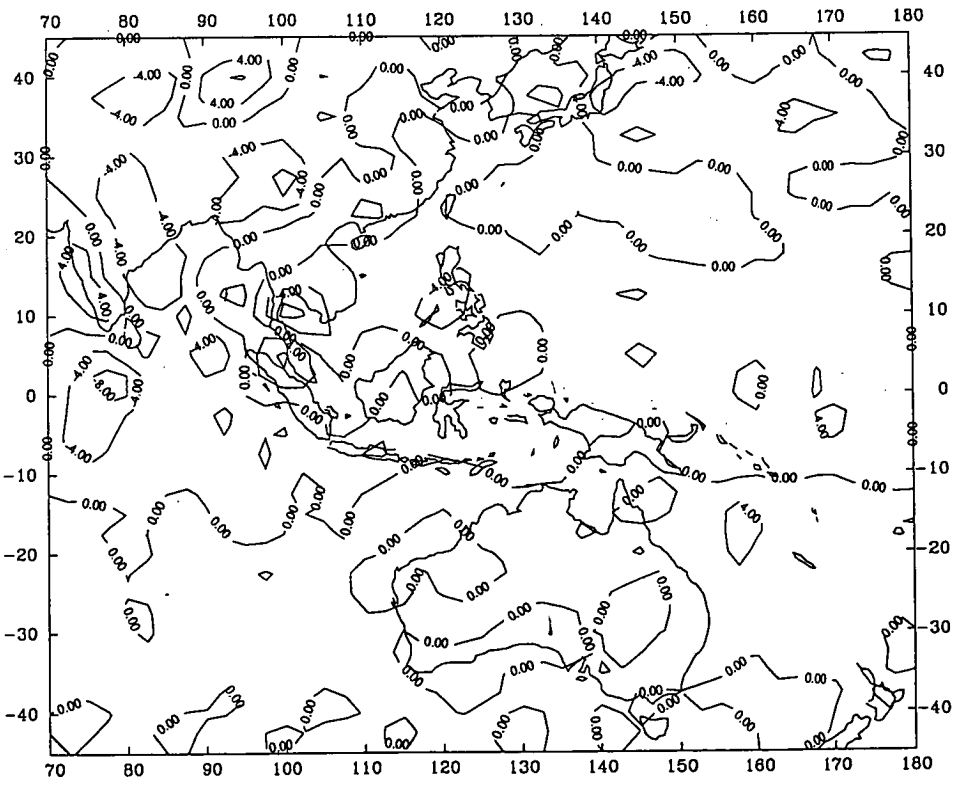

MONTHLY WIND DIVERGENCE AT 850MB (8607)

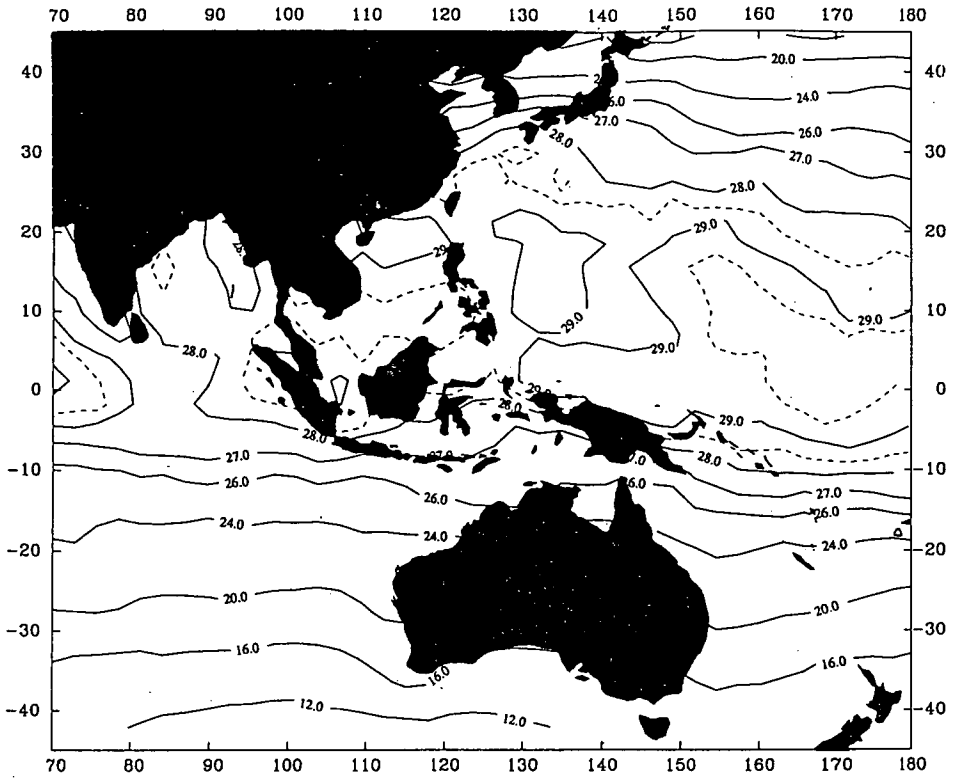

REYNOLDS BLENDED MONTHLY SST (8608)

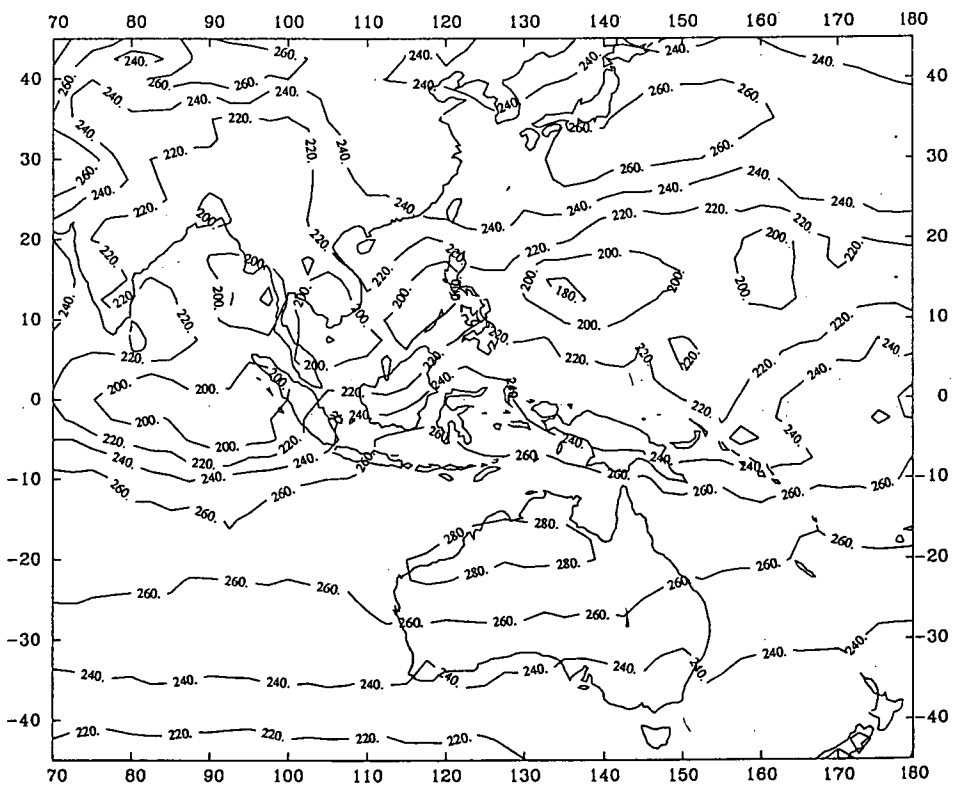

MONTHLY OLR (8608) (UNIT W/M*M)

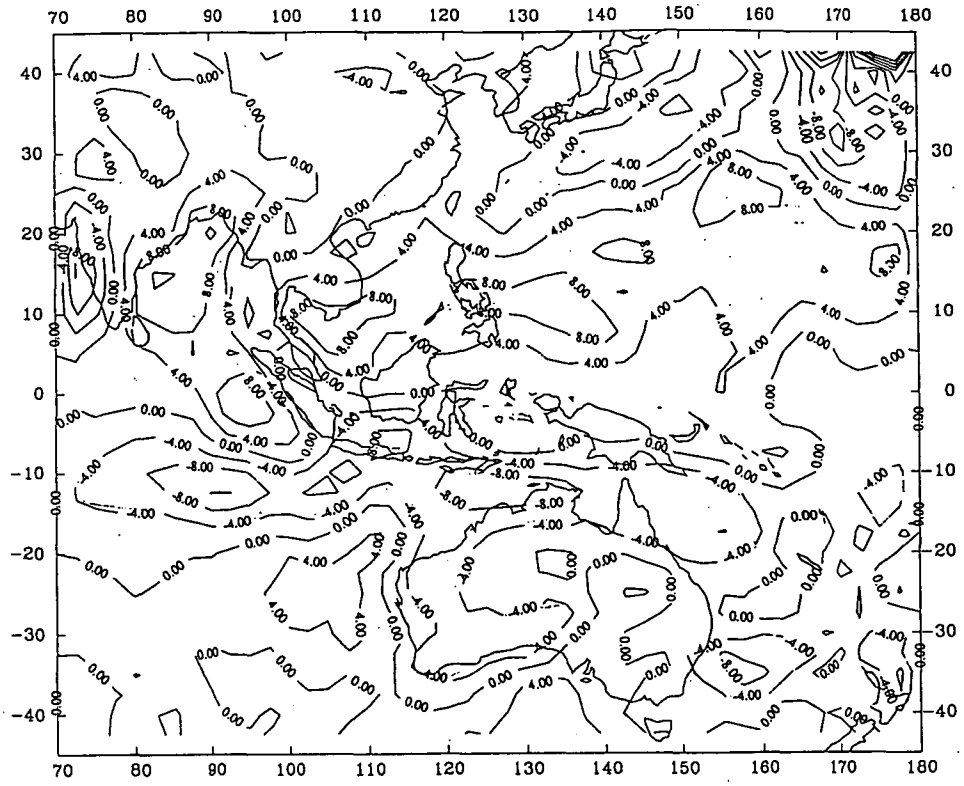

MONTHLY WIND DIVERGENCE AT 200MB (8608)

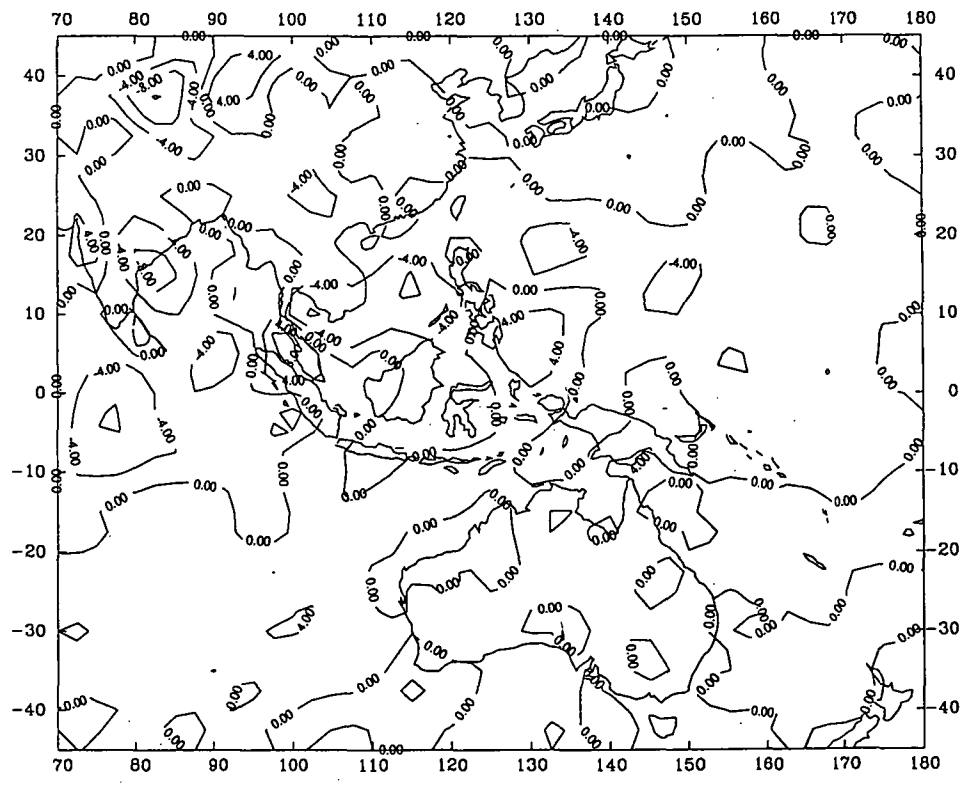

MONTHLY WIND DIVERGENCE AT 850MB (8608)

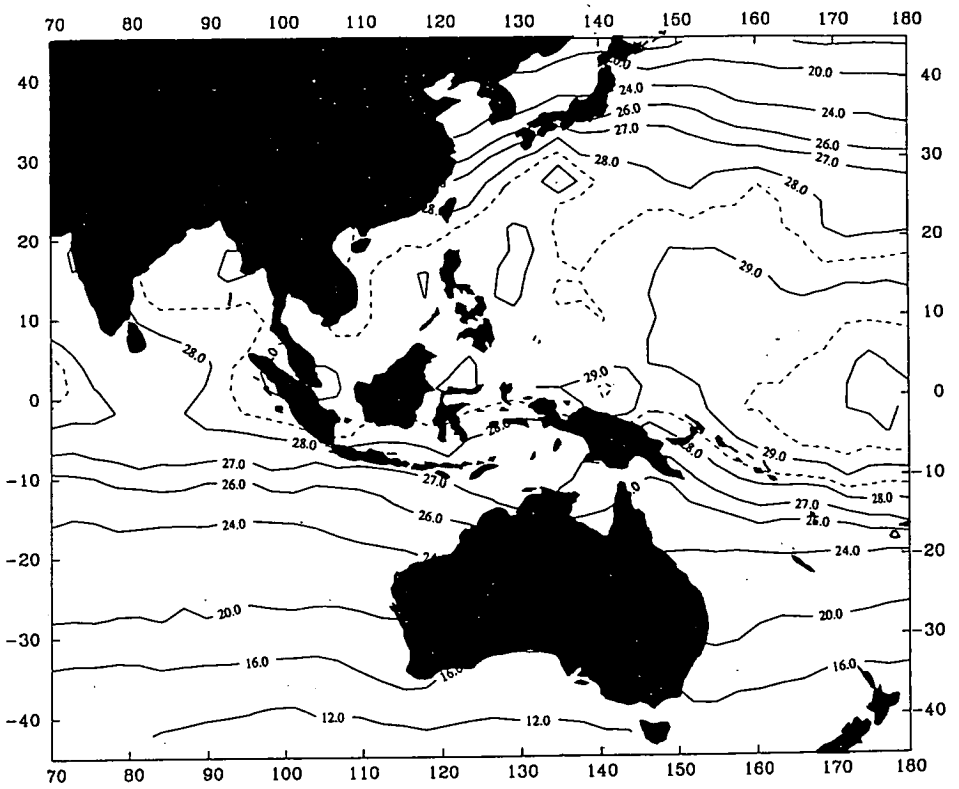

REYNOLDS BLENDED MONTHLY SST (8609)

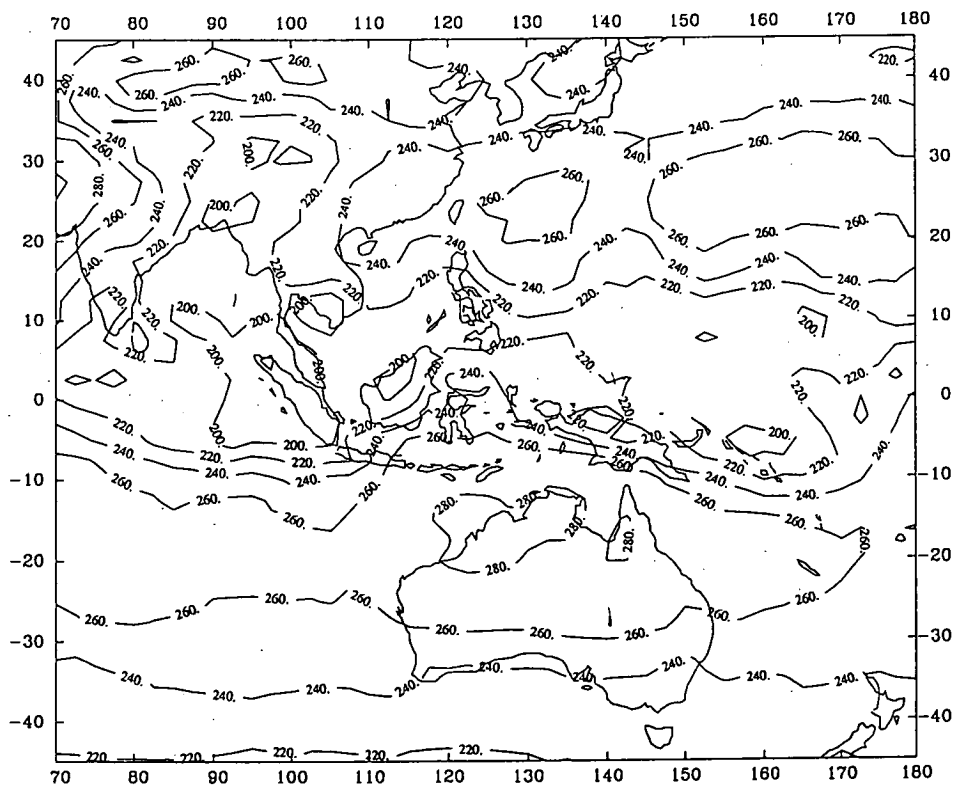

MONTHLY OLR (8609) (UNIT W/M*M)

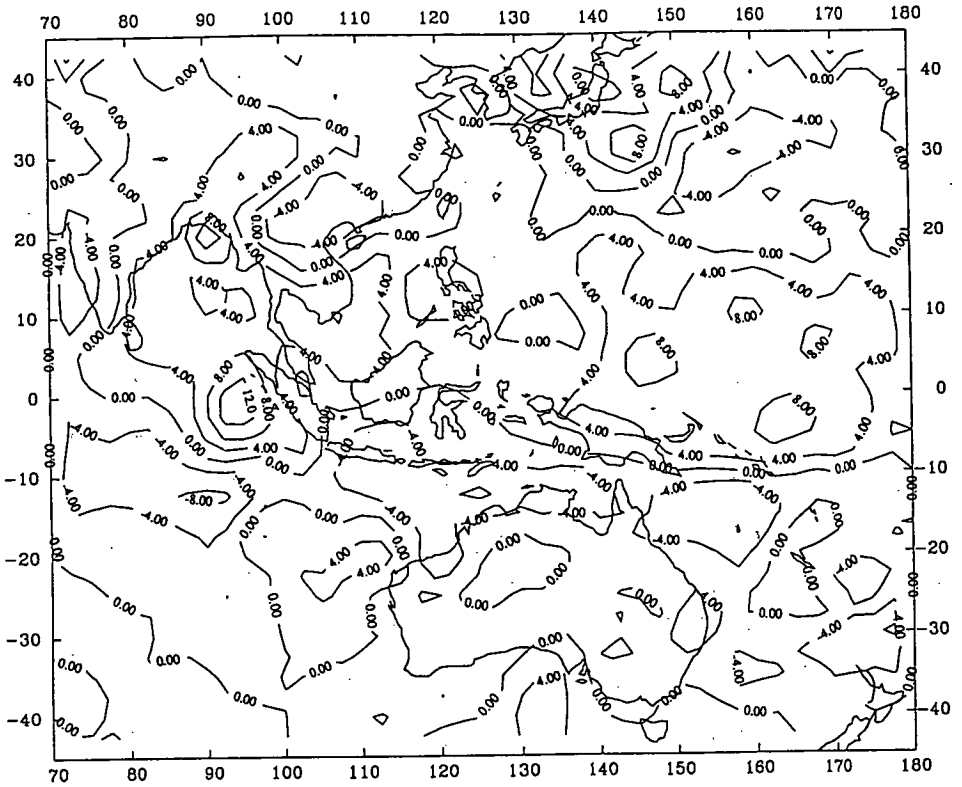

MONTHLY WIND DIVERGENCE AT 200MB (8609)

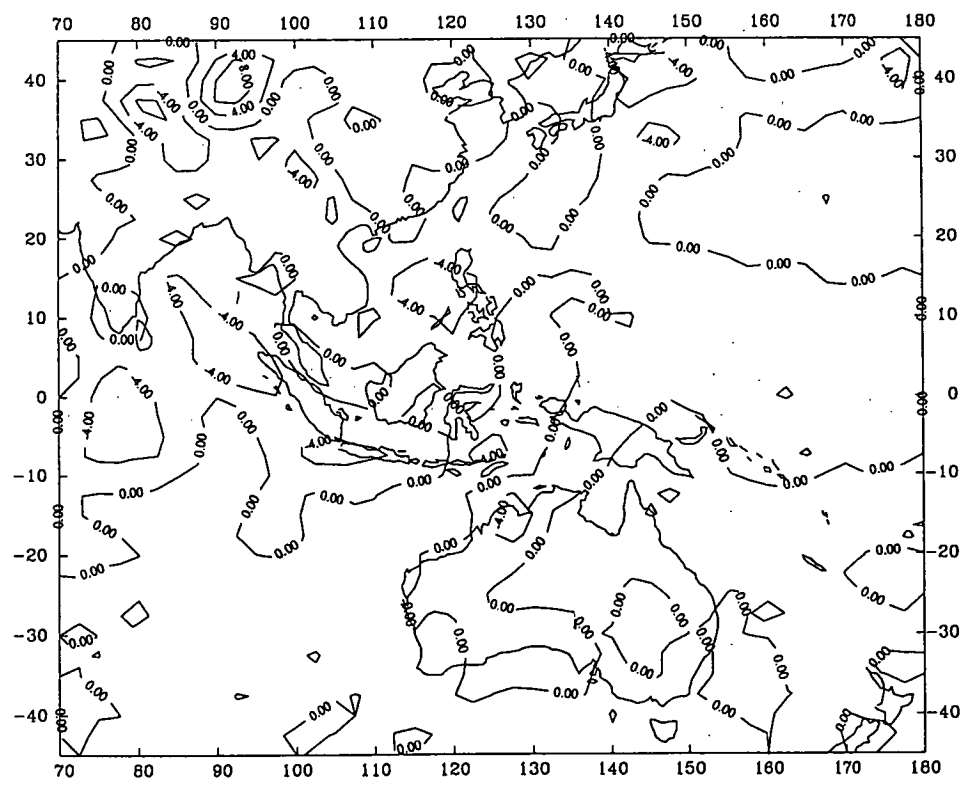

MONTHLY WIND DIVERGENCE AT 850MB (8609)

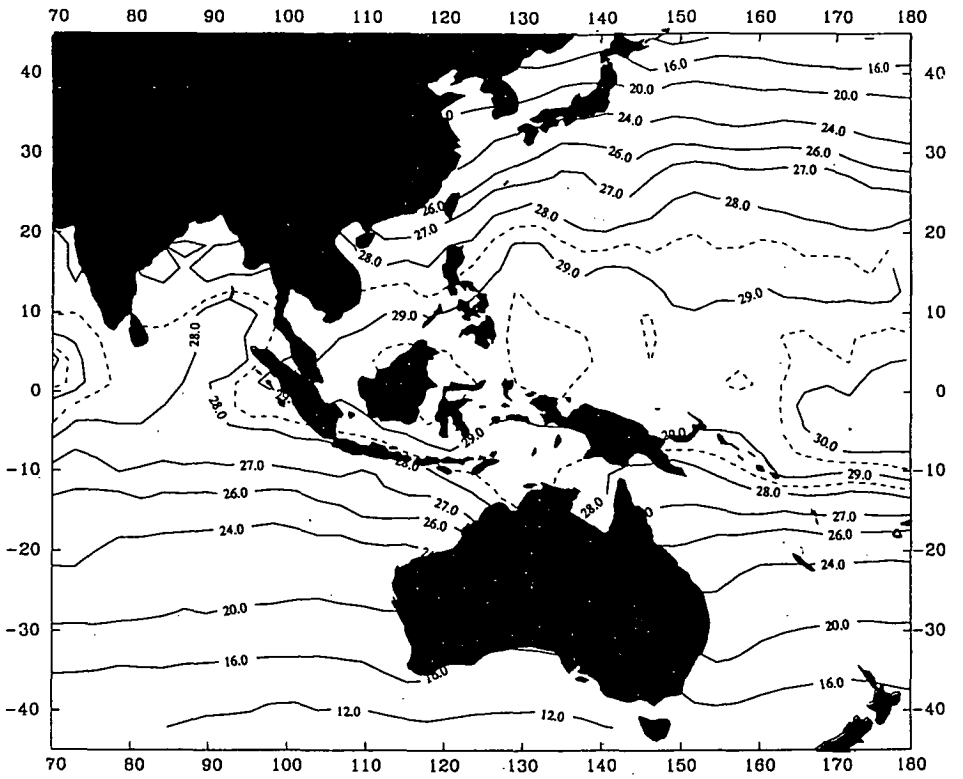

REYNOLDS BLENDED MONTHLY SST (8610)

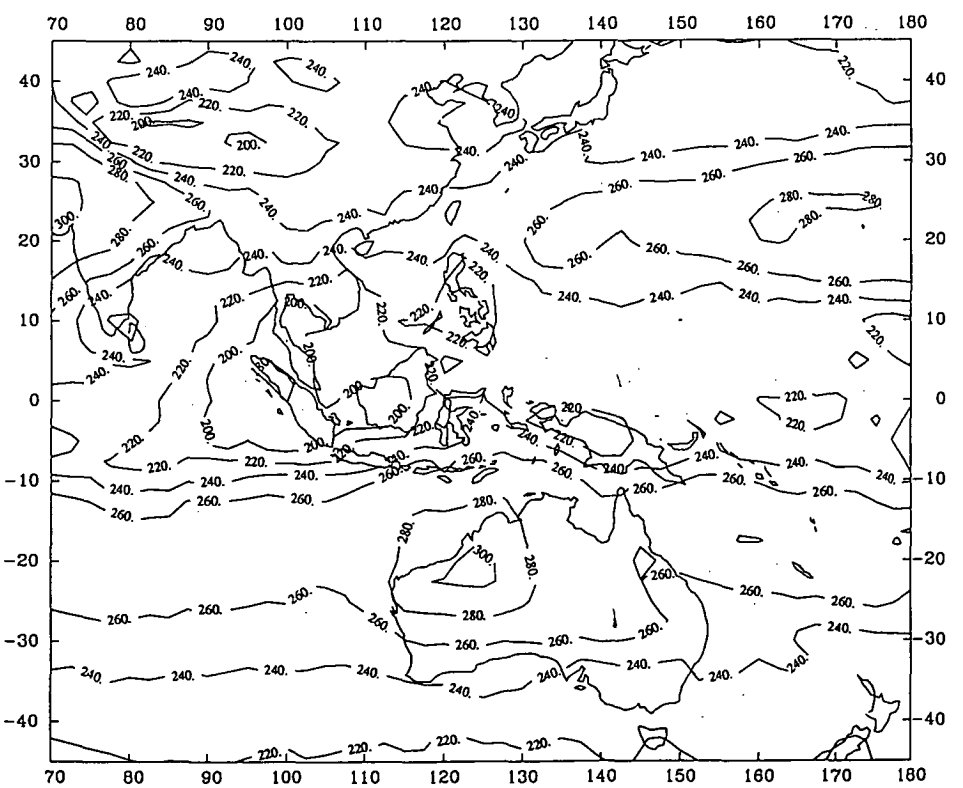

MONTHLY OLR (8610) (UNIT W/M*M)

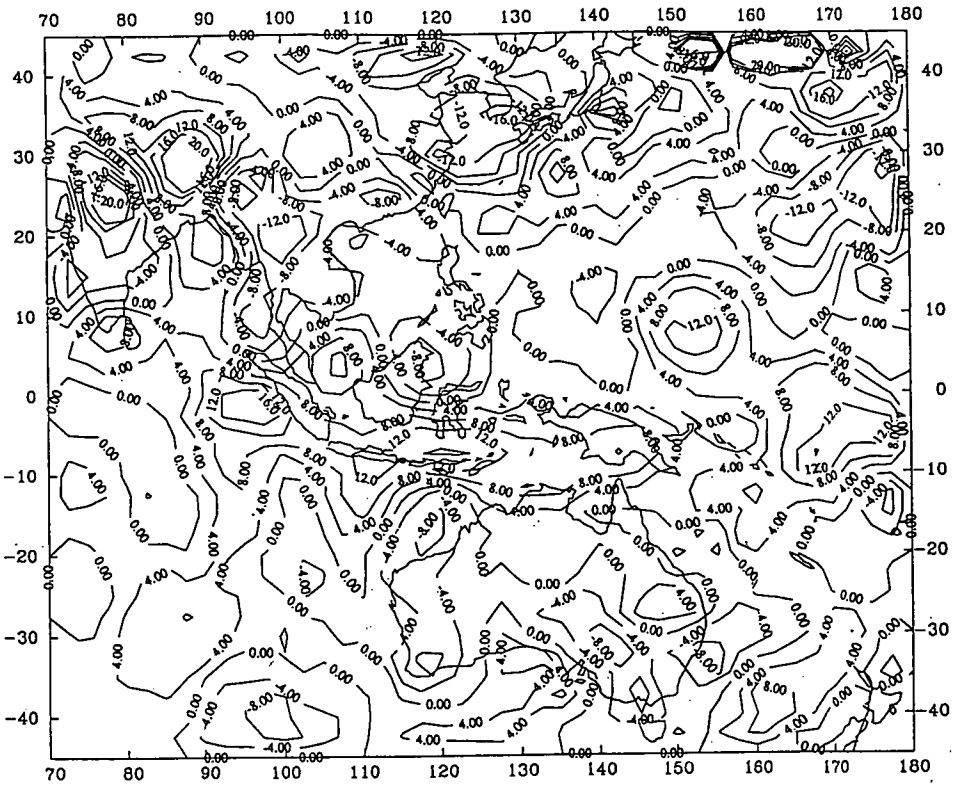

MONTHLY WIND DIVERGENCE AT 200MB (8610)

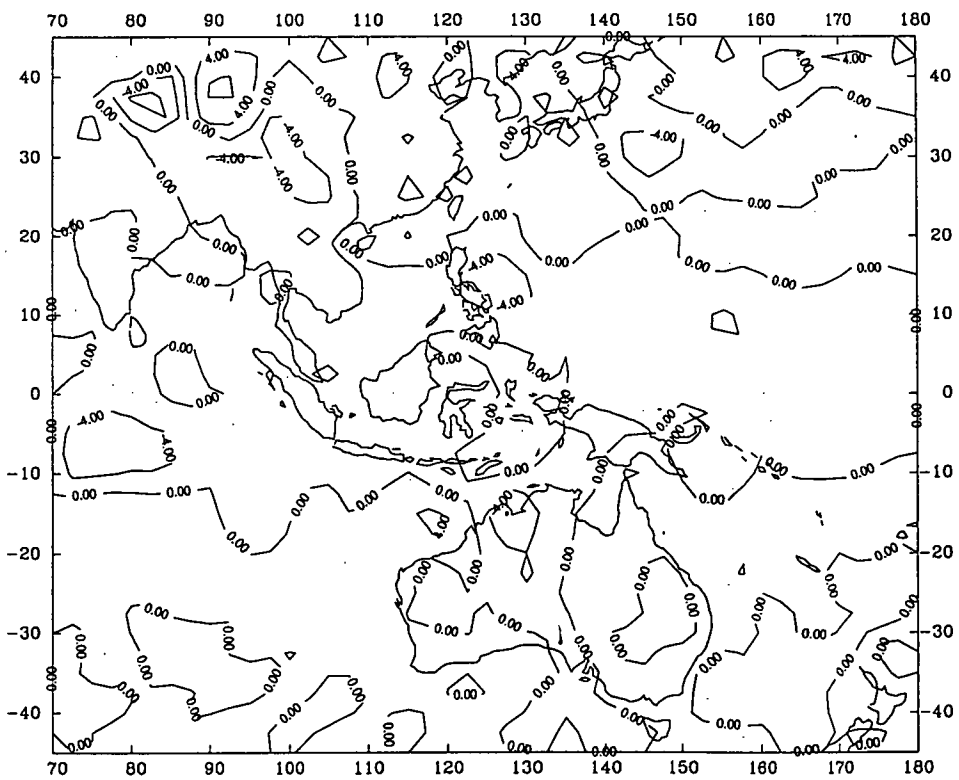

MONTHLY WIND DIVERGENCE AT 850MB (8610)

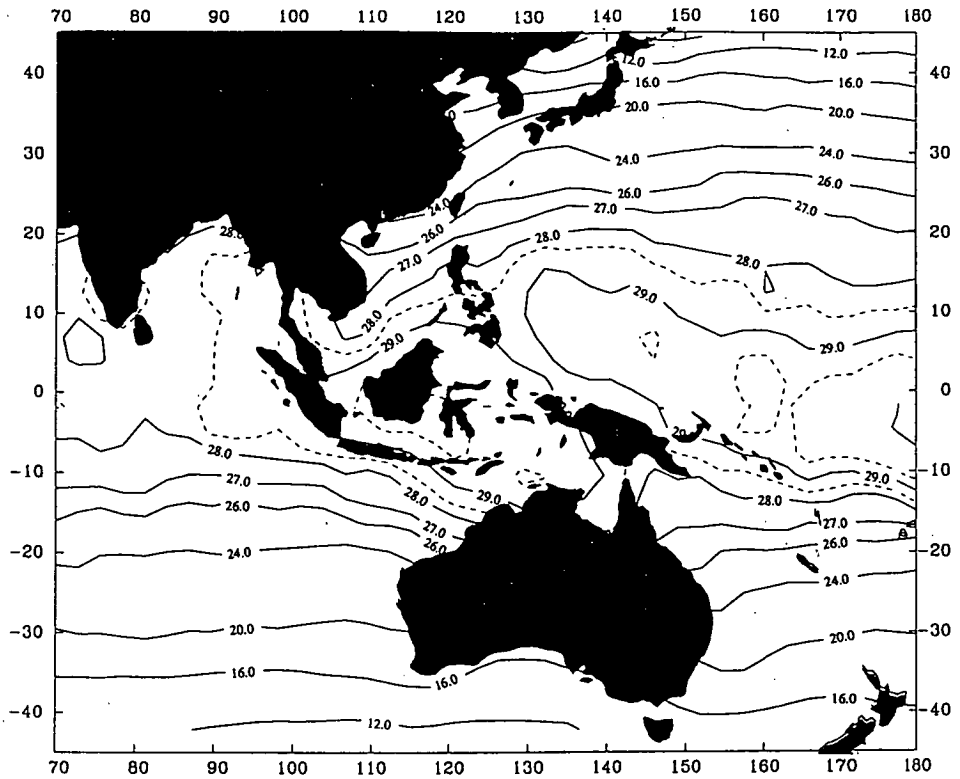

REYNOLDS BLENDED MONTHLY SST (8611)

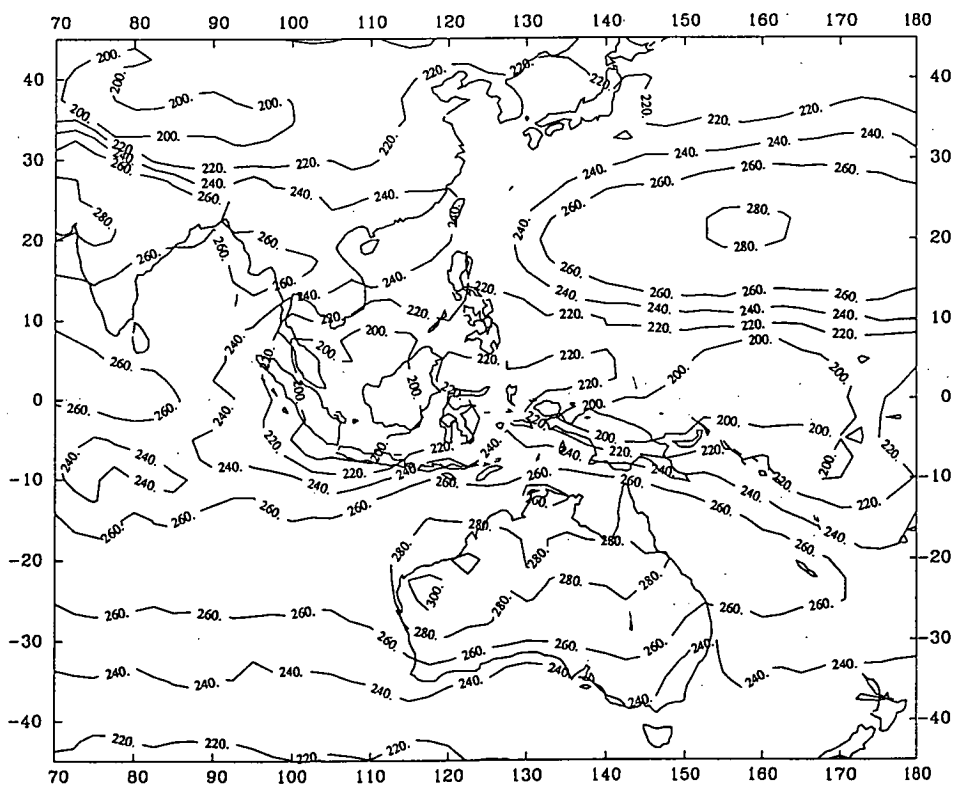

MONTHLY OLR (8611) (UNIT W/M*M)

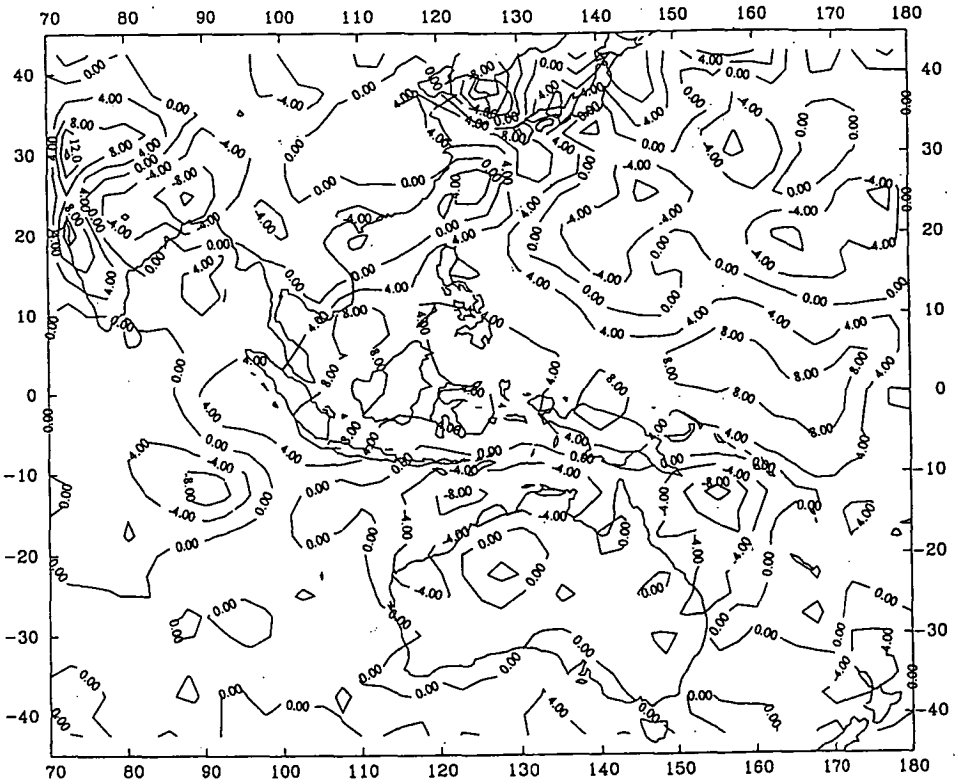

MONTHLY WIND DIVERGENCE AT 200MB (8611)

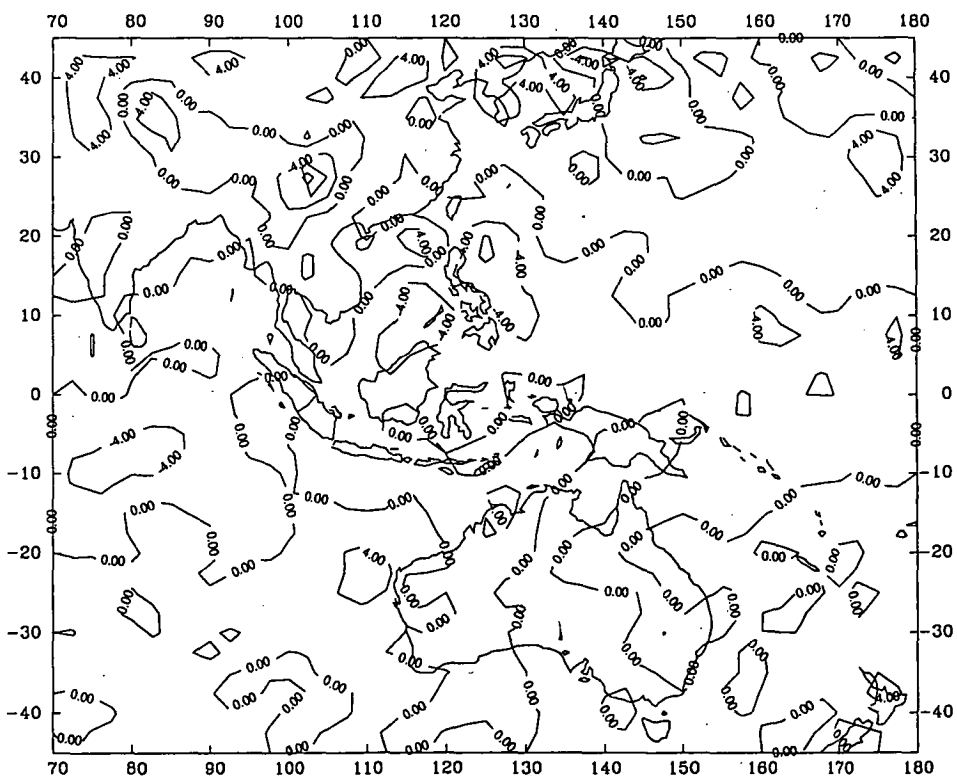

MONTHLY WIND DIVERGENCE AT 850MB (8611)

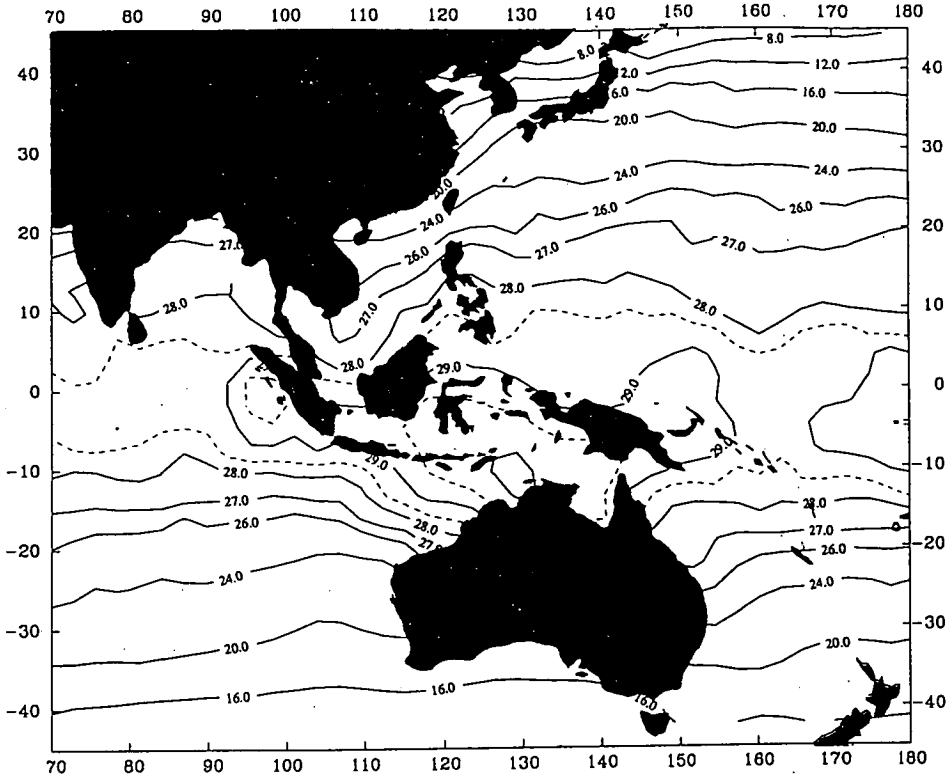

REYNOLDS BLENDED MONTHLY SST (8612)

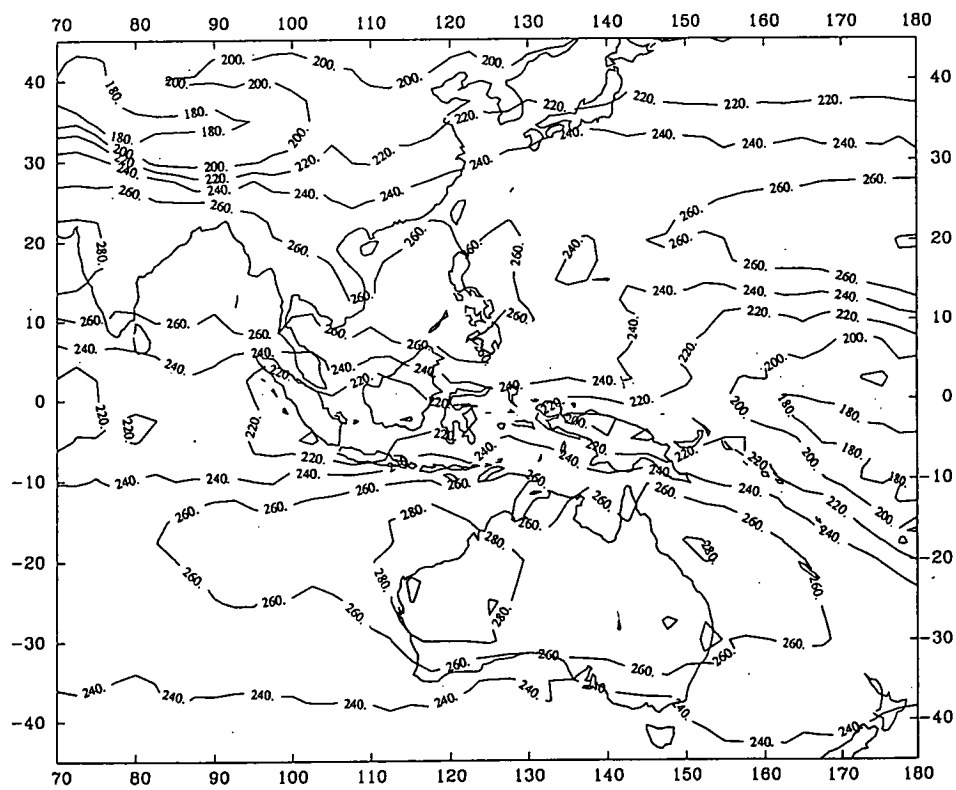

MONTHLY OLR (8612) (UNIT W/M*M)

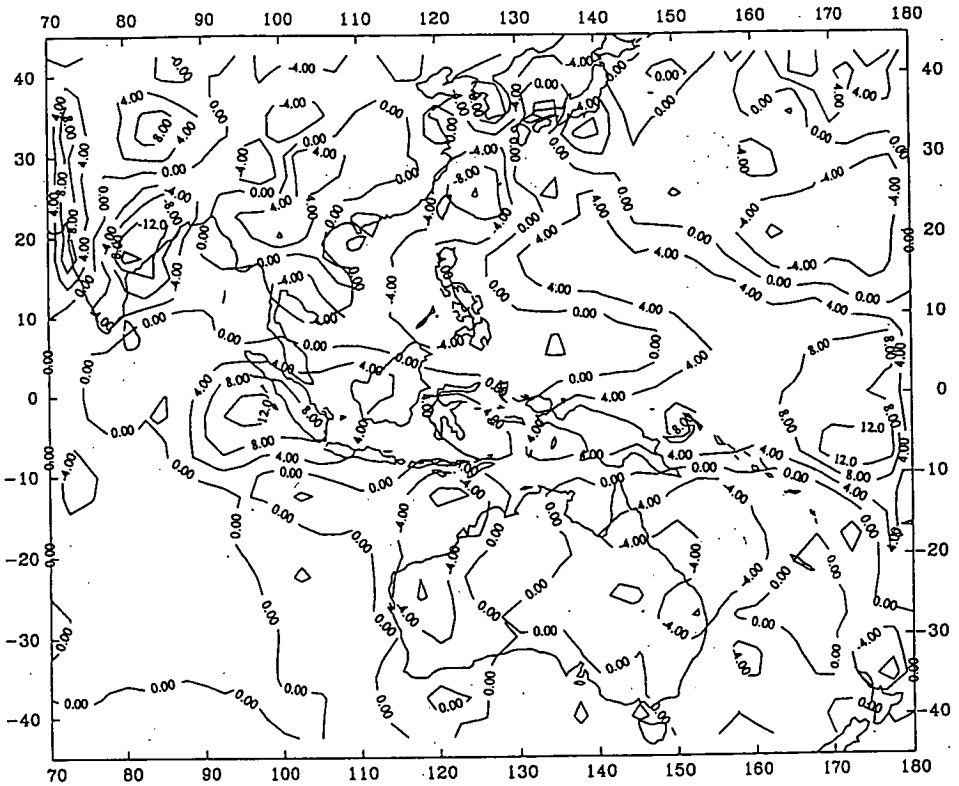

MONTHLY WIND DIVERGENCE AT 200MB (8612)

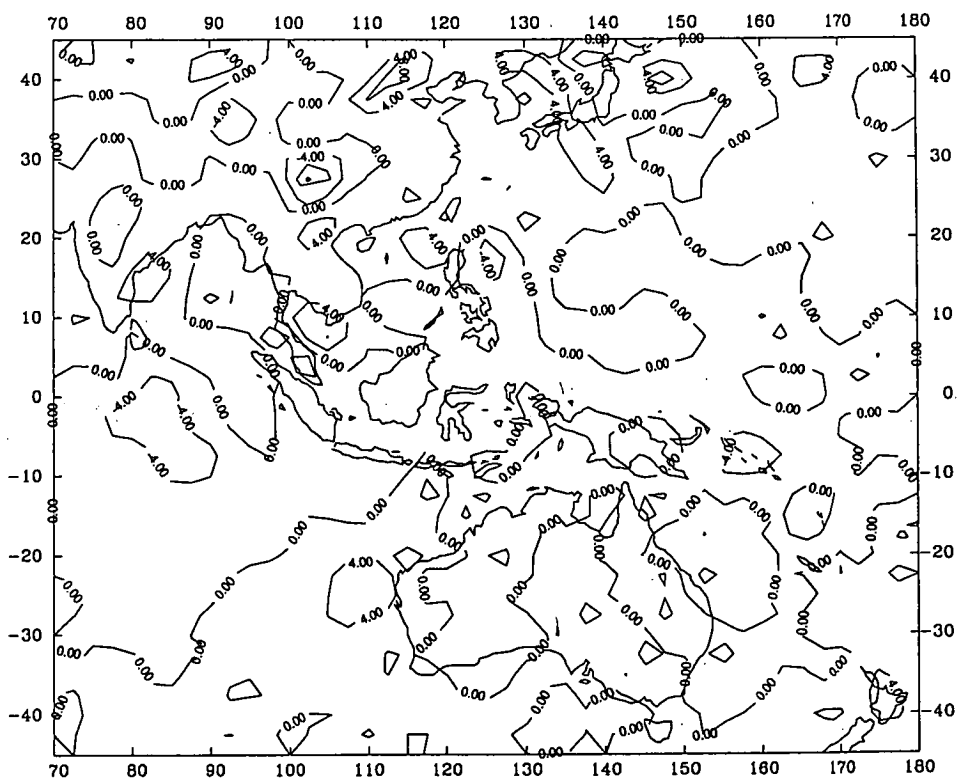

MONTHLY WIND DIVERGENCE AT 850MB (8612)